EJA
European Journal of Anatomy

Volume 26 - Number 6 November 2022

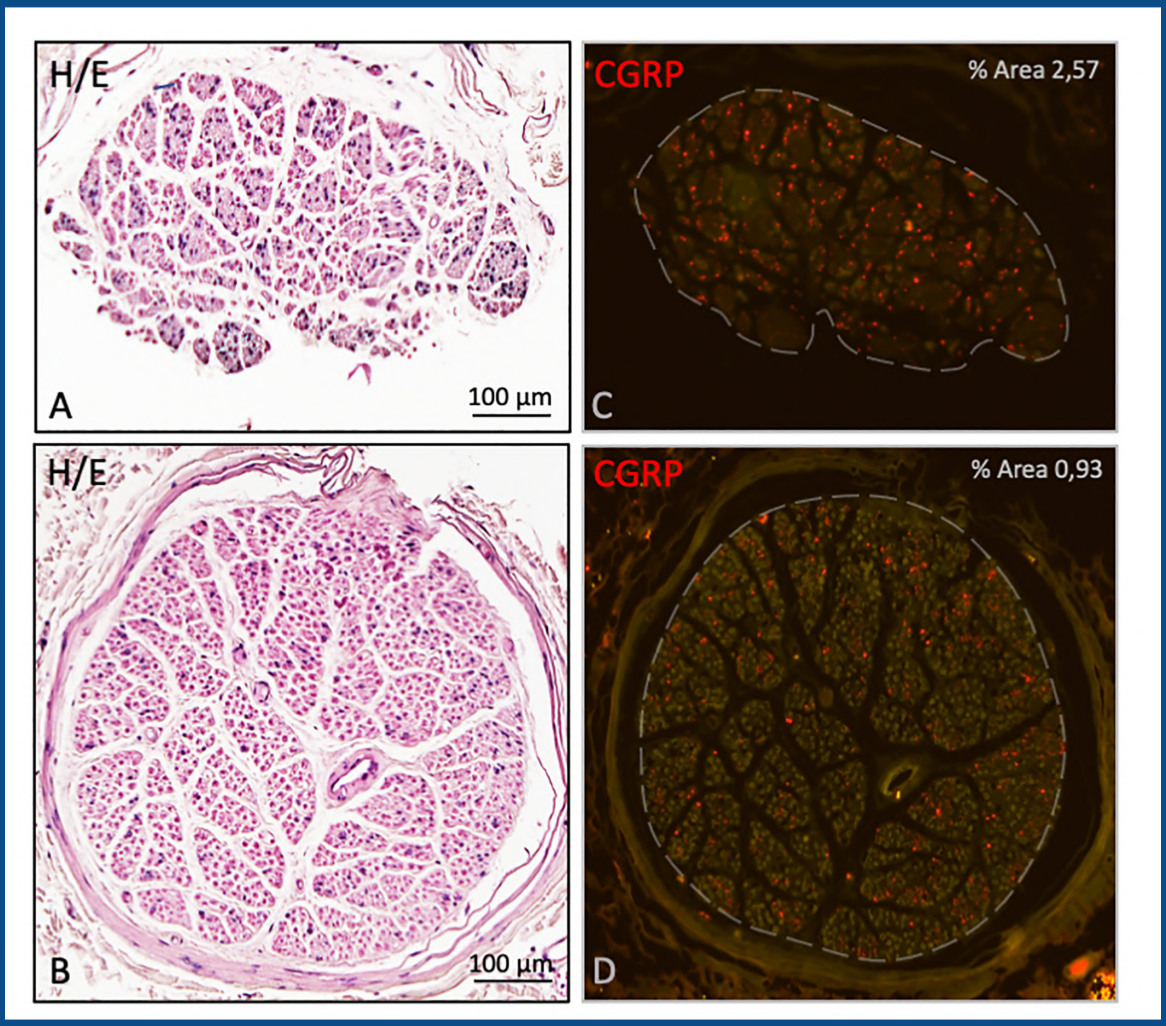

Indexed in:

CLARIVATE
- JCR:2020
- Q4 (21/23)
- I.F. J.C.I.: 0.19

DIALNET

EMBASE / Excerpta Medica

SCOPUS
- SJCR: 2020
- Q4 (31/39)
- I.F.: 0.162

Emerging Sources Citation Index

LATINDEX. Catálogo v1.0 (2002-2017)

Official Journal of the Spanish Society of Anatomy

www.eurjanat.com

EJA
European Journal of Anatomy

Volume 26 - Number 6 November 2022

ORIGINAL ARTICLES

TEACHING IN ANATOMY

Morphometry of extensors of the thumb with comprehensive review

Dhivyalakshmi Gnanasekaran[1], Raveendranath Veeramani[2], Aravindhan Karuppusamy[2]

[1] Dept of Anatomy, Indira Gandhi Medical College and Research Institute (A Government of Puducherry Institution), Puducherry, India
[2] Dept of Anatomy, Jawaharlal Institute of Postgraduate Medical Education and Research [JIPMER], Puducherry, India

SUMMARY

This study was aimed to evaluate the anatomical variations and morphometry of long extrinsic tendons of the thumb namely, extensor pollicis longus and extensor pollicis brevis. Fifty-five upper limbs of formalin embalmed adult cadavers were dissected. The variation in muscle belly, tendon, its course within dorsal wrist compartment and mode of insertion were noted. The extensor pollicis longus was duplicated in 5.5%. Around 25% tendons were fused with extensor pollicis brevis and through the extensor hood insert into the base of the distal phalanx. The extensor pollicis brevis was absent in 2% and tendon was also duplicated in 2%. In case of absent extensor pollicis brevis tendon, one of the slips from the abductor pollicis longus insert into base of the proximal phalanx instead of the extensor pollicis brevis. The extensor pollicis brevis tendon showed various modes of insertion. The overall length of the extensor pollicis longus and extensor pollicis brevis were 121 mm and 90 mm respectively. The thickness of the extensor pollicis longus at the proximal, middle and distal level of insertion were 1.25 mm, 0.76 mm and 0.55 mm respectively, whereas for the extensor pollicis brevis it was 1mm, 0.75 mm and 0.53 mm. The results obtained from this study may be helpful for the hand surgeons in the management of extensor tendon injuries of the thumb, its reconstructive procedures and in differential diagnosis of dorsal wrist pain.

Keywords: Extensor pollicis longus – Extensor pollicis brevis – Thumb – Extrinsic tendons – Extensor of thumb

INTRODUCTION

The extensor pollicis longus (EPL) and extensor pollicis brevis (EPB) muscles provide dynamic stability to the thumb along with other muscles acting on it (Flatt, 2002). The variations in the extensor muscles of the thumb have numerous clinical implications. The EPL muscle belly may be absent (Zadek, 1934) or have an additional belly with variable origin (Mogensen and Mattson, 1980; Beatty et al., 2000; Papaloïzos, 2004; Jscobs et al., 2016). Usually, it has an independent muscle belly, yet sometimes remains fused with adjacent muscles like EPB or with both EPB and abductor pollicis longus (Parsons and Robinson, 1898). The EPL muscle can rarely have two tendons, and the additional tendons were observed to arise either from the single muscle belly or from the additional muscle belly (Beatty

Corresponding author:
Dr. Raveendranath Veeramani. Department of Anatomy, Jawaharlal Institute of Postgraduate Medical Education and Research [JIPMER], Puducherry – 605006, India. Phone: 09043997352. E-mail: dr_raveendra@rediffmail.com

Submitted: March 16, 2022. **Accepted:** June 26, 2022

https://doi.org/10.52083/PMCG7678

et al., 2000; Sawaizumi et al., 2003; De Greef and De Smet, 2006). Double EPL tendons are formed rarely due to the splitting of the tendon distal to its myotendinous junction (Bharambe et al., 2017; Caetano et al., 2004). Wrist pain and the inability of thumb extension have been reported to occur due to the abnormal course of a single EPL tendon or its additional slips in various dorsal wrist compartments like first, third, fourth, and separate compartments (Bharambe et al., 2017; Rosa et al., 2016; Türker et al., 2010; Jscobs et al., 2016; Sevivas et al., 2009; Tordjman et al., 2018). Stenosing tenosynovitis of the third compartment has been reported to occur due to impingement of the EPL muscle belly within it (Mogensen and Mattsson, 1980; Beatty et al., 2000). Compression of the normal-sized EPL tendon in a small dorsal compartment (Mcmahon and Posner, 1994) or due to an enlarged EPL tendon in a normal-sized compartment (Kardashian et al., 2011) have been implicated as one of the causes of trigger thumb.

The incidence of an absence of the EPB muscle reported in the literature varies widely between 3.85 to 18.75% (Brunelli and Brunelli, 1992; Dawson and Barton, 1986). This is because of controversy in the interpretation of findings on the EPB. Dawson and Barton (1986) reported that the EPB muscle, as well as the tendon, was absent, but a slip of the abductor pollicis longus tendon inserts into the base of the proximal phalanx of the thumb instead of the EPB tendon (Dawson and Barton, 1986). Other authors considered this slip as an EPB tendon even when EPB muscle was absent (Nayak et al., 2009 & Kulshreshtha et al., 2007). The EPB tendon also varies in number from one to three (Nayak et al., 2008). Knowledge of duplicated EPB tendon is important in the differential diagnosis of EPB longitudinal split tears that present with dorsal wrist pain (Kroonen et al., 2015). The functional significance of the EPB tendon is doubtful. The method of insertion of the EPB tendon decides if it can be harvested for any reconstructive surgeries on the hand without affecting the thumb extension (Britto and Elliot, 2002; Matev, 1981; Sakellarides and Deweese, 1976). It also decides the course of surgical plan in case of a ruptured EPL or EPB tendon (Strauch and Strauch, 2016; Fujimoto et al., 2009). Kulshreshtha et al. (2007) observed that nearly 75% of the tendons showed wide variations in the method of insertion. Dawson and Barton (1986) considered some of the EPB tendons as thin, weak, and less or doubtful functional value. Joshi and Joshi (2002) considered subjectively that the EPB tendons were mostly very thin or moderately thick. Brunelli and Brunelli (1992), on the other hand, had classified the EPB tendon into three types normal (more than 2mm), thin (1-2 mm), and very thin (1mm). In this study, the details of the point of measurement and the technique adapted were not explained clearly. Kulshreshtha et al. (2007) compared the thickness of the EPB tendon with the abductor pollicis longus and reported that 36% of EPB tendons were relatively thin and less than 33% of the thickness of the abductor pollicis longus. However, it is not clear how the comparison was made. Shigematsu et al. (2015) measured the thickness and width of the EPB tendon, yet the length of the tendon, which is also equally important, was not measured. At the level of the extensor retinaculum, the extensor tendon is round in appearance and has enough strength and bulk to hold a suture. As the tendons continue into the thumb, they become flat and thin with longitudinal fibers that do not hold sutures well (Tsiouri et al., 2009). Thus, the knowledge of the morphometry of the extensors tendons of the thumb is essential for the tendon reconstructive procedures of the hand. Most of the above-mentioned data are obtained from case reports and only very few original studies are available that have documented the morphometry of entire thumb extensor muscles. The present study was done to find the incidence of variation in the muscle belly and the tendons of the EPL and EPB, and also to document the detailed measurements of these tendons.

MATERIALS AND METHODS

The study was approved by the Post Graduate Research Monitoring Committee. Ethical clearance was obtained from the Institute Ethics Committee. The study was then carried out in the Department of Anatomy in the Postgraduate Research Institute. All embalmed cadavers fit to be dissected were included, excluding the cadavers with evidence of

damage to the upper limb. 28 formalin fixed adult cadavers of both genders were taken for the study. After excluding one hand, a total of 55 upper limbs were dissected. The dorsal aspect of the distal forearm and hand was dissected. The extensor tendons inserted into the thumb were identified and traced backward. The extensor retinacular compartment was opened to see the course of the tendons and to trace the muscle bellies. Any variation in its muscle attachments was noted. The dissected specimens were photographed with a digital camera. All the measurements were taken by a single investigator using Mitutoyo digital vernier calliper. The length of the tendon was measured from the distal end of the muscle fibers to the site of the insertion of the tendon. Variation in the insertion of these tendons was documented. The thickness of the tendon was measured at three places as follows: proximal – just after the ending of the muscle fibers at the myotendinous junction, middle – at the middle of the dorsal compartment and, distal – just before its insertion. All relevant data were recorded and analyzed using IBM_PASW STATISTICS ver. 19.0 (SPSS ver 19.0). For left and right side, comparison of data of matched pairs paired t-test was used. For comparison between the genders, independent student t-test was used. All statistical analysis was carried out at a 5 % level of significance and a p-value < 0.05 was considered statistically significant. The results were expressed in mean, standard deviation, and range.

RESULTS

Extensor pollicis longus: muscle belly, tendons and site of insertion

The EPL muscle was present in all the dissected upper limbs. In all the specimens, the EPL muscle originated from the posterior aspect of the middle one-third of the radius and the adjacent interosseous membrane as a separate muscle belly. No variation in the number of muscle bellies was observed. In three cases (5.5%) double EPL tendon was identified. Of these, in one hand the EPL tendon was divided into two tendons about 20 mm distal to its origin from the muscle belly, and in the other two hands a double tendon was observed from the myotendinous junction itself. In all three hands, the two tendons were fused again at the level of the base of the proximal phalanx, then continued to insert into the distal phalanx base (Fig. 1a). Similarly, a separate EPB tendon was also seen in these hands. In the case of a double tendon, both the tendons passed through the same third extensor compartment and related medial to the Lister's tubercle similar to single tendon cases.

Regarding the insertion of the single EPL tendon, in 75% the tendon was inserted independently into the base of the distal phalanx through the extensor hood and in 25% the EPL tendon fused with the EPB tendon and together inserted into the base of the distal phalanx through the extensor hood. (Fig. 1b) Out of the 55 hands dissected, duplicated EPL tendon was observed in three hands. Hence in total measurements of 58 tendons were taken for the analysis. The overall length of the EPL tendon was measured to be 120.68 ± 15.61 mm. The thickness of the tendon at the proximal, middle, and the distal level of insertion were measured as 1.25 ± 0.38 mm, 0.76 ± 0.23 mm, and 0.55 ± 0.22 mm respectively. The details of the analysis carried out to compare the mean length and thickness of EPL tendons showed no significant difference between the genders (Independent student t-test). For comparison between the left and right sides, 27 matched pairs were taken excluding the unpaired hand. Since duplicated EPL tendon was observed in three hands, the mean of the values was taken for each hand and considered as one hand (Paired t-test). This also showed no significant differences (Table 1).

Extensor pollicis brevis: muscle belly, tendons and site of insertion

Out of 55 hands dissected, the EPB muscle was absent in 2% (1 hand) and no duplicated muscle belly was observed. Single EPB tendon was seen in 98% (53 hands) and duplicated tendon in 2% (1 hand). The tendon was duplicated at its origin level from the single muscle belly (Fig. 1c). In the case of a duplicated tendon, the main tendon joins the EPL tendon and inserts into the base of the distal phalanx through the extensor hood. But the accessory EPB tendon was inserted into the extensor hood (Fig. 1c). In the hand where the EPB

tendon was absent, it was found that an accessory tendon from the abductor pollicis longus muscle inserts into the base of the proximal phalanx instead of the normal EPB tendon (Fig. 1d). The separate EPB muscle belly was not seen in any of the dissected hands (54 hands). It was found to be fused with the abductor pollicis longus muscle to a variable extent starting from its origin to till the tendon arises. However, an identifiable plane of separation was found between the distal end of

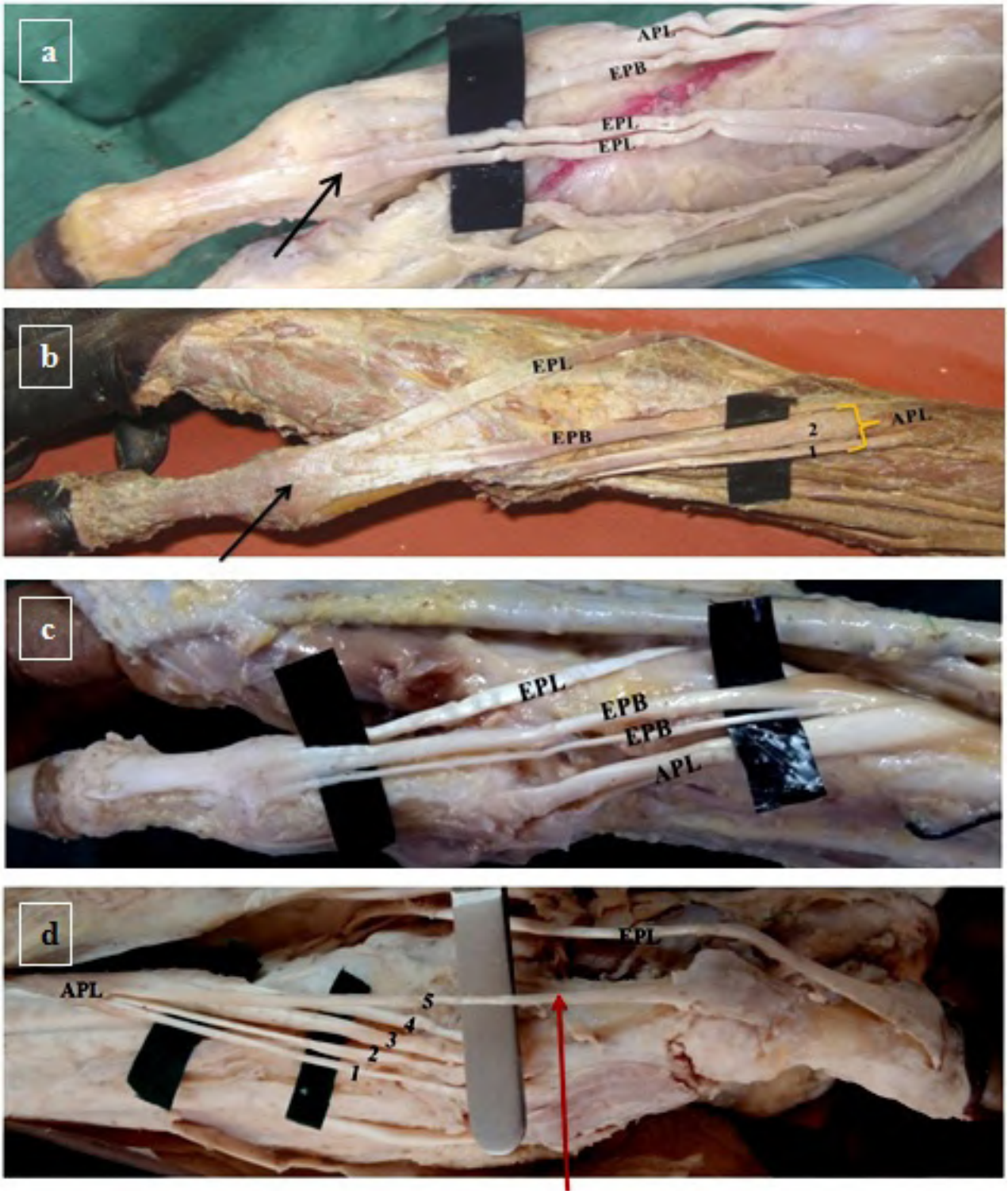

Fig. 1.- a. Duplicated EPL tendons fuses at the level of first metacarpophalangeal joint and insert into the base of distal phalynx. **b.** EPB tendon fuses with the EPL tendon at the level of first metacarpophalangeal joint and together inserts into the base of distal phalynx. **c.** Duplicated EPB tendon at its origin from single muscle belly. **d.** Both muscle belly and tendon of EPB is absent**.** Accessory APL tendon inserts into the base of proximal phalanx instead of the normal EPB tendon. EPB - Extensor pollicis brevis, EPL - Extensor pollicis longus, APL - Abductor pollicis longus.

Table 1. Morphometry of the extensor pollicis longus tendons (mm); SD - Standard deviation.

Sl No	Parameters	Mean ± SD (58 tendons) Range	Gender (58 tendons) Mean ± SD		Side (27 paired hands) Mean ± SD	
			Male (36)	Female (22)	Left (27)	Right (27)
1	Length of the tendon	120.68 ± 15.61 87.12 - 152.68	121.89 ± 17.80	118.71± 11.24	119.63 ± 16.08	120.51 ± 15.88
2	Thickness of the tendon at proximal level	1.25 ± 0.38 0.48 - 2.31	1.33 ± 0.39	1.14 ± 0.32	1.27 ± 0.37	1.27 ± 0.39
3	Thickness of the tendon at the middle	0.76 ± 0.23 0.44 - 1.49	0.75 ± 0.23	0.77 ± 0.24	0.78 ± 0.26	0.74 ± 0.21
4	Thickness of the tendon at distal level	0.55 ± 0.22 0.25 - 1.38	0.57 ± 0.19	0.51 ± 0.26	0.56 ± 0.24	0.56 ± 0.20

Table 2. Morphometry of the extensor pollicis brevis tendons (mm); SD - Standard deviation.

Sl No	Parameters	Mean ± SD (55 tendons) Range	Gender (55 tendons) Mean ± SD		Side (26 paired hands) Mean ± SD	
			Male (33)	Female (22)	Left (26)	Right (26)
1	Length of the tendon	90.00 ± 14.63 66.40 - 118.56	92.97 ± 14.43	85.56 ± 14.10	90.27 ± 13.82	90.64 ± 15.64
2	Thickness of the tendon at proximal level	1.07 ± 0.48 0.26 - 3.23	1.15 ± 0.51	0.94 ± 0.40	1.07 ± 0.35	1.09 ± 0.56
3	Thickness of the tendon at the middle	0.75 ± 0.39 0.17 - 1.68	0.83 ± 0.41	0.64 ± 0.32	0.81 ± 0.40	0.74 ± 0.38
4	Thickness of the tendon at distal level	0.53 ± 0.24 0.14 - 1.45	0.54 ± 0.27	0.51 ± 0.19	0.54 ± 0.20	0.54 ± 0.28

both the EPB and EPL muscles at least in its distal end in 54 hands. In one hand a small slip of tendon arose from the EPB tendon about 2 cm from the distal end of the extensor retinaculum and was inserted into the base of the first metacarpal bone. In all the hands where the EPB tendon was present, it passed through the first dorsal wrist compartment along with abductor pollicis longus. Regarding insertion of EPB tendon, the tendons insert partly to the base of the proximal phalanx and partly to the hood in 26%, completely to the proximal phalanx in 28.30%, completely to the extensor hood in 21%, in 15% the EPB tendon was fused with the EPL tendon at the level of the metacarpophalangeal joint and together inserted into the base of the distal phalanx through the extensor hood (Fig. 1b). The tendon sometimes partly inserts into the base of the proximal phalanx and then joins the EPL tendon to reach the distal phalanx through the hood in 9%.

The EPB was absent in one hand but duplicated in another hand. Hence in total 55 tendons' measurements were taken for the analysis. The overall length of the EPB tendon was measured to be 90.00 ± 14.63 mm. The thickness of the tendon at the proximal, middle, and distal level of insertion was measured as 1.07 ± 0.48 mm, 0.75 ± 0.39 mm and 0.53 ± 0.24 mm respectively. Similar to the EPL tendon, the EPB tendon also showed no significant difference between genders and sides. Out of the 27 matched pairs, the EPB tendon was absent in one hand. Hence 26 matched pairs were taken for comparison of the measurements between the sides. Out of these 26 pairs, in one hand where the duplicated tendon was observed the mean of the value was taken for analysis (Table 2).

DISCUSSION

Extensor policis longus

The EPL is a constant structure found in humans (Yoshida, 1990). The incidence of double muscle bellies reported in two separate cadaveric studies were 2% and 6.6% respectively (Bharambe et al., 2017; Parsons and Robinson, 1898). The muscle

can be absent alone or associated with an absence of EPB muscle (Parsons and Robinson, 1898). Bilateral absence of the EPL muscle has been also reported (Zadek, 1934). In the present study, the EPL muscle was present in all of the dissected hands. No absent or double muscle belly was observed. The EPL muscle is seen mostly as an independent structure, but rarely does it fuse with other extensor muscles such as extensor indicis proprius or extensor pollicis indicis accessorius, or with both EPB and abductor pollicis longus (Parsons and Robinson, 1898; Yoshida, 1990). In the present study, the EPL muscle belly was seen as a distinct structure and there was no fusion with the adjacent muscles.

The most common numerical variation includes the double EPL tendon, however, Parsons and Robinson (1898) reported the triple EPL tendon in 2.3%. A cadaveric study by Thwin et al. (2014) reported that the double EPL tendon was observed in 2 out of 10 dissected specimens, which accounts for 20% which is more compared to the other

Table 3. Review on variation in the number and course of the extensor pollicis longus tendon.

Author / year/ sample size/ region/ type of study	Course of the tendon
Talbot/ 2013/ 1/ USA/ Cadaveric dissection	The tendon divided into two slips and inserted into extensor indicis and normal extensor pollicis longus separately. Course in the compartment not mentioned
Sevivas/ 2009/ 1 upper /France/ clinical case	Additional tendon passed through the separate compartment between the 3rd and 4th compartment
Sawaizumi/ 2003/ 1 upper limb /Japan/ clinical case	1st tendon passed through the separate compartment between 1st and the 2nd compartment 2nd tendon passed over the extensor retinaculum radial to the Lister's tubercle
Rosa/ 2016/ 2 upper limbs/ Brazil/ Cadaveric dissection	2 hands - The additional tendon coursed through the 1st extensor compartment and merged with the extensor pollicis brevis
Papaloïzos/ 2004/ 1 upper limb / Switzerland/ Cadaveric dissection	The additional tendon passed through 4th compartment. Both the tendons fuses at the level of metacarpophalangeal joint
Nishijo/ 2000/ 1/ Japan/ Clinical case	The duplicated tendon passed radial to the lister's tubercle in the 1st compartment
Masada/ 2003/ 1 upper limb/ Japan/ clinical case	Both the tendons passed through the same 3rd compartment
Jscobs/ 2016/ 1 upper limb/ Netherland/ Cadaveric dissection	Both the tendons fuses at the base of the proximal phalanx and continued to insert into the distal phalanx. Course in the compartment not mentioned
Hong/ 2013/ 1 case/ Korea/ clinical case	Only one tendon but the tendon passed through the 3rd compartment at the wrist and at the carpal passed through the 1st compartment and inserted to the radial side of the base of the proximal phalanx and not to the distal phalanx
Turker/ 2010/ 3 cases/ USA/ clinical case report	1st case – Two tendons passed through 3rd and 4th compartment 2nd & 3rd case – 1st tendon passed through the 3rd compartment – 2nd tendon, the extensor pollicis et indicis communis passed through the 4th compartment
Tordjman/ 2018/ 1 case/ France/ clinical case	Accessory tendon passed through the 4th extensor compartment
Beatty/ 2000/ 1 case/ UK/ clinical case	Both the tendons passed through the 3rd extensor compartment
Greef/ 2006/ 1 case/ Turkey/ clinical case	Additional tendon passed through the 4th compartment
Chamberlain/ 1997/ 2 upper limbs/ U K/ clinical case	Both the tendons passed through the 3rd compartment
Abe/ 2004/ 2 cases/ Japan/ clinical study	The extensor pollicis longus tendon ran through the 1st extensor compartment and the 3rd compartment was empty
Rubin/ 2011/ 1 upper limb/ Israel/ Clinical case	The extensor pollicis longus tendon passed radial to the Lister's tubercle and entered through the 1st extensor compartment. Third compartment was absent
Kim/ 2015/ Korea/ 1 upper limb/ clinical case	The tendon passed radial to the Lister tubercle and crossed the extensor carpi radialis in the 2nd extensor compartment. The third compartment was absent

studies cited in the literature. In the present study, the EPL muscle with double tendons was present in 5.5%. The duplicated EPL tendons may remain together in the same third extensor compartment (Chamberlain and Burke, 1997), or the accessory tendons may have an unusual course through the various dorsal extensor compartments (Bharambe et al., 2017; Papaloïzos, 2004; Sevivas et al., 2009; Thwin et al., 2014; Masada et al., 2003; Türker et al., 2010; Rosa et al., 2016; Sawaizumi et al., 2003). In the current study, the double tendons observed in the three hands passed through the same third extensor compartment and were related medial to the Lister's tubercle. The unusual course of the single EPL tendon in the dorsal wrist compartment has led to dorsal wrist pain, the inability of thumb extension, and misdiagnosis of intersection syndrome or de Quervain's tenosynovitis when the double tendon passed through the first compartment (Abe et al., 2004; Rubin et al., 2011; Kim et al., 2016; Hong et al., 2013; Nishijo et al., 2000). This study provides a detailed review on the morphometry of EPL, which could be taken as reference for tendon transfer surgeries (Table 3).

McMahon and Posner (1994) reported a case of trigger thumb due to compression of normal-sized EPL tendon within a small third compartment. At the same time, Kardashian et al. (2011) mentioned a case of snapping of the thumb due to an enlarged EPL tendon in a normal-sized third compartment. To the best of our knowledge, the thickness of the EPL has been the least studied topic till now. From the present study the thickness of the tendon at the proximal, at the middle of the extensor compartment, and the distal level of insertion were measured as 1.25 ± 0.38 mm, 0.76 ± 0.23 mm and 0.55 ± 0.22 mm respectively. The length of the tendon, which is equally important for planning its reconstruction, is measured to be 120.68 ± 15.61 mm.

The knowledge of insertion of the EPL tendon helps in understanding the function of the thumb extension and planning intervention accordingly when it gets injured (Alsharif et al., 2017). Parsons and Robinson (1898) described that the entire EPL tendon inserts into the dorsal aspect of the thumb's distal phalanx in 84.5%, into the terminal phalanx, after receiving a slip of EPB tendon in 12%, and into the terminal phalanx after giving off a slip to the proximal phalanx in 3%. In the present study, about 75% were inserted into the distal phalanx' base alone and received fibers of EPB before insertion into the distal phalanx in 25%. Our study is in accordance with the study by Parsons and Robinson (1898). Caetano et al. (2004) described that the EPL tendon duplicated distal to the extensor retinaculum but again fused at the base of the metacarpophalangeal joint before insertion in 4.8%. The same finding was observed in one case in the present study. Alsharif et al. (2017) reported that the EPL tendon was inserted into the sides of the base of the distal phalanx after splitting and this altered the thumb motion. Colak et al. (2017) documented a variation in which the EPL tendon was inserted into the tuberculum radii. The EPL tendon rupture occurs if additional friction force is being imposed on it due to its course around the Lister's tubercle and also this is the most common site of rupture. It often requires treatment with tendon transfer surgery for restoring the thumb extension function (Sabat et al., 2014). The knowledge of the dimension such as length and thickness of the EPL tendon could aid in the repair or reconstruction surgery and enable to resume of optimal thumb functions.

Extensor pollicis brevis

The EPB, a muscle peculiar to or individualized to a greater degree in humans is sometimes absent or fused with abductor pollicis longus as in the primates (Tubbs et al., 2016). The frequency of absence of EPB muscle belly reported in the literature varies widely. Dawson and Barton (1986) reported that the absence of the EPB muscle belly in 18.75% and Brunelli and Brunelli (1992) in 3.85%. Contrary to this, the frequency of absence of the EPB muscle found in the present study is very low (2% only). Dawson and Barton (1986) reported that in 81.25% the EPB muscle belly was either distinct or fused with the abductor pollicis longus muscle. In our study, the EPB muscle belly was found to be fused with abductor pollicis longus muscle to a variable extent in 98%. The incidence of double EPB tendon reported in two separate cadaveric studies was 2% and 4% respectively

(Joshi and Joshi, 2002; Shigematsu et al., 2014). In the present study, double EPB tendons were found in 2% similar to the study by Joshi and Joshi (2002). However, in a cadaveric study by Nayak et al. (2008) double EPB tendons were identified in 11% and such high frequency may be due to their higher sample size (156 hands) compared to the present study. The same author has found triple EPB tendons in 3.85% of the dissected hands (Nayak et al., 2008). The incidence of the absence of EPB tendon reported by other studies was 0% (Kulshreshtha et al., 2007), 0% (Dawson and Barton., 1986), 2% (Brunelli and Brunelli, 1992), 6.25% (Shigematsu et al., 2014) and 7.8% (Joshi and Joshi, 2002). Such variation in the incidence is because some authors considered one of the accessory tendons of abductor pollicis longus inserted into the base of the proximal phalanx as EPB tendon and reported no absence of EPB tendon in their study (Kulshreshtha et al., 2007; Nayak et al., 2009).

Table 4. Review on variation in the site of insertion of extensor pollicis brevis.

Site of insertion	Authors (Sample size)						
	Dawson and Barton (16 hands)	**Brunelli and Brunelli (52 hands)**	**Kulshreshtha et al (44 hands)**	**Nayak et al (156 hands)**	**Joshi and Joshi (50 hands)**	**Shigematsu et al (144 hands)**	**Present study (55 hands)**
Partly to the proximal phalanx and partly to hood	56.25 %	19.23 %	25 %	-	-	19.4 %	26.42 %
Completely to the proximal phalanx	25 %	-	25 %	Single tendon - 85.25 % Accessory tendon - 11 %	76 %	22.2 %	28.30 %
Completely to the extensor the hood	18.75 %	69.23 %	2 %	-	-	28.5 %	20.75 %
To the distal phalanx	-	7.69 %	-	-	-	-	-
Partly to the base of the proximal phalanx and partly to the extensor hood and majority of the fibres continued along with the EPL to insert into the distal phalanx	-	-	27 %	-	-	9.0 %	15.09 %
Partly to the extensor hood and remaining continued to insert into the base of the distal phalanx along with EPL	-	-	20%	-	-	9.0 %	9.43 %
Joined with EPL to insert into the distal phalanx	-	-	-	-	18 %	-	-
Both proximal phalanx and distal phalanx	-	-	-	-	2 %	-	-
Base of the first metacarpal	-	-	-	3.2 %	4 %	-	-
Absent tendon	6.25 % *	# 3.85 %	6.8 % *	1.2 % *	2 %	# 2.1 %; 5.6 % *	1.82 %

* Dawson and Barton reported that in a case where EPB muscle belly was absent the accessory abductor pollicis longus tendon was found to insert into the base of the proximal phalanx instead. Hence in this study both the EPB muscle and tendon was considered to be absent.
* The same as first was observed but it was considered as EPB tendon arising from the abductor pollicis longus. Hence reported EPB was not absent.
* The accessory tendon from EPL and Abductor pollicis longus inserts into the extensor hood at the metacarpophalangeal joint. Hence it is considered as absent EPB tendon
# Absent EPB tendon

The EPB tendon was inserted completely into the base of the proximal phalanx only in 28.30% and also completely into the extensor hood in 20.75%. Rest 26.42% inserted partly into the proximal phalanx and partly into the extensor hood. Then in 15.09%, part of the tendon was inserted into the proximal phalanx, and the remaining continued distally to the distal phalanx for insertion along with the EPL. But, in 9.43%, the tendons reached the base of the distal phalanx for complete insertion along with the EPL tendon. The above findings of our study go in accordance with the study by Shigematsu et al. (2014) and at the same time differ from others (Table 4), as the insertion of tendons into the extensor hood or its relation to the EPL tendon insertion were not taken into account (Nayak et al., 2008; Joshi and Joshi, 2002).

The overall length of the EPB tendon was measured to be 90.00 ± 14.63 mm and the thickness of the tendon measured at proximal, at the middle of the dorsal compartment, and the distal level was 1.07 ± 0.48 mm, 0.75 ± 0.39 mm, and 0.53 ± 0.24 mm respectively. Shigematsu et al. (2014) measured the thickness and the width of the EPB tendon at the center of the metacarpal bone to be 0.93 ± 0.20 and 2.63 ± 0.61 mm and of the accessory tendons as 0.66 ± 0.17 mm and 1.70 ± 0.52 mm. Our study results cannot be compared with the abovementioned study, as the measurements were taken at a different level. The surgeons need to be aware of the presence or absence of the EPB tendon and variation in the insertion of the tendon with respect to the EPL tendon as it helps in planning the repair or reconstruction of the injured EPB tendon.

REFERENCES

ABE Y, TSUE K, NAGAI E, KATSUBE K, MIYOSHI T (2004) Extensor pollicis longus tenosynovitis mimicking de Quervain's disease because of its course through the first extensor compartment: a report of 2 cases. *J Hand Surg*, 29(2): 225-229.

ALSHARIF MH, ALFAKI MA, ELAMIN AY, MANSSOR EH, TAHA KM, ARAFA EM, ALDOSARI KH (2017) Tendón accesorio del músculo extensor largo del pulgar: reporte de caso de una rara variación anatómica. *Int J Morphol,* 35(4): 1276-1279.

BEATTY JD, REMEDIOS D, MCCULLOUGH CJ (2000) An accessory extensor tendon of the thumb as a cause of dorsal wrist pain. *J Hand Surg,* 25(1): 110-111.

BHARAMBE V, PATEL D, MANVIKAR PR, SHEVADE S, BAJPAYEE PG (2017) A study of extensor pollicis longus and brevis and abductor pollicis longus from the perspective of evolution. *J Med Res,* 3(3): 146-150.

BRITTO JA, ELLIOT D (2002) Thumb function without the abductor pollicis longus and extensor pollicis brevis. *J Hand Surg*, 27(3): 274-277.

BRUNELLI GA, BRUNELLI GR (1992) Anatomy of the extensor pollicis brevis muscle. *J Hand Surg*, 17(3): 267-269.

CAETANO MBF, ALBERTONI WM, CAETANO EB (2004) Anatomical studies of the distal insertion of extensor pollicis longus. *Acta Ortop Bras,* 12(2): 118-124.

CHAMBERLAIN ST, BURKE FD (1997) Bilateral double extensor pollicis tendons. Segmentation or coalition? *Hand Surg*, 2(02): 171-174.

COLAK T, BAMAC B, TEKIN OA, OZBEK A, OZTURK OB (2017) Case report: uncommon insertion of the extensor pollicis longus muscle: clinical and anthropological significance of this variation. *Anthropologist,* 27(1-3): 121-124.

DAWSON S, BARTON N (1986) Anatomical variations of the extensor pollicis brevis. *J Hand Surg Brit Eur,* 11(3): 378-381.

DE GREEF I, DE SMET L (2006) Accessory extensor pollicis longus: a case report. *Eur J Plast Surg*, 28(8): 532-533.

FLATT AE (2002) Our thumbs. In: Taylor & Francis (eds). Baylor University Medical Center Proceedings, pp 380-387.

FUJIMOTO T, TANASE Y, ORIBE T, WATANABE Y (2009) Spontaneous rupture of the extensor pollicis brevis tendon in a baseball pitcher: A case report. *Upsala J Med Sci*, 114(3): 189-192.

HONG J, KIM DK, KANG SH, SEO KM (2013) Anomalous course of the extensor pollicis longus with multiple absences of thumb muscles. *Ann Rehabil Med,* 37(1): 151-155.

JSCOBS K, OOSTRA RJ, ENGELBERT R, HABETS P (2016) Multiple bilateral anatomical variations of the tendons of the forearm and wrist: a case report based on a cadaver study. *Int J Anat Var*, 9: 3-7.

JOSHI SS, JOSHI SD (2002) Applied significance of variations of the first extensor compartment of wrist. *J Anat Soc India,* 51(2): 159-161.

KARDASHIAN G, VARA AD, MILLER SJ, MIKI RA, JOSE J (2011) Stenosing synovitis of the extensor pollicis longus tendon. *J Hand Surg,* 36(6): 1035-1038.

KIM YJ, LEE JH, BAEK JH (2016) Variant course of extensor pollicis longus tendon in the second wrist extensor compartment. *Surg Radiol Anat,* 38(4): 497-499.

KROONEN LT, FERGUSON C, KETSCHKE RA (2015) Longitudinal split tear of the extensor pollicis brevis tendon: Report of 2 cases. *J Hand Surg,* 40(2): 236-239.

KULSHRESHTHA R, PATEL S, ARYA AP, HALL S, COMPSON JP (2007) Variations of the extensor pollicis brevis tendon and its insertion: a study of 44 cadaveric hands. *J Hand Surg Eur Vol,* 32(5): 550-553.

MASADA K, YASUDA M, TAKEUCHI E, MIZUSAWA K (2003) Duplicate extensor tendons of the thumb mimicking rupture of the extensor pollicis longus tendon. *Scand J Plast Reconstr Surg Hand Surg,* 37(5): 318-319.

MATEV IB (1981) Restoration of thumb opposition by displacement of extensor pollicis brevis. *Hand, 1*3(3): 279-284.

MCMAHON MS, POSNER MA (1994) Triggering of the thumb due to stenosing tenosynovitis of the extensor pollicis longus: a case report. *J Hand Surg,* 19(4): 623-625.

MOGENSEN BA, MATTSSON HS (1980) Stenosing tendovaginitis of the third compartment of the hand. *Scand J Plast Reconstr Surg*, 14(1): 127-128.

NAYAK SR, HUSSEIN M, KRISHNAMURTHY A, MANSUR DI, PRABHU LV, D'SOUZA P, POTU BK, CHETTIAR GK (2009) Variation and clinical significance of extensor pollicis brevis: a study in South Indian cadavers. *Chang Gung Med J,* 32(6): 600-604.

NAYAK SR, KRISHNAMURTHY A, PAI MM, PRABHU LV, RAMANATHAN LA, GANESH KUMAR C, THOMAS MM (2008) Multiple variations of the extensor tendons of the forearm. *Rom J Morphol Embryol,* 49(1): 97-100.

NISHIJO K, KOTANI H, MIKI T, SENZOKU F, UEO T (2000) Unusual course of the extensor pollicis longus tendon associated with tenosynovitis, presenting as de Quervain disease--a case report. *Acta Orthop Scand*, 71(4): 426-428.

PAPALOÏZOS M (2004) Accessory extensor pollicis longus. *Scand J Plast Reconstr Surg Hand Surg,* 38(5): 310-313.

PARSONS FG, ROBINSON A (1898) Eighth report of the Committee of Collective Investigation of the Anatomical Society of Great Britain and Ireland, for the year 1897-98. *J Anat Physiol*, 33(Pt 1): 189-203.

ROSA RC, DE OLIVEIRA KM, LEO JA, ELIAS BA, DOS SANTOS PR, DE SANTIAGO HA (2016) Anomalous bilateral contribution of extensor pollicis longus and muscle fusion of the first compartment of the wrist. *Rev Bras Ortop*, 51(2): 235-238.

RUBIN G, WOLOVELSKY A, RINOTT M, ROZEN N (2011) Anomalous course of the extensor pollicis longus:clinical relevance. *Ann Plast Surg,* 67(5): 489-492.

SABAT D, DABAS V, DHAL A (2014) Late extensor pollicis longus rupture following plate fixation in Galeazzi fracture dislocation. *Indian J Orthop*, 48(4): 426-428.

SAKELLARIDES HT, DEWEESE JW (1976) Instability of the metacarpophalangeal joint of the thumb. Reconstruction of the collateral ligaments using the extensor pollicis brevis tendon. *J Bone Joint Surg Am,* 58(1): 106-112.

SAWAIZUMI T, NANNO M, ITO H (2003) Supernumerary extensor pollicis longus tendon: a case report. *J Hand Surg,* 28(6): 1014-1017.

SEVIVAS N, KALOUCHE I, ROULOT E (2009) Double extensor pollicis longus tendon in independent extensor compartments: a case report of an anatomical variation requiring alteration of surgica lstrategy. *Chir Main.* 28(3): 180-182.

SHIGEMATSU S, SHIMIZU H, BEPPU M, HIRATA K (2014) Anatomy of the extensor pollicis brevis associated with an extension mechanism of the thumb metacarpophalangeal joint. *Hand Surg,* 20(1): 201-202.

STRAUCH RJ, STRAUCH CB (2016) Extensor pollicis brevis tendon can hyperextend thumb interphalangeal joint in absence of extensor pollicis longus: Case report and review of the literature. *World J Orthop,* 7(7): 448-451.

TALBOT CE, MOLLMAN KA, PEREZ NM, ZIMMERMAN AM, DREW N, TSUNG I, WADE C, FINNEGAN PS, FREDIEU JR (2013) Anomalies of the extensor pollicis longus and extensor indicis muscles in two cadaveric cases. *Hand,* 8(4): 469-472.

THWIN SS, FAZLIN F, THAN M (2014) Multiple variations of the tendons of the anatomical snuffbox. *Singapore Med J,* 55(1): 37-40.

TORDJMAN D, PIERRART J, BELLITY J, DELGRANDE D, MASMEJEAN E (2018) Accessory extensor pollicis longus: A rare tendon anomaly. *Hand Surg Rehabil*, 37(1): 60-63.

TSIOURI C, HAYTON MJ, BARATZ M (2009) Injury to the ulnar collateral ligament of the thumb. *Hand*, 4(1): 12-18.

TUBBS RS, SHOJA MM, LOUKAS M (2016) *Bergman's comprehensive encyclopedia of human anatomic variation.* 1st edn. Wiley.

TÜRKER T, ROBERTSON GA, THIRKANNAD SM (2010) A classification system for anomalies of the extensor pollicis longus. *Hand,* 5(4): 403-407.

YOSHIDA Y (1990) Anatomical study on the extensor digitorum profundus muscle in the Japanese. *Okajimas Folia Anat Jpn*, 66(6): 339-353.

ZADEK I (1934) Congenital absence of the extensor pollicis longus of both thumbs. Operation and cure. *J Bone Jt Surg*, 16(2): 432-434.

Modification of alprazolam-induced liver injury by bone marrow-derived mesenchymal stem cells and the role of miRNA-192

Heba M. Ali Labib[1, 2]

[1] *Department of Anatomy and Embryology, Faculty of Medicine, Kasr Alainy, Cairo University, Egypt*
[2] *Department of Preclinical Science, College of Osteopathic Medicine, William Carey University, USA*

SUMMARY

The group of drugs known as Benzodiazepines (BDZs) are among the most widely prescribed CNS-depressant drugs. Alprazolam (Alp) is a member of the BDZs family, commonly prescribed as an antipsychotic and anxiolytic agent. Induction of oxidative stress, impairment of cognitive functions and psychomotor skills, conformational alterations in hemoglobin structure and elevation of liver enzymes are among the side effects reported on the use of alprazolam. Several studies have found that alprazolam could favor hepatotoxicity, whereas other studies contradicted those findings. Bone marrow-derived mesenchymal stem cells (BM-MSCs) have been studied as a novel approach for treatment of liver diseases. The current study was designed to assess the biochemical, histopathological and molecular liver alterations in response to oral administration of alprazolam at a dose of 0.3 mg/kg/day for 4 weeks in adult male albino rats and to evaluate the therapeutic effect of BM-MSCs on the alprazolam-induced alterations. Forty adult male albino rats (Sprague Dawley strain; 170-200 g mean body weight) were used. Liver enzymes were measured, isolation and preparation of BM- MSCs were done, and immunohistochemical staining for alpha smooth muscle actin and FGF2 were assessed. Moreover, histological and ultrastructural liver tissue examination and PCR detection of SOD, TNF-α and mirNA-192 were investigated. Animals exposed to alprazolam developed liver injury characterized by significant increase in TNF-α and significant decrease in SOD and miRNA-192 expression. Histological findings provided supportive evidence for the biochemical and molecular analyses. Treatment with stem cells caused a significant alleviation of the alprazolam-induced findings. In conclusion, alprazolam was found to induce liver injury and oxidative stress, which were ameliorated by BM-MSCs administration.

Key words: Alprazolam – BMSCs – TNF-α – SOD – miRNA192

INTRODUCTION

The prospects of morbidity and mortality escalate with drug abuse of prescription psychostimulants and depressants. Benzodiazepines (BZDs) are a group of psychoactive drugs that are recognized

Corresponding author:
Heba Mohamed Ali Labib. Department of Anatomy and Embryology, Faculty of Medicine, Kasr Alainy, Cairo University, Egypt. Postal code, 11562. Province, Cairo. Address,71 El Kasr Al Ainy. Sector, Greater Cairo. Financial number, 1631. Phone: 02-2794782. E-mail: labib_heba@yahoo.com

Submitted: May 7, 2022. **Accepted:** June 26, 2022

https://doi.org/10.52083/IVLL6465

for their anxiolytic, hypnotic and anticonvulsant properties and are extensively used in human pharmaco-therapy (Dinis-Oliveira, 2017).

Alprazolam is a benzodiazepine which is broadly used as an anxiolytic and an antipsychotic drug, as well as in the treatment of acute and sub-chronic insomnia and agitated psychosis (Zareifopoulo and Panayiotakopoulos, 2019). Alprazolam is metabolized in the liver, mainly by the enzyme cytochrome P450 3A4 (CYP3A4). Its maximum recommended daily dose is 10 mg per day (Uehara et al., 2017), whereas the median lethal dose (LD50) of alprazolam is 331-2171 mg/kg in rats (Golovenko et al., 2020).

Although once considered safe, several reports have emerged of alprazolam-induced multiple organ impairment. At a dose of 0.5 mg and higher, alprazolam caused alterations in brain oxidative metabolism and impairment of cognitive and psychomotor skills such as memory affection, with a substantial potential to prompt dependence and abuse. Alprazolam causes cytotoxicity in the vital organs of rats such as the liver and kidney (Chattopadhyay et al., 2019). Alprazolam is considered to be more toxic than other BZDPs. When co-administered with other depressant agents such as ethanol, alprazolam becomes particularly toxic, causing behavioral irritability and aggression (Huang et al., 2018). Chronic administration of alprazolam alone or with central nervous (CNS) stimulants increases oxidative stress and inflammation in the brain and induces neurobehavioral, histopathological and neurotransmitters levels' alterations (Dutt et al., 2020a). By means of spectrophotometry, alprazolam was shown to bind with hemoglobin (Hb), altering the α-helical structure of Hb-subunits. Alprazolam-induced conformational changes in Hb result in changes of its function (Maitra et al., 2007).

Micro RNAs (miRNAs) are small non-coding RNAs which moderate gene expression by targeting 3' UTR of their related messenger RNA (mRNAs), playing a fundamental role in inflammation, carcinogenesis and cell death modulation. Whereas serum-based miRNAs are considered biomarkers in liver injury, several miRNAs expressed in liver tissue surpass the accuracy and sensitivity, as biomarkers, of serum aspartate transaminase/alanine transaminase (AST/ALT) levels. miR-192 is proposed as a serum-based marker for acute liver injury. MicroRNA-192 (*miR-192-5p*) is expressed in the liver in a ubiquitous manner, and its expression has been examined in inflammation-related cancers. miR-192-5p is also considered to be a serum-based biomarker that is highly elevated in several liver diseases. In contrast, down-regulation of miR-192-5p in hepatocytes is seen upon liver damage, where its expression in hepatocytes is regulated by tumor necrosis factor α (TNF-α) (Roy et al., 2016).

In multicellular organisms, stem cells are undifferentiated or partially differentiated cells that have the ability to differentiate into various cell types and to proliferate indefinitely to produce more of the same stem cell. They are the initial type of cell in a cell lineage. They are found in both embryonic and adult organisms, with somewhat different properties in each. Stem cells are different from progenitor cells, which cannot divide indefinitely, and precursor or blast cells, which are usually committed to differentiating into one cell type (Müller et al., 2016).

Stem cells have the ability of long-term clonal self-renewal, by going through repetitive cycles of cell division while maintaining an undifferentiated state, and the ability of multipotency, with the capacity of differentiation into more than one specialized cell type (Kopp et al., 2016). Bone marrow-derived MSCs (BM-MSCs) are adult stem cells with multipotency and multilineage differentiation potential. BM-MSCs have the ability to differentiate into osteoblasts, chondrocytes, adipocytes, fibroblasts, endothelial cells, and smooth and cardiac muscle cells (Scuteri and Monfrini, 2018). In the adult liver, stem cells have been suggested to replace tissue cells, particularly following injury (Kopp et al., 2016).

The tumor necrosis factor (TNF) superfamily is a protein superfamily of type II transmembrane proteins containing TNF homology domain, which form trimers. Members of the TNF superfamily are freed from the cell membrane by extracellular proteolytic cleavage and function as cytokines. They are expressed by immune cells and they control various cell functions, such as immune response, inflammation, proliferation,

differentiation and apoptosis (Aggarwal et al., 2012). TNF-α-induced liver injury occurs via TNF-receptor-1 (TNFR1) signaling and TNFR1 inhibition markedly reduces liver steatosis and triglyceride content. Moreover, inhibition of TNFR1 reduces activation of the MAP kinase MKK7 and its downstream target JNK, leading ultimately to significant improvement in insulin resistance. Apoptotic liver injury, NAFLD activity and alanine aminotransferase (ALT) levels, as well as liver fibrosis are TNF-α-mediated and are decreased by anti-TNFR1 (Wandrer et al., 2020).

Superoxide dismutase (SOD) is an antioxidant enzyme that reduces superoxide radicals and protects against oxidative stress, through break down of H2O2 into H2O and O2. In oxidative-stress-induced liver injury, SOD removes oxygen radical species and protects the integrity of the cells reducing production of reactive oxygen species (ROS) (Lim et al., 2021).

There are seven subfamilies of fibroblast growth factors (FGFs), FGF1 subfamily (FGF1, FGF2) being one of them. These subfamilies of FGFs are tissue specific and have different binding affinities with FGF receptors (FGFRs). Fibroblast growth factor 2 (FGF2) (also named basic FGF) possesses anti-fibrotic effects in liver fibrosis and enhance tissue regeneration. Activated hepatic stellate cells (HSCs) are the main cells responsible for extracellular matrix deposition; the distinctive feature of liver fibrosis. Among the fibroblast growth factor receptors (FGFRs), FGF2 chiefly interacts with FGFR1, highly overexpressed on activated HSCs, and inhibits HSCs' activation, migration and contraction and has thus been investigated in liver fibrosis. FGF2 also plays a critical role in numerous cellular processes including organ development, wound healing and tissue regeneration (Kurniawan et al., 2020).

Actins are a family of multi-functional proteins that form microfilaments. Alpha smooth muscle actin is one of six actin isoforms that are involved in the contractile apparatus of smooth muscles. Alpha-smooth muscle actin is related to hepatic dysfunction and the degree of liver fibrosis. As to its principal role in liver fibrogenesis, α-SMA is one of the most useful immunohistochemical markers indicative of liver fibrosis, and is regarded as a parameter of liver fibrogenesis. The expression of cytoplasmic α-SMA is a histopathological marker for hepatic stellate cells (HSCs) activation responsible for liver fibrogenesis (Udomsinprasert et al., 2020).

It is probable that all psychopharmacological agents are accompanied with a risk of hepatotoxicity. However, the evidence is inadequate for certain conclusions to be drawn about the frequency and severity of psychiatric drug-induced liver injury. Prolonged use of BZDs is accountable for multiple side effects. The liver has a primary role in BZDs metabolism and is particularly prone to BZDs-related toxicity. Few data are available on the long-term impact of BZD administration on liver.

We herein investigate the potential toxic effects of alprazolam on enzymatic levels of Alanine aminotransferase (ALT) and Aspartate aminotransferase (AST) in rat serum. In addition, TNF-α, superoxide dismutase (SOD) and miRNA 192 in liver tissue homogenate are measured and correlated with liver injury with reference to molecular, histological and ultrastructural changes. Moreover, the protective role of mesenchymal bone marrow-derived stem cells against alprazolam-induced liver injury is examined.

MATERIALS AND METHODS

Animals

Forty adult male albino rats weighing (170-200 gm) were obtained from the Animal and Experimental House, Faculty of Medicine, Cairo University. Animals were housed in cages under standard hygienic conditions. All rats were acclimatized to the laboratory environment for two weeks prior to the experiment, where they were adapted to the controlled environmental conditions at a room temperature of 25±2°C, relative humidity 60-70% under a 12h light: 12h dark cycle. All animals were subjected to a 1 hour fasting period prior to drug administration. Food and water were supplied ad libitum. All procedures were done in accordance with the principles of the Ethics Committee, Faculty of Medicine, Cairo University.

Experimental design

The duration of the experiment was five weeks. Rats were equally and randomly divided into four groups (n=10 for each group); normal healthy group (group I), where the rats were housed separately in cages for five weeks without any manipulation; sham control group (group II), in which the rats were given a single intravenous (I.V.) injection (3 x 10^6 cell) of MSCs at the beginning of the fifth week; alprazolam group (group III), in which alprazolam was given daily as a single oral dose of 0.3 mg/kg/day for four weeks; and alprazaolam+stem cells-treated group (group IV), in which alprazolam was given in a manner similar to that of group III, followed by a single I.V. injection (3 x 10^6 cell) of BM-MSCs at the beginning of the fifth week. All rats were sacrificed by the end of week five. All rats of the experiment were closely observed and carefully examined daily throughout the experimental period, in order to record any apparent behavioral changes and/or signs of toxicity. The dose for animal experimentation was calculated by extrapolating the human dose to animal dose based on the body surface area ratio following the table of Paget and Barnes (1964). The dose for alprazolam was recommended by Elmesallamy et al. (2011) and was assessed in its maximum therapeutic dose used for treatment of generalized anxiety disorders.

Chemicals

Alprazolam in the form of white crystalline powder was obtained from Amoun Pharmaceutical Industries Co., Egypt, freshly prepared for oral gavage administration by dissolving it in distilled water (each 0.5 mg dissolved in 5 ml of distilled water).

Preparation of BM-derived MSCs (BMSCs)

Bone marrow was harvested from 6-week-old male white albino rats by flushing the tibiae and femurs with Dulbecco's modified Eagle's medium (DMEM, GIBCO/BRL), supplemented with 10% of fetal bovine serum (GIBCO/BRL). Nucleated cells were isolated with a density gradient [Ficoll/Paque (Pharmacia)] and suspended in complete culture medium supplemented with 1% of penicillin–streptomycin (GIBCO/BRL). Cells were incubated at 37°C in 5% of humidified CO_2. When large colonies developed (80–90% confluence), cultures were washed twice with phosphate-buffered saline (PBS, Lonza Company, Switzerland) and the cells were trypsinized with 0.25% of trypsin in 1mM EDTA (GIBCO/BRL) for 5 min at 37°C. Cells were centrifuged and suspended in serum supplemented medium and incubated in 50 cm^2 culture flask (Falcon, Nunc, Roskilde, Denmark). MSCs were identified by their adherence to the plastic surface.

Labeling of MSCs with PKH26

PKH26 fluorescent linker dye was used for MSCs labeling according to Sigma Protocol (St. Louis, MO). Briefly, cells were centrifuged and washed twice in serum free medium. Cells were pelleted and suspended in dye solution and then were injected intravenously into the tail vein.

Biochemical analysis

The blood samples were collected from the tail vein for biochemical testing of serum alanine aminotransferase (ALT) and aspartate aminotransferase (AST) at 8:00 a.m. at the end of the 5th week. The blood samples were then centrifuged at 3000*g* for 10 min using a bench top centrifuge (KH20R, Kaidalab, China). The sera acquired from the sample tubes were stored frozen at -80°C to be used for analysis at a later time. Afterwards, all animals were anesthetized by use of sodium pentobarbital (40 mg/kg, i.p.) and decapitated after reaching full anesthesia according to the guidelines of the Institutional Animal Care and Use Committee (IACUC). Serum activities of ALT and AST were used to evaluate the liver function.

Histopathological analysis

The liver was rapidly isolated and immersed in freshly prepared 4% *w*/*v* formaldehyde (0.1 M phosphate buffers, pH 7.2) for 48 h and then embedded in paraffin with melting point 55-57°C. 4 µm-thick histological sections were prepared and stained with hematoxylin and eosin for routine histological study and with Masson's trichrome for detection of collagen fiber deposition. Capturing images for microscopic

analysis was performed using light microscope model DM LB2 (Switzerland).

Sections for immunohistochemical study were mounted on charged slides to help adherence of sections to the slides during immunostaining. Immunostaining was done for fibroblast growth factor 2 (FGF2) and alpha smooth muscle actin (α-SMA).

Processing of specimens and stains for light microscopy

Hematoxylin and eosin staining entailed deparaffinization of sections in xylene followed by rehydration in descending grades of ethanol. The sections were stained with hematoxylin for 10 minutes, bluing in tap water was then done, followed by staining with eosin for 1 minute. Sections were cleared in xylene then mounted on slides and covered.

For Masson's trichrome staining, the fixed paraffin sections were stained with Trichrome Stain Kit (Connective Tissue Stain) (ab150686). Sections were deparaffinized and the slides were incubated in preheated Bouin's Fluid then in Weigert's Iron Hematoxylin and rinsed in water. Afterwards, incubation in Biebrich Scarlet/Acid Fuchsin solution was done and the slides were differentiated in phosphomolybdic / phosphotungstic acid solution. Further incubation in Aniline Blue solution for 5-10 minutes and in acetic acid solution followed. Sections were cleared in xylene and mounted in permanent mounting medium.

Fibroblast Growth Factor 2 (FGF2) immunohistochemichal analysis

To perform antibody staining, deparaffinization and rehydration were initially done, followed by antigen unmasking. Afterwards, staining was performed using the chromogenic staining protocol. To prevent non-specific binding of the antibody to the tissues, each section was blocked with 100-400 µl blocking solution for 1 hour at room temperature in a humidified chamber. The blocking solution was removed and 100-400 µl of primary antibody *FGF2 Mouse Polyclonal Antibody (Cat #: PMA5-15276), ThermoFisher Scientific, USA,* was added. Equilibration with Signal Stain Boost Detection Reagent and addition of Signal Stain DAB Chromogen Concentrate and Signal Stain DAB Diluent were done. The final step was counterstaining with hematoxylin, which stains the cell nuclei blue, providing a contrast to the brown color of the DAB chromogen for better visualization of tissue morphology.

Alpha smooth muscle Actin (α-SMA) immunohistochemical analysis

To perform antibody staining, deparaffinization and rehydration were initially done. The sections were mounted on glass slides coated with 0.1% poly-1-lysine. Subsequent blockage of the endogenous peroxidase activity, by incubation in 2.5% methanolic hydrogen peroxide for 30 minutes, was performed. The endogenous biotin was blocked by Biotin Blocking System (Agilent, CA, USA), according to the manufacturer's instructions. Subsequently, the sections were washed three times in phosphate-buffered saline (PBS). The blocking solution was removed and 100-400 µl of primary antibody *Mouse Anti-Alpha Smooth Muscle Actin Monoclonal Antibody (Clone 1A4) (CAT#: NAB201062LS), Creative Biolabs, NY, USA,* was added. After three washings in PBS, the sections were incubated for 30 minutes with the appropriate secondary biotinylated antibody labelled with Avidin-Biotin complex *(ThermoFisher Scientific, USA, code 29339).* The sections were developed with 3-3 diaminobenzidine and finally counterstained with hematoxylin. Negative controls were performed using normal house antiserum instead of the primary antibody, which uniformly demonstrated no reaction.

Immunohistochemistry data interpretation

The evaluation of immunostaining was performed using *OptikalSView camera software, Optika, Italy*. The immune-positive cells were counted in each region of interest (ROI) using a counting grid in relation to their proportion among the total counterstained cell population. The stained areas of the ROI were digitally marked, and the percentage of stained areas was determined and the staining intensity scored according to a four-tier system: 0, no staining;

1+, weak; 2+, moderate; and 3+, strong. In brief, the score of each sample was calculated as the sum of each intensity (0–3) multiplied by the percentage of positive cells (0-100%) determined by immunohistochemistry (IHC). The specimens were immediately examined then stored at 4°C protected from light for long term storage. The microscopic examination was performed by *LABOMED Fluorescence microscope LX400, cat no: 9126000; US.* Using the aforementioned staining scores, the positive areas of positive cells of FGF2 and α-SMA were determined by measuring at least 7-10 randomly selected microscopic fields on each slide. The number of FGF2 and alpha-SMA-positive cells was counted under light microscope at 400 magnifications: only the cells which displayed nuclei on the section were considered.

Processing of specimens for electron microscopy

Transmission electron microscopy (TEM) lab was performed at Cairo University Research Park – Faculty of Agriculture (CURP). Ultra-thin tissue sections were examined by transmission electron microscope JEOL (JEM-1400 TEM) at the candidate's magnification. Images were taken by CCD camera model AMT, optronics camera with 1632 x 1632 pixel format as side mount configuration which uses 1394 fire wire board for acquisition. Microtome sections were prepared at approximately 500-1000 nm thickness with a Leica Ultracut UCT ultramicrotome. The sections were stained with toluidine blue (1X), then sections were examined by Leica ICC50 HD camera. For tissue processing, specimens were cut into 1-2 mm^3 thick pieces, then instantly fixed in 3% gluteraldehyde formol (v/v) in 0.1 M sodium phosphate buffer (pH 7.2-7.4) over night at 4°C. Specimens were additionally processed by washing in buffer, post fixed in 1% osmium tetraoxide, washed in 4 changes of distilled water and dehydrated in ascending grades of ethanol. Next, embedding in Epoxy resin and embedding of the specimens in beam capsules followed. The specimens were sectioned on LKB ultramicrotome utilizing glass knives for ultrathin sections. Ultrathin sections of 0.6-0.8 µm in thickness were acquired from selected blocks, then mounted on copper grids and doubly stained with uranyl acetate and lead citrate. Electron micrographs were taken with clear linear images and without angles or artifacts.

Reverse transcription-real time quantitative PCR for TNF-α, SOD and miRNA 192

Total RNA and miRNA extraction and purification were done from paraffin-embedded tissue using the RNeasy FFEP Kit; cat no: 73504 (Qiagen, Hilden, Germany) according to the manufacturer's protocol. Reverse transcription, in which cDNA was synthesised by reverse transcription reaction using miScript RT-II Transcription Kit; cat no: 218160; (Qiagen, Hilden, Germany) was done. Gene expression analysis was performed by the quantification of TNF-α and SOD genes levels, which were amplified from mRNA using a QuantiTect primer assay primer assays; [Rn_TNF-α _1_SG QuantiTect Primer Assay; cat no: 249900, and Rn_SOD_1_SG QuantiTect Primer Assay, cat no: 249900] respectively and the QuantiTect SYBR Green PCR Kit cat no: 204141 (Qiagen, Germany). The ACTB Primer sequence was used as housekeeper gene. All samples were analyzed using the 5 plex Rotor-Gene PCR Analyzer (Qiagen, Germany). The $2^{\Delta\Delta}$Ct method was conducted for the analysis of gene expression levels, using ACTB as an endogenous reference control for normalization purposes. miRNA 192 expression analysis was performed by the quantification of miR-192 expression level using the SYBR-Green fluorescent-based primer assay (Rn_miR-192*_1 miScript primer assays, assay ID: MIMAT0017147, Qiagen, Germany. The used miRNA sequence was: 5'CUGCCAGUUCCAUAGGUCACAG-3'. The RUN6 primer assay was used as housekeeper gene for normalization. The qPCR was performed in the 5-plex Rotor Gene PCR System (*Qiagen, Hilden, Germany*). The 20 µl reaction mixture / reaction consist of 2x QuantiTect syber green PCR mastermix, 10x miscript universal primer, 2 µl primer assay and 50pg-3ng cDNA. The thermal protocol for the target gene consisted of 15 min for HotStarTaq DNA Polymerase activation at 95°C followed by 40 cycles of denaturation at 94°C for 15 minutes, primer annealing for 30 seconds at 55°C and extension at 70°C for 30 sec). The

$2^{\Delta\Delta}$Ct method was conducted for the analysis of miR-192 expression levels, using RUN6 as an endogenous reference control for normalization purposes.

Data Analysis

Data were statistically described in terms of mean ± standard deviation (± SD). Data were tested for the normal assumption using the Shapiro-Wilk test. Comparison of the study groups was done using one way analysis of variance (ANOVA) test with posthoc multiple 2-group comparisons. Two-sided *p* values < 0.05 were considered statistically significant. All statistical calculations were done using computer program IBM SPSS (Statistical Package for the Social Science; IBM Corp, Armonk, NY, USA) release 22 for Microsoft Windows.

RESULTS

Biochemical Results

There was no statistically significant difference in ALT and AST mean serum levels between the control groups I and II. Also, a non-significant difference was seen between the controls and the alprazolam-treated group III. In addition, there was not sufficient statistical evidence to suggest a significant difference between the alprazolam+stem cells-treated group IV and neither the controls nor the alprazolam-treated group III (Table 1).

Table 1. Effect of alprazolam and alprazolam+stem cells on ALT (U/L) and AST (U/L) serum levels as compared to the controls, represented as mean ± SD.

	Group	Mean ± SD	Versus	p-value
ALT	**I**	33.92±3.7	Group II Group III Group IV	1.000 0.080 0.087
	II	34.10±2.4	Group I Group III Group IV	1.000 0.084 0.092
	III	35.31±6.9	Group I Group II Group IV	0.080 0.084 0.079
	IV	34.63±8.1	Group I Group II Group III	0.087 0.092 0.079
	Group	**Mean ± SD**	**Versus**	**p-value**
AST	**I**	108.13±11.4	Group II Group III Group IV	1.000 0.083 0.090
	II	108.81±9.3	Group I Group III Group IV	1.000 0.089 0.094
	III	109.43±7.5	Group I Group II Group IV	0.083 0.089 1.000
	IV	109.17±3.7	Group I Group II Group III	0.090 0.094 1.000

*p value ≤ 0.05 was deemed statistically significant; SD=standard deviation.

Fluorescence results

Florescent microscopic examination of the unstained sections of liver in the sham control group (II) and in the alprazolam +stem cells treated-group (IV) displayed homing of PKH26 labeled MSCs in the liver tissue (Fig. 1).

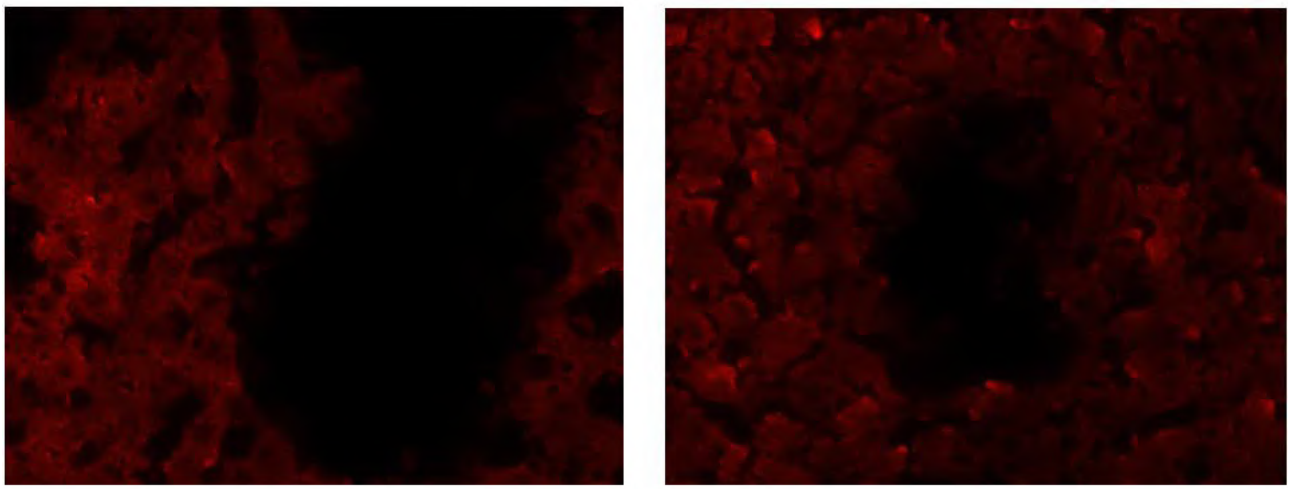

Fig. 1.- PKH26-labeled injected stem cells of the unstained sections of the rat liver in a. sham control group II and b. alprazolam + stem cells-treated group IV showing engraftment of MSCs and their homing in the hepatocytes.

Histopathological Results

Hematoxylin and eosin staining

The hepatic parenchyma of the controls' rats depicted hepatic lobules separated from one another by connective tissue septa where portal areas accommodated the portal triad. Each hepatic lobule featured a central vein from which hepatic plates radiated. The portal areas included a hepatic portal vein, a branch of the hepatic artery and a bile ductile (Figs. 2a and b, 3a and b and 4). Treatment with alprazolam caused focal necrosis, inflammatory cellular infiltration, hepatocyte vacuolization and nuclear pyknosis with sinusoidal dilatation (Figs. 1c, 2c and d and 5a, b). An apparent restoration of hepatic architecture was noticed in the liver of alprazolam+stem cells-treated rats (Figs. 2d, 3e and 5c).

Masson's trichrome staining

Normal liver staining was seen in control and sham control groups I and II (Fig. 6a, b). Pericentral and periportal collagen fibers deposition were seen in alprazolam-treated liver sections (Fig. 6c, d) as indicated by strong blue staining which was apparently reduced in the aplrazoalm+stem cells-treated stained section (Fig. 6e).

Immunohistochemical Staining

Very faint FGF-2 immune-expression was present in control groups I and II (Fig. 7a, b). Strong FGF-2 immune-expression was seen in alprazolam-treated sections (Fig. 7c), as indicated by strong and diffuse brown staining of hepatic parenchyma especially noticed pericentrally. A faint expression was seen in alprazolam+stem cells-treated liver sections (Fig. 7d).

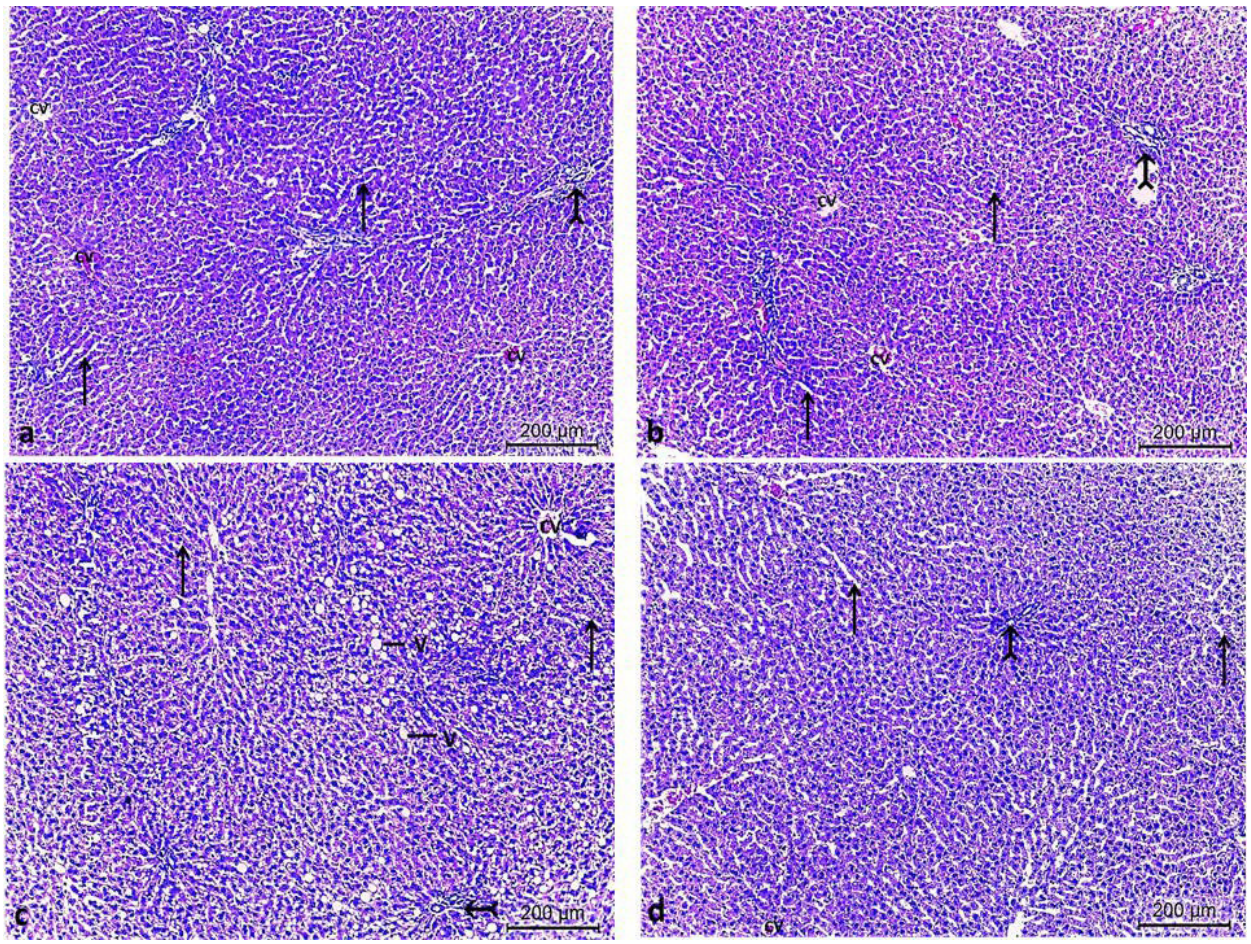

Fig. 2.- Hematoxylin and eosin-stained sections of rat liver in **a.** control and **b.** sham control groups I and II illustrating numerous hepatic lobules, in the center of each is the central vein (CV). The hepatic sinusoids (arrow) appear between the plates of hepatic cells that radiate from the central veins toward the periphery of the hepatic lobule. Branches of the interlobular vessels and bile ducts are seen within the portal areas (tailed arrow) of a hepatic lobule. **c.** Hematoxylin & Eosin-stained sections in alprazolam-treated rat liver showing ballooning and vacuolization (V) of hepatocytes. **d.** Alprazolam+Stem Cells-treated rat liver featuring central vein (CV), hepatic sinusoids (arrow) and branches of the interlobular vessels and bile ducts within the portal areas (tailed arrow) of a hepatic lobule. H&E staining, x100. Scale bars = 200 µm.

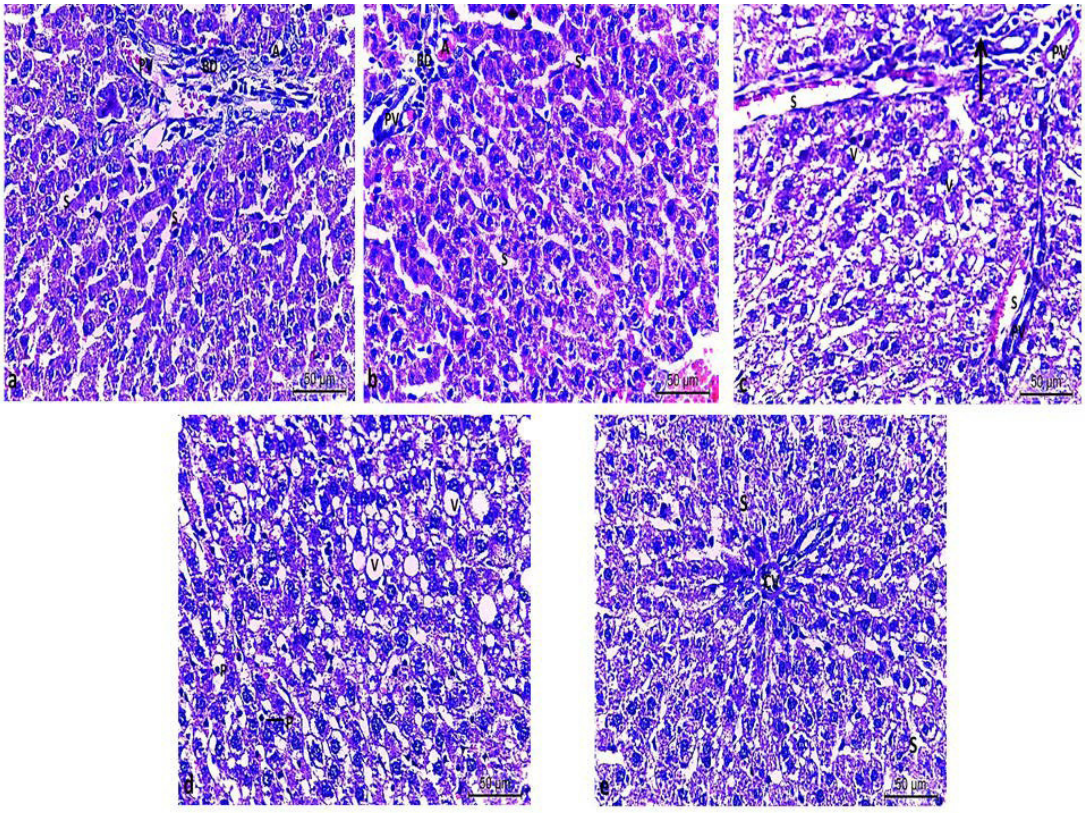

Fig. 3.- Hematoxylin and eosin-stained sections of rat liver. **a.** Liver of control group I and **b.** of sham control group II exhibiting normal architecture. Blood sinusoids (S) intervening between regularly arranged plates of hepatic cells radiate from central veins (CV). Branches of the interlobular vessels; portal vein (PV) and hepatic artery (A), in addition to bile ducts (BD) are seen within the portal areas. **c** and **d.** Liver of alprazolam-treated group III exhibit areas of focal necrosis and intra-lobular mononuclear inflammatory infiltration (arrow), identified around portal veins (PV), dilatation of sinusoids (S), hepatocyte nuclear pyknosis (P) vacuolar degeneration and atrophy of hepatocytes (V) with loss of hepatic architecture. **e.** Liver of alprazolam+stem cells-treated group IV featuring restoration of normal architecture. Blood sinusoids (S) intervene between plates of hepatic cells which radiate from a central vein (CV). H&E, x400. Scale bars = 50 µm.

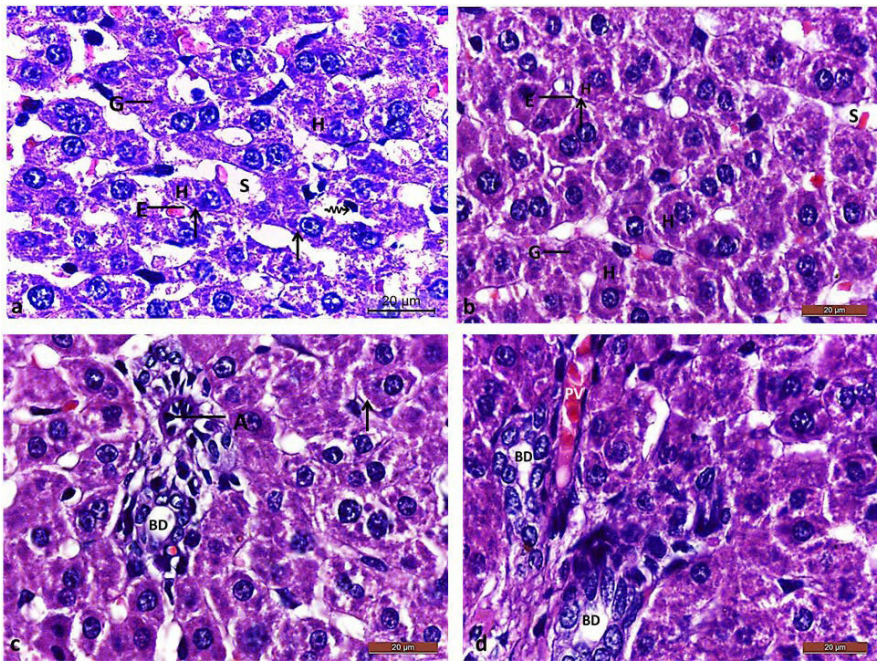

Fig. 4.- Hematoxylin and eosin-stained sections of rat liver in **a.** control group I and **b.** sham control group II showing normal hepatic architecture. Hepatocytes (H) are arranged in plates, between which the sinusoids (S) are situated. The space of Disse (arrow) is visible and appears as a thin bright band between hepatocyte cytoplasm (H) and the thinner, darker band which represents the endothelium (E) where the endothelial cells have flattened nuclei. Glycogen granules are also seen within the hepatocyte cytoplasm (G). Kupffer cells can be recognized by their several processes and an irregular or stellate outline that protrudes into the sinusoids closely associated with sinusoidal spaces (zigzag arrow). Cross section in rat liver stained with H&E in **c.** control and **d.** sham control groups I and II showing the portal area of the hepatic lobule. Branches of the portal vein (PV), bile duct (BD) and hepatic artery (A) are seen as well as space of Disse (arrow). H&E, x1000. Scale bars = 20 µm.

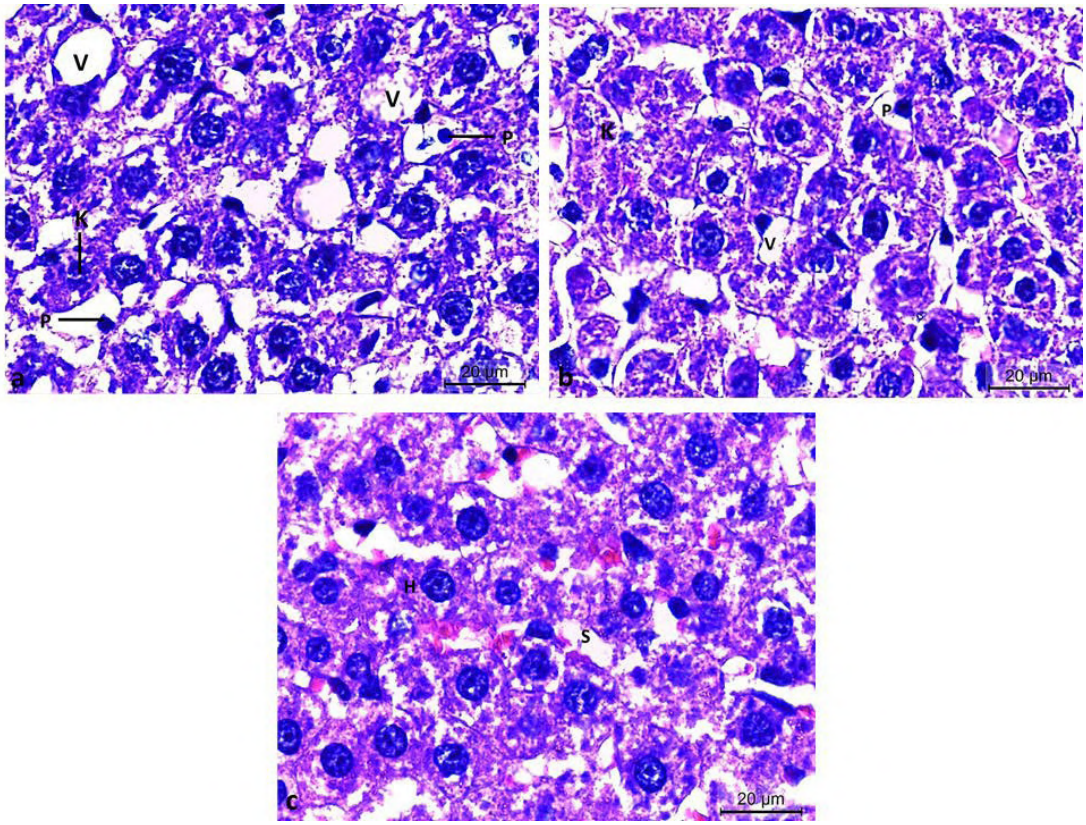

Fig. 5.- a and **b.** Hematoxylin and eosin-stained sections of rat liver in alprazolam-treated group III showing loss of hepatic architecture along with hepatocyte cytoplasmic ballooning and vacuolization (V). Nuclear pyknosis (P) and karyolysis (K) are also featured. **c.** Hematoxylin and eosin-stained section of rat liver in alprazolam+stem cells-treated group IV showing partial improvement of liver architecture with blood sinusoids (S) intervening between hepatocytes (H). H&E, x1000. Scale bars = 20 µm.

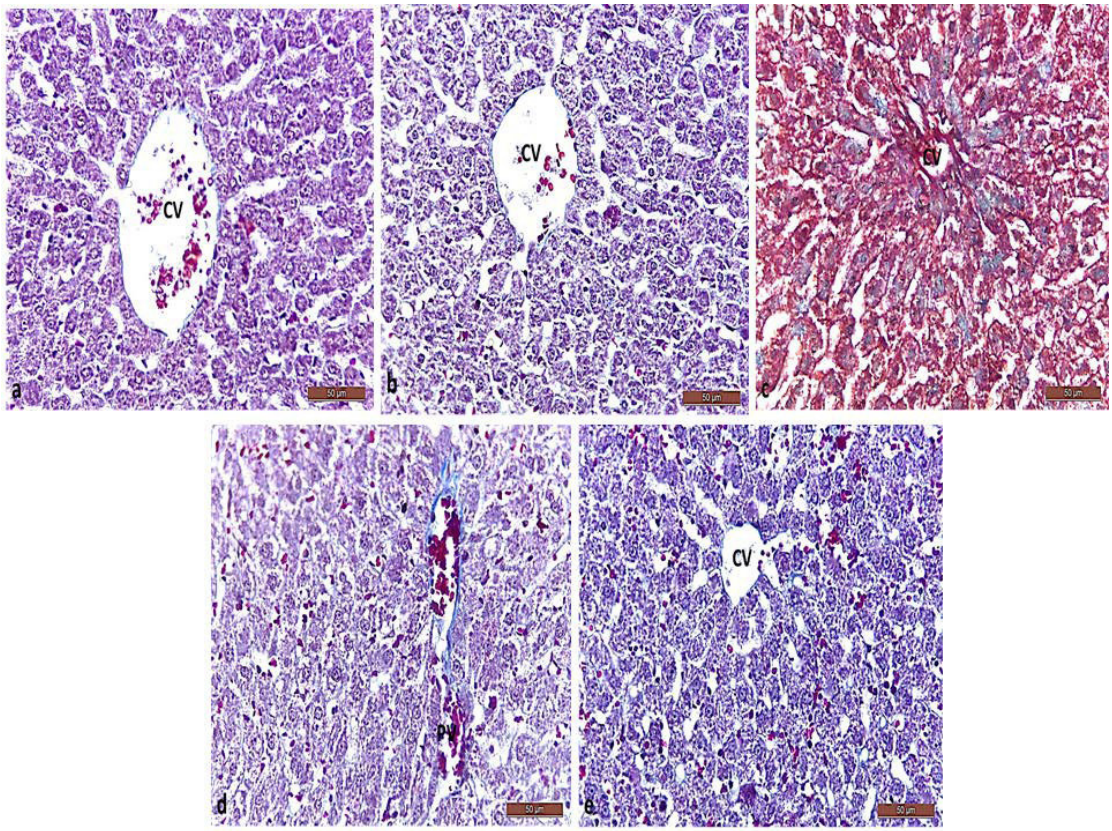

Fig. 6.- Masson's trichrome staining for collagen in rat liver sections. **a.** and **b.** are normal control and sham control groups I and II. **c.** and **d.** Masson's trichrome staining of liver sections in alprazolam-treated group III showing apparent increase in collagen accumulation. Pericentral and periportal fibrosis and deposition of collagen fibers in the hepatic parenchyma are featured. **e.** Masson's trichrome staining in alprazolam+stem cells-treated group IV showing minimal reaction; central vein (CV), portal vein (PV). Masson's trichrome, x400. Scale bars = 50 µm.

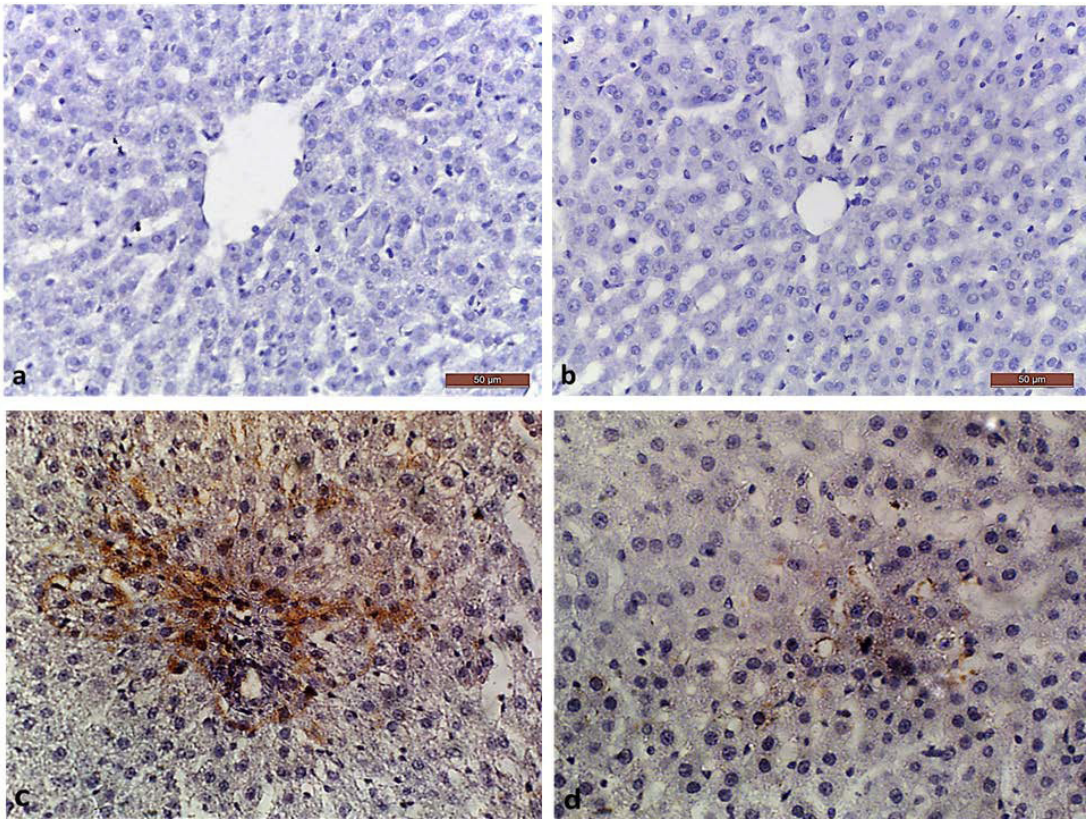

Fig. 7.- FGF-2 immunohistochemical analysis of paraffin-embedded rat liver tissue showing negative expression of FGF2 in **a.** control group I and **b.** sham control group II. **c.** FGF-2 immunohistochemical analysis of paraffin-embedded rat liver tissue in alprazolam-treated group III. Marked cytoplasmic localization of FGF2 (score 4) was observed and distributed in large tissue section. **d.** Alprazolam+stem cells-treated rat liver showing mild cytoplasmic localization of FGF2 (score 2). The sections were stained with biotin labelled FGF2 polyclonal antibody (cat no: PMA5-15276), ThermoFisherScientific, USA, followed with DAB staining. Magnification x400. Scale bars = 50 µm.

Very faint alpha-SMA immune-expression was present in control groups I and II (Fig. 8a, b) along the sinusoids. Alpha-SMA immunopositivity markedly increased in alprazolam-treated sections (Fig. 8c, d) as indicated by strong and diffuse brown staining of hepatic parenchyma. A faint expression was seen in alprazolam+stem cells-treated liver sections (Fig. 8e).

Ultrastructural results

Transmission electron micrographs of liver tissue sections in control and sham control groups I and II showed general architecture of normal hepatocytes. Hepatocytes featured rounded vesicular nuclei, well-formed rough endoplasmic reticulum and mitochondria with few lipid droplets. A regular space of Disse intervened between the hepatocytes and the endothelial cells (Figs. 9 and 10). Hepatic cellular necrosis and vacuolization were seen in alprazolam-treated liver sections. Nuclear chromatinolysis, increased number of lipid droplets and dilatation of space of the Disse were also seen (Fig. 11). Relative restoration and normalization of hepatocyte architecture were seen in alprazolam+stem cells-treated liver sections (Fig. 12).

DISCUSSION

In the present study, a non-statistically significant difference in ALT and AST mean serum levels between the control and alprazolam-treated groups was seen. In agreement with the present study, Li et al. (2017) recorded a non-significant difference in alanine aminotransferase and aspartate aminotransferase serum levels between controls and alprazolam groups upon oral alprazolam administration in low, medium and high doses (5, 10 and 20 mg/kg/day respectively). In contrast to the present findings, Ibrahim et al., (2017) reported a significant elevation in serum ALT and AST upon oral administration of alprazolam at a dose of 0.3 mg/kg/day. Dutt et al. (2020a) recorded a surge in alanine aminotransferase and aspartate

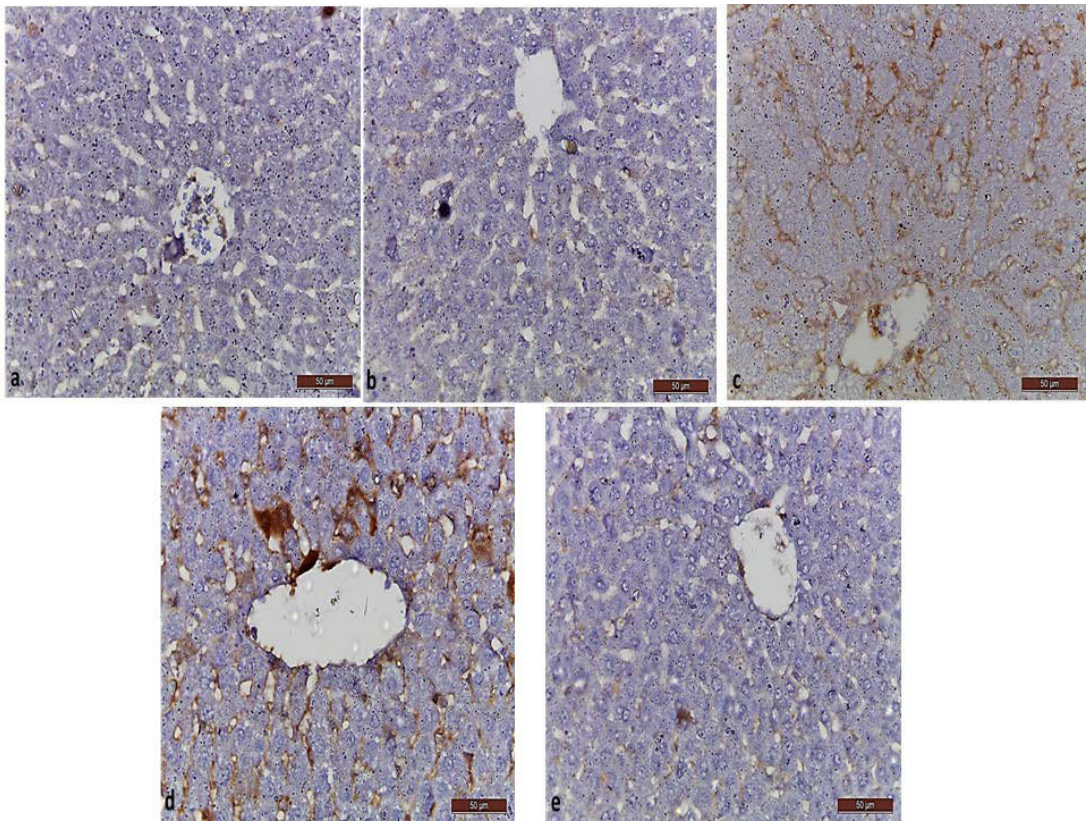

Fig. 8.- Immunohistochemical staining of liver sections stained with alpha smooth muscle actin antibody (α-SMA). **a** and **b** are sections of the control and sham control groups I and II showing negative expression of α-SMA. **c, d.** alprazolam-treated group showing dense brown expression of α-SMA in between hepatic lobules and into hepatic lobules between hepatocytes (score 4). **e.** Alprazolam+stem cells-treated group showing faint expression of α-SMA between hepatocytes (score 2). The sections were stained with Mouse Anti-Alpha Smooth Muscle Actin Monoclonal Antibody (Clone 1A4) (CAT#: NAB201062LS), Creative Biolabs, NY, USA. Magnification x400. Scale bars = 50 µm.

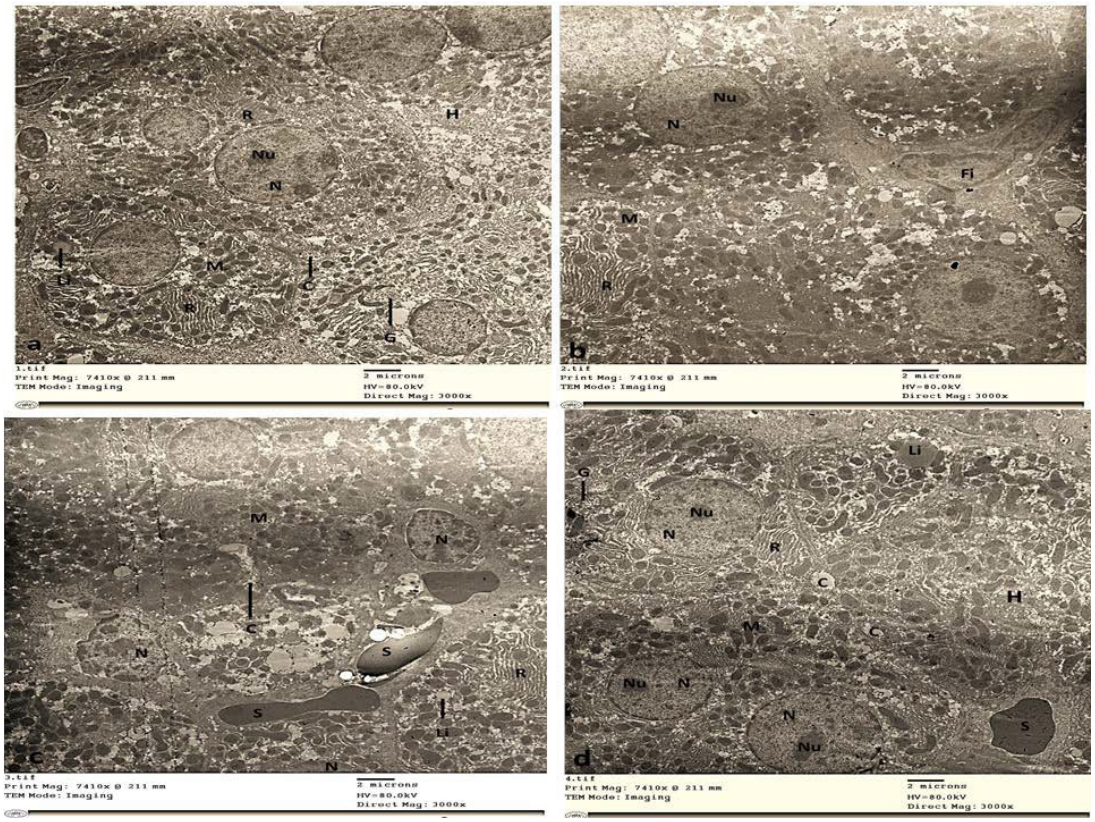

Fig. 9.- Transmission electron micrographs of control and sham control rat liver depicting details of hepatocytes (H). Nucleolus (Nu) in hepatocyte nucleus (N); canaliculus (C); rough endoplasmic reticulum (R); glycogen (G); mitochondria (M); lipid droplets (Li).; fibroblast (Fi); blood sinusoid (S) with blood cells in some. Magnification: ×3,000. Scale bars = 2 µm.

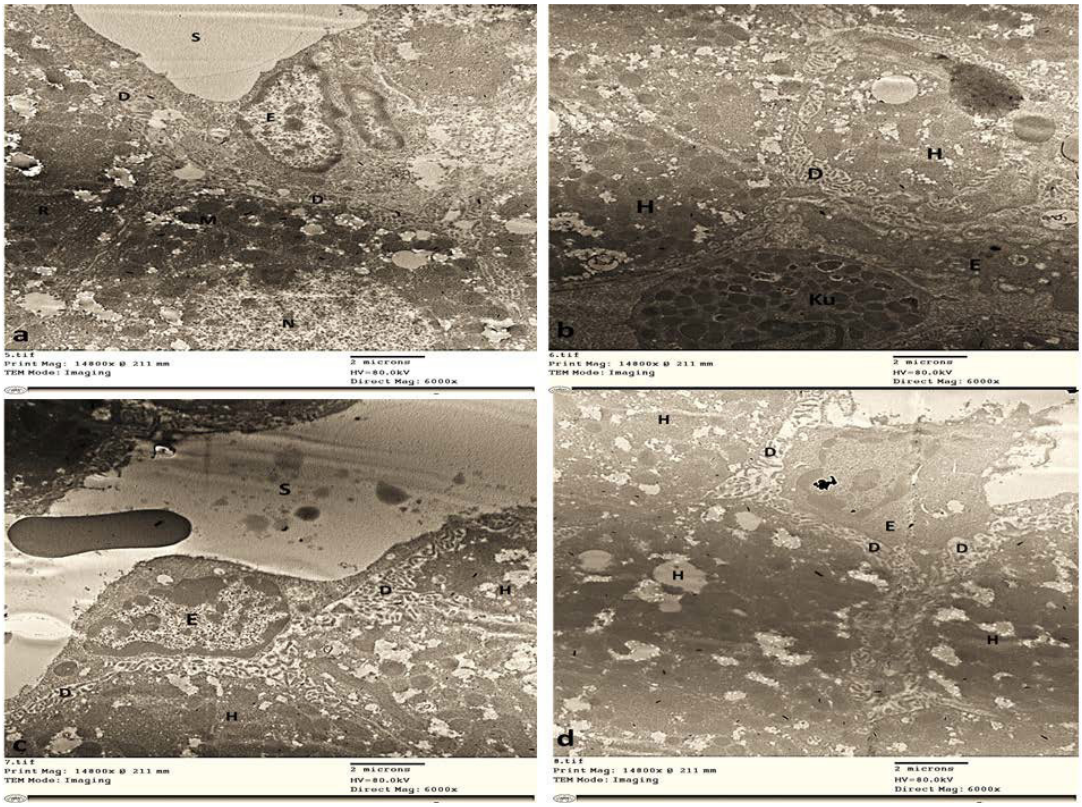

Fig. 10.- Transmission electron micrographs of control and sham control rat liver depicting details of hepatocyte (H); hepatocyte nucleus (N); mitochondria (M); blood sinusoid (S) with blood cells in some; endothelial cells (E); space of Disse (D); portion of a Kupffer cell (Ku); Magnification: ×6,000. Scale bars = 2 µm.

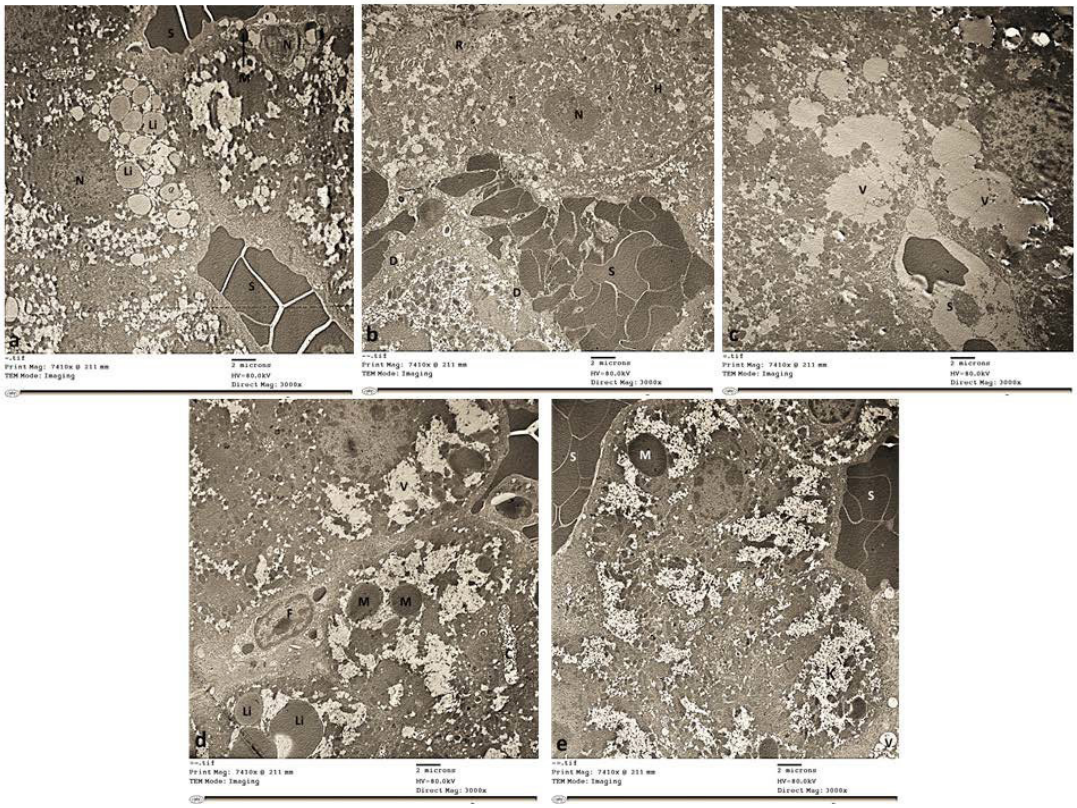

Fig. 11.- Electron micrographs of liver tissue obtained from alprazolam-treated rats showing loss of architecture. Hepatocytes are necrotic with large areas of cytoplasmic vacuolization (V) and karyolysis of the nucleus (K). Note the dilated sinusoids (S) filled with red blood corpuscles (RBCs). Necrotic hepatocyte in the centrilobular area with nuclear chromatinolysis (N) and many lipid droplets (Li). Hepatocyte at the periportal region showing fading nuclei with irregular outlines and clumped chromatin (N), swollen mitochondria (M), accumulated lipid droplets (Li), vesiculated rough endoplasmic reticulum (R) and dilated space od Disse (D). Magnification: ×3,000. Scale bars = 2 µm.

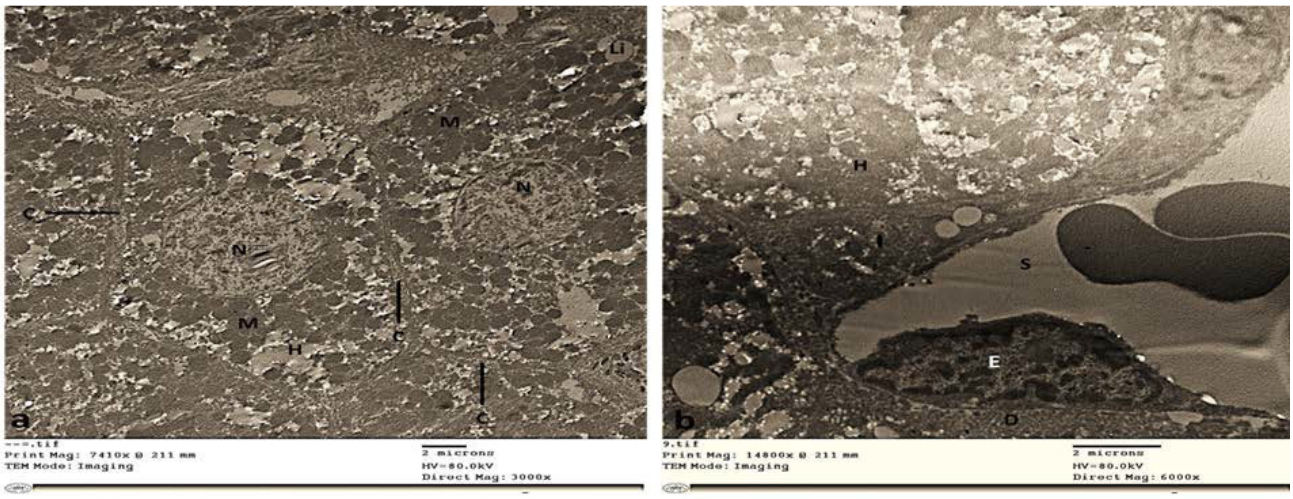

Fig. 12.- Transmission electron micrographs of alprazolam+stem cells-treated rat liver depicting normalization of liver architecture with details of hepatocytes (H). Hepatocyte nucleus (N); mitochondria (M) and lipid droplets (Li). Canaliculus (C); blood sinusoid (S) with blood cells in some of them; endothelial cells (E) and space of Disse (D). Magnification: ×3,000. Scale bars = 2 µm.

aminotransferase serum levels when alprazolam was co-administered with methylphenidate in high doses, whether administered alone or in combination. The authors confirmed that when administered in a low dose, alprazolam caused a non-significant change in the enzyme levels. Dutt et al. (2020b) concluded that the co-administration of alprazolam has augmented the hepato-toxic effects of methylphenidate as proven by the elevated markers for oxidative stress and the reported structural abnormalities in the liver. Dutt et al. (2020a) reported that low, medium and high doses of combined alprazolam and methylphenidate significantly increased lipid peroxidation and decreased SOD levels in liver tissue, whereas in contrast with the current work, the authors stated that individual treatment with alprazolam caused no significant lipid peroxidation except when given in a high dose. According to the authors, the alprazolam-induced reduction in the endogenous SOD levels has augmented the toxic effects of methylphenidate on the liver. The authors suggested that an intercalation of alprazolam with genomic and mitochondrial DNA was a cause for activation of the mechanism involved in cellular death.

In this study, a significant elevation of TNF-α level was seen in the alprazolam-treated group when compared to the control group. In agreement, Dutt et al. (2020b) observed marked increase of neuroinflammation as indicated by elevated levels of TNF-α following chronic administration of alprazolam when used alone and in combination with methylphenidate to evaluate the extent of damage of both drugs on the brain cortex and hippocampus (Table 2).

Schueller et al. (2018) emphasized the diversified role of miRNAs in maintenance of liver homeostasis, and thus their consequent involvement in acute and chronic liver diseases. The authors reported that knockout of DICER1 in hepatoblast-derived cells leads to a significant downregulation of miRNA-192, among other miRNAs, where development of hepatocyitc damage and cellular apoptosis would be seen as a result at 2-4 months of age. MiR-192-5p expression is restricted to hepatocytes. In agreement with the present results, Schueller et al. (2018) revealed a downregulation in intrahepatic expression of miR-192-5p after ischemia and reperfusion (I/R), as well as after CCl4 induced-liver injury. In contrast, the authors reported an increase in miR-192-5p serum levels after I/R, which was linked with the degree of liver damage and the presence of hepatic cell death. The authors added that downregulation of miR-192-5p had a defensive effect in HepG2 cells after H_2O_2 treatment, signifying a role of miR-192-5p in preventing liver injury (see Table 2).

Roy et al. (2016) suggested the involvement of miR-192-5p in the control of liver cell death during acute liver injury and considered it to be a potent

marker of hepatic injury. The authors reported a miR-192-5p down regulation in hepatocytes in acute liver injury, with no alteration in its expression among other cell types, indicating a hepatocyte specificity of miR-192-5p regulation during acute liver injury. The authors discussed the role of binding of TNF to its receptor in initiation of signaling cascades which regulate cell cycle or cell death pathways; NF- κB activation being the most prominent pathway. The authors hypothesized that miR-192-5p is regulated by TNF/NF- κB-dependent signaling cascades in hepatocytes and proposed that miR-192-5p is part of a TNF/LPS-dependent signaling pathway that mediates de-repression of anti- apoptotic genes such as Zeb2 defending hepatocytes against cell death in acute liver injury (Table 2).

In accordance with the present results, Andrade et al. (2000) conducted a study that described three patients with benzodiazepines-induced chronic hepatocellular injury, with findings that are indicative of hepatotoxicity of the benzodiazepine, bentazepam. Their findings showed that a benzodiazepine drug can cause chronic hepatitis after oral usage of the drug at a dose of 25 mg twice a day. Percutaneous liver biopsy showed alteration of the hepatic architecture with obvious portal-to-portal fibrosis and transition to cirrhosis as seen with Masson's trichrome staining. Masson's trichrome staining also showed fibrous expansion of portal areas and tracts, fibrous bands surrounding parenchymal regenerative nodes, with bile duct proliferation and inflammatory infiltration, in which mononuclear cells (lymphocytes and plasma cells) dominated. Parenchymal necrosis with acidophilic bodies, regenerative changes, and hepatocytic cholestasis were also noted. The authors hypothesized that bentazepam-related hepatotoxicity has been rarely detected, despite its extensive use, because benzodiazepines are not usually considered as a cause of liver damage. Moreover, chronic hepatitis may be symptomless or its clinical manifestations may be nonspecific, in absence of jaundice. The authors concluded that their findings, together with two previously published case reports, propose that a benzodiazepine can cause chronic hepatitis and argue in favor of using liver function tests to monitor all patients administered the drug.

Table 2. Effect of alprazolam and alprazolam+stem cells on TNFα, SOD and miRNA192 gene expression as compared to the controls.

	Group	Mean ± SD	Versus	p-value
RQ-TNF-α	**I**	0.89± 0.14	Group II Group III Group IV	1.000 *0.000 *0.001
	II	1.13± 0.32	Group I Group III Group IV	1.000 *0.000 *0.001
	III	5.12 ± 0.44	Group I Group II Group IV	*0.000 *0.000 *0.000
	IV	2.86 ± 0.09	Group I Group II Group III	*0.001 *0.001 *0.000
	Group	**Mean ± SD**	**Versus**	**p-value**
RQ-SOD	**I**	0.91 ± 0.03	Group II Group III Group IV	1.000 *0.000 *0.001
	II	1.10 ± 0.11	Group I Group III Group IV	1.000 *0.000 *0.001
	III	0.01 ± 0.79	Group I Group II Group IV	*0.000 *0.000 *0.000
	IV	0.55 ± 0.83	Group I Group II Group III	*0.001 *0.001 *0.000
	Group	**Mean ± SD**	**Versus**	**p-value**
RQ-miRNA 192	**I**	1.06 ± 0.71	Group II Group III Group IV	1.000 *0.000 *0.001
	II	0.95 ± 0.17	Group I Group III Group IV	1.000 *0.000 *0.001
	III	0.03 ± 0.87	Group I Group II Group IV	*0.000 *0.000 *0.000
	IV	0.44 ± 0.62	Group I Group II Group III	*0.001 *0.001 *0.000

*p value ≤ 0.05 was deemed statistically significant; RQ=Reverse Transcription Quantitation; SD=standard deviation.

In the present study, homing of MSCs in liver hepatocytes was verified through the detection of MSCs labeled with PKH26 by fluorescence microscopy. In line with the present study, El Asmar at al. (2011) reported that the generation of

parenchymal damage is a requirement for effective homing and repopulation of stem cells. The authors mentioned that although molecular mechanisms for stem cells mobilization and homing in the injured liver were poorly understood, possible pathways have been proposed including; Stromal Cell-Derived Factor-1 (SDF- 1)/CXCR4 axis, the proteolytic enzymes matrix metalloproteinases (MMPs), the hepatocyte growth factor (HGF) and the stem cell factor (SCF) where the Chemokine Stromal Cell-Derived Factor-1 (SDF-1) is considered to be a commanding chemo-attractant of hepatic stem cells' homing, migration, proliferation, differentiation and survival. Aliotta et al. (2007) also discussed the mechanisms involved in bone marrow-derived cells (BMDCs) trans-differentiation triggered by tissue injury. Chemokines produced by tissue injury attract BMDCs, producing microvesicles which are then taken up by BMDCs altering the cell phenotype to mimic resident cells.

Ishikawa et al. (2006) stated that growth factors affect cell proliferation and differentiation and allegedly contribute in repair processes of various organs. The authors reported that transplanted GFP-positive bone marrow cells (BMCs) differentiate into hepatocytes via hepatoblast intermediates. The authors also reported that FGF2 assists the differentiation of transplanted BMCs into albumin-producing hepatocytes via Liv2-positive hepatoblast intermediates through the activation of TNF-α signaling. The authors found that co-administration of FGF2 and bone marrow transplantation (BMT) improves liver function and prognosis of mice with liver injury. Padrissa-Altés et al. (2015) used siRNA delivered via nanoparticles and liver-specific gene knockout to study Fgfr role in liver regeneration. The authors reported that normally Fgf15- Fgfr4-Stat3 signaling pathway is vital for injury-induced expression of the Foxm1 transcription factor and consequent cell cycle progression. The authors observed a failure of liver mass restoration in case of Fgfr4 knockdown in mice, which was compensated for by compensatory hypertrophy of hepatocytes. Knockdown of Fgfr4 in mice lacking Fgfr1 and Fgfr2 in hepatocytes caused liver failure due to severe liver necrosis and a defective regeneration. The authors recommend activation of Fgfr signaling as a promising approach for the improvement of the liver's regenerative capacity. These results prove that Fgfr signaling in hepatocytes is crucial for liver regeneration and run in agreement with the results of the present study. Kurniawan et al. (2020) reported that FGF2 interacts with FGFR1 which is highly overexpressed in human liver myofibroblasts. The authors suggested different FGF2-regulated signaling pathways including Janus kinase (JAK), signal transducer and activator of transcription (STAT), extracellular signal regulated kinase (ERK), mitogen-activated protein kinase (MAPK), c-jun N-terminal kinase (JNK) and serine/threonine kinase AKT (also known as protein kinase B, PKB) pathways. The authors added that selective inhibitor of phosphatidylinositol 3-kinase (PI3K) and mitogen- activated protein kinase (MAPKK or MEK) eliminate the protective effects of FGF2, proposing involvement of PI3K/AKT and MEK/ERK signaling pathways in FGF2-mediated effects.

In the present work, alpha-SMA immunopositivity was markedly increased in alprazolam-treated group III. Caprino et al. (2005) mentioned that alpha-SMA expression is a dependable marker of hepatic stellate cells activation, occurring even prior to fibrous tissue formation in chronic hepatitis. The authors confirmed that its expression could be a useful measure for identification of the earliest stages of hepatic fibrosis and monitoring the effectiveness of therapy, whereas later in the disease process, fibrosis deposition would be sustained by other mechanisms. Udomsinprasert et al. (2020) discussed the mechanisms underlying the connection of high expressions of Glypican-3 (GPC-3) and a-SMA with liver fibrosis. The authors stated that GPC- 3 contributes in the regulation of HSCs viability through interacting with hedgehog signaling, which in turn plays a fundamental role in maintaining HSCs viability and activation, which are involved in hepatic fibrogenesis. The authors added that in liver fibrosis, HSCs are activated and transformed into myofibroblasts that secrete several cytokines/growth factors and produce extracellular matrix proteins including α-SMA. In contrast to the present results, Zhao

et al. (2018) recorded that although present in fibrotic skeletal muscles, the expression of α-SMA by myofibroblasts is not demonstrable by immunostaining. The authors found that the level of α- SMA expression by intramuscular fibrogenic cells does not show a positive correlation with the level of collagen gene expression or the severity of skeletal muscle fibrosis in mice with muscular dystrophy. The authors concluded that α-SMA is not a functional marker of fibrogenic cells in skeletal muscle fibrosis accompanying muscular dystrophy.

The histopathological findings of the present study, associated with alprazolam administration, provided supportive evidence for the biochemical and molecular analyses. The present findings are in line with those of Dutt et al. (2020b), who observed an increase in hepatocyte cellular necrosis and vacuolization in addition to alterations in the morphological arrangement of hepatocytes in liver tissue upon co-administration of alprazolam. Despite reporting liver cell cord disorder and liver cell edema, Li et al. (2017) concluded that alprazolam is not hepatotoxic in terms of pathological findings.

Ishikawa et al. (2006) demonstrated the potentiality of BMCs to differentiate into various cell types, including hepatocytes. The authors reported an elevation of serum albumin level and a reduction in liver fibrosis, following bone marrow transplantation (BMT). According to the authors, the mechanism of BMC plasticity involved cell fusion, nuclear reprogramming or trans-differentiation. In the early stage following BMT, the authors observed that genes known to control morphology, such as homeobox, helix-loop-helix transcription factors, and FGFs were up-regulated. However, in later stages, upregulation involved genes linked with hepatocyte differentiation, such as hepatocyte nuclear factor-4 and glucose-6-phosphatase isomerase. Khalil et al. (2021) conducted a study to assess the therapeutic effect of BM-MSCs in carbon tetrachloride (CCl4)-induced liver injury and fibrosis in male rats, relative to standard drugs derived from herbal plants. The authors observed restoration of liver structure and function upon treatment with stem cells in comparison with the standard drugs. BM-MSCs significantly decreased AST, ALT, TNF-α, and increased SOD levels compared to the positive control and the standard drugs groups, with no significant difference between the BM-MSCs-treated group and the normal group. The authors attributed the decrease in serum level of TNF-α after BM-MSCs treatment to deactivation of macrophages and hepatic stellate cells. Histologically, the authors reported a significant improvement in induced hepatic fibrosis, as scored by the METAVIR scoring system, with restoration of normal liver tissue in the BM-MSCs group. Normal tissue with no collagen proliferation was recorded in the BM-MSCs group, as seen with Masson's trichrome staining. The findings of the present work are in agreement with the above findings. Khalil et al. (2021) stated that BM-MSCs either undergo differentiation in the liver tissue or release cytokines/chemokines, by means of a paracrine mechanism, which help reduce inflammation, fibrosis and oxidative stress. The authors hypothesized that BM-MSCs stimulate hepatic regeneration in liver damage either by generation of de novo hepatocytes by means of trans-differentiation and/or cell fusion, paracrine stimulation of endothelial differentiation and vasculogenesis, antifibrogenic modulation of the stromal micro-environment and secretion of hepatotrophic growth factors. The growth factors enhance cell survival, decrease chronic inflammation and diminish fibrosis by inhibiting extracellular matrix (ECM) production and deposition, stimulating myofibroblasts apoptosis. Xiu et al. (2020) discussed the therapeutic role of BMSCs in the treatment of acute liver injury in down-regulation of serum markers such as AST and ALT and reduction of mortality. The authors confirmed that BMSCs transplantation markedly attenuated liver injury and improved the survival of rats in acute liver injury. The authors also stated that mesenchymal stem cells (MSCs) are regulated by the stromal cell-derived factor-1 (SDF-1)/CXC chemokine receptor-4 (CXCR4) signaling axis, which promotes stem cells migration to the inflammation-associated disease sites consequent to the activation of PI3K/Akt signaling pathway in BMSCs that is downstream of CXCR4.

CONCLUSION

This study investigated the hepatic injury associated with oral alprazolam administration and the role of BMSCs. The changes in levels of TNF-α, SOD and miRNA192 indicated alprazolam induced-oxidative stress and liver injury, results that were further supported by the immunohistochemical, histological and ultrastructural findings. There were no significant differences for ALT and AST between control and alprazolam groups as regards the biochemical results. The results indicated a reversal in the previously mentioned findings upon administration of BMSCs. In conclusion, studies investigating frequent and prolonged administration of alprazolam are further needed and administration of BMSCs could be recommended as a therapeutic option in conditions involving alprazolam-induced liver injury.

REFERENCES

AGGARWAL BB, GUPTA SC, KIM JH (2012) Historical perspectives on tumor necrosis factor and its superfamily: 25 years later, a golden journey. *Blood,* 119(3): 651-665.

ALIOTTA JM, SANCHEZ-GUIJO FM, DOONER GJ (2007) Alteration of marrow cell gene expression, protein production, and engraftment into lung by lung derived microvesicles: a novel mechanism for phenotype modulation. *Stem Cells,* 25: 2245-2256.

ANDRADE RJ, LUCENA MI, AGUILAR J, LAZO MD, CAMARGO R, MORENO P, GARCÍA-ESCAÑO MD, MARQUEZ A, ALCÁNTARA R, ALCÁIN G (2000) Chronic liver injury related to use of bentazepam. *Dig Dis Sci,* 45(8): 1400.

CARPINO G, MORINI S, CORRADINI SG, FRANCHITTO A, MERLI M, SICILIANO M, GENTILI F, MUDA AO, BERLOCO P, ROSSI M, ATTILI AF (2005) Alpha-SMA expression in hepatic stellate cells and quantitative analysis of hepatic fibrosis in cirrhosis and in recurrent chronic hepatitis after liver transplantation. *Digest Liver Dis,* 37(5): 349-356.

CHATTOPADHYAY A, DARBAR S, SAHA S, KARMAKAR P (2019) Effects of alprazolam administration on the vital organs of adult Wistar albino rats, biochemical and toxicological studies. *Indian J Pharmaceut Educ Res,* 53(1): 127-132.

DINIS-OLIVEIRA RJ (2017) Metabolic profile of oxazepam and related benzodiazepines: clinical and forensic aspects. *Drug Metab Rev,* 49(4): 451-463.

DUTT M, DHARAVATH RN, KAUR T, CHOPRA K, SHARMA S (2020a) Differential effects of alprazolam against methylphenidate-induced neurobehavioral alterations. *Physiol Behav,* 222: 112935.

DUTT M, DHARAVATH RN, KAUR T, KAUR N, CHOPRA K, SHARMA S (2020b) Co-abuse of alprazolam augments the hepato-renal toxic effects of methylphenidate. *Indian J Pharmacol,* 52(3): 216.

EL ASMAR MF, ATTA HM, MAHFOUZ S, FOUAD HH, ROSHDY NK, RASHED LA, TAHA FM (2011) Efficacy of mesenchymal stem cells in suppression of hepatocarcinogenesis in rats: possible role of Wnt signaling. *J Exp Clin Cancer Res*, 30(1): 1-11.

ELMESALLAMY GE, ABASS MA, ATTA A, REFAT NA (2011) Differential effects of alprazolam and clonazepam on the immune system and blood vessels of non-stressed and stressed adult male albino rats. *Mansoura J Forensic Med Clin Toxicol,* 19(2): 1-25.

GOLOVENKO NY, KOVALENKO VN, LARIONOV VB, REDER AS (2020) Dose and time-dependent acute and subchronic oral toxicity study of propoxazepam in mice and rats. *Int J Pharmacol Toxicol,* 8(1): 1.

HUANG Z, XU Z, WANG H, ZHAO ZQ, RAO Y (2018) Influence of ethanol on the metabolism of alprazolam. *Expert Opinion Drug Metab Toxicol,* 14(6): 551-559.

IBRAHIM NA, IBRAHIM SS, MANNAA FA, ABDEL-WAHHAB KG, ALI MA (2017) Selective amelioration of chronic restraint stress effects on IL-6, liver function and erythrocyte indices by alprazolam or the herb valerian extract in rats. *Egypt J Exp Biol (Zool.),* 13(2): 149-158.

ISHIKAWA T, TERAI S, URATA Y, MARUMOTO Y, AOYAMA K, SAKAIDA I, MURATA T, NISHINA H, SHINODA K, UCHIMURA S, HAMAMOTO Y (2006) Fibroblast growth factor 2 facilitates the differentiation of transplanted bone marrow cells into hepatocytes. *Cell Tissue Res,* 323(2): 221-231.

KHALIL MR, EL-DEMERDASH RS, ELMINSHAWY HH, MEHANNA ET, MESBAH NM, ABO-ELMATTY DM (2021) Therapeutic effect of bone marrow mesenchymal stem cells in a rat model of carbon tetrachloride induced liver fibrosis. *Biomed J,* 44(5): 598-610.

KOPP JL, GROMPE M, SANDER M (2016) Stem cells versus plasticity in liver and pancreas regeneration. *Nature Cell Biol,* 18(3):238-245.

KURNIAWAN DW, BOOIJINK R, PATER L, WOLS I, VRYNAS A, STORM G, PRAKASH J, BANSAL R (2020) Fibroblast growth factor 2 conjugated superparamagnetic iron oxide nanoparticles (FGF2-SPIONs) ameliorate hepatic stellate cells activation in vitro and acute liver injury in vivo. *J Control Release,* 328: 640-652.

LI Y, LIN G, CHEN B, ZHANG J, WANG L, LI Z, CAO Y, WEN C, YANG X, CAO G, WANG X (2017) Effect of alprazolam on rat serum metabolic profiles. *Biomed Chromatogr,* 31(9): e3956.

LIM JY, LEE JH, YUN DH, LEE YM, KIM DK (2021) Inhibitory effects of nodakenin on inflammation and cell death in lipopolysaccharide-induced liver injury mice. *Phytomedicine,* 81: 153411.

MAITRA S, SAHA B, SANTRA CR, MUKHERJEE A, GOSWAMI S, CHANDA PK, KARMAKAR P (2007) Alprazolam induced conformational change in hemoglobin. *Int J Biol Macromol,* 41(1): 23-29.

MÜLLER AM, HUPPERTZ S, HENSCHLER R (2016) Hematopoietic stem cells in regenerative medicine: astray or on the path? *Transfusion Med Hemother,* 43(4): 247-254.

PADRISSA-ALTÉS S, BACHOFNER M, BOGORAD RL, POHLMEIER L, ROSSOLINI T, BÖHM F, LIEBISCH G, HELLERBRAND C, KOTELIANSKY V, SPEICHER T, WERNER S (2015) Control of hepatocyte proliferation and survival by Fgf receptors is essential for liver regeneration in mice. *Gut,* 64(9):1444-1453.

PAGET GE, BARNES JM. TOXICITY TESTS. IN: LAURENCE DR, BACHARACH AL (1964) Evaluation of drug activities pharmacometrics. London and New York: Academic Press, pp 134-166.

ROY S, BENZ F, ALDER J, BANTEL H, JANSSEN J, VUCUR M, GAUTHERON J, SCHNEIDER A, SCHÜLLER F, LOOSEN S, LUEDDE M (2016) Down-regulation of miR-192-5p protects from oxidative stress-induced acute liver injury. *Clin Sci,* 130(14): 1197-1207.

SCHUELLER F, ROY S, VUCUR M, TRAUTWEIN C, LUEDDE T, RODERBURG C (2018) The role of miRNAs in the pathophysiology of liver diseases and toxicity. *Int J Mol Sci,* 19(1): 261.

SCUTERI A, MONFRINI M (2018) Mesenchymal stem cells as new therapeutic approach for diabetes and pancreatic disorders. *Int J Mol Sci,* 19(9): 2783.

UDOMSINPRASERT W, ANGKATHUNYAKUL N, KLAIKEAW N, VEJCHAPIPAT P, POOVORAWAN Y, HONSAWEK S (2020) Hepatic glypican-3 and alpha-smooth muscle actin overexpressions reflect severity of liver fibrosis and predict outcome after successful portoenterostomy in biliary atresia. *Surgery,* 167(3): 560-568.

UEHARA S, UNO Y, NAKANISHI K, ISHII S, INOUE T, SASAKI E, YAMAZAKI H (2017) Marmoset cytochrome P450 3A4 ortholog expressed in liver and small-intestine tissues efficiently metabolizes

midazolam, alprazolam, nifedipine, and testosterone. *Drug Metab Dispos*, 45(5): 457-467.

WANDRER F, LIEBIG S, MARHENKE S, VOGEL A, JOHN K, MANNS MP, TEUFEL A, ITZEL T, LONGERICH T, MAIER O, FISCHER R (2020) TNF-Receptor-1 inhibition reduces liver steatosis, hepatocellular injury and fibrosis in NAFLD mice. *Cell Death Dis,* 11(3): 1-9.

XIU G, LI X, YIN Y, LI J, LI B, CHEN X, LIU P, SUN J, LING B (2020) Sdf-1/cxcr4 augments the therapeutic effect of bone marrow mesenchymal stem cells in the treatment of lipopolysaccharide-induced liver injury by promoting their migration through PI3K/Akt signaling pathway. *Cell Transplant,* 29: 0963689720929992.

ZAREIFOPOULOS N, PANAYIOTAKOPOULOS G (2019) Treatment options for acute agitation in psychiatric patients: Theoretical and empirical evidence. *Cureus,* 11(11): e6152.

ZHAO W, WANG X, SUN KH, ZHOU L (2018) α-smooth muscle actin is not a marker of fibrogenic cell activity in skeletal muscle fibrosis. *PLoS One,* 13(1): e0191031.

Determining nail consistency by quantification of type I keratins

Esther Mingorance Álvarez[1], Rodrigo Martínez Quintana[2], Ana Mª Pérez Pico[3], Raquel Mayordomo[1]

[1] Department of Anatomy and Cell Biology, University Center of Plasencia, University of Extremadura, 10600 Plasencia, Cáceres, Spain

[2] Department of Mathematics, University Center of Plasencia, University of Extremadura, 10600 Plasencia, Cáceres, Spain

[3] Department of Nursing, University Center of Plasencia, University of Extremadura, 10600 Plasencia, Cáceres, Spain

SUMMARY

Nail consistency is a little studied characteristic of the nail plate. Numerous factors can influence its determination, including the anatomy of the nail apparatus, the structure of the nail plate, and the type and quantity of keratins present. To study the relationship between nail consistency and the expression level of type I keratins, a sample was chosen of 32 individuals in the same age group (49.94 ± 3.38 years), 18 with hard consistency nails and 14 with soft consistency nails, with the same number of individuals for each gender. Two buffers with different concentrations of reducing agent (50mM and 200mM) and two antibodies to various type I keratins were analyzed by immunoblotting. The mean extracted protein concentration at 50mM was significantly higher than the concentration at 200mM (p-value<0.001). The expression level obtained with the AE13 antibody did not vary with gender or nail consistency (p-values≥0.942). With the cytokeratin 17 antibody (CTK17), no differences were found by gender (p-value=0.341). However, significant differences were established between hard-consistency and soft-consistency nails (p-values≤0.007) for the two concentrations, and between concentrations for soft consistency nails (p-value=0.001). Hard-consistency nails had a higher expression level of K17. Adding to the elemental analysis between layers and the flexural behavior of the nail plate studied reported in previous studies, this work demonstrates that nail consistency also depends on the quantity of keratins expressed.

Key words: Epithelial keratin – Hair keratin – Immunoblot – Nail consistency – Nail plate

INTRODUCTION

The nail apparatus is a complex, versatile skin appendage (Haneke, 2006; Haneke, 2015) of epidermic origin (McCarthy, 2004). It is located dorsally in the distal phalanges of the fingers and toes, which it protects (Runne et al., 1981; McCarthy, 2004). In addition to epithelial components, the nail apparatus includes vascularization and innervation structures (Bas et al., 1999; Fleckman et al., 2001; de Berker, 2013; Haneke, 2015) with important sensorial and temperature regulating functions (Haneke, 2006; Haneke, 2015). Anatomically, it comprises the

Corresponding author:
Raquel Mayordomo. Department of Anatomy and Cell Biology, University Center of Plasencia, University of Extremadura, Avda. Virgen del Puerto 2. 10600 Plasencia, Cáceres, Spain. Phone: +34636526498; Fax: +34927425209. E-mail: rmayordo@unex.es

Submitted: June 6, 2022. **Accepted:** June 27, 2022

https://doi.org/10.52083/XKZR3881

following principal elements: nail folds (proximal and lateral folds), nail matrix, nail bed, nail plate, eponychium and hyponychium (Fleckman et al., 2001; Haneke, 2006; de Berker, 2013; Fleckman et al., 2013; Haneke, 2015).The nail plate is made up of tightly packed, anucleate keratinized cells (Runne et al., 1981; Haneke, 2006) arranged in three layers: the dorsal, intermediate and ventral layers (Runne et al., 1981). The layers are differentiated by the orientation of the keratin filaments (Farren et al., 2004), the type of keratins present, and the relative thickness of each layer (Kobayachi et al., 1999). These and other factors influence the mechanical functions of the human nail plate and its physical characteristics of toughness, strength, and flexibility (Young et al., 1965; Finlay et al., 1980; Farren et al., 2004), and are also likely to influence nail consistency.

Nail consistency is a characteristic of the nail plate that is not routinely assessed during clinical examination. However, changes in the color, shape or thickness of the nail plate are important signs assessed in podiatry practice, because they can indicate systemic pathologies or nail disorders (Shemer et al., 2013; Baraldi et al., 2015; Zaiac et al 2015). We consider that when examining both normal and pathological nails, consistency should be one of the main factors assessed alongside color, shape, and other characteristics. Soft, medium, and hard consistency nails have been identified, and their relative frequencies have been found to vary with age, gender, and sports activity (Pérez Pico et al., 2017; Pérez Pico et al., 2019). Moreover, studies which develop a predictive mathematical model for nail consistency based primarily on the level of calcium in the dorsal layer of the nail plate (Mingorance Álvarez et al., 2021) and which analyze flexural behavior through fractional modeling (Traver et al., 2021) strengthen the hypothesis that nail consistency varies.

Keratins form the type of intermediate filament characteristic of epithelial tissue (Woodcock-Mitchell et al., 1982). They are very stable filaments that provide integrity and mechanical support to the epithelial cells (Runne et al., 1981). Epithelial keratins are characteristic of epithelial tissue, while hair keratins are the majority type in cutaneous appendages (hair and nails). The structural unit of the fold is the heterodimer (Hatzfeld et al., 1990), a type I (acid) and a type II (basic or neutral) amino acid chain (Moll et al., 1982) assembled by the central α-helical rod domain. This domain is fundamental in the development of upper fold levels (coiled-coil conformation), together with the existence of disulfide bonds that keep the structure stable, particularly in hair keratins (Gniadecka et al., 1998). Human type I keratins are epithelial (K9-10, K12-K20, K23-28) and hair (K31-K40), and human type II keratins are epithelial (K1-K8, K71-K80) and hair (K81-K86) (Schweizer et al., 2006). Numerous studies have permitted characterization of epithelial and hair keratin expression patterns in the different elements of the nail apparatus (Baden et al., 1984; Heid et al., 1988; Moll et al., 1988; Westgate et al., 1997; Waseem et al. 1999; de Berker et al., 2000; McGowan et al., 2000; Perrin et al., 2004; Perrin, 2007; Perrin et al., 2011) some of them in human adults (Table 1). The nail plate contains both

Table 1. Keratin expression in human adult nail apparatus.

	Type I		Type II	
	Epithelial	**Hair**	**Epithelial**	**Hair**
Proximal nail fold	K10, K16, K17		K1, K6	
Eponychium	K10, K16, K17		K5, K6	
Matrix	K10, K14, K16, K17, K18,	K31, K34, K36, K38	K1, K5, K6, K7, K8,	K81, K85, K86
Nail bed	K10, K14, K16, K17		K5, K6, K7, K75	
Nail plate	K17			
Hyponychium	K10, K17		K5	
Digit pulp	K16, K17		K6	

Studies summarized from: de Berker, 2000; McGowan and Coulombe, 2000; Perrin et al., 2004; Perrin, 2007; Perrin et al., 2011.

epithelial and hair keratins (Lynch et al., 1986; Heid et al., 1988; Kitahara et al., 1991), although only 10-20% are epithelial, compared to a majority of hair keratins (Lynch et al., 1986; Heid et al., 1988).

Several factors may influence nail consistency, including the anatomy of the nail apparatus, the structure of the nail plate, and the type, quantity, and assembly of the keratins present. However, few studies have addressed nail consistency and its determining factors. The main objective of this work is to analyze the relationship between nail consistency and the quantification of two type I keratins present in the nail plate (the epithelial keratin K17 and a 44-46 kDa hair keratin doublet) and establish a new line of research to determine whether nail consistency depends on the pattern and/or relative quantity of the keratins expressed in the nail plate.

MATERIALS AND METHODS

Permission and sample description

Permission for the study was obtained from the University of Extremadura Bioethics Committee (Reg. 116/2016). All participants signed an informed consent form and after a physical examination of their feet, they filled in a questionnaire to provide the necessary health information. The inclusion criteria were: aged 40 to 55 years; no diagnosed disease capable of altering nail structure and/or composition; no prescribed medication described as altering nail structure and/or composition; no behaviors or treatments that alter the structure and/or composition of the nails; following a Mediterranean diet.

The final sample comprised 32 adult individuals (16 men and 16 women; 49.94 ± 3.38 years), 18 with hard consistency nails and 14 with soft consistency nails.

Nail consistency and sample collection

Trained personnel determined nail consistency *in vivo* by applying manual pressure to the nail edges in the lateral-medial and dorsal-ventral axis after the foot had been exposed to room temperature for 15 minutes, following the methodology described elsewhere (Pérez Pico et al., 2017). Nail clippers were used to collect samples on the free edge of the first toe, without exceeding the onychocorneal band. Nail samples were immersed in an ultrasound cleaning bath (Elma, Singen, Germany) to clean them and remove skin cells, fibers and nail plate debris, and samples were stored at -20ºC until analysis.

Antibodies

As representatives of type I keratins, AE13 and CTK17 antibodies were analyzed due to their traditional use in the study of nail apparatus keratins, and their relationship with symptoms in the nail plate associated to hereditary human diseases as paquioniquia congenita type 2, respectively.

Mouse monoclonal antibody AE13, kindly provided by Dr TT Sun (New York University), recognizes a 44-46 kDa type I human hair keratin doublet (Lynch et al., 1986). Mouse monoclonal antibody CTK17 (sc-393091, Santa Cruz Biotechnology, Heidelberg, Germany) recognizes 46 kDa type I human epithelial keratins. Mouse monoclonal antibody GAPDH (sc-32233, Santa Cruz Biotechnology, Heidelberg, Germany) was used in 50mM 2-mercaptoethanol immunoblots as loading control. Goat anti-mouse IgG (H+L) HRP conjugate secondary antibody was obtained from Advansta (San José, California, USA).

Extraction procedure, protein quantification and immunoblot

Keratins were extracted following the methodology described elsewhere (Kitahara et al., 1991) for clipped nails. Because it was a two-step sequential extraction procedure, two different buffers were used: buffer I (50mM Tris-HCl, 9M urea, 2mM phenylmethanesulfonyl fluoride and 50mM 2-mercaptoethanol, pH 9) and buffer II (200mM Tris-HCl, 9M urea, 2mM phenylmethanesulfonyl fluoride and 200mM 2-mercaptoethanol, pH 9). Two extracts were obtained from each sample with increasing concentrations of 2-mercaptoethanol, one containing 50mM, in which the epithelial keratins were soluble, and the other containing 200mM, in which the hair keratins were soluble (Kitahara

et al., 1991). Three independent repetitions of the extraction procedure were performed with each sample analyzed. The protein concentration present in the extracts was quantified by the Bradford colorimetric method (Bradford, 1976).

Because the molecular weight of the target keratins was very similar (44-46kDa: AE13 antibody; 46kDa: CTK17 antibody), it was necessary to perform independent immunoblots for each antibody. A total of 3 µg of protein per well was loaded in the immunoblots with the AE13 antibody and 10 µg with CTK17, to avoid problems of membrane saturation and perform the quantification in the linear range. Sodium dodecyl sulfate polyacrylamide gel electrophoresis was performed under denaturing conditions (SDS-PAGE) (Laemmli, 1970) using gels with 10% acrylamide and electrophoresis buffer (25mM Tris, 192mM glycine, 0.1% w/v SDS). Separated proteins were transferred electrophoretically (40mV, for 4h, at 4ºC) to nitrocellulose membranes (GE Healthcare Life Sciences, Freiburg, Germany) with Mini Trans Blot System (Biorad Laboratories, Shanghai, China) using transfer buffer (25mM Tris, 192mM glycine, 20% v/v methanol).

Membranes were treated with blocking solution (50mM Tris-HCl, 75mM NaCl, 0.2% (v/v) Tween-20, pH 7.5, containing 10% (w/v) non-fat milk) for 2h at room temperature, then incubated overnight with primary antibodies AE13 and CTK17 (diluted 1:500 (v/v) in blocking solution) and GAPDH (diluted 1:2000 (v/v) in blocking solution) at 4ºC. Because the extraction conditions with buffer II (200mM) are incompatible with GAPDH protein extraction, Ponceau S stain was used as loading control rather than the GAPDH antibody (Fig. 1). The membranes were then washed (Tris-buffered saline buffer, pH 7.5, with 0.2% Tween-20) three times, for 10 minutes each, and incubated with goat anti-mouse IgG HRP conjugate secondary antibody (diluted 1:10000 in blocking solution) for 1h at room temperature. After four 10-minute washes, HRP chemiluminescent substrate Pierce ELC (Thermo Scientific, Rockford, Illinois, USA) was added for the membranes with the AE13 and CTK17 antibodies, and Clarity Max (Biorad Laboratories, Segrate, Italy) for GAPDH membranes. Membranes were exposed to Hyperfilm ELC (Amersham, Buckinghamshire, UK). Developed films were scanned and band signaling was measured using ImageJ software (http://rsbweb.nih.gov/ij/). The immunoblot results were obtained from three independent repetitions.

Statistics and variables

Statistical treatment was performed using IBM SPSS Statistics for Windows, Version 22.0 (IBM, Armonk, New York, USA). Normality was assessed by the Kolmogorov-Smirnov and Shapiro-Wilk tests. The paired sample T-test and the independent sample T-test were performed. For the two extraction conditions tested (50mM and 200mM), the variables analyzed were mean extracted protein concentration, mean quantification of the expression level with the AE13 antibody, and mean quantification of the expression level with the CTK17 antibody. To compare the extracted protein concentrations and the mean quantifications of the expression level for each antibody, the differences obtained under each extraction condition tested were analyzed. In all analyses the significance level was 0.05.

RESULTS

The three independent repetitions of protein extractions performed at 50mM showed a higher median (3.07, 3.81 and 4.01) and range (4.03, 3.95 and 4.40) than extractions performed at 200mM (2.49, 2.56 and 2.54) and (2.09, 2.39 and 2.17), respectively (Fig. 2). All the variables analyzed followed a normal distribution (p-values≥0.148). The comparison between the mean protein concentration extracted at 50mM and 200mM was independent of gender and nail consistency (p-values≥0.641). At 50mM, the mean extracted protein concentration was significantly higher (3.80 µg/µl) than the concentration obtained at 200mM (2.57 µg/µl) (p-value<0.001) (Fig. 2). Moreover, for each concentration analyzed, no differences were observed either by gender (p-values≥0.167) or nail consistency (p-values≥0.409) (Fig. 2).

Comparison of the mean quantification of the expression level for the AE13 antibody between the two concentrations tested was also

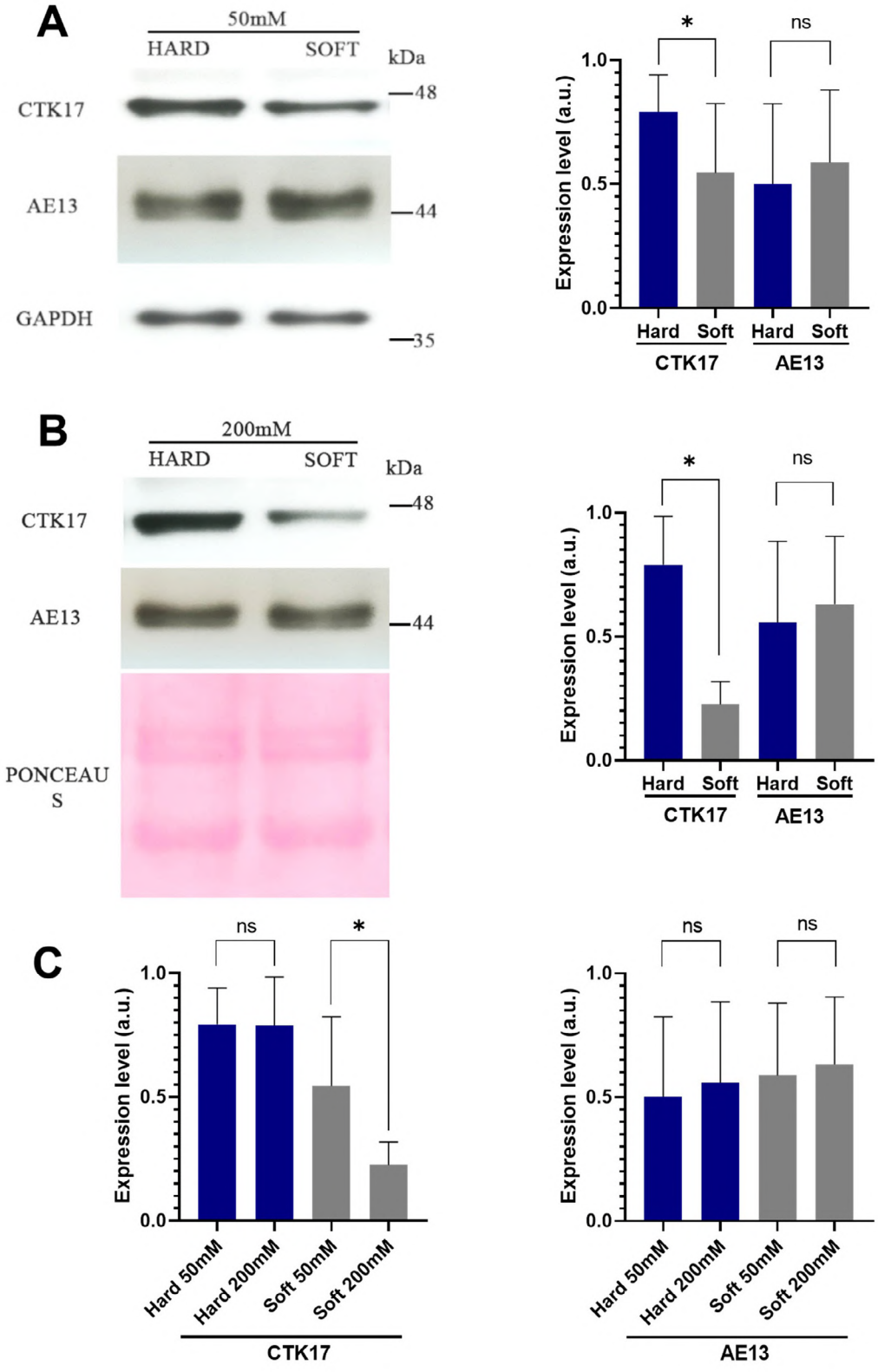

Fig. 1.- Expression level detected with the AE13 and CTK17 antibodies under the two extraction conditions tested (50mM and 200mM). (**A**) extracts obtained at 50mM. (**B**) extracts obtained at 200mM. (**C**) comparison of the expression level between nail consistencies (Hard and Soft). A left, 50mM immunoblot comparing hard- and soft-consistency nails. A right, bar graph comparing the expression level obtained at 50mM for the two antibodies tested by nail consistency. B left, 200mM immunoblot comparing hard- and soft-consistency nails. B right, bar graph comparing the expression level obtained at 200mM for the two antibodies tested by nail consistency. C left, bar graph comparing the expression level obtained for the CTK17 antibody by the two extraction conditions and the two nail consistencies tested. C right, bar graph comparing the expression level obtained for the AE13 antibody by the two extraction conditions and the two nail consistencies tested. 50mM, concentration of 2-mercaptoethanol in the extraction buffer; 200mM, concentration of 2-mercaptoethanol in the extraction buffer; Hard, hard-consistency nails; Soft, soft-consistency nails; kDa, kilodalton; a.u., arbitrary units; *, statistically significant difference ($p<0.05$); ns, not significant; GAPDH, loading control at 50mM; Ponceau S, loading control at 200mM.

independent of gender and nail consistency (p-values≥0.942). Analysis of the results of the mean quantification of the expression level of the extracts obtained at 50mM and 200mM did not show enough evidence to reject that they were the same (p-value=0.516). For each concentration analyzed, no significant differences were observed by gender (p-values≥0.802) or nail consistency (p-values≥0.437) (Fig. 1).

For the CTK17 antibody, the comparison between the mean quantification of the expression level at 50mM and at 200mM did not vary by gender (p-value=0.341), although it varied by nail consistency (p-value=0.001). The data observed on comparing the mean quantification of the expression level of the extracts obtained at 50mM and at 200mM in hard consistency nails did not show enough evidence to reject that they were the same (p-value=0.958). However, significant differences were found on comparing the mean quantification of the expression level in the extracts obtained at 50mM and at 200mM in soft consistency nails (p-value=0.001). For each concentration, no differences were observed in relation to gender (p-values≥0.187), although differences were observed by nail consistency (p-values≤0.007) (Fig. 1).

Quantification of the expression level obtained for the AE13 antibody therefore did not vary either by gender or nail consistency (p-values≥0.942). However, the results obtained with the CTK17 antibody showed significant differences between soft consistency nails and hard consistency nails under each extraction condition tested (at 50mM and at 200mM) (p-values≤0.007) and between soft consistency nails for extracts obtained at 50mM and at 200mM (p-value=0.001).

DISCUSSION

The nail plate is a highly keratinized tissue, given that 90% of the total proteins in the nail plate are keratins or keratin-associated proteins (Rice et al., 2010) and 80-90% of these are hair keratins (Heid et al., 1988; Lynch et al., 1986). However, the extractions performed under less reducing conditions (50mM) showed a higher total protein concentration than extractions at a higher concentration of reducing agent (200mM), in which hair keratins are more soluble than epithelial keratins. Therefore, under more gentle extraction conditions, not only are the epithelial keratins soluble (Kitahara et al., 1991), but other types of proteins (membrane or intracellular) also

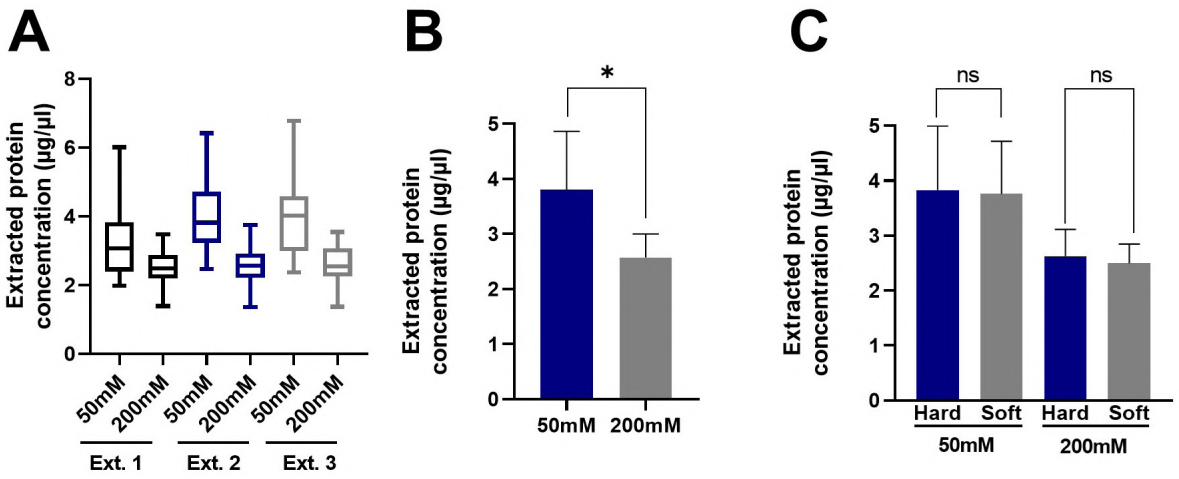

Fig. 2.- Principal results obtained from the extraction experiments. (**A**) Box and whisker plot of the three independent repetitions of the extraction procedure. (**B**) Bar graph comparing the mean extracted protein concentration under the two extraction conditions tested (50mM and 200mM). (**C**) Bar graph comparing the mean extracted protein concentration under the two extraction conditions tested by nail consistency (Hard and Soft). 50mM, concentration of 2-mercaptoethanol in the extraction buffer; 200mM, concentration of 2-mercaptoethanol in the extraction buffer; Ext. 1, independent extraction number 1; Ext. 2, independent extraction number 2; Ext. 3, independent extraction number 3; *, statistically significant difference (p<0.05); ns, not significant; Hard, hard consistency nails; Soft, soft consistency nails.

solubilize, producing a higher extraction yield than under more reducing conditions (Rice et al., 2010). This is the case of the protein glyceraldehyde-3-phosphate dehydrogenase (GAPDH), which participates in glycolysis and was detected only in extracts performed at 50mM, where it was used as loading control. Moreover, the results obtained in the three independent repetitions of protein extraction showed greater variability in extractions performed at 50mM than at 200mM. These results support the hypothesis that a higher diversity of proteins is extracted under less reducing conditions, whereas under more reducing conditions the type of proteins solubilized is more homogeneous and variability is lower. However, the nail plate is not characterized as a very active tissue from a metabolic point of view, because it is made up of cells with pyknotic nuclei or largely denucleated cells (Runne et al., 1981). It is likely that, together with the minority non-keratin proteins present in the nail plate, some hair keratins are also extracted under less reducing conditions (Rice et al., 2010), even though they are almost insoluble in these conditions (Kitahara et al., 1991).

The AE13 antibody was not useful for differentiating between hard- and soft-consistency nails, because its expression level did not vary either by nail consistency or extraction conditions. Previous studies with this antibody reported exclusive staining in extracts obtained under more reducing conditions (Kitahara et al., 1991). However, we cannot state that only hair keratins will be extracted under these conditions, which would explain the expression level of the extracts obtained at 50mM. A minor tendency was observed in the slightly higher expression level in soft-consistency nails, which was higher under the more reducing extraction conditions. Although the results were not statistically significant, the extracts from soft consistency nails may contain a higher relative concentration of target hair keratins of the AE13 antibody than the extracts from hard consistency nails.

The results showed that hard-consistency nails express more K17 than soft consistency nails. K17 has been detected in the nail matrix associated with precursor cells, in the nail bed (McGowan et al., 2000) and in the nail plate (Heid et al., 1988). It has also been associated with epithelia subjected to high physical stress, with high cell turnover rates (Swensson et al., 1998). Nails are constantly subjected to bending forces by activities of daily living (Forslind et al., 1980). It seems logical that hard-consistency nails would be less adapted to these forces than soft-consistency nails, which are probably more flexible and adaptable. These less adaptable nail plates would be subjected to greater stress, which could cause an increase in K17 synthesis and, therefore, a greater presence of this keratin in the nail plate of hard-consistency nails. Moreover, this difference in expression by nail consistency is independent of the extraction conditions, although in soft consistency nails the expression level is higher under less reducing extraction conditions, supporting an earlier description of keratin solubility and reducing power (Kitahara et al., 1991).

Nail consistency varies by age, gender, and sports activity. Adult males and young people who do sport have a higher frequency of hard-consistency nails than adult females and sedentary young people, whose most frequent nail consistencies are medium and soft (Pérez Pico et al., 2017; Pérez Pico et al., 2019). In developing a predictive model of nail consistency, gender was not shown to be a good predictive variable (Mingorance et al., 2021), and neither were the results obtained with the two antibodies tested, because no relation was established between nail consistency and gender. Therefore, although the frequency of each nail consistency varies in the population, hard- and soft-consistency nails show no differences by gender.

CONCLUSIONS

This study provides experimental evidence to show that hard-consistency nails and soft-consistency nails have different expression levels of K17, a type I epithelial keratin, and that expression is greater in hard-consistency nails. The role of K17 in healthy nail plates strengthens the hypothesis that nail consistency varies and establishes differences at molecular level. With greater knowledge of the characteristics of the nail plate, health professionals will be better equipped to prevent, diagnose, and treat numerous nail and

systemic diseases. We consider nail consistency to be one of the key characteristics that health professionals should assess during clinical examination. However, more studies are needed, both to define the determining factors of nail consistency and to associate this characteristic with the most common nail and systemic diseases.

ACKNOWLEDGEMENTS

We thank Dr TT Sun for kindly providing the AE13 antibody, and Jane McGrath for assistance with the translation and final language review. This research was funded by the Extremadura Regional Government and the European Regional Development Fund (ERDF) through a grant to the research group [code CTS020, reference GR18182].

REFERENCES

BADEN HP, KUBILUS J (1984) A comparative study of the immunologic properties of hoof and nail fibrous proteins. *J Invest Dermatol*, 83: 327-331.

BARALDI A, JONES SA, GUESNE S, TRAYNOR MJ, MCAULEY WJ, BROWN MB, MURDAN S (2015) Human nail plate modifications induced by onychomycosis: implications for topical therapy. *Pharm Res*, 32: 1626-1633.

BAS H, KLEINERT JM (1999) Anatomic variations in sensory innervation of the hand and digits. *J Hand Surg Am*, 24(6): 1171-1184.

BRADFORD MM (1976) A rapid and sensitive method for the quantitation of microgram quantities of protein utilizing the principle of protein-dye binding. *Anal Biochem*, 72: 248-254.

DE BERKER D, WOJNAROWSKA F, SVILAND L, WESTGATE GE, DAWBER RP, LEIGH IM (2000) Keratin expression in the normal nail unit: markers of regional differentiation. *Br J Dermatol*, 142: 89-96.

DE BERKER D (2013) Nail anatomy. *Clin Dermatol*, 31: 509-515.

FARREN L, SHAYLER S, ENNOS AR (2004) The fracture properties and mechanical design of human fingernails. *J Exp Biol*, 207: 735-741.

FINLAY AY, FROST P, KEITH AD, SNIPES W (1980) An assessment of factors influencing flexibility of human fingernails. *Br J Dermatol*, 103: 357-365.

FLECKMAN P, ALLAN C (2001) Surgical anatomy of the nail unit. *Dermatol Surg*, 27(3): 257-260.

FLECKMAN P, JAEGER K, SILVA KA, SUNDBERG JP (2013) Comparative anatomy of mouse and human nail units. *Anat Rec (Hoboken)*, 296(3): 521-532.

FORSLIND B, NORDSTROM G, TOIJER D, ERIKSSON K (1980) The rigidity of human fingernails: a biophysical investigation on influencing physical parameters. *Acta Derm Venereol*, 60: 217-222.

GNIADECKA M, NIELSEN OF, CHRISTENSEN DH, WULF HC (1998) Structure of water, proteins, and lipids in intact human skin, hair, and nail. *J Invest Dermatol*, 110: 393-398.

HANEKE E (2006) Surgical anatomy of the nail apparatus. *Dermatol clin*, 24: 291-296.

HANEKE E (2015) Anatomy of the nail unit and the nail biopsy. *Semin Cutan Med Surg*, 34(2): 95-100.

HATZFELD M, WEBER K (1990) The coiled coil of in vitro assembled keratin filaments is a heterodimer of type I and II keratins: use of site-specific mutagenesis and recombinant protein expression. *J Cell Biol*, 110: 1199-1210.

HEID HW, MOLL I, FRANKE WW (1988) Patterns of expression of trichocytic and epithelial cytokeratins in mammalian tissues. II. Concomitant and mutually exclusive synthesis of trichocytic and epithelial cytokeratins in diverse human and bovine tissues (hair follicle, nail bed and matrix, lingual papilla, thymic reticulum). *Differentiation*, 37: 215-230.

KITAHARA T, OGAWA H (1991) The extraction and characterization of human nail keratin. *J Dermatol Sci*, 2: 402-406.

KOBAYACHI Y, MIYAMOTO M, SUGIBAYASHI K, MORIMOTO Y (1999) Drug permeation through the three layers of the human nail plate. *J Pharm Pharmacol*, 51:271-278.

LAEMMLI UK (1970) Cleavage of structural proteins during the assembly of the head of bacteriophage T4. *Nature*, 227: 680-685.

LYNCH MH, O'GUIN WM, HARDY C, MAK L, SUN TT (1986) Acidic and basic hair/nail ("hard") keratins: their colocalization in upper cortical and cuticle cells of the human hair follicle and their relationship to "soft" keratins. *J Cell Biol*, 103: 2593-2606.

MCCARTHY DJ (2004) Anatomic considerations of the human nail. *Clin Podiatr Med Surg,* 21: 477-491.

MCGOWAN KM, COULOMBE PA (2000) Keratin 17 expression in the hard epithelial context of the hair and nail, and its relevance for the pachyonychia congenita phenotype. *J Invest Dermatol*, 114: 1101-1107.

MINGORANCE ÁLVAREZ E, MARTÍNEZ QUINTANA R, PÉREZ PICO AM, MAYORDOMO R (2021) Predictive model of nail consistency using scanning electron microscopy with energy-dispersive X-ray. *Biology (Basel)*, 10: 1-17.

MOLL R, FRANKE WW, SCHILLER DL, GEIGER B, KREPLER R (1982) The catalog of human cytokeratins: patterns of expression in normal epithelia, tumors and cultured cells. *Cell*, 31: 11-24.

MOLL I, HEID HW, FRANKE WW, MOLL R (1988) Patterns of expression of trichocytic and epithelial cytokeratins in mammalian tissues. III. Hair and nail formation during human fetal development. *Differentiation*, 39: 167-184.

PÉREZ PICO AM, VERJANO E, MAYORDOMO R (2017) Relation between nail consistency and incidence of ingrown toenails in young male runners. *J Am Podiatr Med Assoc*, 107: 137-143.

PÉREZ PICO AM, MINGORANCE ÁLVAREZ E, CABALLÉ CERVIGÓN N, MAYORDOMO ACEVEDO R (2019) Importance of preexisting physical factors in the development of dermatological and muscular lesions during hiking. *Int J Low Extrem Wounds*, 18: 161-170.

PERRIN C (2007) Expression of follicular sheath keratins in the normal nail with special reference to the morphological analysis of the distal nail unit. *Am J Dermatopathol*, 29: 543-550.

PERRIN C, LANGBEIN L, SCHWEIZER J (2004) Expression of hair keratins in the adult nail unit: an immunohistochemical analysis of the onychogenesis in the proximal nail fold, matrix and nail bed. *Br J Dermatol*, 151: 362-371.

PERRIN C, LANGBEIN L, SCHWEIZER J, CANNATA GE, BALAGUER T, CHIGNON-SICART B, GARZON JM, BENCHETRIT M, MICHIELS JF (2011) Onychomatricoma in the light of the microanatomy of the normal nail unit. *Am J Dermatopathol*, 33: 131-139.

RICE RH, XIA Y, ALVARADO RJ, PHINNEY BS (2010) Proteomic analysis of human nail plate. *J Proteome Res*, 9: 6752-6758.

RUNNE U, ORFANOS CE (1981) The human nail. Structure, growth and pathological changes. *Curr Probl Derm*, 9: 102-149.

SCHWEIZER J, BOWDEN PE, COULOMBE PA, LANGBEIN L, LANE EB, MAGIN TM, MALTAIS L, OMARY MB, PARRY DAD, ROGERS MA, WRIGHT MW (2006) New consensus nomenclature for mammalian keratins. *J Cell Biol*, 174: 169-174.

SHEMER A, DANIEL CR 3RD (2013) Common nail disorders. *Clin Dermatol*, 31: 578-586.

SWENSSON O, LANGBEIN L, MCMILLAN JR, STEVENS HP, LEIGH IM, MCLEAN WH, LANE EB, EADY RA (1998) Specialized keratin expression pattern in human ridged skin as an adaptation to high physical stress. *Br J Dermatol*, 139: 767-775.

TRAVER JE, TEJADO I, MINGORANCE ÁLVAREZ E, PRIETO-ARRANZ J, MAYORDOMO R, PÉREZ-PICO AM, VINAGRE BM (2021) Fractional modelling of flexural properties of toenail plates: first step for clinical purposes. *Med Eng Phys*, 90: 23-32.

WASEEM A, DOGAN B, TIDMAN N, ALAM Y, PURKIS P, JACKSON S, LALLI A, MACHESNEY M, LEIGH IM (1999) Keratin 15 expression in stratified epithelia: downregulation in activated keratinocytes. *J Invest Dermatol*, 112: 362-369.

WESTGATE GE, TIDMAN N, DE BERKER D, BLOUNT MA, PHILPOTT MP, LEIGH IM (1997) Characterization of LHTric-1, a new monospecific monoclonal antibody to the trichocyte keratin Ha1. *Br J Dermatol*, 137: 24-30.

WOODCOCK-MITCHELL J, EICHNER R, NELSON WG, SUN TT (1982) Immunolocalization of keratin polypeptides in human epidermis using monoclonal antibodies. *J Cell Biol*, 95: 580-588.

YOUNG RW, NEWMAN SB, CAPOTT RJ (1965) Strength of fingernails. *J Invest Dermatol*, 44: 358-360.

ZAIAC MN, WALKER A (2013) Nail abnormalities associated with systemic pathologies. *Clin Dermatol*, 31: 627-649.

Microstructural evidence of reversal of PCOS by steroidal saponins of asparagus racemosus in PCOS induced rats

M. Vani[1], P. Preethi[1], D.H. Gopalan[1], S. Manikandan[2], V. Vijayakumar[3], C. Swathi Priyadarshini[1]

[1]Department of Anatomy, Tagore Medical College and Hospital, Rathinamangalam, Chennai, India
[2]Department of Physiology, Tagore Medical College and Hospital, Rathinamangalam, Chennai, India
[3]Department of Anatomy, Saveetha Medical College and Hospital, Saveetha University, Chennai, India

SUMMARY

The purpose of this study is to investigate the histological and hormonal observations in fructose-fed, letrozole-induced polycystic-ovarian-syndrome (PCOS) rats treated with various doses of extract of asparagus racemosus (EAR) and Steroidal saponin (SAPO). 48 female Wistar albino rats were divided into 8 groups, including Vehicle Control (VC); PCOS; EAR 400 mg/kg; SAPO 40 mg/kg; PCOS + EAR 200 mg/kg; PCOS + EAR 400 mg/kg; PCOS + SAPO 20 mg/kg; PCOS + SAPO 40 mg/kg. PCOS group was administered letrozole at a concentration of 1 mg/kg dissolved in 1% CMC per oral(p.o.) once daily for 28 days. Along with these, rats were allowed free access of 10% fructose solution daily. Calculated dosages of EAR and SAPO were given with oral gavage for 30 days. During experimental period, vaginal smears were collected daily for estrus cycle determination. Rats were sacrificed and blood samples were collected for hormonal assay. Ovaries were removed to proceed with histopathological study. Slides were stained using hematoxylin and eosin (H&E) stains. When compared to the vehicle control group, PCOS ovaries had a higher incidence of ovarian cysts, incomplete luteinization, and a lower number of corpus lutea. Although serum estradiol, progesterone, and Follicle-stimulating hormone (FSH) levels were lower in the PCOS group, testosterone and luteinizing hormone (LH) levels were higher. The findings of this study indicated that taking EAR 400 mg/kg and SAPO 40mg/kg orally could alleviate PCOS-related symptoms. It appears that consuming SAPO 40mg/kg reduces LH and testosterone levels while increasing FSH, estrogen, and progesterone hormone levels. Because of the hormonal balancing nature of these drugs, EAR 400mg/kg- and SAPO 40mg/kg-treated rats had a lower number of cystic follicles and a higher number of corpora lutea. In PCOS rats, this results in a normal process of folliculogenesis and ovulation. In the current study, we observed that SAPO 40mg/kg is better compared to EAR 400mg/kg treatment.

Keywords: PCOS – Asparagus racemosus – Saponin – Hormones

Corresponding author:
Dr. P. Preethi. Department of Anatomy, Tagore Medical College and Hospital, Rathinamangalam, Chennai, India. Phone: 9952907904. E-mail: drpreethimed@gmail.com

Submitted: May 6, 2022. **Accepted:** July 16, 2022

https://doi.org/10.52083/UCXX3672

INTRODUCTION

PCOS has a complex etiology that includes a number of reproductive and metabolic factors. There is no single etiology that can explain the prevalence of PCOS. Furthermore, no single etiological gene or inheritance pattern for PCOS has been identified. The pituitary gland secretes an abnormally large amount of LH into the bloodstream in PCOS, disrupting the normal menstrual cycle. As a result, follicle maturation and ovulation are delayed, which can result in anovulation. The immature follicles that do not mature remain as fluid-filled sacs or cysts. Because of an increased amount of testosterone, these cysts cause hormonal imbalances. In addition, there is an increased level of insulin hormone produced by the pancreas (Anadu et al., 2013).

Polycystic ovaries are many times the size of a normal ovary. There are a lot of immature follicles (subcortical cysts) that cause the ovary to change shape. The ovary turns whitish in color, with multiple cystic follicles surrounded by a dense fibrous capsule. There is hyperthecosis as well as thickening of the tunica albugenea (Krishnamurthy et al., 2009). PCOS women's ovarian and adrenal glands are typically sites of increased androgen production. It is also suggested that PCOS women have an increase in the production of the CYP17 enzyme, which is responsible for the formation of androgens in the ovaries and adrenal glands (Haywood et al., 2004). The ovaries produce a variety of androgens, the most prominent of which is testosterone. Other androgens produced by the ovaries include androstenedione and DHA. The stroma and theca cells produce an excess of testosterone, which is a common and significant feature of polycystic ovary (Nagarthna et al., 2014).

Asparagus racemosus (AR) is a tropical and subtropical Indian plant with medicinal properties. This plant was traditionally used as a fertility tonic. AR's primary active constituents are steroidal saponins (Shatavarins–IV) found in the roots. Shatavarin IV is a sarsasapogenin glycoside composed of two rhamnose molecules and one glucose molecule. RP-HPLC methods were used to isolate five steroidal saponins, shatavarins VI–X, as well as five known saponins, from AR roots (Hayes et al., 2008). AR is best known for its phytestrogenic properties. As people become more aware of the dangers of synthetic estrogens, there has been a surge in interest in plant-derived estrogens, making AR especially important. The molecular structures of the major phytestrogens, isoflavones and coumastans, are compared to 17-estradiol, the most powerful naturally occurring estrogen. The structural similarities between phytestrogens and 17-estradiol are sufficient to allow phytestrogens to occupy the ER, but affinity for the receptor is significantly lower when compared to 17-estradiol (Sharma et al., 2013). Its beneficial uses in correcting menstrual irregularities are mentioned in ancient literature, and they are still prescribed by ayurvedic physicians to correct menstrual irregularities with products available in the market. Clearly, more research is required to define the effect of phytestrogens from AR while also standardizing and characterizing formulations and/or isolated phytestrogens. Furthermore, developing an understanding of the effects of phytestrogens derived from AR versus human estrogens holds great promise for future research (Verma et al., 2014).

Many studies have found that saponin reduces the harmful effects of chemotherapy on reproductive organs. Saponins also possess antioxidant properties (Zhang et al., 2008). The current study was conducted to assess the effect of ethanolic extract of AR roots and steroidal saponins on hypothalamic-pituitary-gonadal axis hormones and histological observations in PCOS rats due to the presence of many compounds affecting gonadotropic and ovarian hormones in asparagus extract, such as steroidal saponins, vitamins, and amino acids.

MATERIALS AND METHODS

Animals

6-week-old Adult female Wistar albino rats (180-225 g) with regular estrus cyclicity were obtained from TANUVAS, Chennai. They were housed in polypropylene cages with paddy husk bedding, standard rat pellets, and ad libitum drinking

water, and acclimatized on a 12-hour light and 12-hour dark schedule in temperatures ranging from 23 to 25°C. The cages are categorized with the group, the animal's weight, and the drug dosage. Before beginning the study, each group of animals was given an average of one week to acclimatize. The experimental study protocol was approved by Tagore Medical College and Hospitals Institutional Animal Ethics Committee (TMC/IAEC/02/003, dated 12.01.2015; TMC/IAEC/01/002, dated 03.12.2016).

Collection and preparation of plant material

AR fresh roots were obtained from Kolapakkam, Vandalur, Chennai, Tamil Nadu, India between July and September and authenticated by the Department of Botany, National Institute of Siddha, Chennai (Voucher no. NISMB1492014, dated December 29, 2014) The specimen was stored at the National Institute of Siddha in Chennai, India, for future use. For a week, AR roots were shade dried. The dried roots were powdered using an electric blender before being subjected to a 48-hour Soxhlet extraction with 99 % ethanol. A rotary flash evaporator was employed to dry the mixture, and the condensed extract was stored in the refrigerator before being used for preliminary phytochemical screening (Harborne, 1973).

Chemicals

Letrozole was purchased from sun pharmaceutical, (Mumbai). Carboxmethlycellulose (CMC) and fructose were purchased from southern India scientific corporation, (Chennai).

Experimental design

The animals were divided into eight groups with each group having 6 animals. Group 1 - 1% CMC administered p.o., for 28 days (Vehicle control). Group 2 -Letrozole 1 mg/kg in 1% of CMC (2 mL/kg) administered p.o., with free access of 10% solution of fructose for 28 days (PCOS). Group 3 - 400 mg/kg of EAR treated p.o., for 30 days (EAR 400). Group 4 - 40 mg/kg of SAPO treated p.o., for 30 days (SAPO 40). Group 5 - PCOS rats +200 mg/kg of EAR treated p.o., for 30days (PCOS + EAR 200). Group 6 - PCOS rats + 400 mg/kg of EAR treated p.o., for 30 days (PCOS + EAR400). Group 7 - PCOS rats +20 mg/kg of SAPO treated p.o., for 30 days (PCOS + SAPO20). Group 8 - PCOS rats+ 40 mg/kg of SAPO treated p.o., for 30 days (PCOS +SAPO40). Throughout the entire study period vaginal smears were taken daily and evaluated microscopically for estrous cycle determination.

Column and thin layer chromatography

A small plug of cotton was pushed at the bottom of the glass column after it had been cleaned and dried vertically. The fractions were eluted with different ratios of solvents such as hexane (low polar), chloroform (middle polar), ethyl acetate (polar), and ethanol (highly polar) in the order of increasing polarity. The fractions collected were then concentrated for use in thin-layer chromatography. TLC plates 20 x 20 cm, 1 mm thick, were taken and cut into appropriate sizes so that samples could be loaded. The column chromatography fractions were used as samples, and individual spots were placed in the TLC plates using a capillary tube. After that, the TLC plate was placed in the solvent chamber for elution. When the sample reached the desired height, the TLC plate was removed from the chamber and stored for drying. The vanillin sulphuric acid solution was prepared, and the TLC plate containing the sample was dipped in it and allowed to dry. The spots obtained were the AR's active compounds known as steroidal saponins (SAPO) (Marston et al., 1997) (Fig. 1 a,b,c,d).

Administration of drugs

Oral gavage was performed using an 18-gauge cannula (feeding tube) with a bulb tip attached to a syringe. The drugs were loaded into a syringe and administered orally. To avoid volume-induced changes, all animals received the same volume of fluid. The cannula was designed to be slightly longer than the distance between the animal's mouth and the last rib. Following the roof of the mouth, the flexible cannula was slowly advanced into the esophagus and then to the stomach, with no resistance. This was accomplished by gently restraining the rats by grasping the loose skin of the neck and back and immobilizing the head.

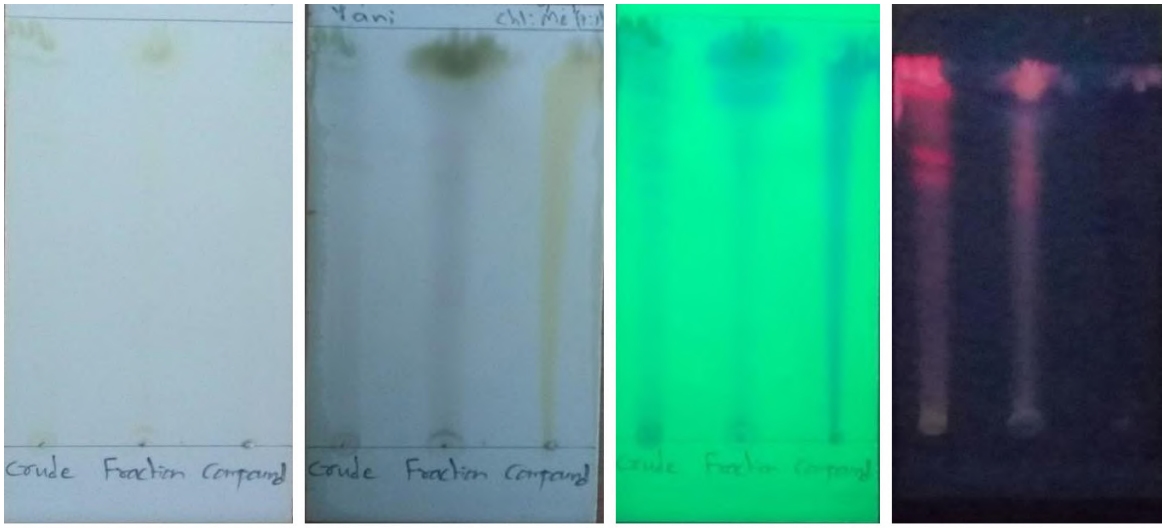

Fig. 1.- a, **b**, **c** and **d** show the visible light, short UV, long UV and vanillin dyed TLC sheet of the crude, fraction and compound AR respectively.

Vaginal smears

Throughout the study, vaginal secretions were collected with a plastic pipette every morning between 9:00 and 10:00 a.m. by inserting the tip into the rat's vagina and filling it with 10 µl of normal saline. On each glass slide, one drop of collected vaginal fluid was placed. Each animal received its own glass slide and pipette tips. The collected vaginal fluid was fixed on slides using a slide warming table and examined under a light microscope (40x). There were three types of cells identified: round and nucleated cells were epithelial cells, irregular cells without a nucleus were cornified cells, and small round cells were leucocytes; their mutual proportion was used for determining different phases of the estrus cycle (Fig. 2).

Blood collection and hormonal assay

After CO2 inhalation, blood samples are taken from the heart via cardiac puncture, which can be accessed via the left side of the chest, through the diaphragm, from the top of the sternum, or by performing a thoracotomy. By inhaling CO2, blood is slowly withdrawn from the heart to prevent it from collapsing while under deep anesthesia. Blood samples were quickly collected into plain sample bottles, allowed to clot, and then centrifuged at 3,000 RPM for 15 minutes to obtain clear serum samples, which were then frozen (-20°C) until hormonal assays were performed. The serum was tested for LH, FSH, testosterone, progesterone, and estrogen levels, among other things. ELISA Kit was used for hormone analysis (Elabscience).

Perfusion of animals

Following CO_2 deep inhalation, rats were cut open through the midline thoraco-abdominal incision and transcardial perfusion with 4% paraformaldehyde in 0.1 M phosphate buffered saline on the left ventricle and the right atrium. When limbs flicker, tissues blanch, and the animal's entire body hardens, this indicates that perfusion has been completed. The ovaries and uterus were carefully dissected and collected as per standard procedure (Gandhare et al., 2013). The organs were washed with cold saline solution and weighed immediately before being fixed in formalin (10% paraformaldehyde solution) for 48 hours. Tissue samples were collected from each organ, processed and stained according to the standard procedure outlined below.

Histological techniques

The ovaries were cut in the equatorial plane and fixed for 48 hours in Gendre's fluid. The fixed ovaries were dehydrated for 2-4 hours using 70% alcohol, 90% alcohol, absolute alcohol, and absolute alcohol II. The dehydrated ovaries were

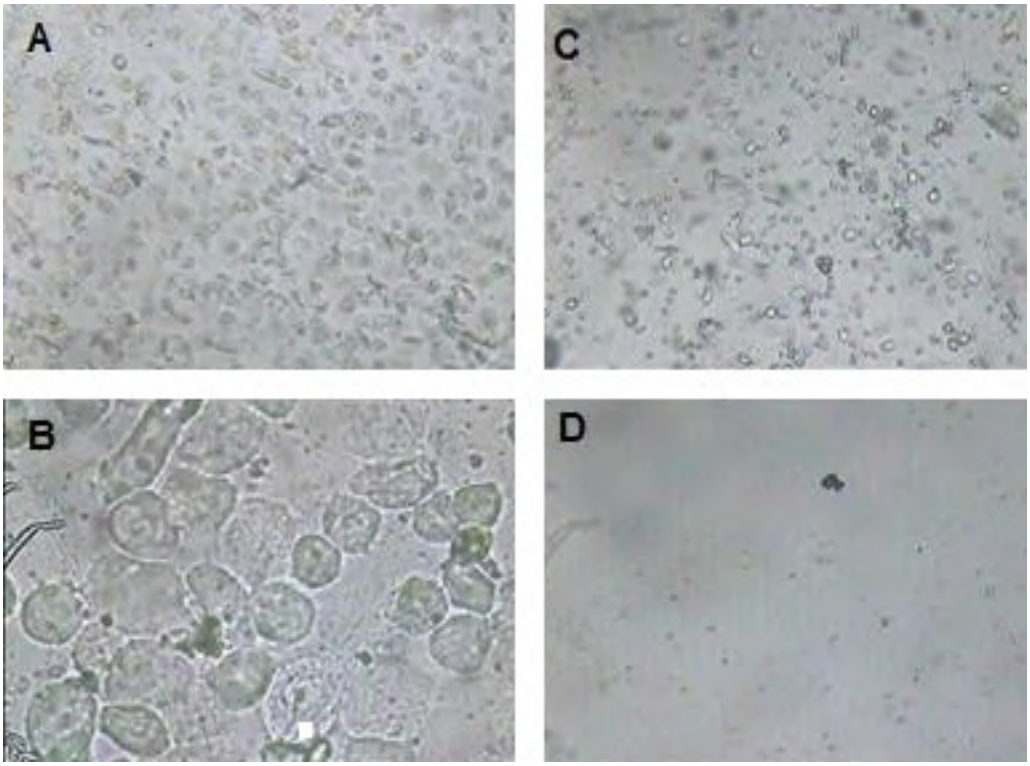

Fig. 2.- Stages of estrous cycles in rats pipette smears unstained with original microscope (x100). **A.** Estrous: large cornified cells inclumps. **B.** Metaestrous: large numbers of leucocytes with smaller numbers of non- nucleated epithelial cells. **C.** Diestrous: mainly leucocytes but with small number of epithelial and cornified cells. **D.** Proestrous: epithelial cells - mostly rounded but some cells showing early stages of cornification of approaching estrous.

then cleared twice in xylene for 3 hours before being impregnated in molten paraffin wax at 60°C for 3 hours with two changes of wax. The ovaries that had been impregnated with wax were now embedded in paraffin wax. The ovaries were embedded by inserting one half from above and the other half from below. Three 5 µm thick sections were taken at different levels in each half of the ovaries using a rotary microtome, then mounted on slides and dried in a hot plate at 40°C. The ovaries section slides were dewaxed with xylene, then removed with absolute alcohol I and II, 95% alcohol, 70% alcohol, and finally water for staining (Culling, 1975).

Haematoxylin and Eosin staining

After hydration, ovarian sections were transferred to haematoxylin and held for 10 minutes, then slides were transferred to a slide washing tray and washed until blue, then placed in flowing tap water for around 10 minutes at pH 8. After bluing the sections, they were dipped in acid alcohol for a few seconds, agitated, and then returned to the slide washing tray until they turned blue again. The slides were counter-stained for 2 minutes in 1 percent eosin and then washed in water to separate the eosin stain. The stained slides are now dehydrated for 10 to 15 seconds in various grades of alcohol, then cleaned for 10 to 15 seconds in xylene, then mounted with DPX and a cover slip (Culling, 1975). Following that, the slides were examined under a light microscope and photomicrographs (Olympus BX51, Japan) were obtained at various magnifications for study.

Statistical analysis

All the results were expressed as Mean ± SEM. The statistical analysis was carried by one-way ANOVA followed by Tukeys multiple comparison tests using SPSS 20.0 version, $P < 0.05$ was considered as significant.

RESULTS

In the present study the values of LH, FSH, estradiol, testosterone, progesterone and histological observations of all the experimental groups were compared with vehicle control group and PCOS group animals.

Follicle stimulating hormone (mIU/mL)

The mean ± SEM of serum concentration of FSH level was noted and shown in the Fig. 3, PCOS group rats shown significant ($p<0.001$) reduction in the level of FSH when compared to vehicle control group. EAR 400 mg/kg and SAPO 40mg/kg alone treated group rats' FSH level was found to be similar to that of the vehicle control group. EAR 200 mg/kg treated to PCOS rats had shown that FSH level was increased but not significant, compared with PCOS group. Treatment with EAR 400 mg/kg, SAPO 20 mg/kg and SAPO 40 mg/kg to PCOS rats showed significant ($p<0.001$) increased FSH level when compared to the PCOS group rats. One-way ANOVA showed that there was a statistically significant difference between the groups ($F=16.60$, $p<0.001$).

Luteinizing hormone (mIU/mL)

The LH serum level mean ± SEM are shown in Fig. 4; in PCOS group rats there was a significant increase ($p<0.001$) in the level of LH compared to vehicle control group. EAR 400 mg/kg and SAPO 40 mg/kg alone treated rats LH level was found to be similar that of vehicle control group. Treatment with EAR 400 mg/kg ($p<0.001$), SAPO 20 mg/kg ($p<0.01$) and SAPO 40 mg/kg ($p<0.01$) in PCOS-induced rats showed significant decrease in the level of LH when compared to the PCOS group. EAR 200 mg/kg treated to PCOS-induced rats had shown that the LH level was altered but not significant compared to the PCOS group and vehicle control group. One-way ANOVA showed that there was a statistically significant difference between the groups. ($F=5.717$, $p<0.001$).

Estrogen (pg/mL)

It can be seen from the Fig. 3, mean ± SEM of estrogen levels. It can be noticed that in PCOS group there is significant ($p<0.001$) reduction in the level of estrogen when compared to vehicle control group. EAR 400 mg/kg and SAPO 40 mg/kg alone treated group rats' estrogen was found to be similar compared to the vehicle control group. Treatment with EAR 400 mg/kg, SAPO 20 mg/kg and SAPO 40 mg/kg in PCOS rats showed significant ($p<0.01$) increase in the level of estrogen when compared to the PCOS group. One-way ANOVA showed that there was a statistically significant difference between the groups ($F=12.99$, $p<0.001$).

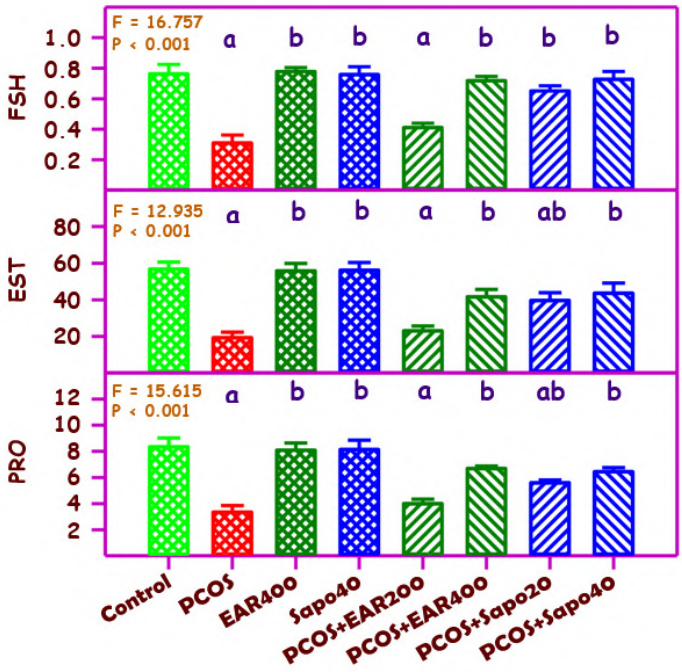

Fig. 3.- The effect of ethanolic extract of Asparagus racemosus (EAR) and its active component saponin (SAPO) in fructose and letrozole induced poly cystic ovary syndrome (PCOS). 20, 40, 200 and 400 are doses per kilogram body weight. Values are mean ± SEM (n = 6 each). Follicle stimulating hormone (FSH) (IU/mL); Estrogen (ngl/mL); Progesterone (ngl/mL). The 'F' and 'P' values are by one way ANOVA with Tukey multiple comparison test. [a] significantly different from vehicle control, [b] significantly different from PCOS.

Testosterone (g/dL)

Fig. 4 shows the mean values of testosterone across the study groups**.** The serum testosterone level increased significantly ($p<0.001$) in PCOS group compared to vehicle control group. EAR 400 mg/kg and SAPO 40 mg/kg alone treated group rat's testosterone were found to be similar compared to the vehicle control group. EAR 200 mg/kg treatment to PCOS rats has not significantly decrease the level of testosterone compared to the PCOS group. Treatment with EAR 400 mg/kg, SAPO 20 mg/kg and SAPO 40 mg/kg to PCOS rats showed significant ($p<0.001$) decrease in the level of testosterone when compared to the PCOS group. One-way ANOVA showed that there was a statistically significant difference between the groups ($F=9.086$, $p<0.001$).

Progesterone (ng/mL)

The mean values of progesterone were shown in Fig. 3. In PCOS group there was a significant ($p< 0.001$) reduction in the level of progesterone compared with vehicle control group. Treatment with EAR 200 mg/kg was not statistically significant with PCOS group. Treatment with EAR 400 mg/kg, SAPO 20 mg/kg and SAPO 40 mg/kg in PCOS rats showed significant ($F=15.32$, $p<0.001$) increase in the level of progesterone when compared to the PCOS group.

Effect of ethanolic extract of AR and SAPO on histology of ovaries

Light microscopic images (40× and 10×) of ovary sections from the vehicle control group, EAR 400 and SAPO 40 (Fig. 5) showed congested vascular spaces with spindle-shaped cells in the medulla. The cortex showed primary and secondary follicles with aggregation of granulosa cells and scanty follicular antrum; few follicles showed intact oocyte; the corpus luteum contains uniform round cells with abundant eosinophilic cytoplasm. In PCOS group (Fig. 6) the medulla and cortex showed multiple follicular cysts of varying sizes with diminished granulosa cells and increased follicular antrum, some atretic follicles and few follicles contain degenerated oocytes. The corpus luteum also showed atrophic changes. After-treatment with EAR and SAPO leads to disappearance of cysts and appearance of corpus luteum and healthy follicles. Sections of EAR 200 mg/kg treatment in PCOS rats exhibited follicles

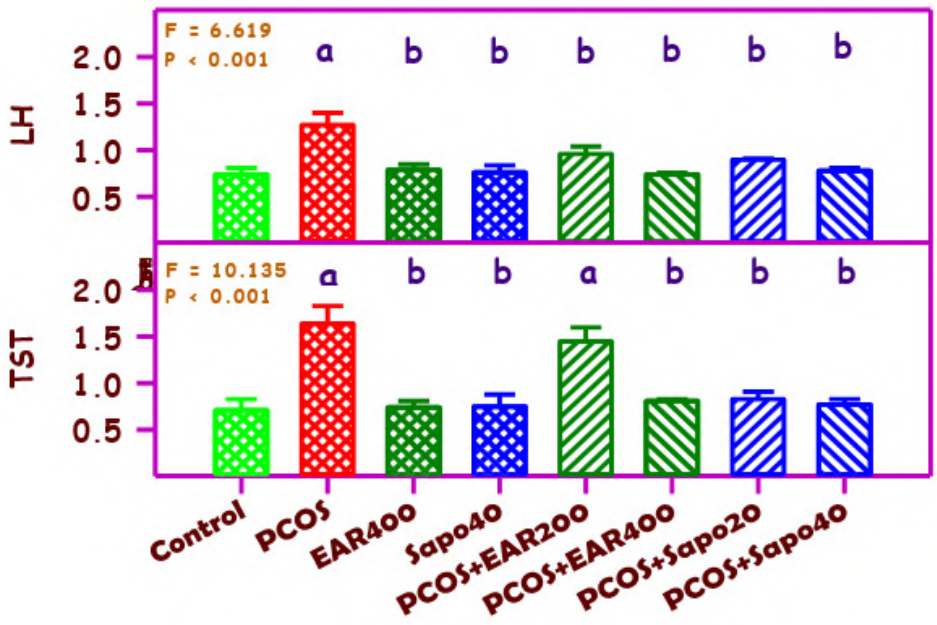

Fig. 4.- The effect of ethanolic extract of Asparagus racemosus (EAR) and its active component saponin (SAPO) in fructose and letrozole induced polycystic ovary syndrome (PCOS). 20, 40, 200 and 400 are doses per kilogram body weight. Values are mean ± SEM (n = 6 each). Luteinizing Hormone (LH) (IU/mL);Testosterone (ngl/dL). The 'F' and 'P' values are by one way ANOVA with Tukey multiple comparison test. [a] significantly different from vehicle control, [b] significantly different from PCOS.

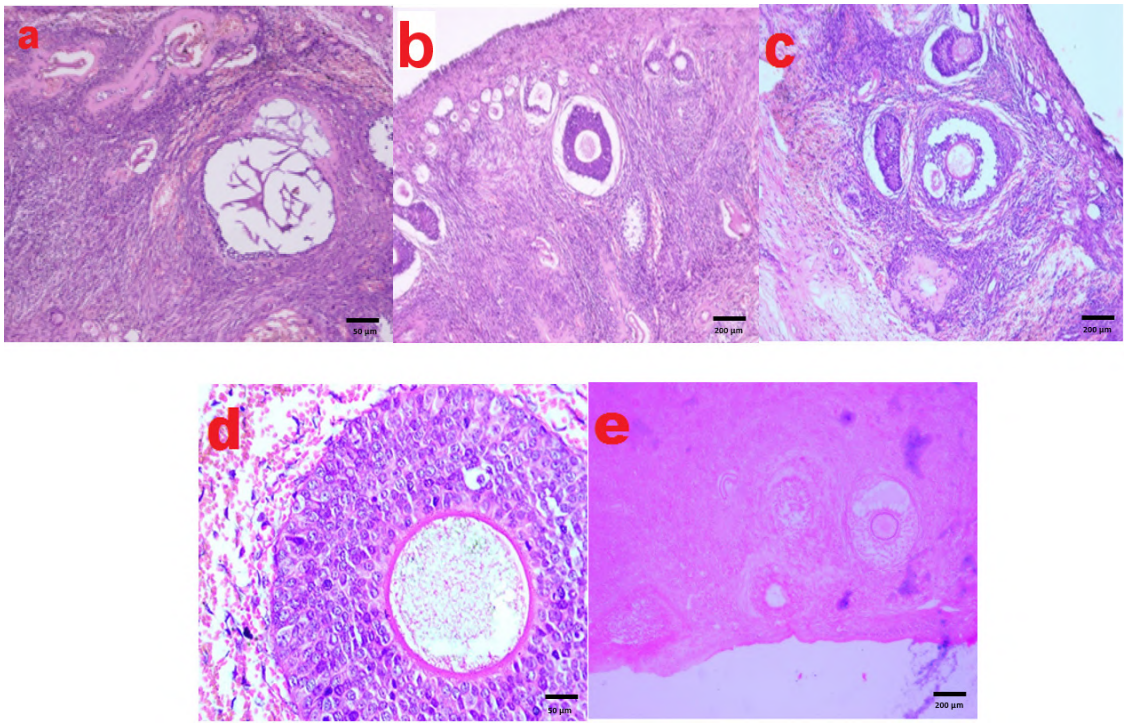

Fig. 5.- Hematoxylin and Eosin-stained microscopic images of vehicle control and drug control group. **a.** congested vascular spaces with spindle shaped cells in medulla. The cortex showed **b.** primary and **c.** secondary follicles with **d.** aggregation of granulosa cells and **e.** scant follicular antrum few follicles showed intact oocyte. Scale bars: a, d = 50 µm.; b, c, e = 200 µm.

larger in size and few corpora lutea (Fig. 7). Cysts were absent and normal-sized healthy follicles at different developmental stages with oocytes were found in section from EAR 400 mg/kg treated PCOS rats (Fig. 7). Sections from SAPO 20 mg/kg and SAPO 40 mg/kg administered PCOS rats show many corpora lutea and antral follicles with clearly differentiated oocyte, granulosa cell layer, corona radiate, cumulus oophorus and thecal cells were observed (Fig. 8).

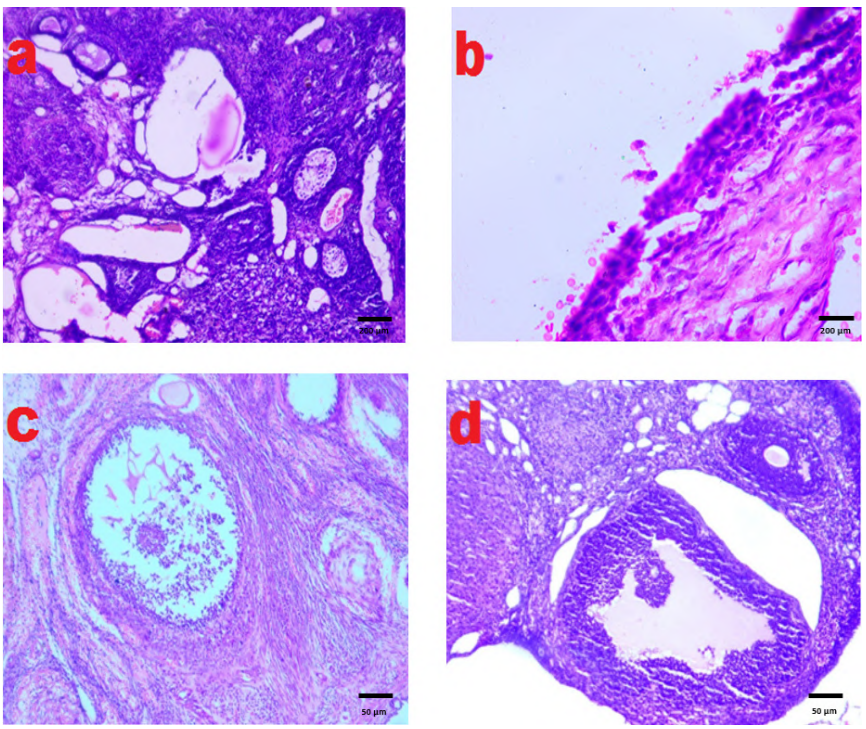

Fig. 6.- Hematoxylin and Eosin-stained microscopic images in PCOS group. **a.** medulla and cortex showed multiple follicular cysts of varying sizes, **b.** with diminished granulosa cells, **c.** some atretic follicles and few follicles contain degenerate oocyte and **d.** increased follicular antrum. Scale bars: a, b = 200 µm.; c, d = 50 µm.

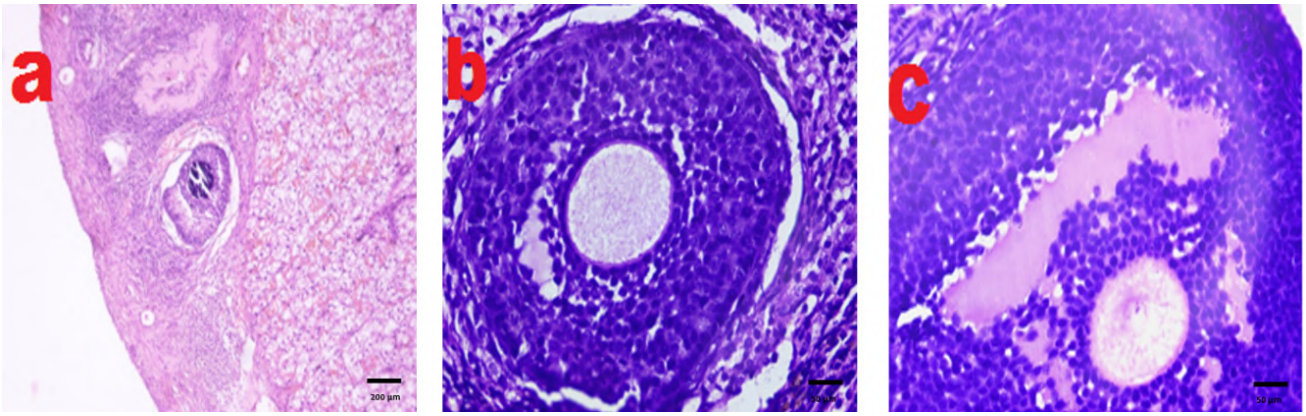

Fig. 7.- Histopathological changes of ovary after treatment with EAR200 and EAR400 in PCOS rats. **a.** appearance of corpora lutea, **b.** appearance of new follicle, **c.** decreasing follicular cyst. Scale bars: a, b = 200 µm.; c = 50 µm.

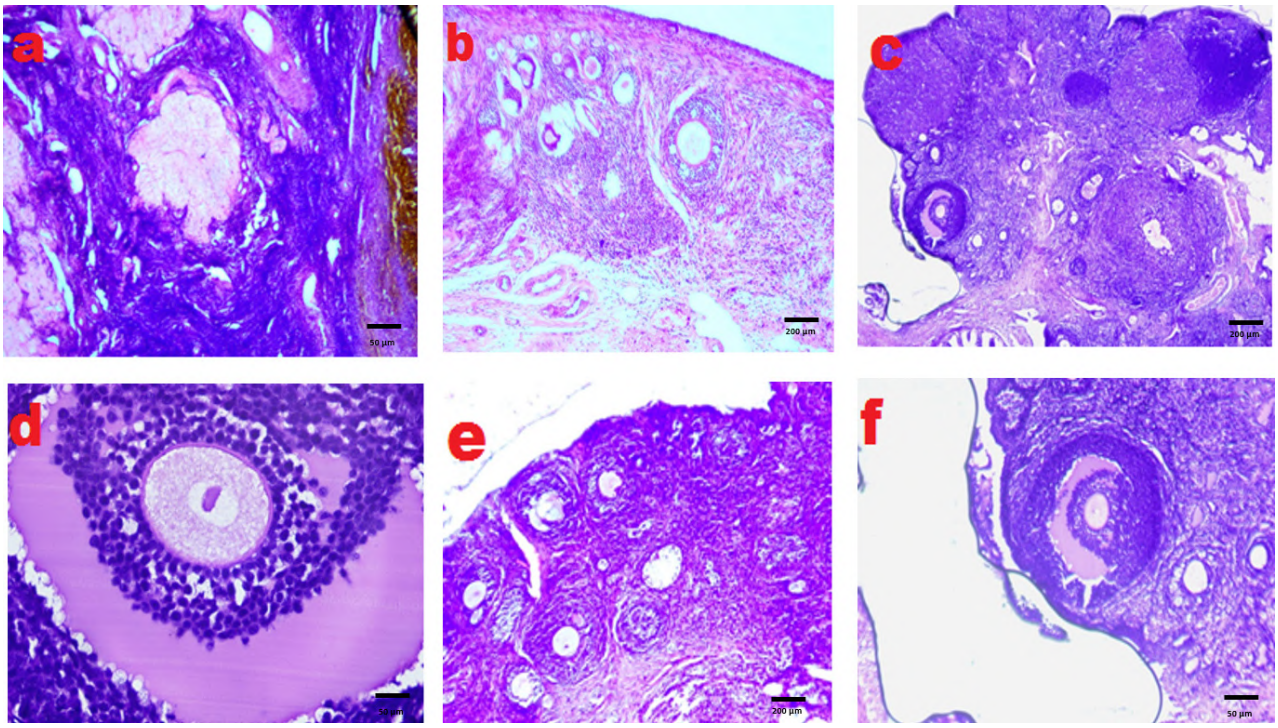

Fig. 8.- Histopathological changes of ovary after treatment with SAPO20 and SAPO40 in PCOS rats. **a.** appearance of numerous corpus luteum, **b.** cortex with many new follicles, **c.** cortex with varying no of corpora lutea, **d.** decreasing of pyknotic granulosa cells, **e.** disappearance of cyst, and **f.** visible granulosa cell layer. Scale bars: a, d, f = 50 µm.; b, c, e = 200 µm.

DISCUSSION AND CONCLUSIONS

PCOS has a wide range of clinical manifestations, including oligomenorrhea and hyperandrogenism, which can lead to metabolic dysfunction (Dickerson et al., 2010). The phenotype PCOS was created in this study, and the effects of EAR roots on the development of follicular growth and the improvement of this disease were investigated using hormonal and histological observations. The current study measured five hormonal parameters: FSH, LH, estradiol, progesterone, and testosterone. The current study found that PCOS increased testosterone and LH levels while decreasing FSH, estrogen, and progesterone levels in PCOS rats. Treatment with EAR and SAPO can increase serum levels of FSH, estrogen, and progesterone while decreasing serum levels of LH and testosterone. In addition, the number of ovarian follicles was found to be lower in the PCOS group of rats. According to the findings, dose-dependent EAR and SAPO treatment restores the hypothalamic-pituitary-gonadal axis hormone imbalance in PCOS rats. Among the various drug doses, the most effective is SAPO 40 mg/kg, which causes an increase in FSH, estrogen, and progesterone while decreasing LH and testosterone levels.

One of the most important diagnostic criteria for PCOS is a change in hormone levels. In some cases, the serum FSH level in PCOS does not change (Durant et al., 2009), and hyperandrogenism and increased serum LH levels are very common (Arifet al., 2016). In the case of PCOS, it could be an increase in testosterone and LH secretion and a decrease in FSH hormone secretion (Karampoor et al., 2014). One possible explanation for sex hormone changes in PCOS is a lack of aromatase enzyme in the ovary, which could increase androgen concentration (Requena et al., 2008).

We used fructose and letrozole to create a PCOS model in rats for 28 days in this study. Letrozole inhibits aromatase activity, resulting in an increase in ovarian androgens by preventing androgens from being converted to estrogens, resulting in hyperandrogenism, a defining feature of PCOS with clinical manifestations of elevated levels of testosterone, increased levels of LH, and decreased levels of FSH. It should also be noted that serum progesterone and estradiol levels were reduced nearly two-thirds of the time in the PCOS group in the current study. Letrozole inhibits testosterone aromatization to estradiol, as previously reported (Gnanadesigan et al., 2014). Letrozole-induced hormonal imbalance resulted in an irregular and/or prolonged estrus cycle in our study. Other studies have found similar results, which support our findings (Maharajan et al., 2010). In light of these findings, female rats were given letrozole, a non-steroidal aromatase inhibitor, along with fructose, which causes increased insulin resistance and hyperinsulinemia. Compensatory hyperinsulinemia is a major contributor to the development of metabolic abnormalities and high androgen levels in women with PCOS (Legro et al., 2013). As a result, our PCOS rat model exhibited all hormonal imbalances that occur in PCOS women, and it is the first model that mimics the real-life situation.

Anovulation is also characterized by low progesterone and estrogen levels, which results in irregular menstrual cycles (Srivastava et al., 2008). In our study, progesterone levels decreased, but treatment with EAR and SAPO increased progesterone and estradiol levels in a dose-dependent manner. Both SAPO 40 mg/kg and EAR 400 mg/kg are extremely effective at increasing progesterone and estradiol levels. AR's previously reported phytestrogenic activity was confirmed by this discovery (Gopumadhavan et al., 2005). Phytestrogens are plant-derived compounds that have estrogen-like properties. The presence of phytestrogens such as phytosterol, saponins, phenols, and flavonoids was discovered in the phytochemical analysis of EAR, demonstrating the efficacy of AR in the treatment of PCOS. This phytestrogenic activity is shared by the active components of AR of steroidal sapogenins such as diosenin, gitogenin, chlorogenin, and ruscogenin; thus, steroidal saponins with hormone-like actions in the body (Anderson et al., 1997). These results indicated that EAR and SAPO had phytestrogenic activity.

Phytestrogens have been shown to bind to two types of estrogen receptors ERα and ERβ, and acts as a pure estrogen antagonist by stimulating Gonadotropin releasing hormone secretion (Osaki et al., 2003) Steroid saponins such as sarsaponin, protodioscin, and diosgenin are the most likely estrogenic components extracted from asparagus roots (Shao et al., 1997). The mechanism of action of the EAR and SAPO may be due to the presence of phytoestrogen. It is thought to be similar to the standard drug clomiphene citrate in normalization of the hormonal level and induction of ovulation. Thus, the current study suggested that the SAPO and EAR both promote regularity of ovarian cycle by correcting hypothalamus pituitary axis function, which in turn may reduce ovarian cyst in rats having PCOS this finding was well supported by (Barton, 2013). Studies on plants with similar compositions to EAR found that plants containing flavonoids and phenolic compounds could help to maintain a natural balance of estrogen and progesterone during the ovarian cycle, and that these plants have specific pharmacological-physiological effects on rebalancing increased or decreased levels of sex hormones. As a result, it is possible that EAR and SAPO could restore estrogen and progesterone hormone balance in PCOS-induced rats via flavonoids and antioxidant activity of AR, which contradicts previous research findings (Liu et al., 2004). As a result, there was a dose-

dependent increase in progesterone and estrogen levels in the groups that received EAR and SAPO.

The positive effects of AR root extract on the folliculogenesis process were reported in a study performed in young females with a dose of 100 mg/kg; it may increase ovarian weight, increase FSH hormones, and may enhance folliculogenesis, as evidenced by a histological study of immature female rats' ovaries (Kalia et al., 2003). Researchers have linked the stimulatory effects of EAR on the ovary to the presence of compounds such as glycosidal flavonoids, saponins, alkaloids, and steroidal compounds (Sharma et al., 2013). Previous research on LH and FSH levels changes in PCOS found a link between an increased level of LH and a decreased level of FSH. Increased LH hormone levels stimulate ovarian theca cells, which in turn stimulates androgen production. (Loffler et al., 2000). Furthermore, androgens may increase the number of FSH receptors in PCOS, resulting in a decrease in the concentration of this hormone and an increase in the level of LH (Requena et al., 2008). In the current study, increased LH levels and a significant decrease in FSH levels were observed in PCOS group rats due to excess antigen production, which causes LH levels to rise and FSH levels to fall. Furthermore, these changes are most likely the result of a mutation in the aromatase enzyme (Requena et al., 2008). Treatment with SAPO 40 mg/kg improved the level of LH and FSH, resulting in an increase in weight and the number of ovary follicles. This study found that SAPO 40 mg/kg improved folliculogenesis when compared to the PCOS group. SAPO 20 mg/kg and EAR 400 mg/kg treatment of PCOS rats was also significant in restoring LH, FSH levels and improving folliculogenesis. EAR and SAPO were found to have a positive and dose-dependent effect on serum LH and FSH levels in PCOS.

AR are high in amino acids and aspartic acid and arginine derivatives. Aspartic acid stimulates gonadotropin-releasing hormone and LH secretion. Tests revealed that this amino acid regulates LH synthesis via looped guanosine monophosphate as a second messenger in the pituitary gland (Pinilla et al., 2001). Asparagus arginine is also converted to nitric oxide, which is one of the most important factors controlling LH and FSH release (Sato et al., 2000). These findings were robustly supported. AR may also act through its amino acid content, eventually resolving the hormonal imbalance.

There was a significant increase in testosterone levels in the PCOS group in the current study. Letrozole inhibited the conversion of androgen substrates into estrogen, resulting in androgen accumulation. This increased testosterone concentration in peripheral blood may be the cause of the rats' prolonged diestrous phase and increased body weight in the study (Abdulghani et al., 2012). Serum testosterone levels were normalized after treatment with EAR 400 mg/kg, SAPO 20 mg/kg, and SAPO 40 mg/kg. The decrease in testosterone concentration in SAPO 40 mg/kg treated rats reflects decreased androgen biosynthesis by the ovary and resulted in a lower percentage of vaginal diestrous days and body weight in PCOS rats, which could be attributed to their ability to lower testosterone concentration in the peripheral blood. Reduced estrogen production caused by aromatase inhibition can result in increased LH secretion in the hypothalamus and pituitary, most likely due to estrogen negative feedback. Previous research has shown that AR reduces testosterone levels in male rats by interfering with steroid production in the adrenal glands (Mishra et al., 2013). SAPO 40 mg/kg treatment resulted in significant testosterone recovery, a good anti-androgenic effect by lowering elevated androgen levels, and prevention of ovarian cell dysfunction in PCOS to improve fertility.

Aside from the positive effects of restoring hormonal balance between gonadotropin and ovarian hormones in alleviating PCOS symptoms, the administration of various antioxidants such as vitamin E and selenium is also regarded as a common treatment approach for this syndrome (Amini et al., 2015). EAR is high in natural antioxidants, including vitamins and minerals like zinc and selenium (Karmakar et al., 2012). According to research findings, polycystic ovary syndrome causes an increase in reactive oxygen species (ROS) in ovarian tissue, and the balance between the oxidant and antioxidant systems is

disrupted. Natural growth of theca interstitial layer is required for normal ovarian function, and oxidative substances and free radicals interfere with regular growth and apoptosis in this layer. It has been established that there is a direct link between reduced oxidative stress and increased oocyte maturation in PCOS and infertile women (Shirsath et al., 2015).

Histopathological examination of ovaries from the PCOS group revealed sub-capsular cysts lined with a thin layer of granulosa cells and hyperplasia of theca cells, which was strikingly similar to human PCOS. Increased intra-ovarian androgen levels have been linked to abnormal follicular growth and an increase in follicular atresia. The PCOS group had a lower number of corpus luteum and developing follicles. Cystic follicles were significantly larger in size than other ovarian follicles with a clear antrum but no oocyte. When comparing PCOS follicles to control follicles, the thickness of the peripheral granulosa layer was reduced while the thickness of the theca layer was increased. Cysts were absent, and normal sized healthy follicles with oocytes were found in sections from the EAR 400 mg/kg, SAPO 20 mg/kg, and SAPO 40 mg/kg treatments, which resulted in the disappearance of cysts and a decrease in the incidence of pyknotic granulosa cells. Ovulation and normal estrous cyclicity were indicated by the presence of a variable number of corpora lutea. Follicles with oocytes and clear, visible granulosa cell layers at various stages of development were observed. The ovarian cortex appeared to be normal, with numerous follicles. These histological findings pointed to the presence of biologically active levels of FSH and LH in the PCOS group, as well as a lack of interplay between granulosa and theca cells, which would otherwise result in ovulation. Another study on the effects of AR extract on ovary tissue found that it increases the number of primary, secondary, and graafian follicles while decreasing the number of atretic follicles in rats (Verma et al., 2014).

Asparagus roots are high in calcium, magnesium, phosphorus, and zinc (Joham et al., 2015). Minerals found in follicular fluid regulate follicle growth and steroidogenesis. Minerals not only act as cofactors in various enzymatic activation systems for oocyte growth and maturation, but also influence ovarian function and fertility. Histological analysis in this study revealed an increase in the number of ovarian follicles and corpus luteum, as well as an increase in the number of atretic follicles in the SAPO-treated groups. This finding corresponds to an increase in hypothalamic-pituitary-gonadal axial hormones.

FSH influences the growth and development of ovarian follicles through the proliferation and differentiation of granulosa cells. Granulosa cells proliferate slowly in the early stages of follicular development, but granulosa cells in preantral follicles respond to FSH stimulation and secrete large amounts of estradiol. As a result, an increase in estrogen due to an increase in follicle number was not unexpected in the current study. The greatest increase in Graffian follicles was seen in the experimental group that received 40 mg/kg of SAPO. This group also had the highest estrogen level. LH affects theca corpus luteum cells, which increases progesterone hormone synthesis (Krishnamurthy et al., 2009). As a result of the increased number of corpora lutea, an increase in progesterone levels was not unexpected according to increased number of corpora lutea in this study. The findings of this study indicated that oral administration of EAR 400 mg/kg and SAPO 40 mg/kg could alleviate PCOS-related symptoms. It appears that consumption of SAPO at a dose of 40 mg/kg reduces levels of LH and testosterone while increasing levels of FSH, estrogen, and progesterone hormones. Because of the hormonal balancing nature of these drugs, EAR 400 mg/kg and SAPO 40 mg/kg treated rats had a lower number of cystic follicles and a higher number of corpus luteum. In PCOS rats, this results in a normal process of folliculogenesis and ovulation. In the current study, we discovered that SAPO 40 mg/kg is superior to EAR 400 mg/kg treatment.

ACKNOWLEDGEMENTS

The authors sincerely thank the management and staff members of their department for the valuable help offered for this study.

REFERENCES

ABDULGHANI M, HUSSIN AH, SULAIMAN SA, CHAN KL (2012) The ameliorative effects of Eurycoma longifolia Jack on testosterone-induced reproductive disorders in female rats. *Reprod Biol*, 12(2): 247-255.

AMINI L, TEHRANIAN N, MOVAHEDIN M, RAMEZANI TF, ZIAEE S (2015) Antioxidants and management of polycystic ovary syndrome in Iran, A systematic review of clinical trials. *Iran J Reprod Med*, 13(1): 1-8.

ANADU U, NDEFO A, EATON A, ROBINSON MG (2013) Polycystic ovary syndrome. *Pharm Therap*, 38(2): 338-355.

ANDERSON JJB, GARNE SC (1997) A pilot study on the breast development in female Wistar rats using an indigenous herbal preparation by topical application. *Nutri Res*, 17(10): 1617.

ARIF M, THAKUR SC, DATTA K (2016) Implication of thymoquinone as a remedy for polycystic ovary in rat. *Pharm Biol*, 54: 674-685.

BARTON D, DOULA CH (2013) How to use fertility herbs to enhance your fertility naturally. Available from http://E;/pcod/fertilityherbsinfertilitytreatmentpregancyherbs.htm. Accessed october 1:14.

CULLING CFA (1975) Handbook of Histopathological and Histochemical techniques, 3rd edn. Oxford University Press, New York, 49(213): 491-492.

DICKERSON EH, CHO LW, MAGUINESS SD, KILLICK SL, ROBINSON J, ATKIN SL (2010) Insulin resistance and free androgen index correlate with the outcome of controlled ovarian hyperstimulation in non-PCOS women undergoing IVF. *Hum Reprod*, 25: 504-509.

DURANT EM, LESLIE NS, CRITCH EA (2009). Managing polycystic ovary syndrome: a cognitive behavioral strategy. *NursWomens Health*, 13: 292-300.

GANDHARE B, KAVIMANI S, RAJKAPOOR B (2013) Acute and subacute toxicity study of methanolic extract of *Ceiba pentandra*(Linn.) on rats. *J Sci Res*, 5 (2): 315-324.

GOPUMADHAVAN S, VENKATARANGANNA MV, RAFIQ M, MADHUMATHI BG, MITRA SK (2005) Evaluation of the estrogenic effect of Menosan using the rat models of uterotrophic assay. *Medicine Update*, 13: 37-41.

GNANADESIGAN E, KUMAR R, MANOHAR U, BALASUBRAMANIAN T (2014) Study of ovarian morphology in high fructose fed mice. *J Biomed Pharm Res*, 3(5): 8-17.

HAYES PY, JAHIDIN AH, LEHMANN R, PENMAN K, KITCHING W, DE VOSS JJ (2008) Steroidal saponins from the roots of asparagus racemosus. *Phytochemistry*, 69: 796-804.

HAYWOOD A, BONE K (2004) Phytotherapy for polycystic ovary syndrome (PCOS). A phytotherapeutics perspective. *Phytother Res*, 46(1): 1-6.

JOHAM AE, TEEDE HJ, RANASINHA S, ZOUNGAS S, BOYLE J (2015) Prevalence of infertility and use of fertility treatment in women with polycystic ovary syndrome: data from a large community-based cohort study. *J Womens Health,* 24(4): 299-307.

KALIA V, JADAV AN, BHUTTANI KK (2003) In vivo effect of asparagus racemosus on serum gonadotrophin levels in immature female wistar rats. 2nd World Congress of Biotech. Dev. of herbal med. nbri. lukhnow., pp 40.

KARMAKAR U, BISWAS S, CHOWDHURY A, RAIHAN S, AKBAR M, MUHIT M, MOWLA R (2012) Phytochemical investigation and evaluation of antibacterial and antioxidant potentials of *Asparagus racemosus*. *Int J Pharmacol*, 8: 53-57.

KARAMPOOR P, AZARNIA M, MIRABOLGHASEMI G, ALIZADEH F (2014) The effect of hydroalcoholic extract of fennel (*foeniculum vulgare*) seed on serum levels of sexual hormones in female Wistar rats with polycystic ovarian syndrome (PCOS). *Arak Med Univ J*, 17: 70-78.

KRISHNAMURTHY MS, HEBBAR (2009) Polycystic ovarian syndrome: Ayurvedic treatment, remedies, diet. *Easy Ayurveda, Health and Lifestyle blog*.

LEGRO RS, ARSLANIAN SA, EHRMANN DA (2013) Diagnosis and treatment of polycystic ovary syndrome: an Endocrine Society clinical practice guideline. *J Clin Endocrinol Metab*, 98: 4565.

LIU J, BURDETTE JE, SUN Y, DENG S, SCHLECHT S, ZHENG W (2004) Isolation of linoleic acid as an estrogenic compound from the fruits of vitex agnus castus L. (chaste-berry). *Phytomedicine*, 11: 18-23.

LOFFLER S, AUST G, KOHLER U, SPANEL-BOROWSKI K (2001) Evidence of leptin expression in normal and polycystic human ovaries. *Mol Hum Reprod*, 7: 1143-1149.

MARSTON A, MAILLARD M, HOSTETTMANN K (1997) The role of TLC in the investigations of medicinal plants of Africa, South America and other tropical regions. *GIT Lab J*, 1: 36-39.

MAHARAJAN H, PADAMNABHI S, LAXMIPRIYA NP (2010) Effect of aloebarbadensis mill. formulation on letrozole induced polycystic ovarian syndrome rat model. *J Ayurveda Integr Med*, 1(4): 273-279.

MISHRA PK, SINGH P, PRAKASH B, KEDIA A, DUBEY NK, CHANOTIYA CS (2013) Essential oil components as plant-based preservatives against fungi that deteriorate herbal raw materials. *Int Biodegrade*, 80: 16-21.

NAGARATHNA PKM, RAJAN PR, KONERI R (2014) A detailed study on Polycystic Ovary syndrome and its treatment with natural products. *Int J Toxicol Pharm Res*, 5(4): 109-120.

OSOSKI AL, KENNELLY EJ (2003) Phytoestrogens: a review of the present state of research. *Phytother Res*, 17: 845-869.

PINILLA L, GONZÁLEZ LC, TENA-SEMPERE M, BELLIDO C, AGUILAR E (2001) Effects of systemic blockade of nitric oxide synthases on pulsatile LH, prolactin, and GH secretion in adult male rats. *Horm Res*, 55: 229-235.

REQUENA A, HERRERO J, LANDERAS J, NAVARRO E, NEYRO JL, SALVADOR C (2008) Use of letrozole in assisted reproduction: a systematic review and meta-analysis. *Hum Reprod Update*, 14: 571-582.

SATO Y, SUKANMAMOTO T (2000) Effect of nitric oxide stimulation on the brain. *Drugs Today*, 36: 83-92.

SHARMA A, SHARMA V (2013) A Brief review of medicinal properties of Asparagus racemosus (Shatawari). *Int J Pure Applied Biosci*, 1(2): 48-52.

SHAO Y, POOBRASERT O, KENNELLY EJ, CHIN CK, HO CT, HUANG MT (1997) Steroidal saponins from Asparagus officinalis and their cytotoxic activity. *Plant Med*, 63: 258-262.

SHIRSATH A, AUNDHAKAR N, KAMBLE P (2015) Study of oxidative stress and antioxidant levels in polycystic ovarian disease. *Int J Health Care Biomed Res*, 3(4): 16-24.

VERMA SP, TRIPATHI VC, DAS P (2014) Asparagus racemosus leaf extract inhibits growth of UOK 146 renal cell carcinoma cell line: simultaneous oncogenic PRCCTFE3 fusion transcript inhibition and apoptosis independent cell death. *Asian Pac J Cancer Prev*,15: 1937-1941.

ZHANG QH, WU CF, DUAN L, YANG JY (2008) Protective effects of total saponins from stem and leaf of Panax ginseng against cyclophosphamide-induced genotoxicity and apoptosis in mouse bone marrow cells and peripheral. *Food Chem Toxicol*, 46: 293-302.

Effect of carnosine on ovarian follicle in rats exposed to electromagnetic field

Ayla Arslan[1], Esra Balcioğlu[2], Mehtap Nisari[1], Betül Yalçin[2], Menekşe Ülger[2], Emel Güler[3], Gökçe Bağcı Uzun[4], Niyazi Acer[5]

[1] Erciyes University Faculty of Medicine, Department of Anatomy, Kayseri, Turkey

[2] Erciyes University Faculty of Medicine, Department of Histology and Embryology, Kayseri, Turkey

[3] Cumhuriyet University Faculty of Medicine, Department of Physical Medicine and Rehabilitation. Algology, Sivas, Turkey

[4] Turgut Ozal University Faculty of Medicine, Department of Anatomy, Malatya Turkey

[5] Arel University Faculty of Medicine, Department of Anatomy, Istanbul, Turkey

SUMMARY

The electromagnetic field (EMF) has an effect on various organs, including the female reproductive system. The purpose of this study was to evaluate the impact of carnosine on ovarian follicle number and diameter in rats exposed to a 900 Megahertz (Mhz) electromagnetic field. In this study, six different groups were used. 40 female rats divided into groups were evaluated. The ovaries of the rats were removed at the end of the study. Routine histological procedures were performed on ovarian tissues. Follicle number and diameter of all groups were calculated and evaluated under the light microscope. When primary follicle number and diameters were compared statistically among the groups, there was a remarkably meaningful difference between the EMF group and the control, 20 mg carnosine and EMF+20 mg carnosine groups ($p<0.05$). There were significant irregularities in the structure of the oocyte and the granulosa cells surrounding the oocyte, especially in the EMF-treated groups. However, the structure of the oocyte and the granulosa cells surrounding the oocyte in the EMF+20 mg carnosine group showed a more regular structure compared to the EMF group. In this study, it can be concluded that the number and diameter of ovarian follicles decreased in rats exposed to electromagnetic field and 20 mg of carnosine may prevent damage caused by EMF.

Key words: Electromagnetic field – Ovarian – Follicle number – Follicle diameter – Carnosine

INTRODUCTION

With the advancement of technology, the electromagnetic field (EMF) effect of many devices that facilitate daily life and the widespread use of these devices adversely affect human health (Feychting et al., 2005). People are constantly exposed to harmful environmental agents, including electromagnetic fields from household appliances (e.g., television, Wi-Fi and microwaves), diagnosis equipment (e.g., magnetic resonance imaging, tomography), industrial tools, smartphones and electronic devices. Also, the recent use of 6 billion mobile phones suggests that EMF is perhaps one of the most hazardous

Corresponding author:
Ayla ARSLAN, PhD, Dr. Erciyes University Faculty of Medicine, Department of Anatomy, 38039, Kayseri, Turkey. Phone: +903522076666. E-mail: aaylaarslan@gmail.com - https://orcid.org/0000-0001-5859-7784

Submitted: May 28, 2022. **Accepted:** July 18, 2022

https://doi.org/10.52083/TESQ7230

environmental factors for humans (Davis et al., 2013). Studies on the impacts of mobile phones on human health have reported that EMF, which is often associated with mobile phone use, causes sleep problems (Huber et al., 2002), fatigue, headaches, and loss of concentration (Oftedal et al., 2000). Cell phones are the most common sources of EMF used near the human body. Kilgallon and Simmons (2005) found a significant reduction in sperm motility in men who kept their mobile phone on their hip or waist field, compared to those who kept their mobile phone elsewhere or did not use one. According to this study, it can be thought that the tissues close to the EMF resources are more impressed. In addition, some studies have shown that EMF causes oxidative stress and DNA damage, leading to deterioration of the structure and function of the cell (Odacı and Ozyılmaz, 2015).

In some animal studies, it was concluded that long-term cell phone use may cause a decrease in sperm development and production, thus reducing fertility in men (Kesari et al., 2011). In their study, researchers found that there was a decrease in Leydig cell numbers in male rats (Saygin et al., 2011). Some researchers have noted that exposure to EMF can lead to embryonic developmental disorders or infertility issues. In one study, it was found that exposure to EMF was associated with miscarriage in women (Belyaev et al., 2016). It has been noted that exposure to radiofrequency EMF during and after pregnancy and breastfeeding does not cause developmental abnormalities in offspring (Shirai et al., 2017). In animal studies, it was shown that EMF decreases the number of follicles in the ovaries (Gul et al., 2009), causes DNA damage in the endometrium and ovary (Diem et al., 2005), increases apoptosis and oxidative stress (Nikolova et al., 2005; Oral et al., 2006).

Carnosine is a histidine derivative, a multifunctional dipeptide synthesized endogenously in the body. It is found in high concentrations in tissues such as heart muscle, skeletal muscle, and brain (Yay et al., 2013). Studies have reported that carnosine has a protective effect on cells against oxidative damage, and that carnosine has antioxidant properties by binding metal ions and scavenging free radicals (Bakardjiev and Bauer, 2000; Brownson and Hipkiss, 2000; Kohen et al., 1988). Also, it has been indicated that carnosine has protective effects against ischemia in tissues and organs such as kidney, brain, myocardium, skeletal muscle and spinal cord (Albayrak et al., 2015; Aydin et al., 2015). *In vivo* studies, it has been reported that carnosine reduces ischemia-reperfusion injury in organs such as testis, brain and kidney (Fujii et al., 2005; Dobrotvorskaya et al., 2011).

Although various frequencies have been used on the ovarian follicles of EMF as a result of the literature review, there is no study yet investigating the effects of 900 Megahertz (MHz) EMF with carnosine application (Khoshbakht et al., 2021; Altındag et al., 2017). The Global Mobile Communication System (GSM)-900 communication system, which is generally, it has an operating frequency of 880–960 MHz, as in Europe and Turkey. Therefore, the purpose of the study was to evaluate the effect of carnosine on ovarian follicle number and diameter in rats exposed to a 900 Mhz electromagnetic field.

MATERIALS AND METHODS

Ethical procedures, Work Plan, Animals and Groups

The work protocol was evaluated and confirmed by the Erciyes University Experimental Animals Ethics Committee (Kayseri, Turkey) (approval number: 2013/82). After getting approval from Erciyes University, the procedures were implemented. Forty female Wistar Albino rats weighing 200-250 g, 16 weeks old, were provided by Erciyes University Experimental Animals Research Center (DEKAM, Kayseri, Turkey). Rats were held in a normal 22 ± 2 °C and 50% ± 5% humidity environment for 12 hours on a light/dark cycle and ventilated with an aspirator. Rats were fed a balanced diet and unlimited water. Rats were placed in normal clear polycarbonate cages. All described experimental and surgical procedures were performed at Erciyes University Experimental Animals Research Center (DEKAM, Kayseri, Turkey).

The animals used were divided into 6 groups without any discrimination. The groups were created as follows.

1. Control group (K): Not exposed to any treatment, EMF, or carnosine injection (n = 10).
2. 2 mg Carnosine group (2 mg car): Rats were not exposed to EMF, but only to carnosine injection (n=5). The rats in this group were injected intraperitoneally with carnosine between 11:00 and 12:00 every day.
3. 20 mg Carnosine group (20 mg car): Rats were not exposed to EMF, but only to carnosine injection (n=5). The rats in this group were injected intraperitoneally with carnosine between 11:00 and 12:00 every day.
4. Electromagnetic field group (EMFG): Rats were exposed to EMF 1 h daily over 28 days (900 MHz) (Onger et al., 2016) (n = 10). Rats were exposed to EMF between 11:00-12:00 every day (Turedi et al., 2016). The specific energy absorption rate (SAR) was approximately 0.008 W/kg for the whole body and 2 W W/kg locally for the head. In addition, the positions of the rats were changed daily during the exposure period (Ulubay et al., 2015).
5. EMFG +2 mg carnosine (EMFG+2 mg car): exposed to EMF (900 MHz) 1 h daily over 28 days (Kerimoglu et al., 2016) (n = 5). During the experimental period, 2 mg intraperitoneal carnosine was administered to this group 30 minutes before EMF exposure (Bae et al., 2013).
6. EMFG +20 mg carnosine (EMFG+20 mg car): exposed to EMF (900 MHz) for 1 hour per day for 28 days (Kerimoglu et al., 2016) (n = 5). During the experimental period, 20 mg intraperitoneal carnosine was administered to this group 30 minutes before EMF exposure (Bae et al., 2013).

After the experimental procedure, the rats were sacrificed and the number of ovarian follicle cells was counted by performing histological studies.

Exposure System

In the current study, the same exposure system design was used as in last studies (Bas et al., 2009). The exposure system used and the EMF application are explained in detail (Kerimoglu et al., 2016; Ragbetli et al., 2007). A special EMF exposure system consisting of a dipole antenna and a circular cage was used (Aslan et al., 2017). The electromagnetic power unit producing 900 MHz continuously regulated EMF (2 W peak output power and 1 ± 0.4 mW/cm^2 power volume) was made in TEKNOPARK Conformity Laboratory (Kayseri, Turkey). The average SAR rate was 2 W/kg and the peak SAR was calculated based on the model with force density indicators made using an EMF meter (Kayseri Technopark) (Bas et al., 2009). Rats were exposed to EMF using a dipole antenna (Bas et al., 2009). The heads of the rats were placed in the direction of the dipole antennae. The gap between the rat and antenna was 1 cm when the rat was placed perpendicular to the antenna. The longitudinal axis of the rats was placed perpendicular to one of the antennae (Bas et al., 2009). All reviews were blinded to the unbiased results obtained.

Histological Procedures

At the end of experimental work, right and left ovaries were removed under anesthesia (Ketolar 50 mg, Pfizer, Turkey). For histopathological examination, ovarian tissues obtained from control and experimental groups were fixed in 10% formaldehyde solution. After fixation, the tissues were embedded in paraffin. Hematoxylin Eosin routine histological (Table 1) follow-ups were performed by taking 5 µm thick sections from the paraffin blocks with a microtome. In order to see the general histological structure, the sections were stained with Masson's trichrome (MT) (Table 2) and examined under the Olimpus BX51 microscope and photographed. Evaluation parameters of follicles were evaluated according to Table 3.

Statistical analysis

All statistical analyses were done in SPSS 22 program. After testing the normality (Kolmogorov-Smirnov and Shapiro-Wilk) of the research data, comparisons between groups were made using the OneWay Analysis of Variance (ANOVA) for normally distributed variables, and multiple comparisons were made with the Tukey test in case of difference. In the variables that did not show normal distribution, comparisons

between groups were made using the Kruskal-Wallis Analysis, and in case of difference, multiple comparisons were made with the Mann Whitney U test. A p value of <0.05 was considered statistically meaningful.

Table 1. Light microscopy tissue preparation technique.

Sequence	Action taken	Duration	Sequence	Action taken	Duration
1	Tap water	1 hour	**7**	Absolute Alcohol	1 hour
2	50% Alcohol	1 hour	**8**	Absolute Alcohol	1 hour
3	%70 Alcohol	1 hour	**9**	Xylene	20 minutes
4	%80 Alcohol	1 hour	**10**	Xylene	20 minutes
5	%96 Alcohol	1 hour	**11**	Xylene	20 minutes
6	Absolute Alcohol	1 hour	**12**	Melted paraffin (60 °C)	1 night

Table 2. Masson's trichrome dyeing technique.

Sequence	Transaction Time	Duration	Sequence	Transaction Time	Duration
1	Oven (60°C)	2 hours	**18**	Phosphomolybdic acid	5 min
2	Xylene I	10 min	**19**	Drying	
3	Xylene II	10 min	**20**	Aniline blue	2-5 min
4	Xylene III	10 min	**21**	Distilled water	2-3 min
5	Absolu Alcohol I	5 min	**22**	%1 lyacetic acid	2 min
6	Absolu Alcohol II	5 min	**23**	%50 Alcohol	5 min
7	%96 Alcohol	5 min	**24**	%70 Alcohol	5 min
8	%80 Alcohol	5 min	**25**	%80 Alcohol	5 min
9	%70 Alcohol	5 min	**26**	%96 Alcohol	5 min
10	%50 Alcohol	5 min	**27**	Absolu Alcohol I	1 min
11	Stream	2 min	**28**	Absolu Alcohol II	2 min
12	Hematoxylin	5-8 min	**29**	Absolu Alcohol III	2 min
13	Stream	5 min	**30**	Xylene I	20 min
14	%1 acid alcohol	1-2 sec	**31**	Xylene II	20 min
15	Stream	1 min	**32**	Xylene III	20 min
16	Asit fuksin	5 min	**33**	Closure (Canada Balsam)	
17	Distilled water	2-3 min			

Table 3. Evaluation parameters of ovarian follicles.

Follicles to be counted	**Primordial follicle:** oocyte with a prominent nucleus and a squamous granulosa cell layer around it
	Primary follicle: oocyte with a prominent nucleus and a layer of cubic granulosa cells around it
	Preantral follicle: oocyte with a prominent nucleus and several layers of granulosa cells around it
	Secondary follicle: oocyte with a prominent nucleus, several layers of granulosa cells around it, and antrum within granulosa cells
	Tertiary follicle: oocyte with prominent nucleus observed pushed aside in the antrum

RESULTS

The statistical results of primary, preantral, secondary and tertiary follicle numbers of the experimental and control groups were given in Table 4. When the mean primary follicle numbers were compared statistically, it was determined that there was an important dissimilarity among the control group and both the 20 mg carnosine group and the EMF group ($p<0.05$). There was no dissimilarity among the mean primary follicle numbers of the groups given 2 mg carnosine and the groups given EMF+20 mg carnosine ($p>0.05$). But there was a statistically significant difference between the two groups and the EMF group ($p<0.05$). When the mean preantral follicle numbers were compared statistically, it was determined that there was no meaningful dissimilarity between the control and 20 mg carnosine groups and the other groups ($p<0.05$). But there was an important dissimilarity between the group exposed to 2 mg carnosine and the EMF group ($p<0.05$). When the mean secondary follicle numbers of the control and experimental groups were compared statistically, there was no dissimilarity among the groups ($p>0.05$). When a comparison was made between the groups in terms of tertiary follicle numbers, it was determined that the only dissimilarity was among the control group and the EMF group ($p<0.05$).

The statistical results of primary, preantral, secondary and tertiary follicle diameters of the experimental and control groups were given in Table 5. When primary follicle diameters were compared statistically among groups, there was an important difference among the control group and the EMF and EMF+2mg carnosine groups ($p<0.05$). There was no significant dissimilarity among the group given 2 mg carnosine and the other groups ($p>0.05$). However, when the group given 20 mg carnosine was compared with the other groups, it was determined that the only dissimilarity was with the EMF group ($p<0.05$). In addition, there was a statistically significant dissimilarity among the EMF group and the control, 20 mg carnosine and EMF+20 mg carnosine groups ($p<0.05$). When the preantral follicle diameter was compared statistically between the groups, there was no meaningful dissimilarity among the control and experimental groups ($p>0.05$). It was defined that there was a statistically important dissimilarity

Table 4. Primary, preantral, secondary and tertiary follicle numbers of control and experimental groups.

	Control	2 mg carnosine	20 mg carnosine	EMF	EMF+2 mg carnosine	EMF+20 mg carnosine	p
Number of Primary Follicles	245±33,56^{a}	216±26,42^{ab}	202±19,34^{bc}	172±34,00^{c}	210±30,97^{abc}	214±38,30^{ab}	,000
Number of Preantral Follicles	73±17,55^{abc}	80±13,57^{ac}	69±12,07^{abc}	59±9,96^{b}	66±17,98^{cb}	73±13,74^{ab}	,058
Number of Secondary Follicles	58±5,87^{a}	56±9,52^{a}	53±7,96^{a}	50±6,19^{a}	52±20,56^{a}	58±16,89^{a}	,509
Number of Tertiary Follicles	7±1,44^{a}	9±1,89^{ab}	7±3,77^{ab}	3±3,37^{b}	7±3,52^{ab}	6±1,66^{ab}	,002

The same letters on the same line indicate the similarity between the groups, and different letters indicate the difference.

Table 5. Primary, preantral, secondary and tertiary follicle diameters of the control and experimental groups.

	Control	2 mg carnosine	20 mg carnosine	EMF	EMF+2 mg carnosine	EMF+20 mg carnosine	p
Primary Follicle Diameter (n=70)	0,41±0,17^{a}	0,37±0,12^{abc}	0,38±0,15^{ac}	0,31±0,09^{b}	0,33±0,13^{cb}	0,38±0,10^{ac}	,000
Preantral Follicle Diameter (n=70)	0,61±0,17^{abc}	0,64±0,23^{a}	0,61±0,21^{abc}	0,54±0,12^{b}	0,55±0,11^{cb}	0,60±0,14^{abc}	,004
Secondary Follicle Diameter (n=70)	1,45±0,46^{a}	1,19±0,45^{b}	1,33±0,49^{ab}	1,19±0,49^{b}	1,34±0,47^{ab}	1,30±0,51^{ab}	,012
Tertiary Follicle Diameter (n=30)	3,09±0,60^{a}	2,80±0,45^{a}	3,15±0,71^{a}	2,18±0,36^{b}	2,84±0,58^{a}	3,06±0,67^{a}	,000

The same letters on the same line indicate the similarity between the groups, and different letters indicate the difference.

among the 2 mg carnosine group and the EMF and EMF + 2 mg carnosine groups ($p<0.05$). When the mean secondary follicle diameters were compared between the groups, it was determined that the statistical dissimilarity occurred among the control group and the group given 2 mg carnosine and the EMF group ($p<0.05$). But there was no dissimilarity among the EMF group and the groups given EMF+2 mg carnosine ($p>0.05$). When the mean tertiary follicle diameters were compared statistically, it was found that there was a statistically remarkable dissimilarity among the EMF group and all other groups ($p<0.05$).

Photomicrography of primary, preantral, secondary and tertiary follicles of the experimental and control groups were given in Figure 1. When the light microscopic images of primary, preantral, secondary and tertiary follicles of the control and experimental groups were examined, the histological images of the control, 2 mg carnosine and 20 mg carnosine groups showed similar structures. There were important irregularities in the structure of the oocyte and the granulosa cells surrounding the oocyte, especially in the EMF-treated groups. However, in the EMF+2 mg carnosine group, there were irregularities in the oocyte and granulosa cells around the oocyte, especially in the secondary and tertiary follicles, as in the EMF group. But the structure of the oocyte and the granulosa cells surrounding the oocyte in the EMF+20 mg carnosine group showed a more regular structure compared to the EMF group.

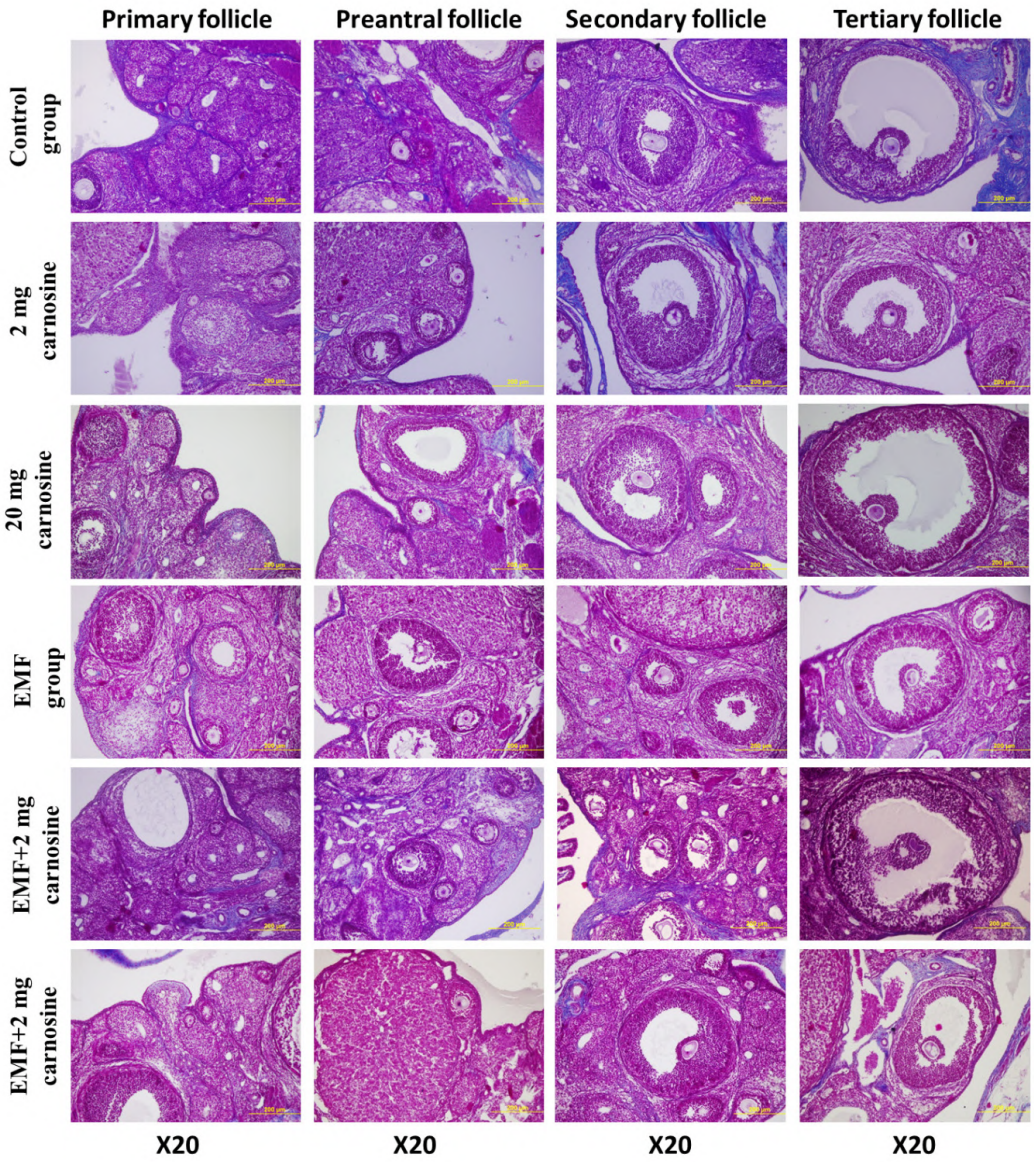

Fig. 1.- Photomicrography of primary, preantral, secondary and tertiary follicles of control and experimental groups (x20).

DISCUSSION

This study demonstrated that exposure to EMF can reduce the mean ovarian follicle count and that this reduction can be ameliorated with higher carnosine dosages. Our findings showed that rats exposed to EMF had a notable lower number of ovarian follicles compared to the control group. Additionally, the structure of the oocyte and the granulosa cells surrounding the oocyte in the groups administered 20 mg carnosine showed a more regular structure compared to the EMF group. The scientists noted that prenatal exposure to 900 MHz EMF could cause pathological changes in the seminiferous tubules in 60-day-old rats and compromise the spermatogenic cycle. They observed that the diameters and epithelial thickness of the seminiferous tubules decreased (Odacı et al., 2016). Studies have shown that environmental electric and magnetic fields can cause deoxyribonucleic acid (DNA) damage and prolong the life of free radicals (Lai and Singh, 2004). Ahmadi et al. (2016) pointed out that EMF radiation has detrimental effects on the implantation of the ovule and the formation of ovarian follicles. Agarwal et al. (2009) examined whether exposure to mobile phones for 1 hour affected human ejaculation of sperm. They concluded that mobile phone may cause male infertility by affecting sperm. Sepehrmanesh et al. (2017) have indicated that exposure to EMF leads to an increase in testicular proteins of adults associated with reproductive damage. Yan et al. (2007) studied the effect on sperm cells of 6 hours a day exposure to EMF from mobile phones for 18 weeks. As a result, they found an increase in sperm cell death in rats. Alchalabi et al. (2015) explained that exposure to 1800 MHz EMF decreasing ovarian follicular development and numbers. Gül et al. (2009) studied the toxic effect of EMF emitted from mobile phones on rat ovarian follicles.

Pregnant rats were exposed to EMF for 11 hours and 45 minutes with mobile phones in standby mode, followed by 15 minutes/12 hours in talk mode with phones during 21 days of gestation. They examined the ovaries of the female offspring. The researchers found a decrease in the number of follicles in the EMF group compared to the control group. Studies in female animals have shown that EMF can cause functional and structural changes in the reproductive system. They reported that EMF exposure can reduce the number of follicles and disrupt the structure of oocytes and follicles in the ovary (Turedi et al., 2016; Khaki et al., 2016; Roshangar et al., 2014). Al-Akhras et al. (2001) significantly reduced fertility was observed in female rats exposed to 50-Hz EMF. Electron microscopy studies have reported that 50 Hz EMF exposure causes degenerative changes in follicle and oocyte cells. Electron microscopy studies have indicated that 50 Hz EMF exposure causes degenerative changes in follicle and oocyte cells (Khaki et al., 2016; Roshangar et al., 2014). Bakacak et al. (2015) reported that ovarian primordial follicle numbers of rats exposed to EMF were notable lower than the control group. Roshangar et al. (2014) investigated the ovarian tissues of 2-day-old mouse pups obtained from mother animals exposed to 50 Hz EMF. They found less developed primordial follicles. In addition, they reported that the integrity of the zona pellucida was disrupted and thinning was observed in the zona pellucida in adult groups.

According to Türedi et al. (2016), rat pups exposed to 900 MHz EMF during prenatal periods were found to show a reduction in the number of primordial and tertiary follicles in the ovarian tissues examined at day 34 postnatally. In addition, they reported an increase in atretic follicle and atretic index, increase in follicle, fibrosis and vasocongestion, albeit at a low level, in the stroma (Turedi et al., 2016). Okatan et al. (2018) stated that there was no dissimilarity among the groups in terms of the number of primordial follicles, primary follicles and Graafian follicles in the EMF group compared to the control group, and only the number of secondary follicles decreased. They reported that exposure to 900 MHz EMF during middle and late adolescence caused changes in ovarian morphology and deterioration in follicle quality. They also concluded that EMF increases oxidative stress and causes a reduce in mitotic activity and secondary follicle numbers. The researchers experimentally analyzed the sepsis-ameliorating therapeutic potential of carnosine against sepsis-induced male albino rats. In their

studies, carnosine was administered in 2 different doses, 25 mg/kg and 50 mg/kg, for 30 sequential days. They reported that after carnosine treatment, the intensity of sepsis was significantly reduced, as evidenced by histopathological analysis (Sun et al., 2017). Oral use of carnosine over a three-month period has been proven to improve the overall appearance of the skin and reduce age-related wrinkles (Babizhayev et al., 2012). In their study, scientists reported that carnosine and vitamin E protect the ovaries from ischemia-reperfusion damage in ovarian torsion, and that carnosine may be especially useful in the treatment of ovarian torsion (Sarac et al., 2018). Studies have shown that carnosine supplementation improves markers of metabolic syndrome in obese diabetic patients (De Courten et al., 2016). One study concluded that carnosine administered intravenously at 100, 500, 1000 and 2000 mg/kg for 14 days was not toxic and reduced cell death (Rajanikant et al., 2007). After reviewing the available literature, we decided to administer 2 mg and 20 mg of carnosine before exposure to EMF for 28 days (Rajanikant et al., 2007). Another study conducted on 75 adult chronic schizophrenia patients aged 18-65 years who were given 2 g of carnosine per day for 3 months showed that carnosine should be considered as an adjunct therapy to improve executive dysfunction in patients with schizophrenia (Chengappa et al., 2012). Khoshbakht et al. (2021) investigated the protective effects of selenium in rat testis tissue exposed to electromagnetic field. They found that serum LH, FSH, GnRH, testosterone level, sperm count, germinal epithelial thickness and seminiferous tubule diameter were significantly decreased in the EM group compared to the control group. In addition, they reported that sperm count, germinal epithelial thickness, seminiferous diameters, serum LH, FSH and GnRH and testosterone levels increased in the EM/SE group compared to the EM group, and sperm abnormality, leptin receptor and apoptotic cells were significantly decreased. Altindag et al. (2017) examined the effects of cell phone exposure on testicular tissue and the protective effects of melatonin use. In the group receiving 2100 MHz radiation, the regular structure of the seminiferous tubules was disrupted, and edema occurred between the seminiferous epithelial cells; they also reported that the seminiferous tubule structure was highly protected in the radiation and melatonin group against the radiation group.

At the end of this study, follicle numbers and diameters were found to be lower in the EMF group and higher in the EMF+20 mg carnosine group. There were marked irregularities in the structure of the oocyte and the granulosa cells surrounding the oocyte in rats exposed to EMF. However, in the EMF+20 mg carnosine group, the oocyte and the granulosa cells surrounding the oocyte exhibited a more regular structure. It was observed that carnosine, which was used as a therapeutic in the experiment, reduced the damage caused by the electromagnetic field. Although we determined that carnosine has a significant effect on preventing electromagnetic field damage, we think that larger studies are needed in terms of long-term effects and possible side effects.

AUTHOR CONTRIBUTIONS

The study was designed by A. Arslan, M. Nisari, E. Balcıoğlu and N. Acer. E. Balcıoğlu, B. Yalçın and M. Ülger collected the data. A. Arslan, E. Balcıoğlu, M. Nisari, and N. Acer analyzed the data. The article was written by A. Arslan M. Nisari, E. Güler and G. B. Uzun. Each author contributed to the evaluation, review of the data, and revision of the manuscript.

ETHICAL STATEMENTS

The study was approved by Erciyes University Animal Ethics Committee with protocol number 13/82 (12.06.2013). Histopathological procedures were performed in Erciyes University Faculty of Medicine, Department of Histology-Embryology.

REFERENCES

AGARWAL A, DESAI NR, MAKKER K, VARGHESE A, MOURADİ R, SABANEGH E, SHARMA R (2009) Effects of radiofrequency electromagnetic waves (RF-EMW) from cellular phones on human ejaculated semen: an *in vitro* pilot study. *Fertil Steril,* 92(4): 1318-1325.

AHMADI SS, AA KHAKI, AINEHCHI N, ALIHEMMATI A, KHATOONI AA, KHAKI A, ASGHARI A (2016) Effect of non-ionizing electromagnetic field on the alteration of ovarian follicles in rats. *Electronic Physician,* 8(3): 2168-2174.

ALBAYRAK S, ATCI IB, KALAYCI M, YILMAZ M, KULOGLU T, AYDIN S (2015) Effect of carnosine, methylprednisolone and their combined application on irisin levels in the 122 plasma and brain of rats with acute spinal cord injury. *Neuropeptides,* 52: 47-54.

ALCHALABI, ASH, AKLILU E, AZIZ AR, MALEK F, RONALD SH, KHAN MA (2015) Exposure to 1800 MHz GSM-like radiofrequency electromagnetic field reduces follicular development and overall fertility of female rats. *S Asia J Exp Biol,* 5(4): 127-136.

ALTINDAG OL, KAPLANOGLU GT, ARAL BS, SEYMEN CM (2017) Possible protective effect of melatonin on testicular tissue in cell phone radiation. *Dicle Med J,* 44(1): 71-80.

AL-AKHRAS MA, ELBETIEHA A, HASAN MK, OMARI IA, DARMANI H, ALBISS B (2001) Effects of extremely low frequency magnetic field on fertility of adult male and female rats. *Bioelectromagnetics,* 22(5): 340-344.

ASLAN A, IKINCI A, BAS O, SONMEZ OF, KAYA H, ODACI E (2017) Long-term exposure to a continuous 900 mhz electromagnet-ic field disrupts cerebellar morphology in young adult male rats. *Biotech Histochem,* 92(5): 324-330.

AYDIN S, OGETURK M, KULOGLU T, KAVAKLI A (2015) Effect of carnosine supplementation on apoptosis and irisin, total oxidant and antioxidants levels in the serum, liver and lung tissues in rats exposed to formaldehyde inhalation. *Peptides,* 64: 14-23.

BABIZHAYEV MA, DEYEV AI, SAVEL'YEVA EL, LANKIN VZ, YEGOROV YE (2012) Skin beautification with oral non-hydrolized versions of carnosine and carcinine: Effective therapeutic management and cosmetic skincare solutions against oxidative glycation and free-radical production as a causal mechanism of diabetic complications and skin aging. *J Dermatolog Treat,* 23(5): 345-384.

BAE ON, KELSEY S, BAEK SH, LEE KY, DORRANCE A. RUMBEIHA W, FITZGERALD SD, FAROOQ MU, NARAVELTA B, BHATT A, MAJID A (2013) Safety and efficacy evaluation of carnosine, an endogenous neuroprotective agent for ıschemic stroke. *Stroke,* 44(1): 205-212.

BAKACAK M, BOSTANCI MS, ATTAR R, YILDIRIM OK, YILDIRIM G, BAKACAK Z, SAYAR H, HAN A (2015) The effects of electromagnetic fields on the number of ovarian primordial follicles: An experimental study. *Kaohsiung J Med Sci,* 31(6): 287-292.

BAKARDJIEV A, BAUER K (2000) Biosynthesis, release and uptake of carnosine in primary cultures. *Biochemistry,* 65(7): 779-782.

BAS O, ODACİ E, MOLLAOGLU H, UCOK K, KAPLAN S (2009) Chronic prenatal exposure to the 900 MHz electromagnet-ic field ınduces pyramidal cell loss in the hippocampus of newborn rats. *Toxicol Industrial Health,* 25(6): 377-384.

BELYAEV I, DEAN A, EGER H, HUBMANN G, JANDRİSOVİTS R, KERN M, KUNDI M, MOSHAMMER H, LERCHER P, MÜLLER K, OBERFELD G, OHNSORGE P, PELZMANN P, SCHEINGRABER C, THILL R (2016) EUROPAEM EMF guideline for the prevention, diagnosis and treatment of EMF-related health problems and diseases. *Rev Environ Health,* 31(3): 363-397.

BROWNSON C, HIPKISS AR (2000) Carnosine reacts with a glycated protein. *Free Radic Biol Med,* 28(10): 1564-1570.

CHENGAPPA KN, TURKIN SR, DESANTI S, BOWIE C R, BRAR JS, SCHLICHT PJ, MURPHY SL, HETRICK ML, BILDER R, FLEET D (2012) A preliminary, randomized, double-blind, placebocontrolled trial of L-carnosine to improve cognition in schizophrenia. *Schizophrenia Res,* 142(1-3): 145-152.

DAVIS DL, KESARI S, SOSKOLNE CL, MILLER AB, STEIN Y (2013) Swedish review strengthens grounds for concluding that radiation from cellular and cordless phones is a probable human carcinogen. *Pathophysiology,* 20(2): 123-129.

DE COURTEN B, JAKUBOVA M, DE COURTEN MP, KUKUROVA IJ, VALLOVA S, KRUMPOLEC P, VALKOVIC L, KURDIOVA T, GARZON D, BARBARESI S, TEEDE HJ, DERAVE W, KRSSAK M, ALDINI G, UKROPEC J, UKROPCOVA B (2016) Effects of carnosine supplementation on glucose metabolism: Pilot clinical trial. *Obesity (Silver Spring),* 24(5): 1027-1034.

DIEM E, SCHWARZ C, ADLKOFEN F, JAHN O, RUDIGER H (2005) Non-thermal DNA breakage by mobile-phone radiation (1800 MHz) in human fibroblasts and in transformed GFSH-R17 rat granulosa cells *in vitro*. *Mutat Res,* 583(2): 178-183.

DOBROTVORSKAYA I, FEDOROVA T, DOBROTA D, BEREZOV T (2011) Characteristics of oxidative stress in experimental rat brain ischemia aggravated by homocysteic acid. *Neurochem J,* 5(1): 42-46.

FEYCHTING M, AHLBOM A, KHEIFETS L (2005) EMF and Health. *Annu Rev Public Health,* 26: 165-189.

FUJII T, TAKAOKA M, TSURUOKA N, KISO Y (2005) Dietary supplementation of L-carnosine prevents ischemia/reperfusion-induced renal injury in rats. *Biol Pharm Bull,* 28(2): 361-363.

GUL A, CELEBİ H, UGRAS S (2009) The effects of microwave emitted by cellular phones on ovarian follicles in rats. *Arch Gynecol Obstet,* 280(5): 729-733.

HUBER R, TREYER V, BORBELY A, SCHUDERER J, GOTTSELIG J, LANDOLT HP, WERTH E, BERTHOLD T, KUSTER N, BUCK A, ACHERMANN P (2002) Electromagnetic fields, such as those from mobile phones, alter regional cerebral blood flow and sleep and waking EEG. *J Sleep Res,* 11(4): 289-295.

KERIMOGLU G, MERCANTEPE T, EROL HS, TURGUT A, KAYA H. COLAKOGLU S, ODACI E (2016) Effects of long-term exposure to 900 Megahertz electromagnetic field on heart morphology and biochemistry of male adolescent rats. *Biotech Histochem,* 91(7): 445-454.

KESARIKK, KUMAR S, BEHARI J (2011) Effects of radiofrequency electromagnetic wave exposure from cellular phones on the reproductive pattern in male wistar rats. *Appl Biochem Biotechnol,* 164(4): 546-559.

KHAKI AA, KHAKI A, AHMADI SS (2016) The effect of non-ionizing electromagnetic field with a frequency of 50 Hz in rat ovary: A transmission electron microscopy study. *Int J Reprod Biomed (Yazd),* 14(2): 125-132.

KHOSHBAKHT S, MOTEJADED F, KARIMI S, JALILVAND N, EBRAHIMZADEH-BIDESKAN AR (2021) Protective effects of selenium on electromagnetic field-induced apoptosis, aromatase P450 activity, and leptin receptor expression in rat testis. *Iran J Basic Med Sci,* 24(3): 322-330.

KILGALLON SJ, SIMMONS LW (2005) Image content influences men's semen quality. *Biol Lett,* 1(3): 253-255.

KOHEN R, YAMAMOTO Y, CUNDY KC, AMES BN (1988) Antioxidant activity of carnosine, homocarnosine, and anserine present in muscle and brain. *Proc Natl Acad Sci USA,* 85(9): 3175-3179.

LAI H, SINGH NP (2004) Magnetic field induced DNA strand breaks in brain cells of the rat. *Environ Health Perspect,* 112(6): 687 694.

NIKOLOVA T, CZYZ J, ROLLETSCHEK A, BLYSZCZUK P, FUCHS J, JOVTCHEV G, SCHUDERER J, KUSTER N, WOBUS AM (2005) Electromagnetic fields affect transcript levels of apoptosis-related genes in embryonic stem cellderived neural progenitor cells. *FASEB J,* 19(12): 1686-1688.

ODACI E, OZYILMAZ C (2015) Exposure to a 900 MHz electromagnetic field for 1 hour a day over 30 days does change the histopathology and biochemistry of the rat testis. *Int J Radiat Biol,* 91(7): 547-554.

ODACI E, HANCI H, YULUG E, TUREDI S, ALIYAZICIOGLU Y, KAYA H, COLAKOGLU S (2016) Effects of prenatal exposure to a 900 MHz electromagnetic field on 60-day-old rat testis and epididymal sperm quality. *Biotech Histochem,* 91(1): 9-19.

OFTEDAL G, WILEN J, SANDSTROM M, MILD KH (2000) Symptoms experienced in connection with mobile phone use. *Occup Med,* 50(4): 237-245.

OKATAN DO, KAYA H, ALIYAZICIOĞLU Y, DEMIR S, COLAKOGLU S, ODACI E (2018) Continuous 900-Megahertz electromagnetic field applied in middle and late-adolescence causes qualitative and quantitative changes in the ovarian morphology, tissue and blood biochemistry of the rat. *Int J Radiat Biol,* 94(2): 186-198.

ONGER ME, GOCER H, CIRAKLI A, KILIC M, KAPLAN S (2016) Effect of electromagnetic wave on bone healing in fixed and unfixed conditions. *J Craniofacial Surg;* 27(6): 1606-1608.

ORAL B, GUNEY M, OZGUNER F, KARAHAN N, MUNGAN T, COMLEKCI S, CESUR G (2006) Endometrial apoptosis induced by a 900-MHz mobile phone: preventive effects of vitamins E and C. *Adv Ther,* 23(6): 957-973.

RAGBETLI MC, OZYURT B, ASLAN H, ODACI E, GOKCIMEN A. SAHIN B, KAPLAN S (2007) Effect of prenatal exposure to diclofenac sodium on Purkinje cell numbers in rat cerebellum: a stereological study. *Brain Res,* 1174: 130-135.

RAJANIKANT GK, ZEMKE D, SENUT MC, FRENKEL MB, CHEN AF, GUPTA R, MAJID A (2007) Carnosine is neuroprotective against permanent focal cerebral ıschemia in mice. *Stroke,* 38(11): 3023-3031.

ROSHANGAR L, HAMDI BA, KHAKI AA, RAD JS, RAD SS (2014) Effect of low-frequency electromagnetic field exposure on oocyte differentiation and follicular development. *Adv Biomed Res,* 3(1): 76.

SARAC M, BAKAL U, KULOGLU T, TARTAR T, AYDIN S, YARDIM M, ARTAS G, KAZEZ (2018) Effects of carnosine and vitamin e on nucleobindin 2 (NUCB2) /nesfatin-1, ghrelin, adropin, and ırisin in experimentally ınduced ovarian torsion. *Ann Clin Lab Sci,* 48(3): 345-354.

SAYGIN M, CALISKAN S, KARAHA N, KOYU A, GUMRAL N, UGUZ A (2011) Testicular apoptosis and histopathological changes induced by a 2.45 GHz electromagnetic field. *Toxicol Ind Health,* 27(5): 455-463.

SEPEHRIMANESH M, KAZEMIPOUR N, SAEB M, NAZIFI S, DAVIS DL (2017) Proteomic analysis of continuous 900-MHz radiofrequency electromagnetic field exposure in testicular tissue: a rat model of human cell phone exposure. *Environ Sci Pollut Res Int,* 24(15): 13666-13673.

SHIRAI T, WANG J, KAWABE M, WAKE K, WATANABE SI, TAKAHASHI S, FUJIWARA O (2017) No adverse effects detected for simultaneous whole-body exposure to multiple-frequency radiofrequency electromagnetic fields for rats in the intrauterine and pre- and postweaning periods. *J Radiat Res*, 58(1): 48-58.

SUN C, WU Q, ZHANG X, HE Q, ZHAO H (2017) Mechanistic evaluation of the protective effect of carnosine on acute lung ınjury in sepsis rats. *Pharmacology,* 100(5-6): 292-300.

TUREDİ S, HANCI H, COLAKOGLU S, KAYA H, ODACI E (2016) Disruption of the ovarian follicle reservoir of prepubertal rats following prenatal exposure to a continuous 900-MHz electromagnetic field. *Int J Radiat Biol,* 92(6): 329-337.

ULUBAY M, YAHYAZADEH A, DENİZ OG, KIVRAK EG, ALTUNKAYNAK BZ, ERDEM G, KAPLAN S (2015) Effects of prenatal 900 MHz electromagnetic field exposures on the histology of rat kidney. *Int J Radiat Biol,* 91(1): 35-41.

YAN JG, AGRESTI M, BRUCE T, YAN YH, GRANLUND A, MATLOUB HS (2007) Effects of cellular phone emissions on sperm motility in rats. *Fertil Steril,* 88(4): 957-964.

YAY A, BALCIOGLU E, YAPISLAR H, OZDAMAR S (2013) Effects of dıabetes and carnosıne on bone structure and mıneral densıty. *J Health Sci,* 23: 203-209.

An exploratory study on the presence of sensory nerves in the caudal part of the trapezius

Inge L. Cox[1,2], Cindy G.J. Cleypool[1], Sander J.A. de Ru[2,3], Ronald L.A.W. Bleys[1]

[1] Department of Anatomy, Division of Surgical Specialties, University Medical Center Utrecht, Utrecht University, The Netherlands
[2] Department of Otorhinolaryngology – Head & Neck Surgery, University Medical Center Utrecht, Utrecht University, The Netherlands
[3] Department of Otorhinolaryngology, Central Military Hospital. Lundlaan 1, 3584 EZ Utrecht

SUMMARY

Intramuscular onabotulinumtoxinA (BTX) injections and nerve decompression surgery both aim to release compressed sensory nerves and are used in the treatment of migraine/headaches. Although for many BTX injection sites, sensory nerves and their potential entrapment sites have been established, for the trapezius this information is incomplete. A macro- and microscopic cadaveric study was performed in which the suprascapular part of the trapezius was explored for the presence of piercing or penetrating nerves and whether these nerves contained sensory nerve fibers. One side of six human cadavers were dissected to reveal trapezius-associated nerves in its suprascapular part. Schematic overview drawings were made of nerves either piercing or penetrating the trapezius in this region. Piercing or penetrating cervical nerves were resected and microscopically studied for the presence of sensory nerve fibers.

For this suprascapular region, correlating potential entrapment sites of the supraclavicular nerves were detected. In all specimens, plexus-like connections between the accessory nerve and branches of the cervical plexus, varying between CII-CV, were observed to innervate the trapezius at locations that showed overlap with BTX injection sites. Moreover, all these nerves contained sensory nerve fibers as confirmed by immunohistochemical staining with the sensory nerve marker CGRP. The presence of potential entrapment sites for supraclavicular nerves and other cervical nerve branches might explain why BTX injection in the suprascapular part of the trapezius show therapeutic effectivity in the treatment of migraine/headaches.

Key words: Cervical plexus – Supraclavicular (scapular) nerves – Entrapment – Migraine headache – Trapezius – OnabotulinumtoxinA – BTX

ABBREVIATIONS

CGRP	Calcitonine gene-related peptide
HE	Hematoxylin eosin
TBS	Tris buffered saline
BTX	OnabotulinumtoxinA

Corresponding author:
Ronald L.A.W. Bleys. University Medical Center Utrecht, Department of Anatomy, Universiteitsweg 100, P.O Box 85060, 3508 AB Utrecht, The Netherlands. Phone: +31 (0)88 7568302; Fax: +31 (0)88 7569030. E-mail: r.l.a.w.bleys@umcutrecht.nl

Submitted: January 9, 2022. **Accepted:** July 25, 2022

https://doi.org/10.52083/OUFY9155

INTRODUCTION

Migraine headache is a debilitating clinical condition which is associated with a high socioeconomic burden (Cady and Dodick, 1999; Stovner et al., 2018). Migraine headache affects both sexes and all age groups, although migraine headaches mostly occur in young adult and middle-aged women (Stovner et al., 2018). Migraine headaches can be divided into two subgroups; 1) episodic migraine, which is characterized by patients suffering from headaches during 14 days or fewer a month, and 2) chronic migraine in which patients have headaches during at least 15 days a month (Schwedt, 2014). Each year, 2.5% of episodic migraine patients turn into chronic patients (Schwedt, 2014). Frequent use of abortive migraine drugs has been associated with this disease progression (Schwedt, 2014). Due to the high disease burden caused by migraine, and because preventive and abortive medication is ineffective or poorly tolerated in a relatively large group of patients, alternative therapies are desired. Migraines are classically considered to represent a central phenomenon; however, various peripheral nerves have been identified as extracranial trigger sites (Guyuron et al., 2000, 2005; Behmand et al., 2003; Mosser et al., 2004; Austad, 2005; Totonchi et al., 2005; Blumenfeld et al., 2010, 2017; Gfrerer and Guyuron, 2017; Muehlberger, 2018; de Ru et al., 2019). Both intramuscular onabolinumtoxinA (BTX) injections causing paralysis of the muscles that are probably strangling the nerves, and decompression surgery were proven to diminish headache burden (Janis et al., 2014). Therapeutic BTX injections result in a significant reduction of up to 9 headache days as described in the PREEMT study (Diener et al., 2010). Furthermore, more recent studies confirm these findings and observe reduction in the use of abortive migraine drugs (Aicua-Rapun et al., 2016; Bilgiç et al., 2021). For most commonly used BTX injection sites – the temporalis region, the frontal region, the occipital region, and cervical paraspinal muscles – the involved sensory nerves and their potential entrapment sites in the pericranial musculature have been identified (Guyuron et al., 2000, 2005; Behmand et al., 2003; Mosser et al., 2004; Austad, 2005; Totonchi et al., 2005; Blumenfeld et al., 2010, 2017; Gfrerer and Guyuron, 2017; Muehlberger, 2018; de Ru et al., 2019; Yi et al., 2021). Especially, the anatomy and possible nerve entrapment sites of the occipital nerves in the upper part of the trapezius were studied extensively (Mosser et al., 2004; Austad, 2005). However, information on potential entrapment sites in the suprascapular part of the trapezius, a region described as additional injection site by Blumenfeld et al., is incomplete. So far, three suprascapular BTX injections sites were described: 1) in the center between the acromion and the necklace line, 2) between the first injection site and the acromion and 3) between the necklace line and the first injection site (Blumenfeld et al., 2017). When reviewing literature on trapezius-associated nerves in this region, potential nerve entrapment sites have been previously observed. These nerve entrapment sites involved the medial, intermediate and lateral supraclavicular nerves, which pierced the muscle or the clavicle (Macalister, 1871; Le Double, 1897; Jelev and Surchev, 2007). Furthermore, some studies hypothesized the existence of a supraclavicular entrapment syndrome, resulting in anterior shoulder girdle pain (Gelberman et al., 1975; Douchamps et al., 2012). How these entrapment sites correlate to the earlier mentioned injection sites is unclear. Therefore, the objective of this study was to confirm the previous observations and to explore the additional injection sites for the presence of sensory nerves piercing or innervating the suprascapular part of the trapezius. The presence, origin, and course of trapezius piercing and innervating nerves were determined by means of cadaveric dissections. If these piercing or penetrating nerves represented other nerves than the supraclavicular nerves (and hence it was unknown if these contained sensory nerve fibers), samples of these nerves were collected and subsequently microscopically studied for the presence of sensory nerve fibers.

MATERIALS AND METHODS

Six human cadavers were used for this study; five males and one female with an age varying between 64-94 years. These bodies entered

the Department of Anatomy of the University Medical Center Utrecht through a body donation program. Written informed consent was obtained during life allowing the use of these bodies for educational and research purposes. No signs of head and/or neck surgery were observed. Whole body preservation was accomplished by arterial perfusion with 3% formaldehyde. Dissections were performed on the right side of the head and neck area only. Skin, platysma and subcutaneous adipose tissue were removed, revealing the sternocleidomastoid, trapezius, and trapezius-associated nerves which were represented by branches of the supraclavicular nerves, the accessory nerve and direct branches of the cervical plexus. Both the sternocleidomastoid and trapezius were dissected and lifted, allowing a better view on relevant neural structures. Small blood vessels were removed if they disturbed the view. Each location where nerves pierced or penetrated the trapezius was documented by both photographs and schematic anatomical drawings.

If these nerves represented nerves other than supraclavicular nerves, they were resected and preserved in 70% ethanol until they were further processed for microscopy (the location of the samples is indicated in Fig. 1). Quantification of the relative contribution of sensory nerve fibers was performed on tissue sections of one level of each nerve only. All samples were placed in increasing percentages of ethanol and xylene, whereafter they were embedded in paraffin and cut into 5 µm thick sections on a microtome (Leica 2050 Super Cut, Nussloch, Germany). Transverse sections of nerves were collected on glass slides, air-dried and subsequently heat fixed for two hours on a slide drying table of 60°C (Medax, 14801, Kiel, Germany). Sections of each sample were routinely stained with hematoxylin/eosin (HE) to provide a general tissue overview and to identify nerves. An adjacent section of each nerve was incubated with antibodies raised against calcitonin gene-related peptide (CGRP) to determine the presence of sensory nerve fibers in these nerves.

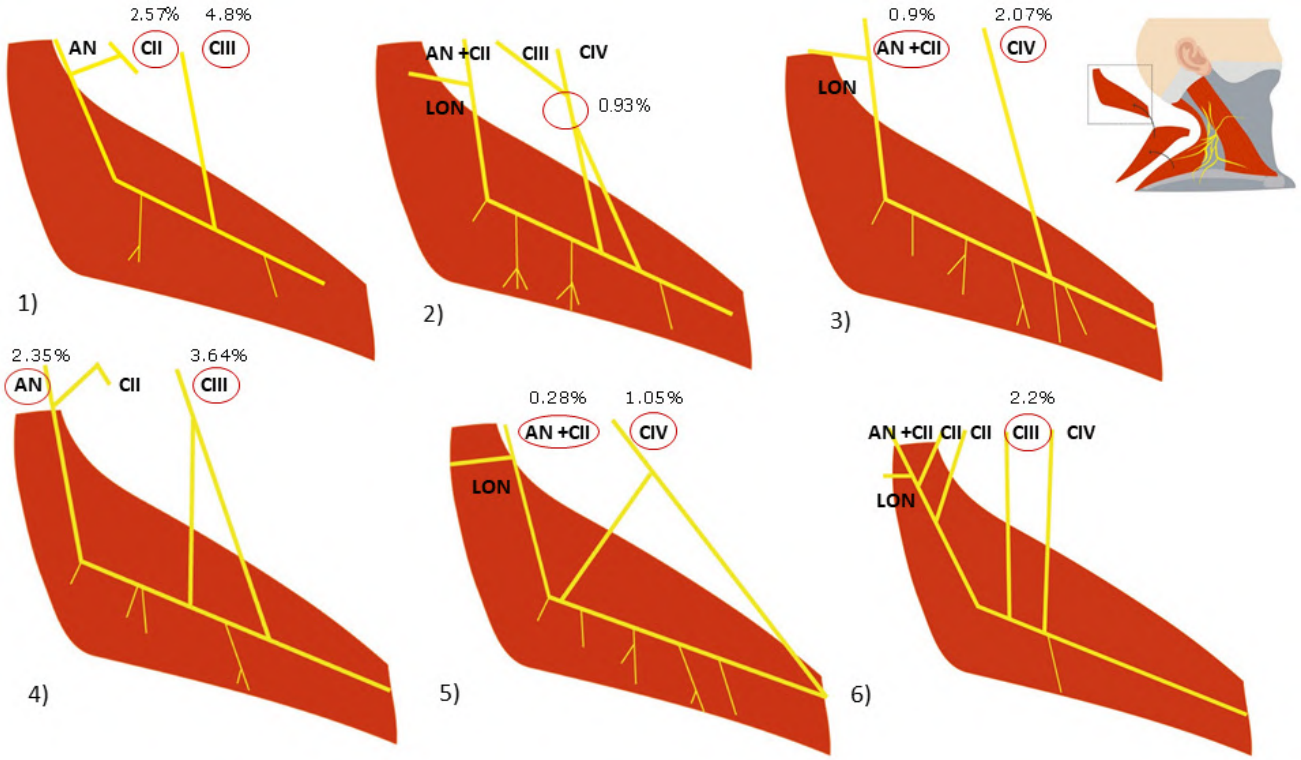

Fig. 1.- Schematic overview of the accessory nerve (AN) forming an accessory-cervical plexus with different branches (CII-CIV) in all six cadavers. In some figures the lesser occipital nerve (LON) is displayed to clarify when AN and CII are already merged. The numbered branches enter the trapezius. In this schematic overview the trapezius has been detached from the clavicle and turned open laterally to reveal a view of the deep surface of the muscle. The muscle is still attached at the level of the acromioclavicular joint. The samples of nerves, which were taken for histochemical analysis are indicated by a red circle. The relative contribution of sensory nerve fibers are expressed as area%.

Immunohistochemistry

Sections were dewaxed in xylene and rehydrated in graded alcohols, followed by 20 min of antigen retrieval in citrate buffer (pH6.0) at 95°C. After washing in Tris-buffered saline (TBS) with 0.05% Tween20 (TBS-T), sections were pre-incubated with 5% Normal Human Serum in TBS for 10 min, followed by incubation with mouse anti-CGRP (Sigma C7133, Saint Louis, USA) 1:1500 overnight at 4°C) in TBS with 3% bovine serum albumin (BSA). Sections were washed with TBS-T several times and incubated for 30 minutes at room temperature with Brightvision Poly-AP Goat-anti-Mouse (ImmunoLogic, Duiven, the Netherlands). After washing with TBS, sections were incubated with liquid permanent red (DAKO, Glostrup, Denmark) for ten minutes. Tissue sections were then washed with distilled water and counterstained with hematoxylin, airdried at 60°C for 90 minutes and cover-slipped using Entellan (Merck, Darmstadt, Germany). Negative controls were obtained by incubation of one additional section with TBS-3%BSA without primary antibodies. Vagus-nerve sections were included as a positive control.

Microscopic imaging

All samples were studied by brightfield (HE) and fluorescent microscopy (CGRP). Stitched overview images (also known as tile scans) of CGRP stained slides were captured with a 10x objective using fluorescent microsocopy. Image acquisition was performed using a DM6 microscope with a motorized scanning stage, a I3 fluorescent filter, a DFC7000 T camera and LASX software (all from Leica, Nussloch, Germany).

Image analysis

Tile scans of CGRP stained nerve sections were analyzed for their relative amount of sensory fibers with respect to the total area of a nerve using Fiji (Schindelin et al., 2012). The outer lining of the neural tissue (thereby excluding the epineurium) was manually selected in each slide and its total area was determined (Fig. 2). A threshold was set allowing to select all CGRP-immune reactive (IR) tissue inside these areas. The pixel area of CGRP-IR nerve tissue was then calculated for each nerve and its amount was then expressed as area% with respect to the total tissue area of the nerve. If a nerve appeared to be composed of multiple smaller nerves, each small nerve was analyzed independently and the results were added up.

RESULTS

All cadavers showed various nerves piercing and/or innervating the trapezius. These represented supraclavicular nerves or branches of the cervical plexus that were joined by branches of the accessory nerve, respectively.

Macroscopic observations

Supraclavicular nerves

In two out of six specimens, three branches of both the lateral and intermediate supraclavicular nerves pierced the trapezius via separate foramina (Fig. 3B, C, and Fig. 4). These foramina correspond with the first two BTX injection sites described by Blumenfeld et al. (2017). Fig. 3A shows the location of BTX injection sites 1-3. All branches originated from ventral rami of the third or fourth cervical spinal nerve. Furthermore, in one of these two specimens the medial supraclavicular nerve pierced through a tendinous arch of the trapezius (Fig. 3B) at a location which might correspond with the third injection site.

Cervical plexus branches and branches of the accessory nerve

No isolated cervical plexus branches or branches of the accessory nerve entered the trapezius in the studied region. In all six specimens several connections between the branches of the cervical plexus (CII-CV) and branches of the accessory nerve were formed prior to entering the trapezius. Each specimen showed an early connection between the accessory nerve and CII. Furthermore, three out of six showed a connection between the accessory nerve and CIII. Lastly four out of six showed connections between the accessory nerve and CIV (Fig. 1). All of them entered the trapezius in the middle portion between the necklace line and the acromion, locations which correspond with the first two injection sites. Unfortunately, some nerves of the sixth dissected cadaver were not preserved due to frailty.

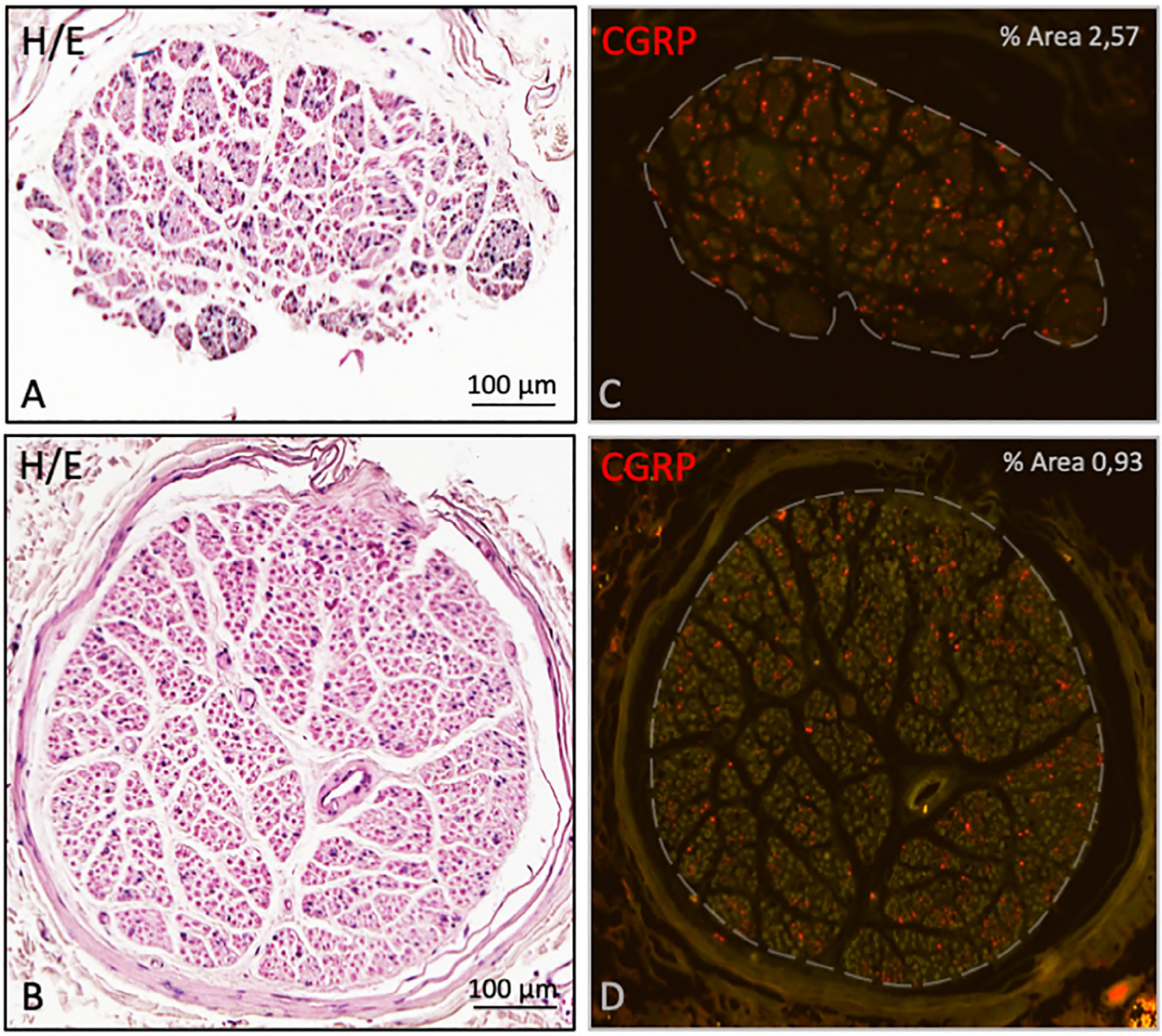

Fig. 2.- Microscopic images of nerves with relative high and low amount of sensory nerve fibers. **A:** Nerve CII of cadaver 1 has a relative high density of senosory nerve fibers. **B:** Nerve CIII/CIV of cadaver 2 has a relative low densitiy of sensory nerve fibers. **C, D:** Grey dotted lines: selection of neural tissue in which the density of sensory nerve fibers is determined.

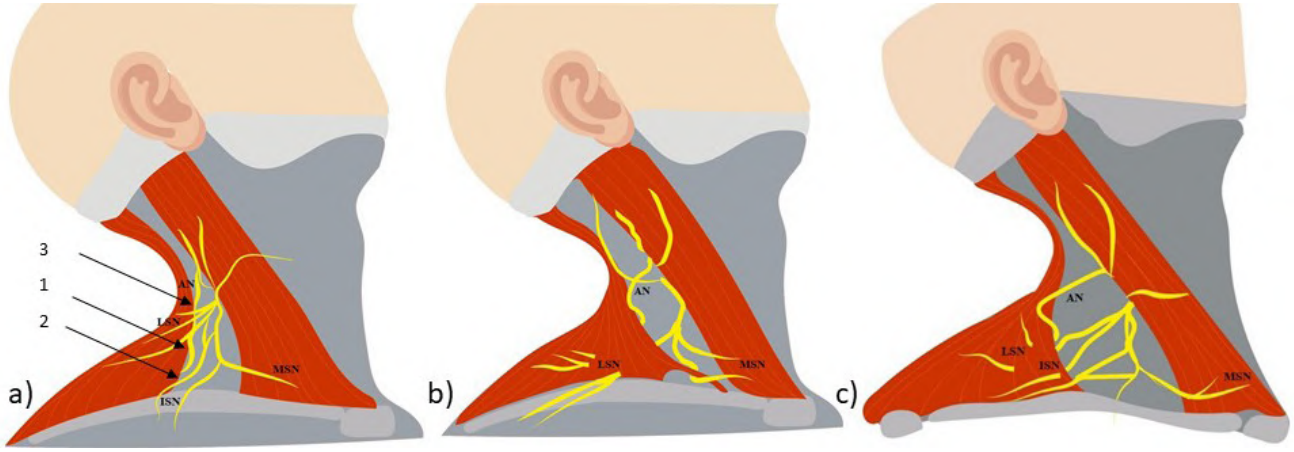

Fig. 3.- Drawing of supraclavicular nerves (lateral (LSN),intermediate (ISN), medial(MSN)), accessory nerve (AN), great auricular nerve, transverse nerve and lesser occipital nerve. **a)** Cadaver 5- male 75 years. Without any potential entrapment sites of the supraclavicular nerves. Thee arrows indicate the location where the BTX injection are commonly placed. **b)** Cadaver 2- male 64 years with potential entrapment sites of the lateral and medial branches of the supraclavicular nerves. **c)** Cadaver 4- male 72 years, with similar entrapment site of the intermediate and lateral branches of the supraclavicular nerve.

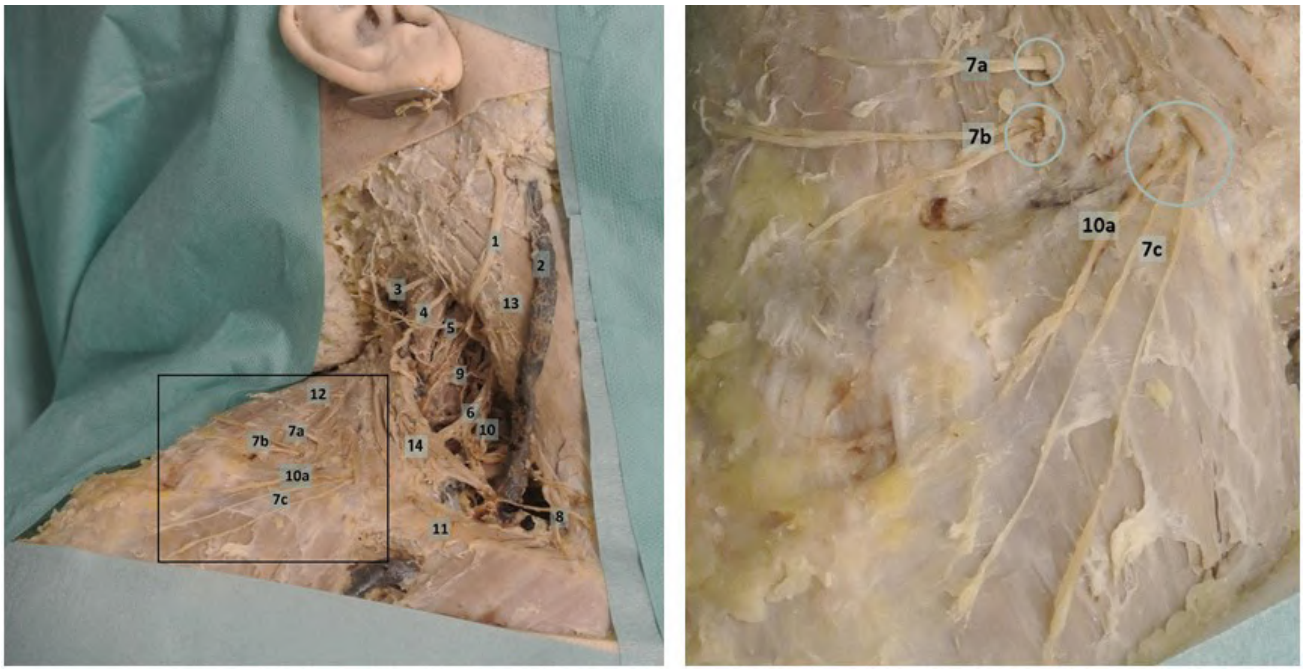

Fig. 4.- Left: Photographic overview of the posterior triangle of the neck in cadaver 2: 1. Great auricular nerve, 2. External jugular vein, 3.Lesser occipital nerve, 4. Accessory nerve, 5. Lesser occipital nerve, 6. CIV, 7.a,b,c Lateral supraclavicular nerve, 8. Medial supraclavicular nerve, 9.CIV, 10. Superficial branch of the transverse cervical artery, 10a Superficial branch of the transverse cervical artery, 11. Clavicle, 12. Trapezius, 13. Sternocleidomastoid, 14.Tendinous arch. **Right:** Enlargement of region of interest.

Microscopic observations

The neural identity of all sampled nerves was confirmed in HE-stained slides as they all represented nerve specific morphological characteristics (Fig. 1). Some nerves were composed of various fascicles within one surrounding epineurium (Fig. 1), whereas other nerves were composed of multiple discrete fascicles, each with their own epineurium. All nerves contained sensory nerve fibers but their number was highly variable (Table 1). The median amount of sensory nerve fibers was 2.34% with an interquartile range of 0.91-2.84.

Quantitative microscopic data on the presence of CGRP-IR nerve fibers in non-supraclavicular nerves are expressed in Table 1. For each nerve the % area of CGPR-IR nerve fibers with respect to the total area of neural tissue is listed. If a nerve was composed of multiple smaller nerve branches, each smaller branch was analyzed separately and the data was pooled and then the %area was calculated.

DISCUSSION

This study shows that in two out of six cases, lateral and intermediate supraclavicular nerves pierced the trapezius. Additionally, in one of these two cadavers, the medial supraclavicular nerve pierced through a tendinous arch formed by the trapezius. These potential entrapment locations of the lateral, intermediate and medial supraclavicular nerves correspond with the second, first and third additional BTX injection site (Blumenfeld et al., 2017), respectively. Since supraclavicular nerves contain sensory fibres (Drake et al., 2014), entrapment of these nerves by the surrounding muscle tissue might result in a pain trigger. This might explain some of the effectivity of BTX injections at these locations; the muscle relaxes and the nerve is no longer entrapped. The occurrence of supraclavicular nerves piercing muscles has been described previously (Macalister, 1871; Le Double, 1897; Jelev and Surchev, 2007). In these studies, nerves piercing the trapezius were mainly observed in conjunction with anatomical variations. These variations comprised a broader attachment of the trapezius to the clavicle which forces the supraclavicular nerves to pierce through it, or a tendinous arch formed over the supraclavicular nerves (Macalister, 1871; Le Double, 1897; Jelev and Surchev, 2007). Jelev and Surchev (2007) solely found one nerve piercing the lateral

part of the trapezius without any anatomical anomalies in one cadaver. Both previous and current findings show that supraclavicular nerve entrapment sites are rare, and, if present, they are mostly located in the medial or more lateral part of the trapezius, close to the acromion and above the clavicle. It is interesting to note that branches of the plexus-like formation consisting of cervical nerve branches and the accessory nerve were found entering the trapezius in all six cadavers. Immunohistochemical analysis confirmed that the cervical nerve branches of these plexus contained sensory nerve fibers, more specifically nociceptive fibers, since CGRP is known for staining nociceptive nerves (Patil et al., 2018). The presence of sensory nerve fibers in cervical branches has been described previously in both animals (Zhao et al., 2006) and humans (Tubbs et al., 2011). Both articles consider the fibers to be proprioceptive, although both studies did not use a specific proprioceptive staining. Based on the immunostaining used in the current study, we hypothesize that these nerves are potentially nociceptive and might detect pain within the trapezius region. Consequently, the muscle paralysis caused by BTX injections might result in less compression of these nerves. In this way, additional migraine/headache trigger reduction due to BTX injections in this region becomes plausible. The relief of migraine headaches after the release of extracranial sensory nerves might be explained by a theory on convergence mechanism (Piovesan et al., 2003). This theory suggests that pain registered by a CI or CII branch can excite the caudal part of the spinal trigeminal nucleus via the lateral cervical nucleus (Piovesan et al., 2003). This could explain why pain registered in the neck (by CI or CII branches) can be perceived as referred pain in areas normally innervated by the trigeminal nerve (Piovesan et al., 2003).

Table 1. Study measurements, including gender, age, length (*head till toe), width (**left acromion till right acromion).

Cadaver	Nerve	% Area CGRP-IR tissue	# nerve branches	Area neural tissue	Area CGRP-IR tissue
1	CII	2.57	1	84260	2169
	CIII	4.8	1	247575	10189
			2	114133	7171
2	CIII/CIV	0.93	1	244570	2268
3	AN/CII	0.9	1	22235	167
			2	45793	346
			3	160183	1734
			4	18367	282
			5	11345	16
	CIV	2.07	1	177382	3022
			2	54396	1776
4	AN	2.35	1	43954	969
			2	196799	3841
			3	89505	2762
			4	32712	975
	CIII	3.64	1	130363	4791
			2	88768	3194
5	AN/CII	0.28	1	61749	172
			2	142682	541
			3	8836	18
			4	49724	12
	CIV	1.05	1	98059	1034
6	CIII	2.2	1	130671	2880

Recommendations

As this study on a relatively small group of specimens was just an exploratory study, more anatomical dissection is needed in this region of interest. Moreover, clinical studies using BTX injections in patients who specifically point out the trapezius as additional trigger site should be performed to further evaluate its efficacy. Furthermore, next to evaluation of subjective symptom improvement, advanced imaging techniques might be used to objectify the degree of nerve compression. For example, using functional magnetic resonance imaging (fMRI) in patients before and after administrating BTX could be of great interest.

Limitations

The low number of included study specimens might be considered a limitation. However, even with this low number, this study clearly underlines previous observations on the heterogeneity of trapezius-piercing nerves. Another limitation was caused by the fragility of some small nerve branches, which resulted in less sampling. Despite these limitations, this exploratory study is a first step in identifying possible treatment options for pain triggers in the trapezius and provides support for further studies on the functional efficacy of trapezius BTX injections.

ACKNOWLEDGEMENTS

We thank Simon Plomp and Marco Rondhuisof the Department of Anatomy of the University Medical Center Utrecht for their assistance with respect to technical anatomical procedures.

AUTHORS'CONTRIBUTIONS

IC designed the study, performed the dissections and histological examination, interpretated the data, designed the figures and wrote the manuscript.

CC supervised the project, performed the histological examination, and helped writing the manuscript.

JR initiated, supervised the project and helped writing the manuscript.

RB initiated, supervised the project and helped writing the manuscript.

REFERENCES

AICUA-RAPUN I, MARTÍNEZ-VELASCO E, ROJO A, HERNANDO A, RUIZ M, CARRERES A, PORQUERES E, HERRERO S, IGLESIAS F, GUERRERO AL (2016) Real-life data in 115 chronic migraine patients treated with Onabotulinumtoxin A during more than one year. *J Headache Pain*, 17: 10-13.

AUSTAD ED (2005) The lesser and third occipital nerves and migraine headaches: Discussion. *Plast Reconstr Surg*, 115: 1759-1760.

BEHMAND RA, TUCKER T, GUYURON B (2003) Single-site botulinum toxin type A injection for elimination of migraine trigger points. *Headache J Head Face Pain*, 43: 1085-1089.

BILGIÇ AB, AKPINAR CK, BORU UT, RAMAZANOGLU L (2021) Peripheral nerve blockade and botox treatment in chronic migraine: a comparative study. *J Curr Med Res Opin*, 4: 878-885.

BLUMENFELD A, SILBERSTEIN SD, DODICK DW, AURORA SK, TURKEL CC, BINDER WJ (2010) Method of injection of onabotulinumtoxina for chronic migraine: A safe, well-tolerated, and effective treatment paradigm based on the preempt clinical program. *Headache*, 50: 1406-1418.

BLUMENFELD AM, SILBERSTEIN SD, DODICK DW, AURORA SK, BRIN MF, BINDER WJ (2017) Insights into the functional anatomy behind the PREEMPT injection paradigm: guidance on achieving optimal outcomes. *Headache*, 57: 766-777.

CADY RK, DODICK DW (1999) Diagnosis and treatment of migraine. *Clin Cornerstone*, 1: 21-32.

DIENER HC, DODICK DW, AURORA SK, TURKEL CC, DEGRYSE RE, LIPTON RB, SILBERSTEIN SD, BRIN MF (2010) OnabotulinumtoxinA for treatment of chronic migraine: Results from the double-blind, randomized, placebo-controlled phase of the PREEMPT 2 trial. *Cephalalgia*, 30: 804-814.

DOUCHAMPS F, COURTOIS AC, BRUYÈRE PJ, CRIELAARD JM (2012) Supraclavicular nerve entrapment syndrome. *Joint Bone Spine*. 79(1): 88-89.

DRAKE R, VOGL AW, MITCHELL AWM, TIBBITTS R, RICHARDSON P (2014) Chapter 8 Head and Neck. In: Gray's Atlas of Anatomy E-Book, Elsevier Health Sciences.

GELBERMAN RH, VERDECK WN, BRODHEAD WT (1975) Supraclavicular nerve-entrapment syndrome. *J Bone Joint Surg*, 57: 119.

GFRERER L, GUYURON B (2017) Surgical treatment of migraine headaches. *Acta Neurol Belg*, 117: 27-32.

GUYURON B, VARGHAI A, MICHELOW BJ, THOMAS T, DAVIS J (2000) Corrugator supercilii muscle resection and migraine headaches. *Plast Reconstr Surg*, 106: 429-434.

GUYURON B, KRIEGLER JS, DAVIS J, AMINI SB (2005) Comprehensive surgical treatment of migraine headaches. *Plast Reconstr Surg*, 115: 1-9.

JANIS JE, BARKER JC, JAVADI C, DUCIC I, HAGAN R, GUYURON B (2014) A review of current evidence in the surgical treatment of migraine headaches. *Plast Reconstr Surg*, 134: 131S-141S.

JELEV L, SURCHEV L (2007) Study of variant anatomical structures (bony canals, fibrous bands, and muscles) in relation to potential supraclavicular nerve entrapment. *Clin Anat*, 20: 278-285.

LE DOUBLE A-F (1897) Traité des variations du système musculaire de l'homme: Et de leur signification au point de vue de l'anthropologie zoologique. Schleicher frères.

MACALISTER A (1871) Additional observations on muscular anomalies in human anatomy (3rd series), with a catalogue of the principal muscular variations hitherto published. *Trans Roy Irish Acad Sci*, 25: 1-134.

MOSSER SW, GUYURON B, JANIS JE, ROHRICH RJ (2004) The anatomy of the greater occipital nerve: Implications for the etiology of migraine headaches. *Plast Reconstr Surg*, 113: 693-697.

MUEHLBERGER T (2018) Migraine surgery: a clinical guide to theory and practice. Springer.

PATIL MJ, HOVHANNISYAN AH, AKOPIAN AN (2018) Characteristics of sensory neuronal groups in CGRP-cre-ER reporter mice : Comparison to lines. *PLoS One*, 112747: 1-27.

PIOVESAN EJ, KOWACS PA, OSHINSKY ML (2003) Convergence of cervical and trigeminal sensory afferents. *Curr Pain Headache Rep*, 7: 377-383.

RU JA DE, FILIPOVIC B, LANS J, VEEN EL VAN DER, LOHUIS PJ (2019) Entrapment neuropathy: a concept for pathogenesis and treatment of headaches—a narrative review. *Clin Med Insights Ear, Nose Throat,* 12: 117955061983494.

SCHINDELIN J, ARGANDA-CARRERAS I, FRISE E, KAYNIG V, LONGAIR M, PIETZSCH T, PREIBISCH S, RUEDEN C, SAALFELD S, SCHMID B, TINEVEZ J-Y, WHITE DJ, HARTENSTEIN V, ELICEIRI K, TOMANCAK P, CARDONA A (2012) Fiji: an open-source platform for biological-image analysis. *Nat Methods*, 9(7): 676-682.

SCHWEDT TJ (2014) Chronic migraine. *Br Med J*, 348: g1416.

STOVNER LJ, NICHOLS E, STEINER TJ, ABD-ALLAH F, ABDELALIM A, AL-RADDADI RM, ANSHA MG, BARAC A, BENSENOR IM, DOAN LP, EDESSA D, ENDRES M, et al. (2018) Global, regional, and national burden of migraine and tension-type headache, 1990-2016: a systematic analysis for the Global Burden of Disease Study 2016. *Lancet Neurol*, 17: 954-976.

TOTONCHI A, PASHMINI N, GUYURON B (2005) The zygomaticotemporal branch of the trigeminal nerve: An anatomical study. *Plast Reconstr Surg*, 115: 273-277.

TUBBS RS, SHOJA MM, LOUKAS M, LANCASTER J, MORTAZAVI MM, HATTAB EM, COHEN-GADOL AA (2011) Study of the cervical plexus innervation of the trapezius muscle: Laboratory investigation. *J Neurosurg Spine*, 14: 626-629.

YI K-H, LEE H-J, CHOI Y-J, LEE K, LEE J-H, KIM H-J (2021) Anatomical guide for botulinum neurotoxin injection: Application to cosmetic shoulder contouring, pain syndromes, and cervical dystonia. *Clin Anat*, 34: 822-828.

ZHAO W, SUN J, ZHENG JW, LI J, HE Y, ZHANG ZY (2006) Innervation of the trapezius muscle: Is cervical contribution important to its function? *Otolaryngol Head Neck Surg*, 135(5): 758-764.

Morphometry of the harvestable surface area of quadriceps tendon using a simple tracing method: A common ACL autograft

Sabiha Latiff, Oladiran I. Olateju

School of Anatomical Sciences, Faculty of Health Sciences, University of the Witwatersrand, 7 York Road, Parktown, 2193, Johannesburg, South Africa

SUMMARY

Several tendons can be used as autografts for anterior cruciate ligament reconstruction, and the choice often depends on the surgeons' preferences. The quadriceps tendon is a commonly used autograft. This study presented, for the first time, the morphometry of the harvestable area of the QT using a simple tracing method. Adult cadavers of South Africans of European Ancestry were carefully dissected to expose the tendon. Then the tendon outline (pre-marked to enhance visibility) was then traced on a firmly secured wax paper which assumed the curvature of the tendon *in situ*. The tracing was then scanned (with its inscribed scale bar) and the morphometrics were measured on the digitized images using an imageJ software. The limb length was also measured in order to normalize all the measurements. Despite the observable difference in the surface area of the quadriceps tendon in each individual, there was no significant difference. For the other measurements, there were no side or sex differences except for the straight distal width which is sexually dimorphic. Some paired parameters showed a strong correlation but the correlation between the limb length and other measurements was weak. These data will be useful for pre-operative planning of anterior cruciate ligament reconstruction and will shed more light into the usability of the quadriceps tendon as a graft with respect to healing at the donor site and the return of knee function.

Key words: Quadriceps tendon – Morphometry – Harvestable area – Tendon tracing – Anterior cruciate ligament reconstruction

INTRODUCTION

The knee joint is a stable joint owed to the menisci and ligaments that provide structural stability to the joint. The two fibro-cartilaginous menisci act as shock absorbers and improve knee joint congruency by aligning the femoral and tibial condyles during joint movement. Ligaments such as the extra-capsular (e.g., medial and lateral collateral ligaments) and the intra-articular (e.g., anterior and posterior cruciate ligaments) aid knee function and also stabilize it. Despite its stability, the medial collateral ligament

Corresponding author:
Oladiran I. Olateju. School of Anatomical Sciences, Faculty of Health Sciences, University of the Witwatersrand, 7 York Road, Parktown, 2193, Johannesburg, Republic of South Africa. Phone: +27 11 717 2763; Fax: +27 11 717 2422. E-mail: Oladiran.Olateju@wits.ac.za

Submitted: March 4, 2022. **Accepted:** July 27, 2022

https://doi.org/10.52083/TDBN2622

and the anterior cruciate ligament (ACL) are the most injured with the ACL requiring a surgical reconstruction using a graft (Hurley et al., 2018; Lalwani et al., 2020).

The harvested graft must closely match the size and biomechanical strength of the ACL. Factors such as the length of the harvestable graft, location, post-surgery recovery of the donor site must be considered when choosing a graft (Hamada et al., 1998; Shelton and Fagan, 2011; Reboonlap et al., 2012; Janssen et al., 2013; Sun et al., 2020). Grafts come in a variety of options, e.g., synthetic graft, allograft or autograft (Legnani et al., 2010; Macaulay et al., 2012; Hulet et al., 2019). Consequently, the choice of graft often depends on the surgeons' preferences based on their clinical trainings and experiences (Mall et al., 2012). No ideal graft exists for ACL reconstruction, so the search for an optimal graft continues. Each graft has its own advantages and disadvantages and may differ extensively in everyone (Romanini et al., 2010; Cerulli et al., 2013; Dhammi et al., 2015). From an anatomical point of view, there are morphological differences amongst individuals of different sexes, race and ethnicity, which means that the choice of graft in an individual may not be solely based on a surgeon's preference (Xerogeanes et al., 2013; van Zyl et al., 2016; Gupta et al., 2017; Vadgaonkar et al., 2018). This study explored the morphometric profile of the QT, a commonly used autograft (Frank et al., 2017), with the aim that it could serve as a guide to surgeons when choosing autografts.

Restoration to the native anatomical footprint is the most important factor in the ACL reconstruction which entails that the graft being 1) biomechanically similar to the ACL; 2) easily harvestable; 3) easily secured surgically and 4) able to have a rapid healing process (Iriuchishima et al., 2013; Dhammi et al., 2015). In addition, the graft size should be customizable to the patient's native ACL morphometry (Hulet et al., 2019). The QT is one of the strongest tendons in the human body situated on the anterior compartment of the thigh, where it serves as a conjoint tendon for the quadriceps femoris muscles (i.e., rectus femoris, vastus intermedius, vastus medialis and vastus lateralis). The QT with its muscles flexes the hip, extends the knee joint and keeps the knee from buckling when standing – an action that enables walking (Ilan et al., 2003; Slone et al., 2015).

The QT has gained popularity for use as a graft because of its favourable biomechanics, low donor-site morbidity, large cross-sectional area, predictability of healing outcome and ease of harvest (Slone et al., 2015; Heffron et al., 2019). To increase the QT graft effectiveness, the central QT–bone construct is recommended for the ACL reconstruction providing low donor site morbidity, adequate size and high tensile strength (Fulkerson and Langeland, 1995; Harris et al., 1997; Stäubli et al., 1999; DeAngelis and Fulkerson, 2007; Geib et al., 2009; Slone et al., 2015; Shani et al., 2016). The QT is considerably thick and wide and provides abundant harvestable tissue (Fulkerson and Langeland, 1995) but little information on the extent of the harvestable tendon area exists in the literature. Thus, this study presents data on the morphometric profiles (i.e., the surface area, length and widths) of the harvestable area of the QT using a simple tracing method. Correlation of paired parameters was also performed to reveal any relationship. It is envisaged that this study will shed more light, and create an awareness on, the suitability and usability of the QT graft in individuals. Knowledge of this may further strengthen its popularity as an autograft.

MATERIALS AND METHODS

Demographic of samples

Lower limbs of adult formalin–fixed cadavers of South Africans of European ancestry were used in the study. This study assumed a mean of 73.5 mm (standard deviation = 12.3 mm) for females and a mean of 81.1 mm (standard deviation = 10.6 mm) for males for the length of the QT (measured from the musculotendinous junction of rectus femoris to the superior aspect of patella) (Xerogeanes et al., 2013) to determine the sample size required for the present study. At 80% statistical power and a significance level of 5%, the minimum sample size required was 74 cadavers (i.e., 37 cadavers per sex). Consequently, the final sample size was 40 female (79 lower limbs assessed) and 39 male cadavers (77 lower limbs assessed). The QT in

both limbs of each cadaver was measured, and any cadaver limb with obvious physical scars or deformities was excluded from the study. The cadavers were housed in the School of Anatomical Sciences at the University of the Witwatersrand, Johannesburg, South Africa for teaching purposes. This study was performed in line with the principles of the Declaration of Helsinki. Waiver was granted by the Human Research Ethics Committee (Medical) of the University of the Witwatersrand (Ethics Waiver Number: W-CJ-140604-1). The mean age of the male cadavers was 76.2 years (range: 53 – 96 years) while that of the female cadavers was 75.3 years (range: 46 – 96 years).

Dissections

To expose the QT, the cadaver was placed in a supine position with the lower limbs fully extended. For the dissection (by S.L. and O.I.O. – anatomists with experiences in human morphometry), a longitudinal incision on the anterior surface of the lower limb was made extending from midway of the thigh to midway of the leg and passing through the centre of the patella. Transverse incisions perpendicular to the longitudinal incision were made at the proximal end, at the level of the patella and at the distal end to expose the region of interest and to allow for adequate space for observation and morphometric measurements. Subsequently, the skin, subcutaneous fascia, fat, fascia lata, and crural fascia were carefully removed without altering the QT morphology.

Morphometry of QT

For the QT morphometry (by S.L. and O.I.O.), the knee was flexed at an angle of about 45° and then the QT was carefully wiped with a dry absorbent cloth. A non-elastic transparent wax paper (dimension: 5 cm x 5 cm x 19 µm; superior wax paper – donated by Superhaze Trading Company, Tongaat, South Africa) was then carefully placed so that it assumed the curvatures of the underlying QT (Fig. 1). The wax paper on the tendon was firmly secured with pins. Subsequently, a permanent marker was used in order to trace out the margins of the tendon onto the wax paper. To further enhance visibility and accuracy of the tracing, the margins of the tendon were pre-marked with a permanent marker before placing the wax paper onto the QT.

The wax paper was removed after the tracing and a known scale bar was drawn on it. The wax paper with its inscribed scale bar was then scanned at 300 dpi using an Epson workforce DS-50000 scanner. From the digitized image, the surface area (SA), straight distal width (SDW), curved distal width (CDW) and length of tendon (LOT) for the QT were measured from the digitized image using an ImageJ 1.47v software (NIH, USA). Each parameter was measured twice and the average of the two measurements was used for the analyses. The parameters for the QT are described in Table 1. In order to normalize the data, the length of each lower limb at full extension from the anterior superior iliac spine to the medial malleolus was also measured using a measuring tape (Sabharwal and Kumar, 2008; Gupta et al., 2017). The raw data of the measurements were normalized by

Table 1. Parameters for the quadriceps tendon.

Parameter	Acronym	Description
Surface area	SA	Area of tendon which is defined by the margins of the tendon i.e. infero-medial border – vastus medius; infero-lateral border – vastus lateralis; inferior border – tendon attachment on the base (superior border) of patella using the medial and lateral borders of the patella as the landmarks
Straight distal width	SDW	Measurement taken as 'a crow flies' at the inferior border of QT using the medial and lateral borders of the patella as landmarks
Curved distal width	CDW	Measurement taken along the curvature of the inferior border of QT using the medial and lateral borders of the patella as landmarks
Length of tendon	LOT	Maximum height from the highest peak at the musculotendinosus junction of QT to the halfway of the CDW at the inferior border of the tendon

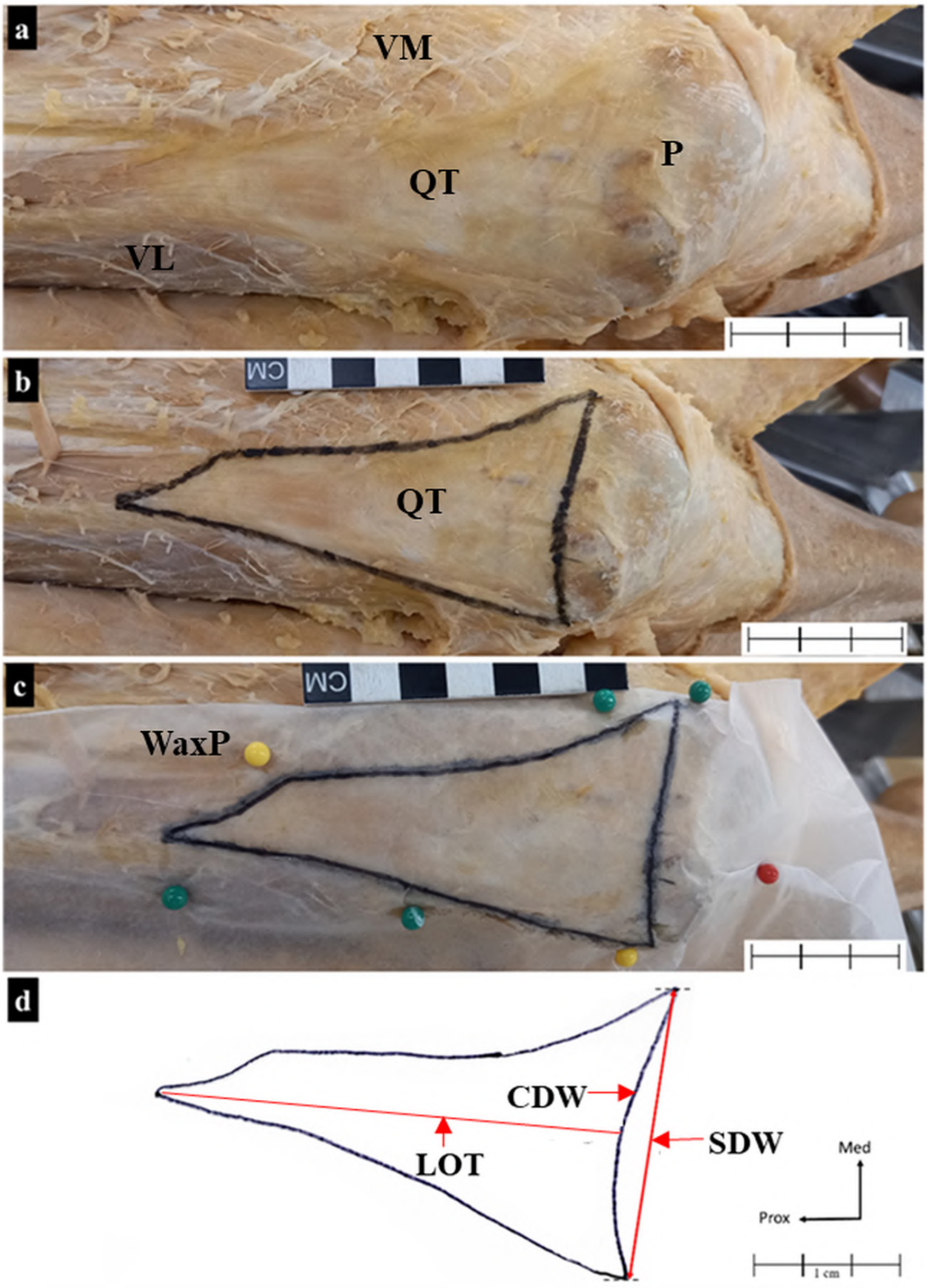

Fig. 1.- Illustrations of the QT tracings on the anterior compartment of the thigh showing (**a**) the exposed QT after removing the superficial structures, (**b**) the highlighted QT margins (i.e. its extent) with a permanent marker in order to improve visibility and tracing accuracy, (**c**) the QT tracing on a superimposed wax paper secured by coloured pins to assume the curvature of QT and (**d**) the digitized image of the traced tendon on the wax paper from which parameters were measured. VM – Vastus medialis, VL – Vastus lateralis, P – patella, QT – Quadriceps tendon, WaxP – Wax paper, LOT – length of tendon, CDW – curved distal width, SDW – straight distal width, Prox – proximal; Med – medial.

dividing the obtained values of the SA, SDW, CDW and LOT by the corresponding lower limb length (LLL).

Statistical analyses

An intra-observer reliability test was conducted (by S.L) at the beginning of the data collection where two independent sets of measurements were taken from the same cadavers at two weeks apart. A Lin's Concordance test (ρc) was performed to determine the level of precision and accuracy between the test and retest measurements. Data collection was then carried out after the reliability test revealed that the level of agreement was substantial (i.e. ρc > 0.95) (Landis and Koch, 1977; McBride, 2005). To test for normality, a Shapiro-Wilk test was carried out for each measurement. All the normalized data were not normally distributed thus a Mann-Whitney U test was used for sex or side comparison. To determine a possible correlation between any two paired parameters, a Pearson's correlation was used for normally distributed raw data, while a Spearman's correlation was used for not normally distributed raw data. All statistical analyses were performed using a SPSS software (version 22.0; IBM, US). Statistical difference of 5% was regarded as significant for all the statistical analyses.

RESULTS

Test of reliability of measurements

The ρc values for the measurements of the QT are shown in Table 2. The ρc values ranged from 0.969 for SA to 0.999 for LOT. Based on these results, all the measurements of the QT are considered to have an error low enough to be acceptable.

Table 2. Lin's concordance correlation of reproducibility for the measurements of the quadriceps tendon.

Parameter	ρc
SA	0.969
LOT	0.999
SDW	0.995
CDW	0.989
LLL	0.997

SA – surface area; LOT – length of tendon; SDW – straight distal width; CDW – curved distal width; LLL – length of lower limb

Morphometry of the lower limb

To reiterate, the measurements for the QT in each cadaver were normalized using the corresponding LLL. There was no significant side difference ($p > 0.05$) in the LLL in both sexes (Table 3). In both limbs, the mean LLL of the male cadavers was significantly higher than the mean LLL of the female cadavers ($p < 0.05$).

Morphometry of the quadriceps tendon

The descriptive analyses of the data for each side and according to sex for the QT are shown in Table 4. For all the measurements from the female or the male cadavers, there was no statistically significant difference in sides (i.e. left vs right). Similarly, no significant difference was obtained when the measurements in the female cadavers were compared with the male cadavers except for the SDW of the male left limb which was significantly higher than the female left limb ($p = 0.033$). Despite the non-significant difference between the measurements from both limbs, the SA measure of one limb was different from the other limb in most of the individual cadavers assessed (Fig. 2). This is an indication that the surface area of the QT in both limbs are morphometrically different in some individuals compared to the similarity of the measurements for the LLL (for illustrative purposes) in both limbs of the same cadaver (Fig. 2).

Correlation analyses on the measurements of the quadriceps tendon

The correlations between any paired QT dimensions showing a clear detail about the strength of their relationships are shown in Table 5. Only paired measurements that revealed moderate (range 0.4-0.69) or strong correlations (range 0.7-1.0) (Schober et al., 2018) are presented. Using the Pearson's or Spearman's correlation (R), strong correlations were observed between the paired measurements of SDW and CDW ($R \geq 0.7$) in both limbs of the female and the male cadavers. A strong correlation was also observed between SA and LOT ($R \geq 0.7$) except for the left lower limb in the female that showed a moderate correlation ($R \geq 0.6$). In addition, the relationship of the LLL (male or female) with each measurement was

Table 3. Comparison between the measurements of the left and the right lower limb lengths.

	Left			Right			
	Number of limbs assessed	**Mean (median) (mm)**	**SD**	**Number of limbs assessed**	**Mean (median) (mm)**	**SD**	**p**
Female	40	860.6* (857.5)	50.21	39	860.846* (865.0)	48.39	0.979
Male	39	926.7* (925.0)	35.88	38	927.474* (920.5)	38.06	0.926

*Significant difference p = 0.0000 (M > F). SD – standard deviation

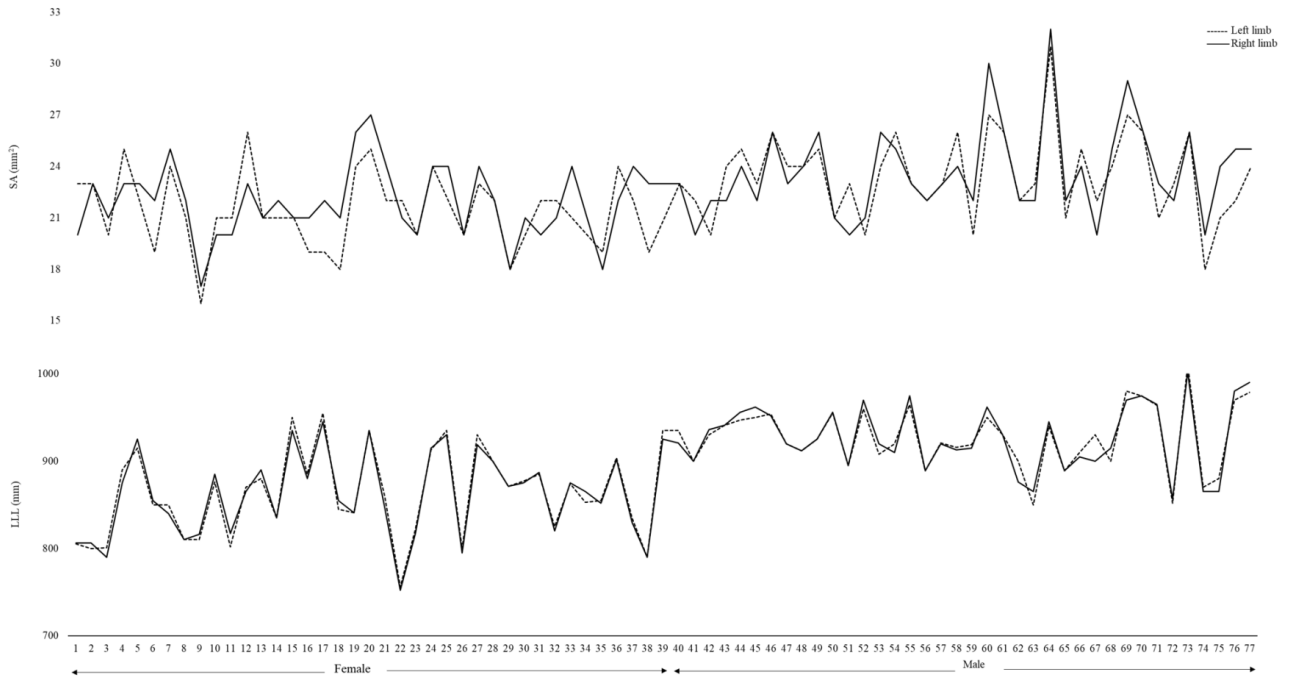

Fig. 2.- Line graphs showing patterns of variation in SA of QT or LLL of both limbs for each individual cadaver. The measurement of SA of one limb is visibly different from the other limb in the cadavers assessed compared to the measurements of LLL in both limbs that are visibly similar.

determined. Only moderate correlation was observed in the paired parameters of LLL vs SA or LLL vs CDW for the male right limb.

DISCUSSION

In the event of an ACL injury, repair of the ligament is necessary to restore the anatomical and functional biomechanics of the damaged ligament (Macaulay et al., 2012). Poor management or treatment plan will lead to unbearable pain, knee function impairment, deterioration of the surrounding cartilage as well as increasing the chances of developing osteoarthritis (Øiestad et al., 2010; Hijazi et al., 2015; Shultz, 2015; Sayampanathan et al., 2017). Surgical repair using an autograft sourced from the patient is the commonly used approach for ACL reconstruction. Various tendons can be used as an autograft however the preference for an autograft often depends on the clinical training and experience of the surgeon.

Generally, human height is a useful parameter for stature in anthropometry and morphometry studies (Xerogeanes et al., 2013; Gupta et al., 2017; Krebs et al., 2019). However, when the height of the subject cannot be accurately measured as in the case of cadavers due to post-mortem variation in body sizes (Cardoso et al., 2016; Ferorelli et al., 2017), the lower limb is often used to indicate stature (Treme et al., 2008; Chiang et al., 2012;

Table 4. Comparison of the measurements of the left and right quadriceps tendon.

	Left					Right					
		Raw		Normalized			Raw		Normalized		
	Number of limbs assessed	Mean (mm)	Mean (mm^2)	Mean	SD	Number of limbs assessed	Mean (mm)	Mean (mm^2)	Mean	SD	p
Female											
SA	40		21.23	0.025	0.003	39		21.90	0.025	0.002	0.440
LOT	40	78.77		0.092	0.016	39	84.75		0.099	0.014	0.052
SDW	40	49.96		0.058*	0.007	39	51.58		0.060	0.008	0.735
CDW	40	53.18		0.062	0.008	39	54.75		0.064	0.008	0.344
Male											
SA	39		23.44	0.025	0.003	38		23.74	0.026	0.003	0.421
LOT	39	86.51		0.093	0.013	38	91.23		0.098	0.013	0.104
SDW	39	57.24		0.062*	0.006	38	56.15		0.061	0.006	0.544
CDW	39	60.74		0.066	0.006	38	60.63		0.065	0.007	0.442

*Significant difference p = 0.033 (M > F). SA_{QT} – surface area; LOT_{QT} – length of tendon; SDW_{QT} – straight distal width; CDW_{QT} – curved distal width; SD – standard deviation

Table 5. Correlation coefficient between measurements of the left and right quadriceps tendon.

	Female				Male			
	SA	LOT	SDW	CDW	SA	LOT	SDW	CDW
Left								
SA		0.6*				0.7*	0.4***	
LOT								
SDW				1.0*				
CDW							0.9*	
LLL								
Right								
SA		0.7*		0.4**		0.8*		0.4**
LOT								
SDW	0.5**			1.0*				
CDW							0.8*	
LLL					0.5**			0.4***

*p < 0.0001. **p < 0.01. ***p < 0.05 . SA – surface area; LOT – length of tendon; SDW – straight distal width; CDW – curved distal width; LLL – length of lower limb

Sundararajan et al., 2016; Mohd Asihin et al., 2018; Sakti et al., 2019; Dziedzic et al., 2020). Even though the LLL parameter used in the present study is consistent with the previous studies, the focus of this study was not to determine stature in this population group. Instead, LLL was used to normalize the measurements and to determine the relationships between the LLL and other measurements. On another note, limb length was significantly higher in the male cadavers than in the female cadavers, which is consistent with previous reports that measured limb length in different population groups: e.g., an American population (Treme et al., 2008), a Chinese population (Chiang et al., 2012) and a South Sulawesi population (Sakti et al., 2019).

In morphometric studies of structures (e.g., tendons or ligaments in the lower limb), some

measurements may indicate a leg dominance when a measurement on one limb is significantly different from a similar measurement of the other limb: e.g., in semitendinosus tendon (Pichler et al., 2008; Bundi et al., 2016) and patellar ligament (Olateju et al., 2013). Factors such as age, sex, lifestyle and activity level of an individual may contribute to leg dominance as well as tendon pathology arising from injuries (Latiff et al., 2021). In a study by Gupta et al. (2017), the limb length of both sides was not significantly different and is consistent with the findings of the present study. This means that leg dominance may not be associated with limb length but may be directly linked to the tendon or ligament morphometries as is the case in Pichler et al. (2008), Olateju et al. (2013) and Bundi et al. (2016). In this study, none of the measurements exhibited a leg dominance as there were no significant differences when the measurements from both limbs were compared. This is also consistent with the cadaveric studies by Hijazi et al. (2015) and Tanpowpong et al. (2019).

The morphometric profile of the QT provides useful information that is beneficial to ACL reconstruction (Lippe et al., 2012). The large harvestable tissue area of the QT is an important feature that makes it a commonly used autograft. Other advantages of the QT is that it can be reliably harvested (Sheean et al., 2018), and that it has a similar ultrastructure to other graft sources: e.g., patellar tendon and hamstrings (Macaulay et al., 2012). This study presents data on the surface area of the QT which have not been collected before. The surface area of the QT was similar in both sexes and in both limbs in the population group assessed. Unfortunately, there is no report in the literature to compare with the present findings, so it is not discussed further. The data on the surface area of the QT may be of benefit to the rate of recovery at the harvest site, since the QT has been shown to have more collagen content (Hadjicostas et al., 2007) which contributes to its tensile strength (Shani et al., 2016; Krebs et al., 2019; Latiff and Olateju, 2022). The implication of this is that the remaining collagen content after the harvesting of a graft should be sufficient for the QT to recover quicker and function more satisfactorily than the patellar tendon, which has a lesser collagen content (Hadjicostas et al., 2007) and a smaller surface area than the QT (unpublished report). It is thus suggested that the surface area of the QT should be considered in pre-operative planning where the QT is being considered as a graft in an individual.

Morphologically, the QT of the population group assessed was similar to a previous study (Lippe et al., 2012). Some cadavers exhibited a dual peak (51%) while others had a single peak (49%). The dual peaks are because the vastus lateralis and vastus medialis become tendons (i.e., the QT) before inserting at the base of the patella (Lippe et al., 2012). Understanding and acknowledging this characteristic feature of the QT is important during harvesting in order to avoid harvesting from the short peak (which is mostly positioned medially) instead from the long peak that provides adequate graft tissue (i.e., the maximum tendon length) for harvesting (Lippe et al., 2012). In this study, the maximum tendon length was taken from the more prominent peak in the case of dual peaks (Lippe et al., 2012; Tanpowpong et al., 2019).

The average maximum tendon length for both limbs in this study was 81.76 mm in the female and 88.87 mm in the male. Due to differences in morphometric approaches and other factors such as age, race and ethnicity (Gupta et al., 2017), other studies report a lower maximum tendon length. Yamasaki et al. (2021) reported a QT length of about 59.5 mm in a MRI study on a Japanese population, while a QT length of 61 mm was reported in cadavers by Harris et al. (1997) and a length of 63 mm in a Thai population by Tanpowpong et al. (2019). However, other studies reported a maximum tendon length within the range observed in the present study. For example, Stäubli et al. (1999) reported an average tendon length of about 86 mm for both limbs, Krebs et al. (2019) reported an average of about 83 mm in a cadaveric study while Thi and Ha (2021) and Lippe et al. (2012) reported averages of about 79 mm and 88 mm respectively. With similarities in the mean QT length, it seems that the in-situ tendon tracing and methodologies used in the present study were adequate. Likewise, the QT length in the

present study was not sexually dimorphic despite the observed higher tendon length in the male than in the female. This however contradicts the MRI study by Xerogeanes et al. (2013) that found a significant higher tendon length in males (~81.1 mm) than in females (~73.5 mm). A cadaveric study in a Saudi Arabian population also reported a significantly higher QT length in males (Hijazi et al., 2015).

To give a further detailed morphometry that could be used pre-operatively, the straight and curved distal widths (SDW and CDW) were measured on the tracings. The tendon tracings provided an additional advantage in that the actual/curved widths can be easily measured unlike in radiological records: e.g., MRI. One or both measurements may be adequate for pre-operative investigation and planning when a QT autograft is being considered. The study however did not find a significant difference between the straight and curved distal widths in the population group assessed. In addition, the SDW or the CDW did not reveal a side difference. However, SDW (not the CDW) exhibited a sex dimorphism where the male QT width was wider than the female. This is consistent with the report by Hijazi et al. (2015) despite the narrower widths reported compared to this study. The present study found SDW to be about 50.8 mm in the female and about 56.7 mm in the male (left and right limbs combined), while the QT widths of about 26.7 mm in the female and about 28.5 mm in the male (left and right limbs combined) were reported by Hijazi et al. (2015). Thi and Ha (2021) reported a narrower QT distal width (~ 36.0 mm) as well. On the other hand, Lippe et al. (2012) (~43.3 mm), Krebs et al. (2019) (~44.8 mm) and Tanpowpong et al. (2019) (~46.2 mm) reported QT distal widths in cadavers within the range observed in the present study.

One advantage the QT has over the other commonly used autografts (e.g., semitendinosus and patellar tendons) is that the area of harvestable tissue is high. Harvesting a standard 10–mm wide (Adams et al., 2006; Shelton and Fagan, 2011; Iriuchishima et al., 2013; Hijazi et al., 2015) and a 70–mm long (van Eck et al., 2010) QT tissue for an ACL reconstruction means that there is sufficient tissue that can be harvested and at the same time leave sufficient tissue for tendon functionality and healing at the harvest site. This is also highlighted in other reports (Xerogeanes et al., 2013; Krebs et al., 2019; Yamasaki et al., 2021). Based on the observed morphometries of the tendon length (female: 52.1 – 116.7 mm and male: 67.3 – 121.8 mm) and width (female: 35.8 – 68.9 mm and male: 48 – 70.1 mm) of the QT in the present study, about 8% (i.e., 6 limbs out of 77) of the male limbs and about 17% (i.e., 13 limbs out of 79) of the female limbs fall short of the required dimensions of a QT autograft, and thus these individuals may not qualify for an ACL reconstruction using the QT autograft. Interestingly, these observations were found bilaterally in 3 cadavers (i.e., 1 male and 2 females). This means that the QT would not be suitable as an autograft in these individuals if they were to undergo an ACL reconstruction. In comparison to Tanpowpong et al. (2019), about 61% of the Thai population group assessed were considered not suitable for a QT autograft due to their short QT length. In these individuals, a bone–patellar tendon–bone autograft could be an alternative (Yamasaki et al., 2021). Predicting the size of the autograft for use in surgery may be a difficult task (Krebs et al., 2019) but this is where morphometric studies have become useful (Helito et al., 2015; Zakko et al., 2017).

It may be possible that the QT of one limb may be adequate but not the other limb. Depending on the strategies or plans of the surgeon, the QT may be harvested from the limb with a damaged ACL or from the undamaged limb (Shelbourne and Urch, 2000; von Essen et al., 2021). However, there is a need for caution as there are individuals with observable differences in the morphometry of the QT of both limbs. For these individuals and depending on which leg is injured, the surgeon must be cautious in choosing which graft to use. Thus, the preference of the surgeon based on the surgical training and experience may not be applicable but rather by an informed decision provided by tendon morphometry. It is not advisable to harvest a graft from an injured limb, as there is a high risk of compounding the problem in this limb. In the event of harvesting a graft from the contralateral limb, as explained by Shelbourne and Urch (2000), the trauma of the surgery is

divided between the limbs, and this allows the patient to focus on the rehabilitation process for each limb. For the recovery of both knees and the return of knee functions, patients may not have to worry about a major loss of strength in the limb where the ACL was reconstructed as the graft was harvested from the non-injured limb. Even though a non-injured limb is being 'disturbed', this proves to be advantageous for recovery of both limbs (Shelbourne and Urch, 2000).

In the present study, correlation between paired parameters of the QT was tested to determine the relationship between them. A strong correlation was found between the distal width (i.e., straight and curved) in both limbs and for both sexes. A strong correlation was also found between the SA and LOT (except for the female left limb that was moderate). This relationship is another important factor to consider during pre-operative investigation of the QT. Correlation was also extended to determine the relationship between the LLL and other QT measurements. It is important to note that the height of a subject and the length of limb in the same subject may not be directly related. Interestingly, none of the parameters paired with the LLL showed a strong correlation unlike in previous reports by Xerogeanes et al. (2013) and Krebs et al. (2019) that found a strong correlation between the height of individual and the tendon length.

In conclusion, the cadaveric approach used in this study is considered reliable and reproducible, evident by the results of the test of reliability. It is true that a cadaveric approach has many limitations, e.g., sample size, tissue shrinkage, population representation, etc., but it provides a 3–dimensional structure from which several measurements can be obtained *in situ* (Olateju et al., 2013). The QT provides an abundant harvestable tissue which is superior to other tendons (e.g., patellar or semitendinosus tendon), but surgeons must be cautious as the QT in some individuals may not be adequate as an autograft. When it comes to faster healing and integration of graft, the benefits of the bone–patellar tendon–bone autograft cannot be matched by the QT. This makes the patellar tendon a popular graft choice, especially when a faster return to activity level is desired. However, a bone–patellar tendon–bone autograft may be inadequate in a surgical approach, like in an all-inside ACL reconstruction, where it becomes difficult to appropriately shorten the graft length (Slone et al., 2016). In a procedure like this, a QT graft is preferred because of its large harvestable area and accessibility. The discussed morphometric data of the QT will contribute to knowledge and will be beneficial for pre-operative planning for ACL reconstruction.

ACKNOWLEDGEMENTS

The authors sincerely thank those who donated their bodies to science so that anatomical research could be performed. Results from such research can potentially increase mankind's overall knowledge that can then improve patient care. Therefore, these donors and their families deserve our highest gratitude. We are grateful to the School of Anatomical Sciences of the University of the Witwatersrand for giving access to the Human Collections.

Author contributions

S.L.: Data collection, Data analyses, Manuscript editing.

O.I.O.: Project development, Data collection, Data analyses, Manuscript writing.

Funding

A student support funding to S. Latiff from The Hillensberg Trust. Both authors certify that they have no affiliations with or involvement in any organization or entity with any financial interest or non-financial interest in the subject matter or materials discussed in this manuscript.

Ethics approval

Approval was granted (Ethics Number: W-CJ-140604-1) by the Human Research Ethics Committee (Medical) of the University of the Witwatersrand, Johannesburg, South Africa. The study was performed in accordance with the ethical standards as laid down in the 1964 Declaration of Helsinki and its later amendments

REFERENCES

ADAMS DJ, MAZZOCCA AD, FULKERSON JP (2006) Residual strength of the quadriceps versus patellar tendon after harvesting a central free tendon graft. *Arthrosc -J Arthrosc Relat Surg*, 22(1): 76-79.

BUNDI B, KIGERA J, GIKENYE G (2016) Semitendinosus tendon for solitary use in anterior cruciate ligament reconstruction. *Ann Afri Surg*, 13(2).

CARDOSO HF, MARINHO L, ALBANESE J (2016) The relationship between cadaver, living and forensic stature: A review of current knowledge and a test using a sample of adult Portuguese males. *Forensic Sci Int*, 258: 55-63.

CERULLI G, PLACELLA G, SEBASTIANI E, TEI MM, SPEZIALI A, MANFREDA F (2013) ACL Reconstruction: choosing the graft. *Joints*, 1(1): 18-24.

CHIANG ER, MA HL, WANG ST, HUNG SC, LIU CL, CHEN TH (2012) Hamstring graft sizes differ between Chinese and Caucasians. *Knee Surg Sports Traumatol Arthrosc*, 20(5): 916-921.

DEANGELIS JP, FULKERSON JP (2007) Quadriceps tendon-a reliable alternative for reconstruction of the anterior cruciate ligament. *Clin Sports Med*, 26(4): 587-596.

DHAMMI IK, REHAN-UL-HAQ SK (2015) Graft choices for anterior cruciate ligament reconstruction. *Indian J Orthop*, 49(2): 127-128.

DZIEDZIC DW, BOGACKA U, KOMARNIȚKI I, CISZEK B (2020) Morphology and morphometry of the semitendinosus distal tendon in adults and foetuses. *Folia Morphol*, 79(2): 339-349.

FERORELLI D, DELL'ERBA A, SOLARINO B (2017) Body length estimation during the post mortem interval: preliminary study. *Rom J Leg Med*, 25(4): 369-372.

FRANK RM, HIGGINS J, BERNARDONI E, CVETANOVICH GC, BUSH-JOSEPH CA, VERMA NN, BACH Jr BR (2017) Anterior cruciate ligament reconstruction basics: bone–patellar tendon–bone autograft harvest. *Arthrosc Tech*, 6(4): e1189-e1194.

FULKERSON JP, LANGELAND R (1995a) An alternative cruciate reconstruction graft: The central quadriceps tendon. *Arthrosc - J Arthrosc Relat Surg*, 11(2): 252-254.

GEIB TM, SHELTON WR, PHELPS RA, LAUREN C (2009) Anterior cruciate ligament reconstruction using quadriceps tendon autograft: intermediate-term outcome. *Arthrosc - J Arthrosc Relat Surg*, 25(12): 1408-1414.

GUPTA R, MALHOTRA A, MASIH GD, KHANNA T (2017) Equation-based precise prediction of length of hamstring tendons and quadrupled graft diameter by various anthropometric variables for knee ligament reconstruction in Indian population. *J Orthop Surg*, 25(1).

HADJICOSTAS PT, SOUCACOS PN, BERGER I, KOLEGANOVA N, PAESSLER HH (2007) Comparative analysis of the morphologic structure of quadriceps and patellar tendon: a descriptive laboratory study. *Arthrosc - J Arthrosc Relat Surg*, 23(7): 744-750.

HAMADA M, SHINO K, MITSUOKA T, ABE N, HORIBE S (1998) Cross-sectional area measurement of the semitendinosus tendon for anterior cruciate ligament reconstruction. *Arthrosc - J Arthrosc Relat Surg*, 14(7): 696-701.

HARRIS NL, SMITH DAB, LAMOREAUX L, PURNELL M (1997) Central quadriceps tendon for anterior cruciate ligament reconstruction. Part I: Morphometric and biomechanical evaluation. *Am J Sports Med*, 25(1): 23-28.

HEFFRON WM, HUNNICUTT JL, XEROGEANES JW, WOOLF SK, SLONE HS (2019) Systematic review of publications regarding quadriceps tendon autograft use in anterior cruciate ligament reconstruction. *ASMAR*, 1(1): e93-e99.

HELITO CP, HELITO PVP, BONADIO MB, PÉCORA JR, BORDALO-RODRIGUES M, CAMANHO GL, DEMANGE MK (2015) Correlation of magnetic resonance imaging with knee anterolateral ligament anatomy: a cadaveric study. *Orthop J Sports Med*, 3(12).

HIJAZI MM, KHAN MA, ALTAF FMN, AHMED MR, ALKUSHI AG, SAKRAN AMEA (2015) Quadriceps tendon and patellar ligament. *Prof Med J*, 22(09): 1192-1195.

HULET C, SONNERY-COTTET B, STEVENSON C, SAMUELSSON K, LAVER L, ZDANOWICZ U, STUFKENS S, CURADO J, VERDONK P, SPALDING T (2019) The use of allograft tendons in primary ACL reconstruction. *Knee Surg Sports Traumatol Arthrosc*, 27(6): 1754-1770.

HURLEY ET, CALVO-GURRY M, WITHERS D, FARRINGTON SK, MORAN R, MORAN CJ (2018) Quadriceps tendon autograft in anterior cruciate ligament reconstruction: a systematic review. *Arthrosc - J Arthrosc Relat Surg*, 34(5): 1690-1698.

ILAN DI, TEJWANI N, KESCHNER M, LEIBMAN M (2003) Quadriceps tendon rupture. *J Am Acad Orthop Surg*, 11(3): 192-200.

IRIUCHISHIMA T, SHIRAKURA K, YORIFUJI H, AIZAWA S, FU FH (2013) Size comparison of ACL footprint and reconstructed auto graft. *Knee Surg Sports Traumatol Arthrosc*, 21(4): 797-803.

JANSSEN RPA, VAN DER VELDEN MJF, PASMANS HLM, SALA HAGM (2013) Regeneration of hamstring tendons after anterior cruciate ligament reconstruction. *Knee Surg Sports Traumatol Arthrosc*, 21(4): 898-905.

KREBS N, YAISH A, O'NEILL N (2019) Anatomic evaluation of the quadriceps tendon in cadaveric specimens: application for anterior cruciate ligament reconstruction graft choice. *Spartan Med Res J*, 4(1).

LALWANI R, ROHIT S, SHEETAL K, ATHAVALE SA (2020) New insights in anterior cruciate ligament morphology: implications for anterior cruciate ligament reconstruction surgeries. *Anat Cell Biol*, 53(4): 398-404.

LANDIS JR, KOCH GG (1977) The measurement of observer agreement for categorical data. *Biometrics*, 33(1): 159-174.

LATIFF S, OLATEJU OI (2022) Quantification and comparison of tenocyte distribution and collagen content in the commonly used autografts for anterior cruciate ligament reconstruction. *Anat Cell Biol*, 55(3): 304-310.

LATIFF S, BIDMOS M, OLATEJU OI (2021) Morphometric profile of tendocalcaneus of South Africans of European ancestry using a cadaveric approach. *Folia Morphol*, 80(1): 196-203.

LEGNANI C, VENTURA A, TERZAGHI C, BORGO E, ALBISETTI W (2010) Anterior cruciate ligament reconstruction with synthetic grafts. A review of literature. *Int Orthop*, 34(4): 465-471.

LIPPE J, ARMSTRONG A, FULKERSON JP (2012) Anatomic guidelines for harvesting a quadriceps free tendon autograft for anterior cruciate ligament reconstruction. *Arthrosc - J Arthrosc Relat Surg*, 28(7): 980-984.

MACAULAY AA, PERFETTI DC, LEVINE WN (2012) Anterior cruciate ligament graft choices. *Sports Health*, 4(1): 63-68.

MALL NA, MATAVA MJ, WRIGHT RW, BROPHY RH (2012) Relation between anterior cruciate ligament graft obliquity and knee laxity in elite athletes at the national football league combine. *Arthrosc - J Arthrosc Relat Surg*, 28(8): 1104-1113.

MCBRIDE GB (2005) A proposal for strength-of-agreement criteria for Lin's concordance correlation coefficient. *NIWA client report: HAM2005-062* 45: 307-310.

MOHD ASIHIN MA, BAJURI M, AHMAD J, SYED KAMARUDDIN SF (2018) Pre-operative ultrasonographic prediction of hamstring autograft size for anterior cruciate ligament reconstruction surgery. *Ceylon Med J*, 63(1): 11.

ØIESTAD BE, HOLM I, AUNE AK, GUNDERSON R, MYKLEBUST G, ENGEBRETSEN L, AARSLAND FOSDAHL M, RISBERG MA (2010) Knee function and prevalence of knee osteoarthritis after anterior cruciate ligament reconstruction: A prospective study with 10 to 15 years of follow-up. *Am J Sports Med*, 38(11): 2201-2210.

OLATEJU OI, PHILANDER I, BIDMOS MA (2013) Morphometric analysis of the patella and patellar ligament of South Africans of European ancestry. *S Afri J Sci*, 109(9): 1-6.

PICHLER W, TESCH NP, SCHWANTZER G, FRONHÖFER G, BOLDIN C, HAUSLEITNER L, GRECHENIG W (2008) Differences in length and cross-section of semitendinosus and gracilis tendons and their effect on anterior cruciate ligament reconstruction: A cadaver study. *J Bone Joint Surg Am*, 90(4): 516-519.

REBOONLAP N, NAKORNCHAI C, CHARAKORN K (2012) Correlation between the length of gracilis and semitendinosus tendon and physical parameters in Thai males. *J Med Assoc Thai*, 95(10): S142-S146.

ROMANINI E, D'ANGELO F, DE MASI S, ADRIANI E, MAGALETTI M, LACORTE E, LARICCHIUTA P, SAGLIOCCA L, MORCIANO C, MELE A (2010) Graft selection in arthroscopic anterior cruciate ligament reconstruction. *J Orthop Traumatol*, 11(4): 211-219.

SABHARWAL S, KUMAR A (2008) Methods for assessing leg length discrepancy. *Clin Orthop Relat Res*, 466(12): 2910-2922.

SAKTI M, YURIANTO H, PASALLO P, HIDAYATULLAH S, FAISAL A, SUBAGIO ES (2019) Anthropometric parameters measurement to predict 4-strand hamstring autograft size in single bundle anterior cruciate ligament reconstruction of South Sulawesi population. *Int J Surg Open*, 21: 58-63.

SAYAMPANATHAN AA, HOWE BKT, BIN ABD RAZAK HR, CHI CH, TAN AHC (2017) Epidemiology of surgically managed anterior cruciate ligament ruptures in a sports surgery practice. *J Orthop Surg*, 25(1).

SCHOBER P, BOER C, SCHWARTE LA (2018) Correlation coefficients: appropriate use and interpretation. *Anesth Analg*, 126(5):1763-1768.

SHANI RH, UMPIEREZ E, NASERT M, HIZA EA, XEROGEANES J (2016) Biomechanical comparison of quadriceps and patellar tendon grafts in anterior cruciate ligament reconstruction. *Arthrosc - J Arthrosc Relat Surg*, 32(1): 71-75.

SHEEAN AJ, MUSAHL V, SLONE HS, XEROGEANES JW, MILINKOVIC D, FINK C, HOSER C (2018) Quadriceps tendon autograft for arthroscopic knee ligament reconstruction: use it now, use it often. *Br J Sports Med*, 52(11): 698-701.

SHELBOURNE KD, URCH SE (2000) Primary anterior cruciate ligament reconstruction using the contralateral autogenous patellar tendon. *Am J Sports Med*, 28(5): 651-658.

SHELTON WR, FAGAN BC (2011) Autografts commonly used in anterior cruciate ligament reconstruction. *J Am Acad Orthop Surg*, 19(5): 259-264.

SHULTZ SJ (2015) ACL injury risk in the physically active: why are females more susceptible? *Kinesiol Rev*, 4(1): 52-62.

SLONE HS, ROMINE SE, PREMKUMAR A, XEROGEANES JW (2015) Quadriceps tendon autograft for anterior cruciate ligament reconstruction: a comprehensive review of current literature and systematic review of clinical results. *Arthrosc - J Arthrosc Relat Surg*, 31(3): 541-554.

SLONE HS, ASHFORD WB, XEROGEANES JW (2016) minimally invasive quadriceps tendon harvest and graft preparation for all-inside anterior cruciate ligament reconstruction. *Arthrosc Tech*, 5(5): e1049-e1056.

STÄUBLI HU, SCHATZMANN L, BRUNNER P, RINCÓN L, NOLTE LP (1999) Mechanical tensile properties of the quadriceps tendon and patellar ligament in young adults. *Am J Sports Med*, 27(1): 27-34.

SUN J, WEI XC, LI L, CAO XM, LI K, GUO L, LU JG, DUAN ZQ, XIANG C, WEI L (2020) Autografts vs synthetics for cruciate ligament reconstruction: a systematic review and meta-analysis. *Orthop Surg*, 12(2): 378-387.

SUNDARARAJAN SR, RAJAGOPALAKRISHNAN R, RAJASEKARAN S (2016) Is height the best predictor for adequacy of semitendinosus-alone anterior cruciate ligament reconstruction? A study of hamstring graft dimensions and anthropometric measurements. *Int Orthop*, 40(5): 1025-1031.

TANPOWPONG T, TANASANSOMBOON T, HUANMANOP T, THAMYONGKIT S, JARUPRAT P, INKARATANA T (2019) Anatomical study of quadriceps tendon for anterior cruciate ligament reconstruction. *Asian Biomed*, 13(5): 179-183.

THI C, HA NDP (2022) Applied anatomy of the quadriceps tendon related to the technique of harvesting the quadriceps tendon graft. *Tech Orthop*. (in Press).

TREME G, DIDUCH DR, BILLANTE MJ, MILLER MD, HART JM (2008) Hamstring graft size prediction: A prospective clinical evaluation. *Am J Sports Med*, 36(11): 2204-2209.

VADGAONKAR R, PRAMEELA MD, MURLIMANJU BV, TONSE M, KUMAR CG, MASSAND A, BLOSSOM V, PRABHU LV (2018) Morphometric study of the semitendinosus muscle and its neurovascular pedicles in South Indian cadavers. *Anat Cell Biol*, 51(1): 1-6.

VAN ECK CF, ILLINGWORTH KD, FU FH (2010) Quadriceps tendon: the forgotten graft. *Arthrosc - J Arthrosc Relat Surg*, 26(4): 441-442.

VON ESSEN C, HALLGREN A, BARENIUS B, ERIKSSON K (2021) Utilizing a contralateral hamstring autograft facilitates earlier isokinetic and isometric strength recovery after anterior cruciate ligament reconstruction: a randomised controlled trial. *Knee Surg Sports Traumatol Arthrosc*, 29(8): 2684-2694.

XEROGEANES JW, MITCHELL PM, KARASEV PA, KOLESOV IA, ROMINE SE (2013) Anatomic and morphological evaluation of the quadriceps tendon using 3-dimensional magnetic resonance imaging reconstruction: Applications for anterior cruciate ligament autograft choice and procurement. *Am J Sports Med*, 41(10): 2392-2399.

YAMASAKI S, HASHIMOTO Y, HAN C, NISHINO K, HIDAKA N, NAKAMURA H (2021) Patients with a quadriceps tendon shorter than 60 mm require a patellar bone plug autograft in anterior cruciate ligament reconstruction. *Knee Surg Sports Traumatol Arthrosc*, 29(6): 1927-1935.

ZAKKO P, VAN ECK CF, GUENTHER D, IRRGANG JJ, FU FH (2017) Can we predict the size of frequently used autografts in ACL reconstruction? *Knee Surg Sports Traumatol Arthrosc*, 25(12): 3704-3710.

VAN ZYL R, VAN SCHOOR AN, DU TOIT P, LOUW E (2016) Clinical anatomy of the anterior cruciate ligament and pre-operative prediction of ligament length. *SA Orthop J*, 15(4).

Morinda lucida and Annona *muricata* reduced hepatic lipid peroxidation and promoted melatonin/TNFα/p53-mediated apoptosis in sodium arsenite-induced toxicity in rats

Adelaja Akinlolu[1], Adeoye Oyewopo[2], Risikat Kadir[2], Mubarak Ameen[3], Victor Owoniyi[2], Fauzeeyah Adam[2], Shukrat Okeleye[2]

[1] *Department of Anatomy, Faculty of Basic Medical Sciences, University of Medical Sciences Ondo, Ondo State, Nigeria*

[2] *Department of Anatomy, Faculty of Basic Medical Sciences, University of Ilorin, Ilorin, Kwara State, Nigeria*

[3] *Department of Chemistry, Faculty of Physical Sciences, University of Ilorin, Ilorin, Kwara State, Nigeria*

SUMMARY

Arsenic-induced carcinogenesis can result in cancers of the liver in exposed organisms. This study evaluated anticancer potentials of MLF1 and AMF1 extracted from *Morinda lucida* and *Annona muicata* leaves respectively in Sodium arsenite (SA)-induced toxicity in rats.

Sixty adult female rats were randomly divided into 12 groups (n = 5). Group 1 was control. Group 2 received 5-weeks administrations of 10 mg/kg bodyweight of SA. Groups 3-6 received SA-dose for 2 weeks followed by 3-weeks post-treatments with MLF1-doses and AMF1-doses respectively. Groups 7-10 received only 5-weeks administrations of MLF1-doses and AMF1-doses respectively. Groups 11 and 12 received 5-weeks co-administrations of SA-dose with high-doses of MLF1 and AMF1 respectively. Drugs/extracts were administered orally. Liver histopathology (Heamatoxylin and Eosin) and ELISA concentrations of sera Melatonin and TNF-alpha were evaluated. Malondialdehyde (thiobarbituric-acid assay) and p53 (ELISA) levels were evaluated in liver homogenates. Data were statistically analysed.

Results showed normal liver histology in Groups 1-12. Post-treatments of SA-induced toxicity with MLF1 and AMF1 resulted in significant ($P \leq 0.05$) and non-significant decreased levels ($P \geq 0.05$) of Malondialdehyde, TNF-alpha and p53, but significant ($P \leq 0.05$) and non-significant increased Melatonin levels ($P \geq 0.05$) in Groups 3-12 compared with Group 2. MLF1 and AMF1 possess anticancer, antioxidant, pro-Melatonin, anti-inflammatory and hepato-protective potentials.

Key words: *Annona muricata* – Lipid peroxidation – Melatonin – *Morinda lucida* – p53 – TNF-alpha

INTRODUCTION

Arsenic compounds are ubiquitously present in nature and are dissipated into the environment

Corresponding author:
Dr Adelaja Akinlolu. Department of Anatomy, Faculty of Basic Medical Sciences, University of Medical Sciences Ondo, Ondo State, 234351103 Nigeria. Phone: +2348062765308. E-mail: aadelaja@unimed.edu.ng

Submitted: July 15, 2022. **Accepted:** July 28, 2022

https://doi.org/10.52083/GSIJ9555

through agricultural and industrial processes and medical applications (World Health Organization, 2001; International Agency for Research on Cancer, 2012; Aliyu et al., 2015). Arsenic-induced cytotoxicity is a via of increased generation of free radicals and further confinement of oxidative stress in body organs resulting in damages to DNA, proteins and lipids (Jomova et al., 2011), as well as increased micronuclei frequency and chromosomal aberrations. Arsenic is a carcinogen and can lead mainly to cancers of the skin, lung, bladder, liver and kidney in exposed organisms (Jomova et al., 2011; Singh et al., 2011). The resolution of carcinogenesis in experimental studies is assessed via activities of biomarkers of lipid peroxidation (Malondialdehyde) (Akinlolu et al., 2012; Lampiao and Du Plessis, 2013), oxidative stress/DNA damage (Melatonin) (Lampiao and Du Plessis, 2013; Zamfir et al., 2014; Mohammadi et al., 2016), inflammation/immune-response (TNF-alpha) (Liu et al., 2004, Zahr et al., 2010; Chu, 2013) and apoptosis (p53) (Chang et al., 2010; Toshinori and Akira, 2011; Xiao et al., 2013).

The ubiquitous environmental presence and pro-carcinogenic potentials of SA make the search for possible plant diets or anticancer compounds that may prevent or counteract SA-induced toxicity quite relevant. *Morinda lucida* (ML) is an ethno-medicinal plant often grown in Nigeria. The leaf extract of ML possesses trypanocidal, antimalarial activities, aortic vaso-relaxant effect, oral hypoglycemic property (Adejo et al., 2014; Adeleye et al., 2018) and antioxidant potentials (Akindele and Obi, 2020). *Annona muricata* (AM) is a member of the Annonaceae family with a long history of ethno-medicinal use (Moghadamtousi et al., 2015; Agu and Okolie, 2017). AM possesses anticancer, anticonvulsant, anti-arthritic, anti-parasitic, antimalarial, hepato-protective and anti-diabetic potentials (Moghadamtousi et al., 2015; Agu and Okolie, 2017). In addition, AM leaf extract was reported to have antioxidant potential, as well as capacity to reduce lipid peroxidation (Justino, 2018).

Rats, mice and humans share about one third of the genome. This includes the majority of coding regions and significant non-coding DNA regions under neutral selection, potentially containing regulatory regions. In addition, some hormones and genes associated with antioxidant defense mechanism and human cancers, such as Melatonin, TNFα and p53 seem to be highly conserved across mammalian evolution, and have counterparts in the rat genome (Simon, 2004; Akinlolu and Shokunbi, 2010). Therefore, this study evaluated the effects of fractionated and isolated compounds from *Morinda lucida* leaves (MLF1) and *Annona muricata* leaves (AMF1) on lipid peroxidation and immuno-modulations of Melatonin, TNF-alpha and p53 proteins in Sodium arsenite (SA)-induced oxidative stress, hepato-toxicity, inflammation and mutagenesis in rats.

MATERIALS AND METHODS

Ethical Approval

Ethical approval for this study was sought and received from the Ethical Review Committee of the University of Ilorin, Nigeria. Appropriate measures were observed to ensure minimal pain or discomfort of rats used in this study. The ethical approval number is UERC/ASN/2018/1161. Furthermore, this research study was conducted in accordance with the internationally accepted principles for laboratory animal use and care as provided in the European Community guidelines (EEC Directive of 1986; 86/609/EEC), the Directive 2010/63/Eu of the European Parliament and of the Council of 22 September 2010 on the protection of animals used for scientific purposes, and the Guidelines of the U.S. Public Health Service and NIH regarding the care and use of animals for experimentation (NIH publication #85-23, revised in 985).

Collection, authentication and deposition of *Morinda lucida* and *Annona muricata* leaves

Freshly cut leaves of *Morinda lucida* (ML) and *Annona muricata* (AM) were obtained locally from forest reserves in Ilorin and samples identified, authenticated and deposited at the herbarium of the same Department of Botany, Faculty of Life Sciences of the study institution. ML and AM leaves were assigned Herbarium Identification Numbers UITH/004/1103 and UITH/003/1106 respectively.

Preparations and ethanolic extractions of *Morinda lucida* and *Annona muricata* leaves

ML and AM leaves were air-dried at the laboratory unit of the Department of Chemistry, Faculty of Physical Sciences of the study institution. The dried leaves of ML and AM were grround to powder form and extracted with ethanol. Thereafter, ethanol was separated from ML and AM and Column chromatography was done to get different fractions of ML and AM.

Column chromatography fractionation of ethanol extracts of *Morinda lucida* and *Annona muricata* leaves

The ethanol extracts of ML and AM leaves were fractionated in a silica gel open column, using n-hexane, dichloromethane, ethyl acetate and ethanol in an increasing order of polarity (N-hexane: Dichloromethane [3;1,3:2,1:1,1:2,1:3]; Dichloromethane; Dichloromethane: Ethylacetate [3:1,3;2, 1:1, 1:2, 1;3]; Ethylacetate; Ethylacetate: Methanol [3:1, 3:2, 1:1, 1:2, 1:3] and Methanol. Thirty-six eluents of 250 ml each of ML, and thirteen eluents of 250 ml each of AM. The resulting eluents were pooled based on the color of the solvents that elute them to give a total of 9 combined ML and 5 combined AM fractions**.** MLF1 and AMF1 fractions which had the best preliminary antioxidant potentials were used for testing anticancer potentials of plants' extracts in this study.

Chemicals and Reagents

Sodium arsenite was a product of Sigma-Aldrich Japan Co. (Tokyo, Japan), and was purchased from Emed Ejeson enterprises in Ilorin, Kwara State, Nigeria. Normal Saline was obtained from MOMROTA pharmaceutical company in Ilorin, Kwara State, Nigeria.

Animal Care and Feeding

A total number of sixty (60) female Wistar rats with an average weight of 200 g were used in this study. The rats were acclimatized for 5 days, received water ad libitum and kept in the animal house of the Faculty of Basic Medical Sciences of the study institution. The animals were fed daily with standard diet. The animals were grouped into twelve with five animals each in a wire gauzed cage. The total number of rats and the number of rats per group were as determined and approved by the policy guidelines of laboratory animal use and care of the University Ethical Review Committee of the study institution. The animals were kept under a normal room temperature of 37°C and double-crossed ventilation.

Experimental Procedures and Drugs Administration

Group 1 received physiological saline. Group 2 received 10 mg/kg bodyweight of Sodium arsenite (SA) for 5 weeks. Groups 3 and 4 received 10 mg/kg bodyweight SA for 2 weeks followed by treatments with 7.5 and 15 mg/kg bodyweight of MLF1 respectively for another 3 weeks. Groups 5 and 6 received 10 mg/kg bodyweight SA for 2 weeks followed by treatments with 7.5 and 10 mg/kg bodyweight of AMF1 respectively for another 3 weeks. Groups 7 and 8 received 7.5 and 15 mg/kg bodyweight of MLF1 respectively for 5 weeks. Groups 9 and 10 received 7.5 and 10 mg/kg bodyweight of AMF1 respectively for 5 weeks. Group 11 received co-administrations of 15 mg/kg bodyweight MLF1 and 10 mg/kg bodyweight SA for 5 weeks. Group 12 received co-administrations of 10 mg/kg bodyweight of AMF1 and 10 mg/kg bodyweight SA for 5 weeks. All drugs and extract were administered orally. Bodyweights (g) of all rats were measured on Day 1 of experimental procedure and at the end of each week.

Histopathological evaluations of the Liver

At the end of the experimental procedures, following animal sacrifice, the liver of each rat was excised and a lobe fixed in 10% formal saline of at least five times of its volume. Liver tissues were processed for light microscopy using conventional histological procedures. Tissue sections were stained via Haematoxylin and Eosin method as previously described by Akinlolu et al. (2017).

Evaluations of Lipid peroxidation

The thiobarbituric acid assay (TBARS assay) method was used to quantify Malondialdehyde

concentrations in liver homogenates of all rats of Control and Experimental Groups as previously described by Akinlolu et al. (2017).

Sera Melatonin, Sera TNFα and Liver tissues' p53 proteins concentrations using Enzyme Linked Immunosorbent Assay (ELISA)

The thoracic cavity of each rat was exposed and 5 mls blood sample collected via the ventricles of the heart into Lithium heparinized bottles. The blood samples were centrifuged and the serum was used for ELISA analyses of concentrations of Melatonin and TNFα proteins in all rats of Control and Experimental Groups using ELISA technique. In addition, liver tissues were isolated immediately after animal sacrifice and then subjected thorough homogenization using porcelain mortar and pestle in ice-cold 0.25 M sucrose, in the proportion of 1 g to 4 ml of 0.25 M sucrose solution. The tissue homogenates were filled up to 5 ml with additional sucrose and collected in a 5 ml serum bottle. Homogenates were thereafter centrifuged at 3000 revolution per minute for 15 minutes using a centrifuge (Model 90-1). The supernatant was collected with Pasteur pipettes and placed in a freezer at -4°C, and thereafter assayed for concentrations of p53 protein in the liver tissues of all rats using ELISA technique.

Statistical Analyses

Statistical analyses were conducted using the 2019 Statistical Package for the Social Science software Version 23.0. Computed data of concentrations of biomarker was expressed as arithmetic means ± standard deviation and were subjected to statistical analyses using One-way Analysis of Variance to test for significant difference amongst Groups 1-12. Degree of freedom (df): (between groups and within groups) and F-values were computed. Scheffe Post-hoc analysis was used for separation of Mean values amongst Groups 1-12. Significant difference was confirmed at 95% confidence interval with $P \leq 0.05$.

RESULTS

Histopathological evaluations of the Liver

Histopathological evaluations showed normal histoarchitectures of the liver in rats of Groups 1-12 (Figs. 1-12). There were normal cellular density and staining characteristics of hepatocytes, hepatic sinusoids, and central veins. The nuclei of hepatocytes were well characterized with no apparent large vacuolations around them.

Table 1. Malondialdehyde (MDA) concentrations (mean±SD) (µmol/ml) in liver tissues of rats.

Groups of rats	Doses of drug/extract administered	MDA (Mean±SD) (µmol/ml)	*P≤0.05*: Group-2 versus Groups 1 and 3-12
1	Physiological saline (5 weeks)	2.22 ± 0.39	0.16
2	10 mg/Kg bodyweight Sodium arsenite (SA) (5 weeks)	2.99 ± 0.10	
3	10 mg/Kg bodyweight SA (2 weeks) + 7.5 mg/Kg bodyweight *Morinda lucida* (3 weeks)	2.43 ± 0.79	0.52
4	10 mg/Kg bodyweight SA (2 weeks) + 15 mg/Kg bodyweight *Morinda lucida* (3 weeks)	2.34 ± 0.79	0.39
5	10 mg/Kg SA (2 weeks) + 7.5 mg/Kg bodyweight *Annona muricata* (3 weeks)	2.95 ± 0.89	0.96
6	10 mg/Kg bodyweight SA (2 weeks) + 10 mg/Kg bodyweight *Annona muricata* (3 weeks)	2.31 ± 0.78	0.45
7	7.5 mg/Kg bodyweight *Morinda lucida* (5 weeks)	2.43 ± 0.38	0.20
8	15 mg/Kg bodyweight *Morinda lucida* (5 weeks)	2.34 ± 0.37	0.26
9	7.5 mg/Kg bodyweight *Annona muricata* (5 weeks)	2.35 ± 0.39	0.20
10	10 mg/Kg bodyweight *Annona muricata* (5 weeks)	2.44 ± 0.37	0.99
11	Co-administration of 15 mg/Kg bodyweight *Morinda lucida* + 10 mg/Kg bodyweight SA (5 weeks)	2.39 ± 0.61	0.38
12	Co-administration of 10 mg/Kg bodyweight *Annona muricata* + 10 mg/Kg bodyweight SA (5 weeks)	2.52 ± 0.63	0.49

Malondialdehyde (MDA) concentrations in Liver tissues of rats

Results showed statistically non-significant higher (*P≥0.05*) MDA levels in rats of Group 2 when compared with Group 1 (Table 1 and Fig. 13). In addition, results showed statistically non-significant lower (*P≥0.05*) MDA levels in rats of Groups 3-12 when compared with Group 2 (Table 1 and Fig. 13).

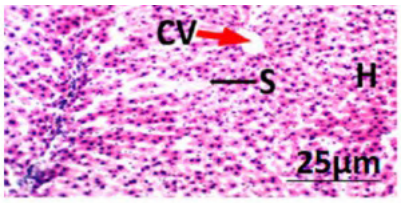

Fig. 1

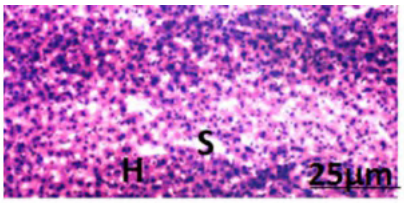

Fig. 2

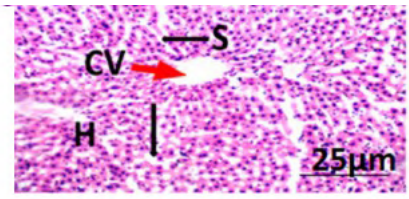

Fig. 3

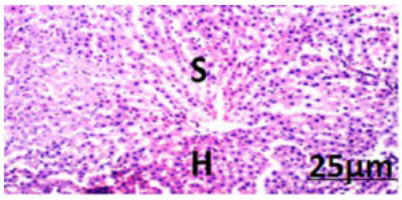

Fig. 4

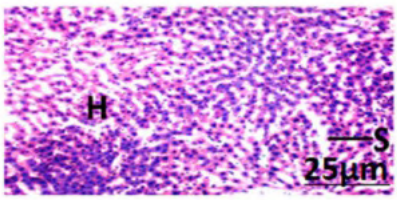

Fig. 5

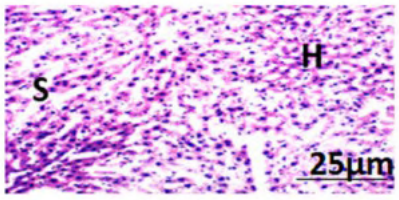

Fig. 6

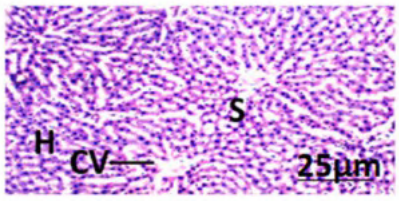

Fig. 7

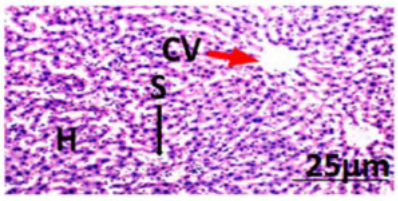

Fig. 8

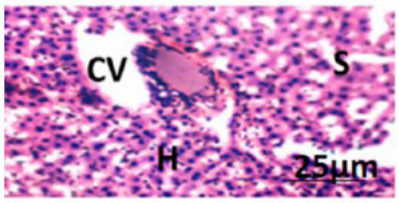

Fig. 9

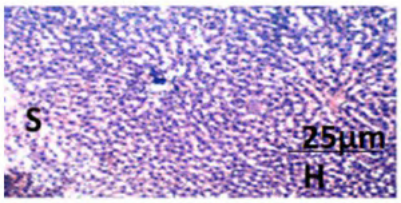

Fig. 10

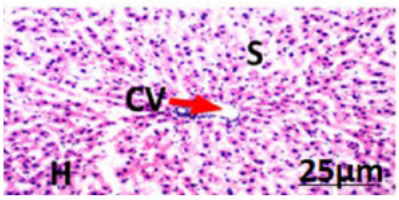

Fig. 11

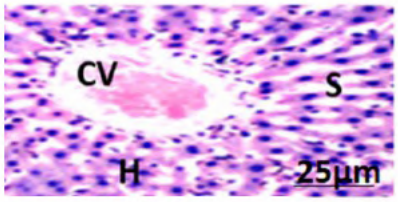

Fig. 12

Fig. 1.- Liver of rat of control group 1, which received normal saline. Haematoxylin and Eosin (x 100). H = Hepatocytes, S = Blood sinusoids and CV = Central Vein. Histopathological evaluations showed normal histoarchitecture of the liver components. **Fig. 2.**- Liver of rat of experimental group 2, which received 100 mg/kg bodyweight of lead acetate only. Haematoxylin and Eosin (x 100). H = Hepatocytes, S = Blood sinusoids and CV = Central Vein. Histo-pathological evaluations showed normal histoarchitecture of the liver components. **Figs. 3. and 4.**- Liver of rat of experimental groups 3 and 4, which received 100 mg/Kg bodyweight lead acetate (2 weeks) + 7.5 and 15mg/Kg bodyweight *Morinda lucida* (3 weeks) respectively. Haematoxylin and Eosin (x 100). H = Hepatocytes, S = Blood sinusoids and CV = Central Vein. Histopathological evaluations showed normal histoarchitecture of the liver components. **Figs. 5 and 6.**- Liver of rat of experimental groups 5 and 6, which received 100 mg/Kg bodyweight lead acetate (2 weeks) + 7.5 and 10mg/Kg bodyweight *Annona muricata* (3 weeks) respectively. Haematoxylin and Eosin (x 100). H = Hepatocytes, S = Blood sinusoids and CV = Central Vein. Histopathological evaluations showed normal histoarchitecture of the liver components. **Figs. 7 and 8.**- Liver of rat of experimental groups 7 and 8, which received only 7.5 and 15 mg/Kg bodyweight *Morinda lucida* (3 weeks) respectively. Haematoxylin and Eosin (x 100). H = Hepatocytes, S = Blood sinusoids and CV = Central Vein. Histopathological evaluations showed normal histoarchitecture of the liver components. **Figs. 9 and 10.**- Liver of rat of experimental groups 9 and 10, which received only 7.5 and 10 mg/Kg bodyweight *Annona muricata* (3 weeks) respectively. Haematoxylin and Eosin (x 100). H = Hepatocytes, S = Blood sinusoids and CV = Central Vein. Histopathological evaluations showed normal histoarchitecture of the liver components. **Fig. 11.**- Liver of rat of experimental group 11, which received co-administration of 100 mg/Kg bodyweight lead acetate + 15 mg/Kg bodyweight *Morinda lucida* (5 weeks). Haematoxylin and Eosin (x 100). H = Hepatocytes, S = Blood sinusoids and CV = Central Vein. Histopathological evaluations showed normal histoarchitecture of the liver components. **Fig. 12.**- Liver of rat of experimental group 12, which received co-administration of 100 mg/Kg bodyweight lead acetate + 10 mg/Kg bodyweight *Annona muricata* (5 weeks). Haematoxylin and Eosin (x 100). H = Hepatocytes, S = Blood sinusoids and CV = Central Vein. Histopathological evaluations showed normal histoarchitecture of the liver components.

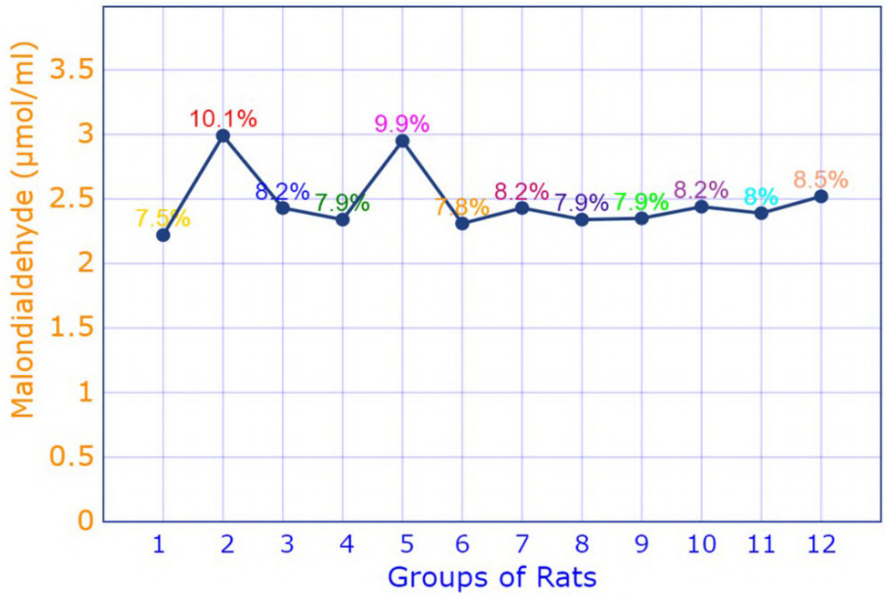

Fig. 13.- Concentrations of Malondialdehyde (µmol/nl) in liver homogenates of rats.

Sera Melatonin concentrations in rats

Results showed statistically significant lower (*P≤0.05*) levels of Melatonin in rats of Group 2 when compared with Group 1 (Table 2 and Fig. 14). In addition, results showed statistically significant higher (*P≤0.05*) levels of Melatonin in rats of Groups 4 - 10 when compared with Group 2 (Table 2 and Fig. 14). However, there were statistically non-significant higher (*P≥0.05*) levels of Melatonin in rats of Groups 3 and 12 when compared with Group 2 (Table 2 and Fig. 14).

Table 2. Melatonin concentrations (mean±SD) (ng/ml) in sera of rats.

Groups of rats	Doses of drug/extract administered	Melatonin (Mean±SD) (ng/ml)	*P*≤0.05: Group-2 versus Groups 1 and 3-12
1	Physiological saline (5 weeks)	0.29 ± 0.01	0.05*
2	10 mg/Kg bodyweight Sodium arsenite (SA) (5 weeks)	0.21 ± 0.08	
3	10 mg/Kg bodyweight SA (2 weeks) + 7.5 mg/Kg bodyweight Morinda lucida (3 weeks)	0.26 ± 0.03	0.94
4	10 mg/Kg bodyweight SA (2 weeks) + 15 mg/Kg bodyweight Morinda lucida (3 weeks)	0.31 ± 0.04	0.04*
5	10 mg/Kg SA (2 weeks) + 7.5 mg/Kg bodyweight Annona muricata (3 weeks)	0.39 ± 0.02	0.03*
6	10 mg/Kg bodyweight SA (2 weeks) + 10 mg/Kg bodyweight Annona muricata (3 weeks)	0.36 ± 0.03	0.03*
7	7.5 mg/Kg bodyweight Morinda lucida (5 weeks)	0.42 ± 0.04	0.02*
8	15 mg/Kg bodyweight Morinda lucida (5 weeks)	0.43 ± 0.07	0.02*
9	7.5 mg/Kg bodyweight Annona muricata (5 weeks)	0.33 ± 0.03	0.03*
10	10 mg/Kg bodyweight Annona muricata (5 weeks)	0.58 ± 0.07	0.02*
11	Co-administration of 15 mg/Kg bodyweight Morinda lucida + 10 mg/Kg bodyweight SA (5 weeks)	0.21 ± 0.08	0.99
12	Co-administration of 10 mg/Kg bodyweight Annona muricata + 10 mg/Kg bodyweight SA (5 weeks)	0.24 ± 0.07	0.95

* = Statistically significant difference

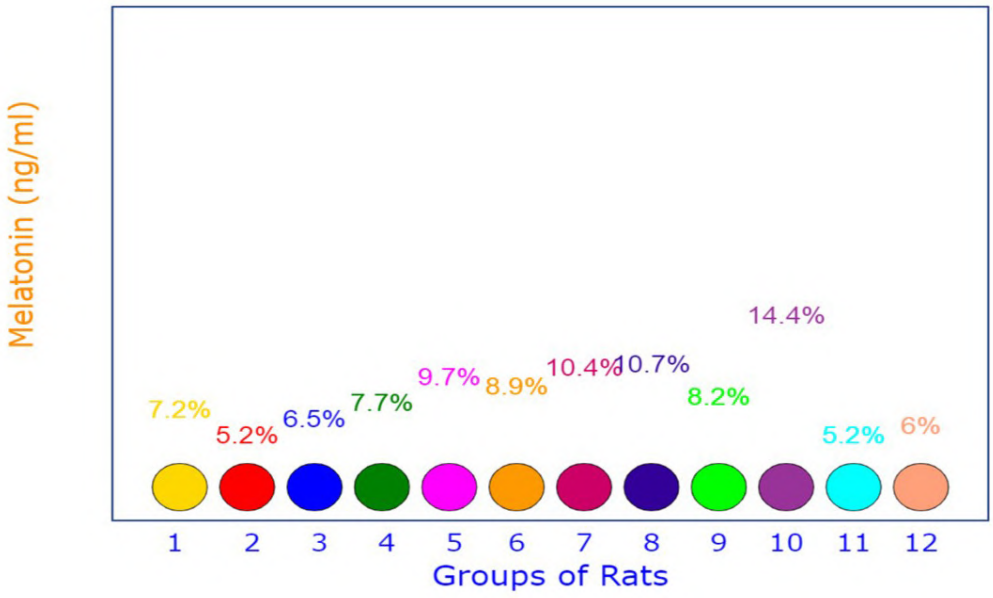

Fig. 14.- Melatonin concentrations (ng/ml) in sera of rats.

Sera TNFα concentrations in rats

Results showed statistically significant higher (P≤0.05) levels of TNFα in rats of Group 2 when compared with Group 1 (Table 3 and Fig. 15). In addition, results showed statistically significant lower (P≤0.05) levels of TNFα in rats of Group 11 when compared with Group 2 (Table 3 and Fig. 15). However, there were statistically non-significant lower (P≥0.05) levels of TNFα in rats of Groups 3 – 10 and 12 when compared with Group 2 (Table 3 and Fig. 15).

Table 3. Sera TNF-α concentrations (mean±SD) (ng/ml) in rats.

Groups of rats	Doses of drug/extract administered	TNFa (Mean±SD) (ng/ml)	*P≤0.05*: Group-2 versus Groups 1 and 3-12
1	Physiological saline (5 weeks)	5.73 ± 6.58	0.03*
2	10 mg/Kg bodyweight Sodium arsenite (SA) (5 weeks)	20.19 ± 4.40	
3	10 mg/Kg bodyweight SA (2 weeks) + 7.5 mg/Kg bodyweight *Morinda lucida* (3 weeks)	16.85 ± 4.34	0.46
4	10 mg/Kg bodyweight SA (2 weeks) + 15 mg/Kg bodyweight *Morinda lucida* (3 weeks)	13.35 ± 4.44	0.19
5	10 mg/Kg SA (2 weeks) + 7.5 mg/Kg bodyweight *Annona muricata* (3 weeks)	16.94 ± 4.69	0.34
6	10 mg/Kg bodyweight SA (2 weeks) + 10 mg/Kg bodyweight *Annona muricata* (3 weeks)	14.38 ± 4.23	0.22
7	7.5 mg/Kg bodyweight *Morinda lucida* (5 weeks)	16.94 ± 6.88	0.62
8	15 mg/Kg bodyweight *Morinda lucida* (5 weeks)	14.38 ± 6.57	0.86
9	7.5 mg/Kg bodyweight *Annona muricata* (5 weeks)	13.88 ± 6.58	0.92
10	10 mg/Kg bodyweight *Annona muricata* (5 weeks)	13.98 ± 6.56	0.91
11	Co-administration of 15 mg/Kg bodyweight *Morinda lucida* + 10 mg/Kg bodyweight SA (5 weeks)	4.74 ± 4.26	0.02*
12	Co-administration of 10 mg/Kg bodyweight *Annona muricata* + 10 mg/Kg bodyweight SA (5 weeks)	13.35 ± 4.44	0.24

* = Statistically significant difference

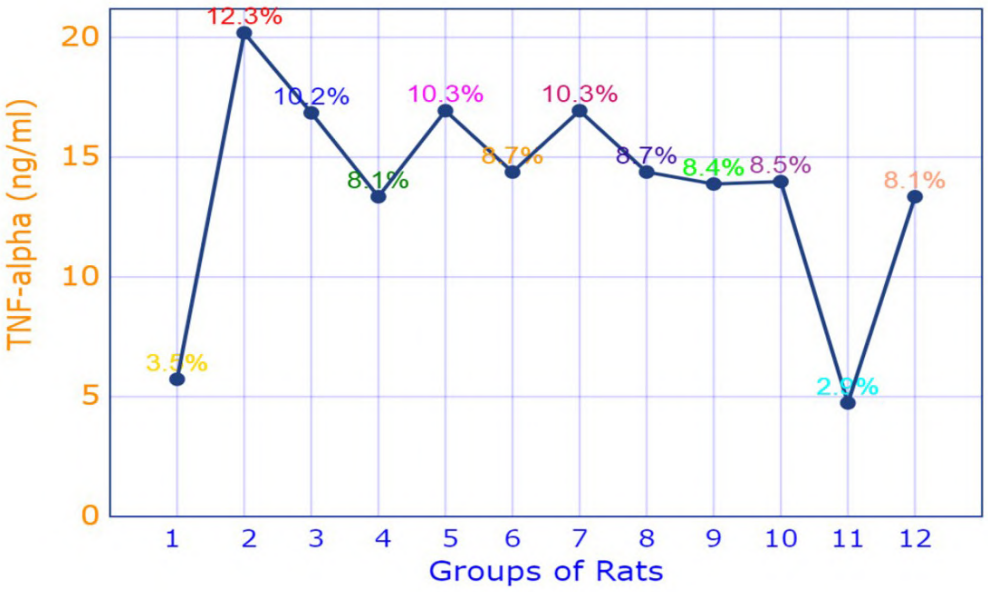

Fig. 15.- Sera concentrations (ng/ml) of TNF-alpha in rats.

p53 concentrations in Liver tissues of rats

Results showed statistically significant higher (*P≤0.05*) levels of p53 in rats of Group 2 when compared with Group 1 (Table 4 and Fig. 16). In addition, results showed statistically significant lower (*P≤0.05*) levels of p53 in rats of Groups 3-11 when compared with Group 2 (Table 4 and Fig. 16). However, there were statistically non-significant lower [*P≥0.05*] levels of p53 in rats of Group 12 when compared with Group 2 (Table 4 and Fig. 16).

Table 4. p53 concentrations (mean±SD) (ng/ml) in liver tissues of rats.

Groups of rats	Doses of drug/extract administered	p53 (Mean±SD) (ng/ml)	*P≤0.05*: Group 2 versus Groups 1 and 3-12
1	Physiological saline (5 weeks)	6.74 ± 1.92	0.02*
2	10 mg/Kg bodyweight Sodium arsenite (SA) (5 weeks)	45.75 ± 2.76	
3	10 mg/Kg bodyweight SA (2 weeks) + 7.5 mg/Kg bodyweight *Morinda lucida* (3 weeks)	24.40 ± 3.19	0.04*
4	10 mg/Kg bodyweight SA (2 weeks) + 15 mg/Kg bodyweight *Morinda lucida* (3 weeks)	16.5 ± 2.65	0.03*
5	10 mg/Kg SA (2 weeks) + 7.5 mg/Kg bodyweight *Annona muricata* (3 weeks)	26.20 ± 2.88	0.03*
6	10 mg/Kg bodyweight SA (2 weeks) + 10 mg/Kg bodyweight *Annona muricata* (3 weeks)	25.21 ± 2.73	0.03*
7	7.5 mg/Kg bodyweight *Morinda lucida* (5 weeks)	17.58 ± 0.38	0.04*
8	15 mg/Kg bodyweight *Morinda lucida* (5 weeks)	13.41 ± 1.80	0.03*
9	7.5 mg/Kg bodyweight *Annona muricata* (5 weeks)	22.1 ± 3.16	0.04*
10	10 mg/Kg bodyweight *Annona muricata* (5 weeks)	20.72 ± 4.45	0.04*
11	Co-administration of 15 mg/Kg bodyweight *Morinda lucida* + 10 mg/Kg bodyweight SA (5 weeks)	31.13 ± 2.89	0.05*
12	Co-administration of 10 mg/Kg bodyweight *Annona muricata* + 10 mg/Kg bodyweight SA (5 weeks)	39.28 ± 5.44	0.07

* = Statistically significant difference

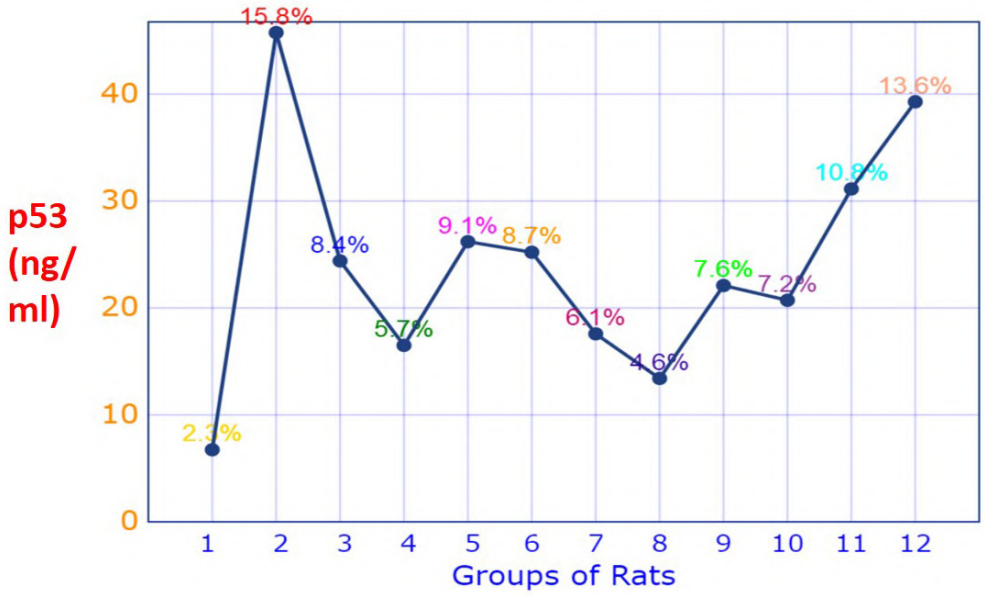

Fig. 16.- Concentrations of p53 (ng/ml) in liver homogenates of rats.

DISCUSSION

Histopathological evaluations showed normal histoarchitectures of the liver in rats of Groups 1-12 (Figs. 1-12). This implied that administrations of 10 mg/kg bodyweight of sodium arsenite (SA), 7.5 and 15 mg/kg bodyweight of MLF1 (extracted from Morinda lucida leaves) and 7.5 and 10 mg/kg bodyweight of AMF1 (extracted from Annona muricata leaves) to rats did not result in evident histopathology of the liver after 5 weeks of exposure.

Lipid peroxidation results in compromised cell membrane and cellular damage, and it is implicated in inflammation and carcinogenesis (Akinlolu et al., 2012). Malondialdehyde is a resultant mutagenic aldehyde product of lipid peroxidation (Akinlolu et al., 2012). Hence, increased Malondialdehyde levels imply increased oxidative stress. Results showed statistically non-significant higher ($P \geq 0.05$) Malondialdehyde levels in rats of Group 2 when compared with Group 1 (Table 1 and Fig. 13). This implied that the administration of 10 mg/kg bodyweight of SA resulted in increased oxidative stress in rats of Group 2.

Do MLF1 and AMF1 have cyto-protective and antioxidant potentials against SA-induced oxidative stress? Post-treatments of SA-induced oxidative stress with MLF1-doses and AMF1-doses resulted in decreased Malondialdehyde levels in rats of Groups 3-6 when compared with Group 2 (Table 1 and Fig. 13). Hence, MLF1 and AMF1 possess cyto-protective and antioxidant potentials.

Do MLF1 and AMF1 have chemo-preventive and antioxidant potentials against SA-induced oxidative stress? The co-administrations of SA-dose with 15 mg/kg bodyweight of MLF1 and 10 mg/kg bodyweight of AMF1 resulted in decreased Malondialdehyde levels in Groups 11 and 12 when compared with Group 2 (Table 1 and Fig. 13). Therefore, MLF1 and AMF1 possess chemo-preventive antioxidant potentials.

Melatonin is a mitochondria-targeted antioxidant (Russel et al., 2016), which inhibits lipid peroxidation by directly scavenging resulting alkoxyl radical and by maintaining cellular glutathione levels (which is otherwise reduced in oxidative stress) (Lampiao and Du Plessis, 2013; Zamfir et al., 2014; Mohammadi et al., 2016; Russel et al., 2016). Melatonin also inhibits the release of pro-inflammatory cytokines and downregulates cyclooxygenase-2, resulting in anti-inflammation and inhibition of cancer growth and metastasis (Lampiao and Du Plessis, 2013; Zamfir et al., 2014). Melatonin is mainly metabolized in the liv-

er (Lampiao and Du Plessis, 2013), hence its strong involvement in the resolutions of hepato-toxicity, hepatic oxidative stress and mutagenesis. Increased melatonin levels are thus associated with reduced DNA and cellular damage, decreased oxidative stress, inflammation and proliferation.

Results showed statistically significant lower ($P \leq 0.05$) levels of melatonin in rats of Group 2 when compared with Group 1 (Table 2 and Fig. 14). This implied that the administration of 10 mg/kg bodyweight of SA resulted in prominent reduction in the antioxidant system in rats of Group 2.

Do MLF1 and AMF1 have cyto-protective and antioxidant potentials against SA-induced prominent reduction in the antioxidant system? Post-treatments of SA-induced prominent reduction in the antioxidant system with doses of MLF1 and AMF1 resulted in increased Melatonin levels in rats of Groups 3-6 when compared with Group 2 (Table 2 and Fig. 14). Hence, MLF1 and AMF1 possess pro-melatonin, cyto-protective and prominent promotion of the antioxidant system potentials.

Do MLF1 and AMF1 have chemo-preventive and antioxidant potentials against SA-induced prominent reduction in the antioxidant system? The co-administration of SA-dose with 10 mg/kg bodyweight of AMF1 resulted in increased Melatonin levels in Groups 11 and 12 when compared with Group 2 (Table 2 and Fig. 14). Therefore, AMF1 possesses pro-Melatonin, chemo-preventive and prominent promotion of the antioxidant system potentials.

TNF-alpha (TNFα) is a pro-inflammatory cytokine and its upregulation resulted in induction of necrosis and consequent apoptosis (necroptosis) in animal models (Liu et al., 2004, Zahr et al., 2010; Chu, 2013). Hence, TNFα is a biomarker of interest in the evaluation of inflammation, tumor progression and cancer cells survival. Results showed statistically significant higher ($P \leq 0.05$) levels of TNFα in rats of Group 2 when compared with Group 1 (Table 3 and Fig. 15). Therefore, this implied that the administration of 10 mg/kg bodyweight of SA resulted in induction of cancer-associated inflammation and upregulation of TNFα in rats of Group 2.

Do MLF1 and AMF1 have cyto-protective and anti-inflammatory potentials against SA-induced cancer-associated inflammation? Post-treatments of SA-induced cancer-associated inflammation with doses of MLF1 and AMF1 resulted in the downregulation of TNFα levels in Groups 3-6 when compared with Group 2 (Table 3 and Fig. 15). Hence, MLF1 and AMF1 possess cyto-protective, anti-inflammatory and anticancer potentials.

Can MLF1 and AMF1 protect the organism and prevent SA-induced cancer-associated inflammation? The co-administrations of 10 mg/kg bodyweight of SA with 15 mg/kg bodyweight of MLF1 and 10mg/kg bodyweight of AMF1 resulted in decreased TNFα levels in Groups 11 and 12 when compared with Group 2 (Table 3 and Fig. 15), and thus protected the rats against SA-induced cancer-associated inflammation. This suggests that MLF1 and AMF1 possess chemo-preventive anti-inflammatory potentials.

p53 trans-activates several apoptotic and cell-cycle arrest-induction genes in response to inflammation, DNA damage, chromosomal aberrations, mutagenesis and carcinogenesis. p53 is usually expressed as a functionally latent form at a very low level in normal condition as mediated majorly by proteasomal degradation actions of RING-finger type E3 ubiquitin protein ligase MDM2. However, in response to DNA damage, there is upregulation, accumulation and activation of p53 in the cell nucleus via post-translational modifications such as phosphorylation and acetylation. Following successful repair of DNA and cellular damage, p53 level returns to normal low level (Chang et al., 2010; Toshinori and Akira, 2011; Xiao et al., 2013).

Results showed statistically significant higher ($P \leq 0.05$) levels of p53 in rats of Group 2 when compared with Group 1 (Table 4 and Fig. 16). This result implied that administration of 10 mg/kg bodyweight of SA resulted in mutagenesis with consequent upregulation of p53 in rats of Group 2. It must be noted that with increased upregulations of Malondialdehyde and TNFα levels, and reduced Melatonin levels, in only the rats of Group 2 (Tables 1-3 and Figs. 13-16), the characteristic expected immune response and DNA/cell-damaged repair mechanism is induction of apoptosis and

upregulation of p53 pro-apoptotic gene (Chang et al., 2010; Toshinori and Akira, 2011; Xiao et al., 2013). In the absence of cancer treatment, the sustained upregulation of p53 in rats of SA-only treated Group 2 at the end of the 5-week experimental procedure implied rapid and sustained SA-induced mutagenesis. This will gradually inhibit and prolong the DNA repair mechanism of p53 until its actions are spent out in-order to allow for un-inhibited mutagenesis. Consequently, cancer-cells survival and tumorigenesis will prevail.

Do MLF1 and AMF1 have cyto-protective and anticancer potentials against SA-induced mutagenesis? Post-treatments of 10 mg/kg bodyweight of SA-induced p53 upregulation with doses of MLF1 and AMF1 in rats of Groups 3-6 resulted in significant downregulations of p53 levels when compared with Group 2 (Table 4 and Fig. 16). This implied that MLF1 and AMF1 possess pro-apoptotic, tumor suppression and anticancer potentials that will bring p53 to normal levels after the resolution of mutagenesis.

Can MLF1 and AMF1 protect the organism and prevent SA-induced mutagenesis? The co-administrations of 10mg/kg bodyweight of SA with 15 mg/kg bodyweight of MLF1 and 10mg/kg bodyweight of AMF1 resulted in decreased p53 levels in Groups 11 and 12 when compared with Group 2 (Table 4 and Fig. 16), and thus protected the rats against SA-induced mutagenesis. This suggests that MLF1 and AMF1 possess chemo-preventive, pro-apoptotic and anticancer potentials.

Overall, the observations of this study suggest that post-treatments with doses of MLF1 (extracted from Morinda lucida leaves) and AMF1 (extracted from Annona muricata leaves) following exposure to sodium arsenite resulted in decreased malondialdehyde, TNF-alpha and p53 levels, and increased melatonin levels. This indicates that MLF1 and AMF1 conferred a degree of cyto-protective, antioxidant, pro-melatonin, hepatoprotective, anti-inflammatory and anticancer potentials against sodium-arsenite-induced toxicity, and are recommended for further evaluation as potential drug candidates for the treatment of cancers.

ACKNOWLEDGEMENTS

The authors acknowledge the technical support of Laboratory staff members of the Departments of Anatomy and Chemistry of the University of Ilorin, Nigeria, the Central Research Laboratory, Ilorin, Nigeria.

REFERENCES

ADELEYE OO, AYENI OJ, AJAMU MA (2018) Traditional and medicinal uses of *Morinda lucida*. *J Medicinal Plants Stud*, 6(2): 249-254.

ADEJO GO, ATAWODI SE, AMEH DA, IBRAHIM S (2014) Anti-peroxidative, protective and ameliorative properties of methanol extract of all parts of *Morinda Lucida* Benth in CCl_4-induced liver injury. *Natural Products Chem Res*, S1: 003.

AGU KC, OKOLIE PN (2017) Proximate composition, phytochemical analysis, and in vitro antioxidant potentials of extracts of *Annona muricata* (Soursop). *Food Sci Nutri*, 5(5): 1029-1036.

AKINDELE F, OBI FO (2020) Antioxidant potential of *Morinda lucida* and *Psidium guajava* extracts and actions against paracetamol-induced kidney and liver injuries in rats. *Am Int J Biol Life Sci*, 2(1): 6-17.

AKINLOLU AA, SHOKUNBI MT (2010) Histological effects of 25mg/kg/bodyweight of artemether on the trapezoid nuclei of Wistar rats. *Acta Histochem*, 112: 193-198.

AKINLOLU A, SALAU BA, AKINGBOLA T (2012) Lipid peroxidation in Nigerians affected with heamatological malignancies. *African J Medicine Med Sci*, 41(Supplement): 145-148.

AKINLOLU AA, BAYODE OE, GHAZALI OK, AMEEN OM (2017) The effects of *Moringa oleifera* on lipid profile status, heart histology and liver histochemistry in adult Wistar rats. *CHRISMED J Health Res*, 4: 104-109.

ALIYU M, OYERONKE A, ODUNOLA MAG, ABDULLAHI BS, UCHE SN, MOHAMMED AI (2015) Inhibitory effects of sodium arsenite and acacia honey on acetylcholinesterase in rats. *Int J Alzheimer's Disease*, Article ID 903603: 1-7.

CHANG T, PING L, NANCY L, WU YY, QI-LONG Y (2010) Production of *p53* gene knockout rats by homologous recombination in embryonic stem cells. *Nature*, 467: 211-213.

CHU W-M (2013) Tumor necrosis factor. *Cancer Lett*, 328(2): 222-225.

INTERNATIONAL AGENCY FOR RESEARCH ON CANCER (2012) Monographs on the Evaluation of Carcinogenic Risks to Humans. Arsenic, Metals and Dusts. Volume 100C. A review of Human Carcinogens. IARC Working Group on the Evaluation of Carcinogenic Risk to Humans [Online]. In: Lyon (France): IARC on Cancer; 2012 [cited 2022 Mar 19]. Retrieved from: https://monographs.iarc.fr/wp-content/uploads/2018/06/mono100C.pdf

JOMOVA K, JENISOVA Z, FESZTEROVA M, BAROS S, LISKA J, HUDECOVA D, RHODES CJ, VALKO M (2011) Arsenic: toxicity, oxidative stress and human disease. *J Appl Toxicol*, 31(2): 95-107.

JUSTINO AB, MIRANDA NC, FRANCO RR, MARTINS MM, SILVA NMD, ESPINDOLA FS (2018) Annona muricata Linn leaf as a source of antioxidant compounds with in vitro andtidiabetic and inhibitory potential against α-amylase, α-glucosidase, lipase, non-enzymatic glycation and lipid peroxidation. *Biomed Pharmacother*, 100: 83-92.

LAMPIAO F, DU PLESSIS SS (2013) New developments of the effect of melatonin on reproduction. *World J Obs Gyn*, 2(2): 8-15.

LIU H, MA Y, PAGLIARI LJ, PERLMAN H, YU C, LIN A, POPE RM (2004) TNF-induced apoptosis of macrophages following inhibition of NF-B: A central role for disruption of mitochondria. *J Immunol*, 172: 1907-1915.

MOGHADAMTOUSI SZ, FADAEINASAB M, NIKZAD S, MOHAN G, ALI MH, KADIR AH (2015) Annona muricata (*Annonaceae*): A review of its traditional uses, isolated acetogenins and biological activities. *Int J Mol Sci*, 16(7): 15625-15658.

MOHAMMADI M, REZAIE MJ, ROSTAMZADEH A, ALLAHVEISI A, MOHAMMADI HR, MOHAMMADI F (2016) Signalling pathways of melatonin in prevention of liver disorders via suppressing of oxidative stress in cellular level. *Biomed Pharmacol J*, 9(2).

RUSSEL JR, JUAN CM, DUN-XIAN T, ROSA MS, MOISES A-J, LILAN Q (2016) Melatonin as an antioxidant: under promises but over delivers. *J Pineal Res*, 61: 253-278.

SIMON NT (2004) Of rats and men. *Genome Biol,* 5(3): 314.

SINGH AP, GOEL RK, KAUR T (2011) Mechanisms pertaining to arsenic toxicity. *Toxicol Int*, 18(2): 87-93.

TOSHINORI O, AKIRA N (2011) Role of p53 in cell death and human cancers. *Cancers*, 3: 994-1013.

WORLD HEALTH ORGANIZATION (2001) Arsenic and Arsenic Compounds (Environmental Health Criteria 224, 2nd ed.) [Online]. In: Geneva: World Health Organization, International Programme on Chemical Safety; 2001 [cited 2022 Mar 19]. Retrieved from: https://www.who.int/ipcs/publications/ehc/ehc_224/en/.

XIAO LI-J, SHUANG Z, EN-HONG Z, XIN Z, WEN-FENG G, YASUO T, ZHENG H-C (2013) Clinicopathological and prognostic significance of Ki-67, caspase-3 and p53 expression in gastric carcinomas. *Oncol Lett*, 6(5): 1277-1284.

ZAHR NM, LUONG R, SULLIVAN EV, PFEFFERBAUM A (2010) Measurement of serum, liver, and brain cytokine induction, thiamine levels, and hepatopathology in rats exposed to a 4-day alcohol binge protocol. *Alcohol Clin Exp Res*, 34(11): 1858-1870.

ZAMFIR CAA, POPESCU CR, GHEORGHE DC (2014) Melatonin and cancer. *J Med Life*, 7(3): 373-374.

Retromolar canal: a classic analysis with CBCT in South Indian population

Karthikeya Patil[1], C.J. Sanjay[1], K.R. Renuka Devi[1], D. Nagabhushana[1], S. Viveka[1], M.S. Girish[2]

[1] Department of Oral Medicine and Radiology, JSS Dental College and Hospital, JSS Academy of Higher Education and Research, Mysuru-570015, India

[2] Department of Pedodontics and Preventive Dentistry, JSS Dental College and Hospital, JSS Academy of Higher Education and Research, Mysuru-570015, India

SUMMARY

The Retromolar canal (RMC) is an anatomic variation, the identification of which has become a clinical obstacle as the demand for surgical procedures in the retromolar area of the mandible has increased. The inferior alveolar nerve innervates the third molar and some of the muscles around the posterior region of the mandible, making surgical treatments in the retromolar area more challenging. The aim of this study was to evaluate the incidence of RMC using Cone Beam Computed Tomography (CBCT) and to evaluate the prevalence, course, and pattern of occurrence of RMC. CBCT images of 160 patients were collected and screened in the three spatial planes on both right and left sides for the presence of RMC. The incidence rates were determined according to gender, location, and type of RMC. Obtained data were subjected to statistical analysis. Out of the 160 subjects examined, 116 (72.5%) subjects presented with RMCs. It was found that 44 out of 72 males (45%) and 72 of 88 (68%) females presented with retromolar canals. Type B was the most common type. Based on the results of this study, retromolar canal should be considered as a normal anatomical variation rather than a rare finding. CBCT is suggested for a detailed evaluation and identification of the course of RMC before any surgical procedures to avoid post-operative complications. Very few studies have been conducted in Indian population and this study analysed the incidence of the RMC using CBCT images of South Indian population.

Key words: RMC – Cone beam computed tomography – Mandibular canal – Third molar

INTRODUCTION

Anatomical variations may influence predisposition to clinical examination, investigation and patient management. Inability to recognise the anatomical alterations may result in a fatal complication. Such an anatomical variation is RMC. RMC is an unusual anatomic variant in the retromolar triangle, which is a tiny triangular-shaped area in the jaw posterior to the third molar tooth following a course, and curves in posterosuperior direction to open into the retromolar fossa. It comprises neurovascular bundles which provide innervation to third molars. (Patil et al., 2013) Olivier postulated two types of inferior alveolar nerve (IAN) main trunk arrangements based on

Corresponding author:
Dr Sanjay CJ. Reader. Department of Oral Medicine and Radiology, JSS Dental College and Hospital, JSS Academy of Higher Education and Research, Mysuru-570015, India. Phone: +91 9742565566. E-mail: drsanjaycj_dch@jssuni.edu.in

Submitted: May 6, 2022. **Accepted:** August 13, 2022

https://doi.org/10.52083/RAKK7944

50 mandible dissections in 1927 (Olivier, 1928). Type I: the dental branches emerge from the undivided trunk just posterior to the roots that would supply the teeth (66 percent). Type II: The nerve divides into two sections shortly after entering the mandibular canal; a larger mental branch leaves the mandible at the mental foramen without providing any dental branches to the teeth, while a smaller branch forms a plexus and supplies the teeth (34 percent). According to the research in the late 1980's Ossenberg et al. (1987) identified three different patterns of RMCs due to inadequate fusing of distinct mandibular canal nerves from the incisors, primary molars, and permanent molars during embryonic development. (Kawai et al., 2012; Von Arx et al., 2011; Lizio et al., 2013). The evaluation of the RMC is required to minimize traumatization of the contents of this canal during tooth extraction, bone harvesting procedures, and implant insertion (Jablonski et al., 1985; Pannalal et al., 2021; Kikuta.et al., 2018). Cone beam computed tomography (CBCT) made substantial effect on determining RMC than other imaging modalities. (Han et al., 2014). Only a very few studies discussed the RMC evaluation in the Indian population. This study used CBCT scans to impart knowledge about the frequency and prevalent type of retromolar canal course in the South Indian population.

MATERIALS AND METHODS

This is a cross sectional study of subjects who had undergone CBCT examination of posterior mandible during the period of September 2020 to September 2021 from the Department of Oral medicine and radiology. Retrospective and prospective CBCT images were acquired and examined for the presence of RMCs. This study was approved by the Ethical Committee of the Institution (IEC protocol number: 96/2020).

CBCT Images of 160 patients aged between 21-86 years were selected by quota sampling method. CBCT images with optimum diagnostic quality showing retromolar regions were selected. Radiographs having posterior mandibular dental implants, those with clinical or radiographic signs of any pathologies, and those with a history of trauma to the posterior mandibular region and who had been treated with surgical intervention were all excluded. Images of the selected subjects were made using a Planmeca Promax 3D Mid CBCT machine. The tube voltage was set at 90 kVp, the tube current at 5.6 mA and the exposure time at 9.0 s. The height of the field of view (FOV) and the diameter both were 4 cm, and the voxel size was 0.08 mm. All RMCs evident on CBCT were included in the study irrespective of their diameter. The visibility of the retromolar area scan slice was inspected bilaterally in all three sections (sagittal, coronal, axial). All measures were assessed twice by both examiners, with a one-week break between each measurement. The inter- and intra-examiner reliabilities were assessed using Cohen's kappa by examining 10% of the subjects by both the examiners in each survey. The kappa values for the inter- and intra-examiner reliability was 0.82-0.88.

Eventually, RMC was classified into three groups for the purpose of the study – A, B, C based on its origin, course, and relationship to the coronal region of the third molar and the retromolar fossa.

Based on the hypothesis of Patil et al. (2013), RMC was classified into the following three types:

- Type A: RMC branched off the mandibular canal distal to the 3rd molar and proceeded superiorly to open into the retromolar fossa.
- Type B: canals ran between the retromolar fossa and the radicular part of the third molar.
- Type C: the canal originated from the mandibular foramen in the ramus region, coursed anteroinferiorly and then anterosuperiorly to open into the retromolar fossa.

Statistical analysis

The data were recorded into a Microsoft Office Excel Sheet (version 2019) and analyzed with the Statistical Package for Social Sciences (SPSS 22.0) A comparison of gender and age groups was made. To determine whether there was a statistically significant difference between the means in groups, descriptive statistics, and Pearson Chi-Square tests were applied to the data. Kappa statistics was adopted to determine the inter and intra examiner reliability in assessment of RMC.

RESULTS

Of the 160 subjects examined, 116 (72.6%) subjects presented with RMCs, among which 78 (48.8%) subjects presented with unilateral RMC and 38(23.8%) presented with bilateral RMC. On comparing both genders it was found that 44 out of 72 males and 72 out of 88 females_presented with RMCs. Hence females had higher incidence on statistical comparison among the genders in occurrence of RMCs and were found to be statistically significant. (p=0.00) (Table 1).

Table 1. Distribution of subjects among genders with unilateral/bilateral occurrence of retromolar canals.

	Unilateral	Bilateral	Absent
MALE	30(41.7%)	14(19.4%)	28(38.9%)
FEMALE	48(54.5%)	24(27.3%)	16(18.2%)
TOTAL	**78(48.8%)**	**38(23.8%)**	**44(27.5%)**

The distribution of subjects with different types of RMCs based on age groups is described in Tables 2, 3. The most common type of RMC in male is type B (30.6%), followed by type A (11.1%) and type C (2.8%). The common type of RMC in female is type B (31.8%), followed by type A (11.4%) and type C (2.3%). The difference in distribution of RMC among gender was found to be statistically significant (p=0.00).

Among different age groups on the right side, type B was the most common in patients aged 20-30 years (29.7%), in 31-40 years (26.7%), in 41-50 years (44.4%), in 51-60 years (35.7%). Patients aged above 60 years had both type A and Type B in equal incidence in our study (Figs. 1, 2). Type C (Fig. 3) was the least common type occurred in different age groups. Among different age groups on left side, type B was the most common in patient aged 20-30 years (40.5%), in 31-40 years (40.0%), in 41-50 years (22.2%), in 51-60 years (35.7%).

Table 4 depicts the bilateral distribution of RMC among gender. Among males, combination types A+B (50.0%) and B+C (50.0%) had equal incidence. Type B+C had higher incidence in females (77.8%). Type A+C was found only in males in our study. Other combination patterns, such as A+A, B+B, and C+C, include the remaining frequencies. Table 5 shows the prevalence of retromolar canal in different populations, as published in previous studies.

Table 2. Distribution of types of RMC in different age on right side.

TYPE	20-30YR	31-40 YR	41-50YR	51-60 YR	ABOVE 60
A	10(13.5%)	4(13.3%)	0	2(7.1%)	2(20.0%)
B	22(29.7%)	8(26.7%)	8(44.4%)	10(35.7%)	2(20.0%)
C	2(2.7%)	2(6.7%)	0	0	0
TOTAL	**74**	**30**	**18**	**28**	**10**

Table 3. Distribution of types of RMC in different age on left side.

TYPE	20-30YR	31-40 YR	41-50YR	51-60 YR	ABOVE 60
A	8(10.8%)	4(13.3%)	2(11.1%)	0	0
B	30(40.5%)	12(40.0%)	4(22.2%)	10(35.7%)	4(40.0%)
C	4(5.4%)	2(6.7%)	2(11.1%)	0	0
TOTAL	**74**	**30**	**18**	**28**	**10**

Table 4. Distribution of bilateral type of RMC among gender.

	A+B	B+C	A+C
MALE	4(33.3%)	4(22.7%)	2(100.0%)
FEMALE	8(66.7%)	14(77.8%)	0
TOTAL	**12(100.0%)**	**18(100.0%)**	**2(100.0%)**

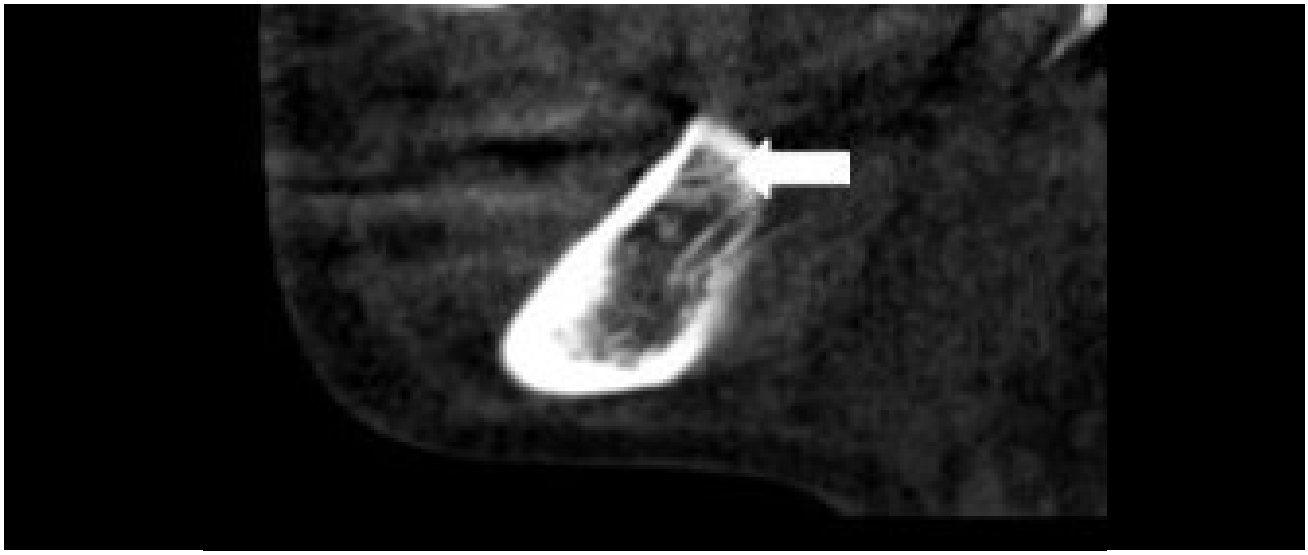

Fig. 1.- Sagittal section of CBCT illustrating Type A- retromolar canal branched off the mandibular canal distal to the 3rd molar and proceeded superiorly to open into the retromolar fossa.

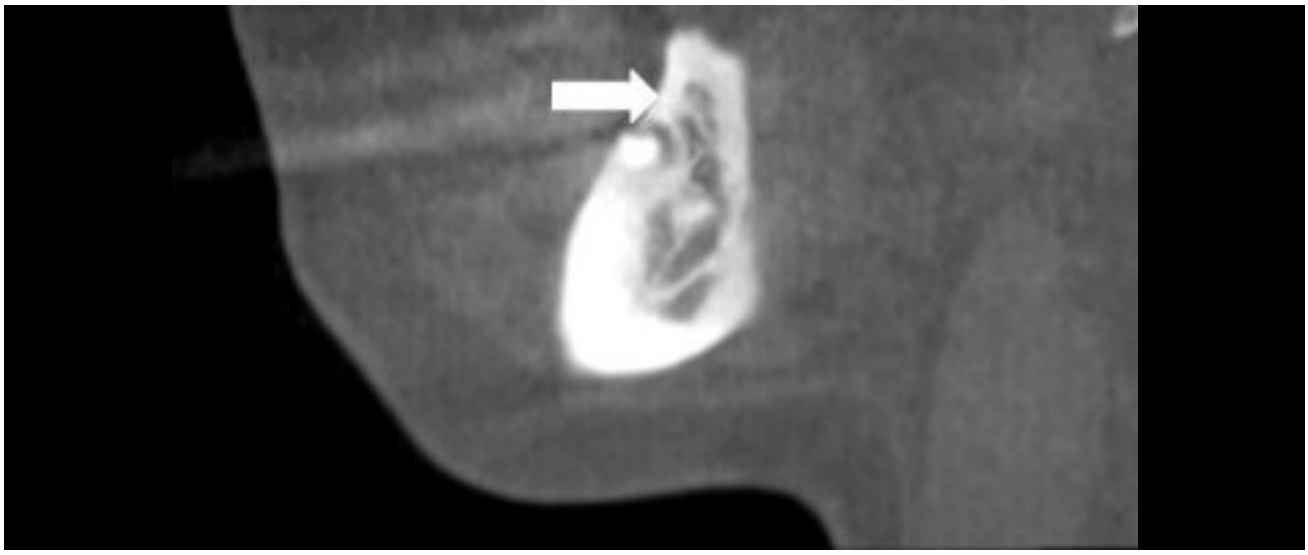

Fig. 2.- Sagittal section of CBCT illustrating Type B- canals ran between the retromolar fossa and the radicular part of the third molar.

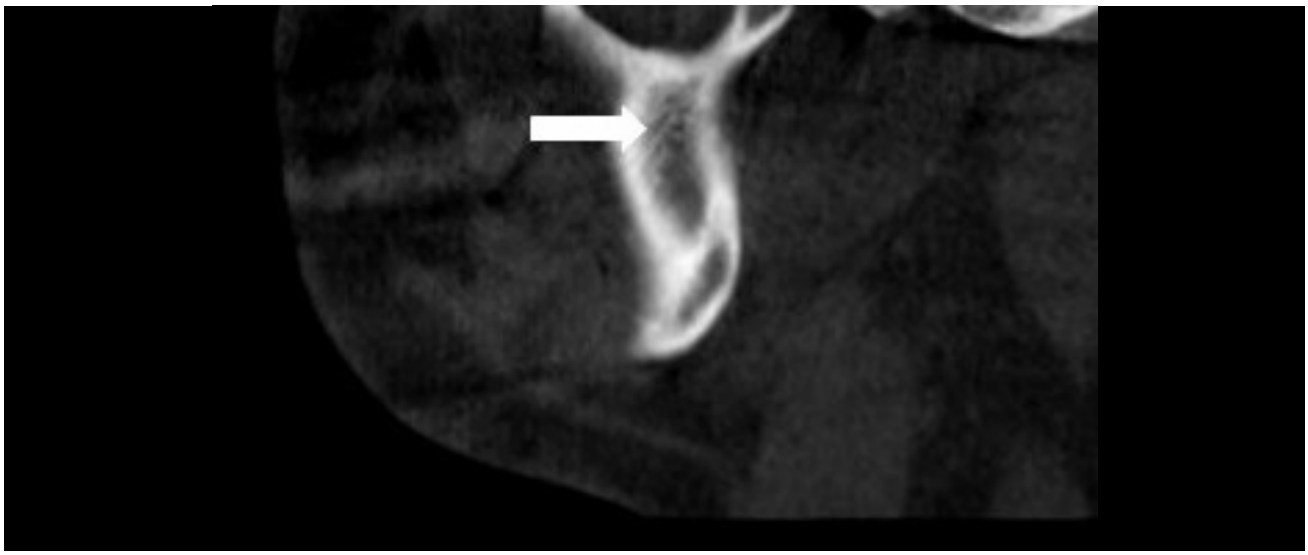

Fig. 3.- Sagittal section of CBCT illustrating Type C-the canal originated from the mandibular foramen in the ramus region, coursed anteroinferiorly and then anterosuperiorly to open into the retromolar fossa.

Table 5. Prevalence of retromolar canal in different populations as reported in previous studies.

AUTHOR	YEAR	POPULATION	NUMBER OF SUBJECTS	% PREVALENCE
Patil et al.	2013	JAPAN	171	75.4
Lizio et al.	2013	ITALY	233	14.6
Muinelo-Lorenzo et al.	2014	SPAIN	225	36.8
Han and Hwang	2014	SOUTH KOREA	446	8.5
Rashsuren et al.	2014	SOUTH KOREA	755	11.5
Sisman et al.	2015	TURKEY	947	26.7
Jamalpour et al.	2016	IRAN	179	12.8
Ahuja et al.	2018	INDIA	80	20
Badry et al.	2020	EGYPT	214	11.2
Oliveira de Gringo	2021	BRAZIL	200	24.5
Present Study	2022	INDIA	160	72.5

DISCUSSION

The RMC is an anatomic variation that originates behind the third molar in the mandibular canal and goes anterosuperiorly to the retromolar foramen (RMF) in the retromolar fossa (Fig. 4). Carter et al. (1971) discovered that the IAN or the retromolar branch that travels through the RMC give rise to a neural branch to the mandibular molars. However, Jablonski et al. (1985) identified an aberrant buccal nerve arising from the IAN within the mandible's ramus, travelling through the RMC, emerging through the RMF, and then continuing forward and upward to penetrate the buccinator muscle. On CBCT research, RMC is now highly recognized. The RMC, however, comprises the retromolar nerve, which is a normal branch of the IAN, as revealed in prior anatomical investigations. Iwanaga et al. (2022) in their study concluded that RMC should be regarded the typical anatomy or normal variant of the inferior alveolar canal. However, few other researchers in their studies concluded that RMC is a branch of inferior mandibular canal. (Naitoh et al., 2009; Langlais et al., 1985). But still there exists a controversy in differentiating the mandibular canal and RMC and hereby in our study we suggest a word forum for consensus in support of the various literatures that are tabulated in Table 5.

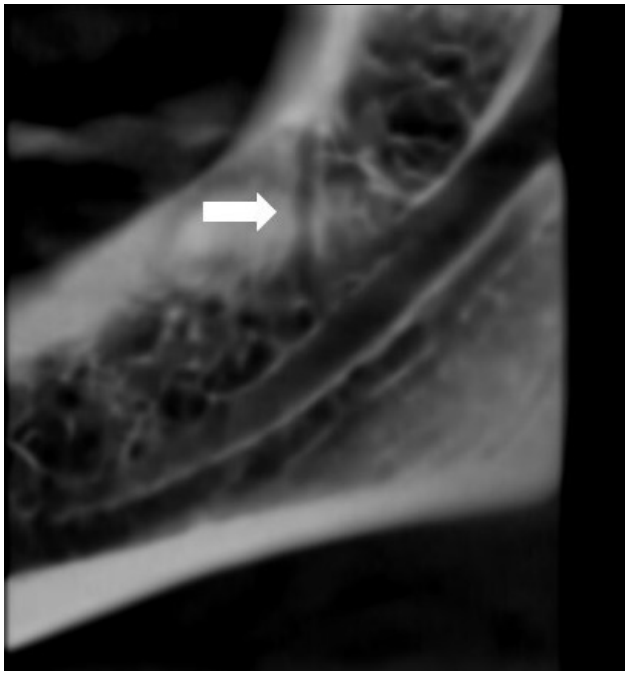

Fig. 4.- CBCT sagittal section showing retromolar canal.

Myelinated nerve fibers are present, along with multiple venules and an artery confirmed by histopathological examinations. During embryologic development, three different mandibular canals appeared in each hemimandible, and from each canal different inferior dental nerves emerged and innervated the three mandibular regions, according to an anthropological study by Chavez et al. (1996). These three canals combine to form a single canal during the fetal growth period of bone remodeling and apposition. Bifurcation or trifurcation is an anatomical variation caused by incomplete union of these three channels.

Anatomical variations such as the supplemental foramen, which acts as an escape route for the impulse to transmit pain, were noted by Rood (1976)

in a case of failure to attain mandibular anesthesia. Some writers have also documented failures in attaining mandibular anesthesia and the existence of a bifid mandibular canal on radiological examination. For the categorization of RMCs in this study, we used Patil et al. (2013) approach. It proved to be the most practical categorization. The type B canal that begins at the RMF and terminates in the radicular section of the 3rd molar was not included in Ossenberg (1987) or Jamalpour et al. (2016) classifications.

CONCLUSION

In conclusion, knowledge of this anatomical variance and its assessment before surgery involving the posterior mandible like extraction of an impacted third molar, bone harvesting as a donor site for bone graft surgery and sagittal split osteotomy may warn the clinician about possible inadequate pre-surgical anesthesia, unexpected bleeding or local altered sensation post-operatively through damage to the vessels and nerves through the RMC. It is, therefore, important to confirm the course and location of the RMC prior to surgical procedures. Since there is no comprehensive study that includes all types of retromolar canals in the Indian population, this study can be considered as the standard incidence of the RMC using CBCT images of South Indian population.

REFERENCES

AHUJA SB, BHARDWAJ NS, DANG V, AHUJA R, MATHUR H (2018) Prevalence of RMC and foramen: A cone beam computed tomography study. *J Indian Acad Oral Med Radiol.* 30: 216-222.

BADRY MSM, EL-BADAWY FM, HAMED WM (2020) Incidence of retromolar canal in Egyptian population using CBCT: a retrospective study. *Egypt J Radiol Nucl Med*, 51: 46.

CHAVEZ ME, MANSILLA J, POMPA JA, KJAER I (1996) The human mandibular canal arises from three separate canals innervating different tooth groups. *J Dent Res*, 75: 1540-1544.

CAROLINE PAULA OLIVEIRA DE GRINGO, EYMI VALERY CAZAS DURAN DE GITTINS, CÁSSIA MARIA FISCHER RUBIRA (2021) Prevalence of RMC and its association with mandibular molars: study in CBCT. *Surg Radiol Anat*, 43: 1785-1791.

CARTER RB, KEEN EN (1971) The intramandibular course of the inferior alveolar nerve. *J Anat,* 108: 433-440.

FREITAS D, DE FREITAS SILVA GB, ALESSANDRA M, ALEXANDRE FS, DA SILVA MB, GOMES TC (2015) Incidence and classification of bifid mandibular canals using cone beam computed tomography. *Braz J Oral Sci*, 14: 294-298.

HAN SS, HWANG YS (2014) Cone beam CT findings of RMCs in a Korean population. *Surg Radiol Anat*, 36: 871-876.

IWANAGA J, TAKESHITA Y, MATSUSHITA Y, HUR MS, IBARAGI S, TUBBS RS (2022) What are the retromolar and bifid/trifid mandibular canals as seen on cone-beam computed tomography? Revisiting classic gross anatomy of the inferior alveolar nerve and correcting terminology. *Surg Radiol Anat,* 44: 147-156.

JABLONSKI NG, CHENG CM, CHENG LC, CHEUNG HM (1985) Unusual origins of the buccal and mylohyoid nerves. *Oral Surg, Oral Med, Oral Pathol,* 60(5): 487-488.

JAMALPOUR M, SHOKRI A, FALAH-KOSHKI S, ZAVAREIAN A (2016) Evaluation of RMCs with cone-beam computed tomography in an Iranian adult population: a retrospective study. *Int J Clin Dentist*, 9(4): 233-240.

KIKUTA S, IWANAGA J, NAKAMURA K, HINO K, NAKAMURA M, KUSUKAWA J (2018) The RMCs and foramina: radiographic observation and application to oral surgery. *Surg Radiol Anat,* 40(6): 647-652.

KAWAI T, ASAUMI R, SATO I, KUMAZAWA Y, YOSUE T (2012) Observation of the retromolar foramen and canal of the mandible: a CBCT and macroscopic study. *Oral Radiol*. 28: 10-14.

LANGLAIS RP, BROADUS R, GLASS BJ (1985) Bifid mandibular canals in panoramic radiographs. *J Am Dent Assoc,* 110: 923-926.

LIZIO G, PELLICCIONI GA, GHIGI G, FANELLI A, MARCHETTI C (2013) Radiographic assessment of the mandibular RMC using cone-beam computed tomography. *Acta Odontol Scand,* 71: 650-655.

MAHMOUD SAYED, MAHMOUD BADRY, FATMA MOSTAFA EL-BADAWY, WALAA MOHAMED HAMED (2020) Incidence of RMC in Egyptian population using CBCT: a retrospective study. *Egyptian J Radiol Nuclear Med,* 51: 46.

MUINELO-LORENZO J, SUAREZ-QUINTANILLA JA, FERNANDEZ ALONSO A, MARSILLAS-RASCADO S, SUAREZ-CUNQUEIRO MM (2014) Descriptive study of the bifid mandibular canals and retromolar foramina: cone beam CT vs panoramic radiography. *Dentomaxillofac Radiol*, 43(5): 20140090.

NAITOH M, HIRAIWA Y, AIMIYA H, ARIJI E (2009) Observation of bifid mandibular canal using cone-beam computerized tomography. *Int J Oral Maxillofac Implants,* 24: 155-159.

OLIVIER E (1928) The inferior dental canal and its nerve in the adult. *Br Dent J,* 49: 356-358.

OSSENBERG NS (1987) Retromolar foramen of the human mandible. *Am J Physn Anthropol*, 72: 119-128.

ORHAN K, AKSOY S, BILECENOGLU B, SAKUL BU, PAKSOY CS (2011) Evaluation of bifid mandibular canals with cone-beam computed tomography in a Turkish adult population: A retrospective study. *Surg Radiol Anat,* 33: 501-507.

PATIL S, MATSUDA Y, NAKAJIMA K, ARAKI K, OKANO T (2013) RMCs as observed on cone-beam computed tomography: Their incidence, course, and characteristics. *Oral Surg Oral Med Oral Pathol Oral Radiol*, 115: 692-699.

PANNALAL V, DEOGHARE A, FATING C, JHA S, BIRANJAN R (2021) The elusive retromolar foramen and RMC: A CBCT study. *IP Int J Maxillofac Imaging*, 7(3): 118-124.

RASHSUREN O, CHOI J-W, HAN W-J, KIM EK (2014) Assessment of bifid and trifid mandibular canals using cone beam computed tomography. *Imaging Sci Dentist,* 44: 229-236.

ROOD JP (1976) The analgesia and innervation of mandibular teeth. *Br Dent J,* 140: 237-239.

TANTANAPORNKUL W, OKOUCHI K, FUJIWARA Y, YAMASHIRO M, MARUOKA Y, OHBAYASHI N (2007) A comparative study of cone beam computed tomography and conventional panoramic radiography in assessing the topographic relationship between the mandibular canal and impacted third molars. *Oral Surg Oral Med Oral Pathol Oral Radiol Endod*, 103: 253-259.

SISMAN Y, ERCAN-SEKERCI A, PAYVEREN-ARIKAN M, SAHMAN H (2015) Diagnostic accuracy of cone-beam CT compared with panoramic images in predicting RMC during extraction of impacted mandibular third molars. *Medicina Oral Patologia Oral y Cirugia Bucal,* 20: 74-81.

VON ARX T, HÄNNI A, SENDI P, BUSER D, BORNSTEIN MM (2011) Radiographic study of the mandibular RMC: an anatomic structure with clinical importance. *J Endod,* 237: 1630-1635.

The anatomical variations of the hepatic veins in a South African sample

Leoné Pretorius, Geney Gunston, Kentse Mpolokeng

Department of Human Biology, University of Cape Town, Cape Town, South Africa

SUMMARY

A preoperative understanding of the anatomy of the hepatic veins and any variation thereof is pivotal for successful hepatic surgeries, as these vessels serve as a hepatic field guideline in living donor liver transplantations (LDLT) and hepatic resections. To date, numerous morphological variations in different populations other than a South African population have been published and thus the following research study was conducted to investigate and document morphological variations in a South African population. The following descriptive study aimed to contribute to a better preoperative understanding of hepatic vein anatomy impacting surgeries conducted in South Africa. This research study was conducted on 40 livers from donated bodies of 20 females and 20 males, used for academic purposes in the Department of Human Biology, at the University of Cape Town. The age range was between 33 to 105 years old with an average age of 75. The livers were removed, and the liver tissue was scraped away to expose the hepatic veins from their origin of the inferior vena cava (IVC) to their terminating branching points within the various hepatic segments. All the livers presented all three major hepatic veins, 90.0% of the livers had a common trunk (n = 36), and the remaining 10.0% had no common trunk (n = 4). The major and minor hepatic veins were observed for all the livers. This study found various morphological variations in a South African population that are of clinical significance with a high prevalence of accessory right hepatic veins.

Key words: Blood supply – Hepatic veins – Liver – Hepatic resection – LDLT

INTRODUCTION

A preoperative comprehension of the anatomy of the hepatic venous system is essential for ensuring successful hepatic surgeries and the preservation of hepatic venous drainage postoperatively (Singh et al., 2012; Nayak et al., 2016; Brentjies et al., 2018). This is seen to be true in advances in new surgical procedures such as living donor liver transplantations (LDLT), which was developed due to the need for donor livers exceeding the existing cadaveric supply and hepatectomies for patients with end-stage liver disease or cirrhosis (Cheng et al., 1997; Orguc et al., 2004; Uchida et al., 2010).

During the embryological gestation period, the hepatic diverticulum (liver primordium or liver bud) forms as a ventral outgrowth from the caudal portion of the endodermal wall of the foregut in the first three to four weeks (Bodzin, 2019; Mcpherson and Anthony, 2019; Sureka et al., 2019). The

Corresponding author:
Dr. Kentse Mpolokeng. Department of Human Biology, University of Cape Town, Anzio Rd, Observatory, Cape Town, 7935, South Africa. Phone: +27214066932. E-mail: kentse.mpolokeng@uct.ac.za

Submitted: June 21, 2022. **Accepted:** August 23, 2022

https://doi.org/10.52083/UHPV1823

hepatic diverticulum then continues to enlarge, with the right lobe developing at a quicker rate than the left lobe and continues to divide into a cranial and caudal portion, forming the liver parenchyma and gallbladder respectively (Mcpherson and Anthony, 2019). During this period the liver receives its blood supply from the portal and umbilical veins, with the primordial portal veins developing from the caudal portion of the vitelline veins and the cranial portion forming the primordial hepatic veins (Bodzin, 2019).

Vitelline or omphalomesenteric veins are responsible for the transport of blood from the yolk sac to the sinus venosus (Ashworth, 2020). These veins mature to form the portal vein, anastomose across the duodenum, and traverse the septum transversum (Ashworth, 2020).

During the fifth week, the left cranial portion of the vitelline vein deteriorates, leaving the right proximal vitelline vein to merge with the cranial portion of the primary hepatic vein and gives origin to the three major hepatic veins, together with the hepatic portion of the inferior vena cava (IVC) (Sureka et al., 2019).

The major hepatic veins commonly consist of the right hepatic vein (RHV), middle hepatic vein (MHV), and left hepatic vein (LHV), which are responsible for draining the liver of deoxygenated blood through the suprahepatic portion of the IVC (Abdel-Misih and Bloomston, 2010; Sureka et al., 2019; Standring, 2021). The MHV and LHV commonly merge to form a common trunk, and the RHV is generally known to be the largest vein of the three major hepatic veins (Abdel-Misih and Bloomston, 2010). These veins are responsible for draining the different liver segments as classified by the Couinaud system which is founded on the anatomy of the biliary vasculature and surgical resectable sections (Mcpherson and Anthony, 2019; Standring 2021). Minor hepatic veins may consist of one to five vessels, exist in addition to the three major hepatic veins, and mostly drain the caudate lobe independently within the IVC (Standring, 2021).

The hepatic veins generally serve as a guide for the hepatectomy plane during surgery (Nayak et al., 2016). This is seen during hepatic surgeries such as LDLT where either the right or left liver segments as required by the recipient are removed and harvested from the living donor (Orguc et al., 2004). Anatomical variations should be considered to ensure the preservation of the hepatic venous outflow in both the recipient and donor as these variations could alter the hepatectomy field and surgical procedures accordingly (Cheng et al., 1997; Paspulati, 2017).

To date, numerous morphological variations within these hepatic veins have been studied in different populations, e.g., China, India, Turkey, etc. but studies regarding a South African population have not yet been found in the published literature. This study was performed to investigate and document morphological variations in a South African population and to analyze if sex or age was a contributing factor for the variations observed. This study ultimately aimed to contribute to a better preoperative understanding of hepatic vein anatomy that could impact surgeries conducted in South Africa.

MATERIALS AND METHODS

This was a cross-sectional observational study with a descriptive analysis within a cadaveric sample and was conducted in the dissection halls in the Department of Human Biology at the University of Cape Town. The sample consisted of 45 formalin preserved bodies. The livers were pre-dissected or removed from these bodies by undergraduate medical and postgraduate honors students during their academic training. The abdomen and relevant structures were dissected with the IVC dissected close to the diaphragm superiorly and close to the liver inferiorly. The attachments of the coronary, falciform, and triangular ligaments and surrounding fascia had also been dissected to freely retrieve the liver from the abdominal cavity during these dissections.

After removal, the livers were soaked in buckets of warm water and fabric softener – a fluid generally used to soften the fabric of clothes when washed (Britannica Dictionary), between 24-72 hours preceding the scraping of the liver tissue. The livers were submerged in a mixture of 10 liters warm water and a cap (75 ml) of liquid fabric

softener that was mixed into the bucket of water to prevent the tissue from drying out and to help soften the liver tissue. The method of using fabric softener was utilized, as some liver tissue proved to be tougher compared to other livers and was sought to facilitate the softening of those liver tissues. Using the fabric softener together with the soaking process helped to ease the scraping and dissection of the liver tissue to expose the hepatic veins. The use of fabric softener has not yet been seen mentioned in the previous cadaveric studies such as those conducted by Shilal and Tuli (2015), Nand and Rai (2020), and Vinh Tran et al. (2020) to help with the ease of dissection to expose the hepatic veins under investigation.

After soaking, each liver was removed individually and placed on a block where the IVC, which was still intact, was cut open posteriorly. The exposed hepatic portion of the IVC served as a landmark for the origin and course for scraping the hepatic veins. The visceral peritoneum was removed by hand whereafter the superficial surface of the liver was scraped by a blunt scalpel to loosen the hepatic tissue. The tissue was then further scraped with both ends of a teaspoon and forceps which served as a curette, tracing the hepatic veins from their origin from the IVC to their terminating branches while taking care not to damage these vessels. Any vessels, hepatic arteries, portal, and biliary system or tissue that did not form part of the hepatic veins and obscured their course were removed by cutting them free with dissection scissors.

Five bodies were excluded after the livers from these bodies were investigated, and it was found that the hepatic veins were damaged. Of the remaining 40 bodies, that presented with intact and unaltered hepatic vein morphology; 50.0% (n = 20) were adult female individuals and the other 50.0% (n = 20) were adult male individuals that were included in this study. The age range of the sample was between 33 to 105 years old, and the average age was 75 with ± 14 standard deviations (SDs).

After dissection the hepatic veins were investigated to observe if all three major veins were found to be present, if the LHV and MHV drained via a common trunk into the IVC, which vein was observed to be the largest, and how many major and minor hepatic veins were found to be present together with any variations within these vessels. The vessels were classified using the Couinaud system. The MHV and Cantlie boundary-field amid the IVC and gallbladder fossa, divided the liver into a right and left lobe that was used to further classify hepatic veins as being the LHV, MHV, and RHV (Fig. 1, Mcpherson and Anthony, 2019).

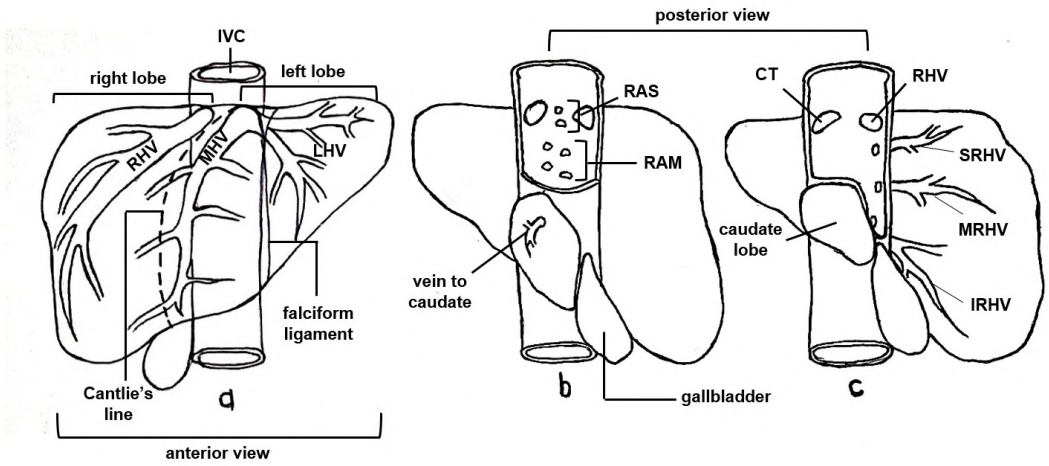

Fig. 1.- Illustration for the classification of hepatic veins documented in this research study. (**a**) Presents the anterior view of the liver separated into a left and right lobe by Cantlie's line and hepatic veins (RHV - right hepatic vein, MHV - middle hepatic vein, LHV - left hepatic vein) with relation to the inferior vena cava (IVC) and falciform ligament. Figure 1 b and c, represent the posterior and interior view of the liver and hepatic portion of the IVC, respectively. (**b**) Illustrates the nomenclature used for the minor hepatic veins found in relation to the MHV (RAS – right anterior superior veins, RAM – right anterior middle veins). (**c**) Illustrates the nomenclature used for the minor hepatic veins found in relation to the RHV and right posterior hepatic segment (SRHV – superior right hepatic vein, MRHV – middle right hepatic vein, IRHV – inferior right hepatic vein, CT – Common trunk of the LHV and MHV).

A common trunk for the LHV and MHV was identified and classified as such where the two vessels were seen to join and drain as one vessel within the IVC (Fig. 1), as opposed to the absence of a common trunk where these vessels were seen to drain separately into the IVC.

The major and minor hepatic veins were classified as per the description by Standring (2021) and counted. The minor hepatic veins that were smaller than the back tip of a dissection probe or those in which the origin and the course could not be traced were excluded.

Classification of any minor hepatic veins originating from the IVC and terminating within the hepatic tissue was achieved through the segmentation and sectioning of the liver. Vertical and horizontal planes exist that divide the right lobe into a right anterior and posterior section with four segments (V, VI, VII, & VIII) and the left lobe into a left medial and lateral section with three segments (II, III, IV; Couinaud system; Yip and Fenwick, 2013; Mcpherson and Anthony, 2019). These vessels that were found with the MHV were classified according to the section of the liver they were found to drain, namely the right anterior superior (RAS) and right anterior middle (RAM) segments (Fig. 1).

Minor hepatic veins that were found regarding the RHV and the right posterior section of the liver respectively were identified and classified when present as per the literature as the superior RHV (SRHV), middle RHV (MRHV), and inferior RHV (IRHV, Fig. 1). Any minor hepatic veins that drained the caudate lobe (hepatic segment I) were classified as the caudate veins (Fig. 1, Yip and Fenwick, 2013). Digital photographs were taken of the anterior and posterior aspects of the livers before and after dissections were carried out as part of the documentation for this study.

Statistical analysis

The statistical program IBM SPSS Statistics (version 27) was used to input and run statistical analysis for the data obtained. To test the significance within the categorical data for the incidence of the largest hepatic vein and the formation of a common trunk against sex of the population under study a Chi-Square Test was performed. Similarly, testing the significance of categorical and continuous variables; sex against age, the incidence of the largest hepatic vein against age, or the incidence of minor hepatic veins observed against sex, a One-Way ANOVA test was performed. Testing the significance within continuous variables such as the incidence of minor hepatic veins against age was achieved through performing a One-Sample T-Test.

A p-value < 0.05 and a confidence interval of 95.0% was used for all three of these tests to determine if the results were significant. These tests were mainly performed to test the significance of morphological findings when compared to the sex and age of the sample under study. For data to be tested for its significance with sex and age, no data had to be missing and the number of valid cases observed had to be five or more. Thus, data that did not meet the criteria together with observations that presented as a constant could not statistically be analyzed.

No ethical approval was needed as permission to use the bodies had already been granted by the Inspector of Anatomy in the Western Cape Government to the University of Cape Town for medical and research activities. All the bodies were handled ethically as outlined in the body donation program of the University and by strictly adhering to the Human Tissue Act of 2003.

RESULTS

For the 40 livers included in this study, all major hepatic veins (RHV, MHV, & LHV) were found to be intact and present. The formation of a common trunk between the MHV and LHV was found in 36 livers out of the 40 and in the remaining four livers these vessels drained separately into the suprahepatic portion of the IVC (Fig. 2). Variation for the length of the common trunk was seen and any junction even in the form of a common orifice (Fig. 2) of the MHV and LHV was classified as a common trunk.

The RHV was observed to be the largest hepatic vein followed by the MHV (Table 1; Fig. 3). It was seen that in three livers the LHV formed the largest hepatic vein, and there was one liver in which the RAM hepatic vein formed the largest hepatic vein (Table 1).

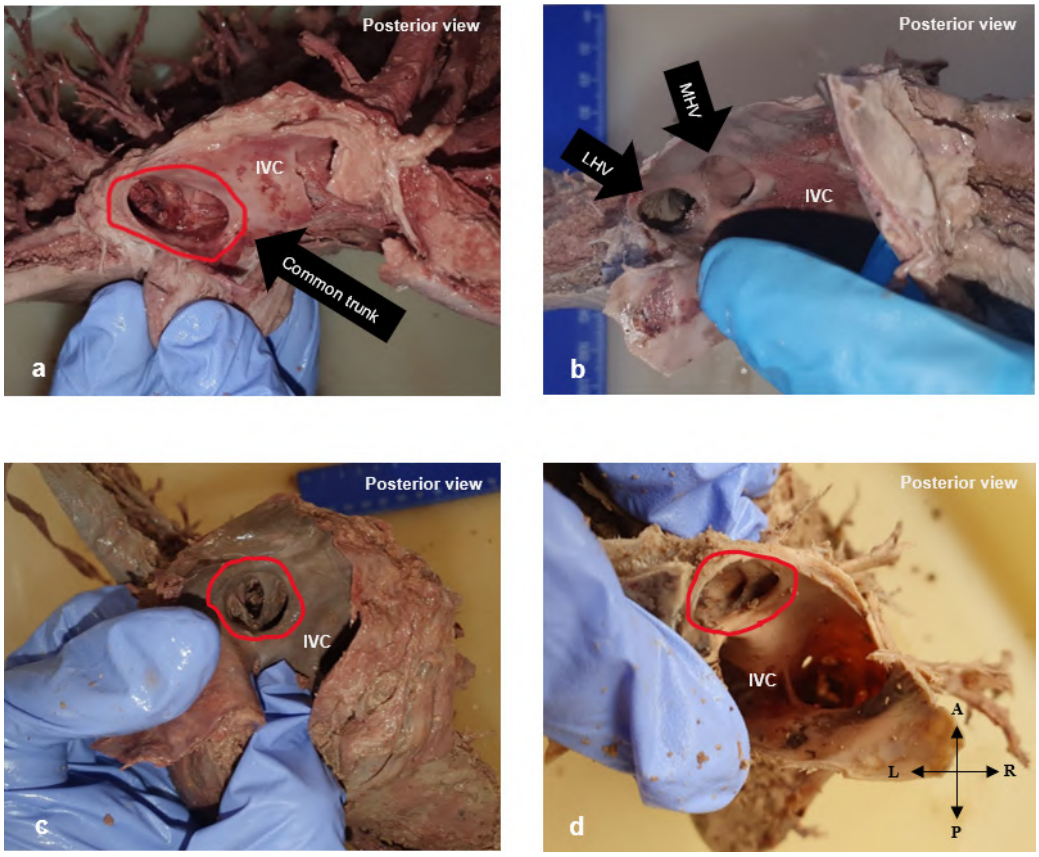

Fig. 2.- Occurrence and variation of a common trunk between the middle hepatic vein (MHV) and left hepatic vein (LHV). (**a**) Presents a common trunk between the MHV and LHV which drain as a single vessel into the suprahepatic portion of the inferior vena cava (IVC). (**b**) Indicates the absence of a common trunk between the MHV and LHV seen in this study and can be seen draining as two separate vessels into the IVC. (**c** and **d**) represent the incidence of variation for the length of a common trunk between the MHV and LHV and show these vessels sharing more of a common orifice**.** Arrow key: A – anterior; R- right; P – posterior; L- left.

The major hepatic veins were made up of two, three, or four vessels (Fig. 4) and were seen in 52.5% (n = 21), 32.5% (n = 13), and 15.0% (n = 6) respectively. Out of these vessels, accessory veins were found in 7.5% (n = 3) through an additional LHV, in 2.5% (n = 1) through the presence of a RAM hepatic vein, in 10.0% (n = 4) through the presence of a single MRHV, and in 5.0% (n = 2) through the presence of a single IRHV. The presence of these accessory veins contributed to a higher incidence of vessels classified as major hepatic veins than expected when a common trunk was present or absent.

Table 1. The largest major hepatic veins.

Hepatic vein	Frequency	Percentage
LHV	3	7.5%
MHV	13	32.5%
RHV	23	57.5%
RAM	1	2.5%
Total	40	100.0%

The minor hepatic veins ranged from two to nine with one incidence of 13 veins (Fig. 5a). A large proportion of livers presented with two to five minor hepatic veins, followed by seven and eight minor hepatic veins, and the remaining numbers of hepatic veins (6, 9, 13) were observed for a smaller proportion of the livers investigated (Fig. 5a). The further subdivision and classification of the minor hepatic veins revealed that: caudate veins were present in all livers, 12.5% (n = 5) had RAS hepatic veins, 55.0% (n = 22) had RAM hepatic veins, 60.0% (n = 24) presented the SRHV, 57.5% (n = 23) presented the MRHV, and 55.0% (n = 22) presented the IRHV.

The veins that originated from the IVC and coursed to terminate within the caudate lobe ranged from one to five vessels (Fig. 5b). The highest incidence was recorded for one to two veins seen in 77.5% (n = 31), followed by the remaining vessels being three to four in count seen in 17.5% (n = 7), and lastly five vessels in count seen in 5.0% (n = 2).

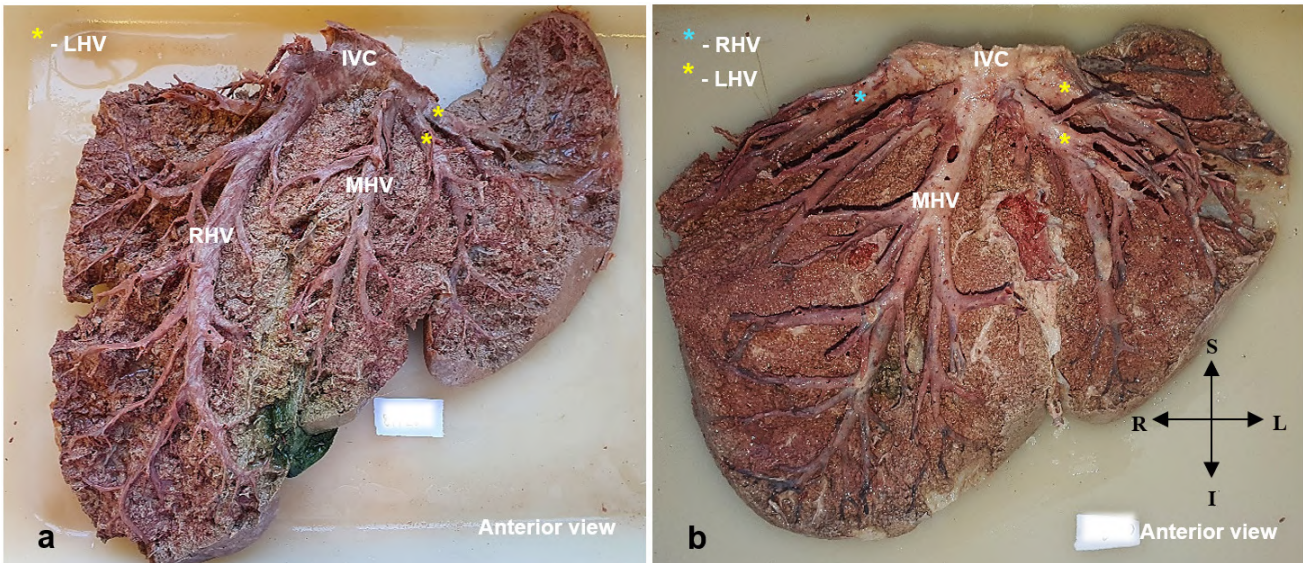

Fig. 3.- Representation of the largest hepatic vein observed for this research study. (**a**) Representing the incidence of the right hepatic vein (RHV) as the largest hepatic vein for the respective liver, draining into the inferior vena cava (IVC) in relation to the middle and left hepatic veins (MHV & LHV). (**b**) Representing the incidence where the middle hepatic vein was observed to be the largest. Arrow key: S – superior; L – left; I – inferior; R – right

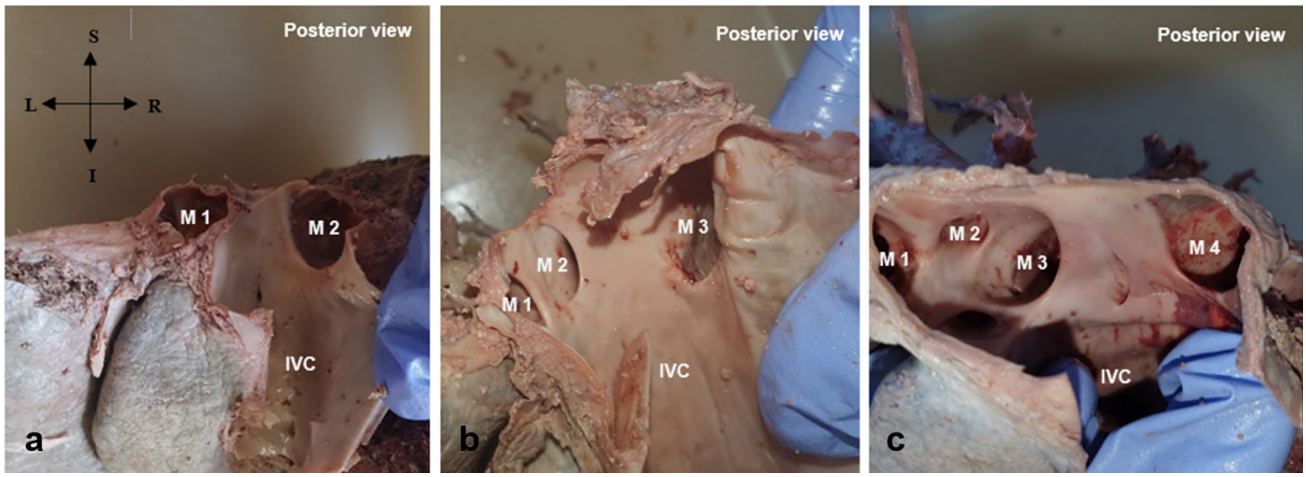

Fig. 4.- (**a-c**) Presence of the major hepatic veins (M) seen in this research study. These vessels can be seen to drain individually into the inferior vena cava (IVC) posteriorly and were counted as M1, M2, M3, or M4. Arrow key: S – superior; R – right; I – inferior; L – left.

Out of the 22 livers that had RAM hepatic veins (Fig. 5c), the veins were mostly present as one single vessel in 30.0% (*n* = 12) of the livers, followed by two to three vessels present in 12.5% (*n* = 5, respectively) of the livers. The presence of one single RAS hepatic vein was only seen in 12.5% (*n* = 5) of the livers included in this research study (Fig. 6). Most livers 87.5% (*n* = 35) did not have any RAS hepatic veins.

The presence of accessory right hepatic veins was observed for most of the livers and was either seen together as SRHV, MRHV, & IRHV; SRHV & MRHV; SRHV & IRHV; MRHV & IRHV respectively, or as one single vessel (Fig. 7). The presence of the SRHV out of the accessory right hepatic veins observed was present in 50.0% (*n* = 20) of the livers as one single vessel or as two vessels in 10.0% (*n* = 4) of the livers (Table 2).

Observations for the MRHV ranged from one to three vessels with the majority seen to have only one single vessel in 37.5% (*n* = 15) of the livers, followed by two vessels in 17.5% (*n* = 7) of the livers, and only one liver had three vessels (Table 2). The presence of the IRHV was mostly seen for 47.5% (*n* = 19) of the livers as one single vessel or two vessels in 7.5% (*n* = 3, Table 2).

Table 2. The prevalence of the accessory right hepatic veins.

Number of Veins	Frequency	Percentage
Superior		
0	16	40.0%
1	20	50.0%
2	4	10.0%
Middle		
0	17	42.5%
1	15	37.5%
2	7	17.5%
3	1	2.5%
Inferior		
0	18	45.0%
1	19	47.5%
2	3	7.5%
Total	**40**	**100.0%**

DISCUSSION

The sample size presented to be a confounding factor that could have influenced the observations and frequencies obtained. Although, the sex of the sample was evenly distributed, and no significant difference was found between the sex and age of the sample. The study was subject to the author's interpretations and observations that could have altered the classification of variations, although classification systems were sought and utilized to minimize any bias. Furthermore, the fact that the major hepatic veins that were found to be present and intact for all the livers were beneficial in identifying accessory veins in this study. This is supported when compared to studies such as Nand and Rai (2020) where two specimens had no LHV for the 50 livers investigated.

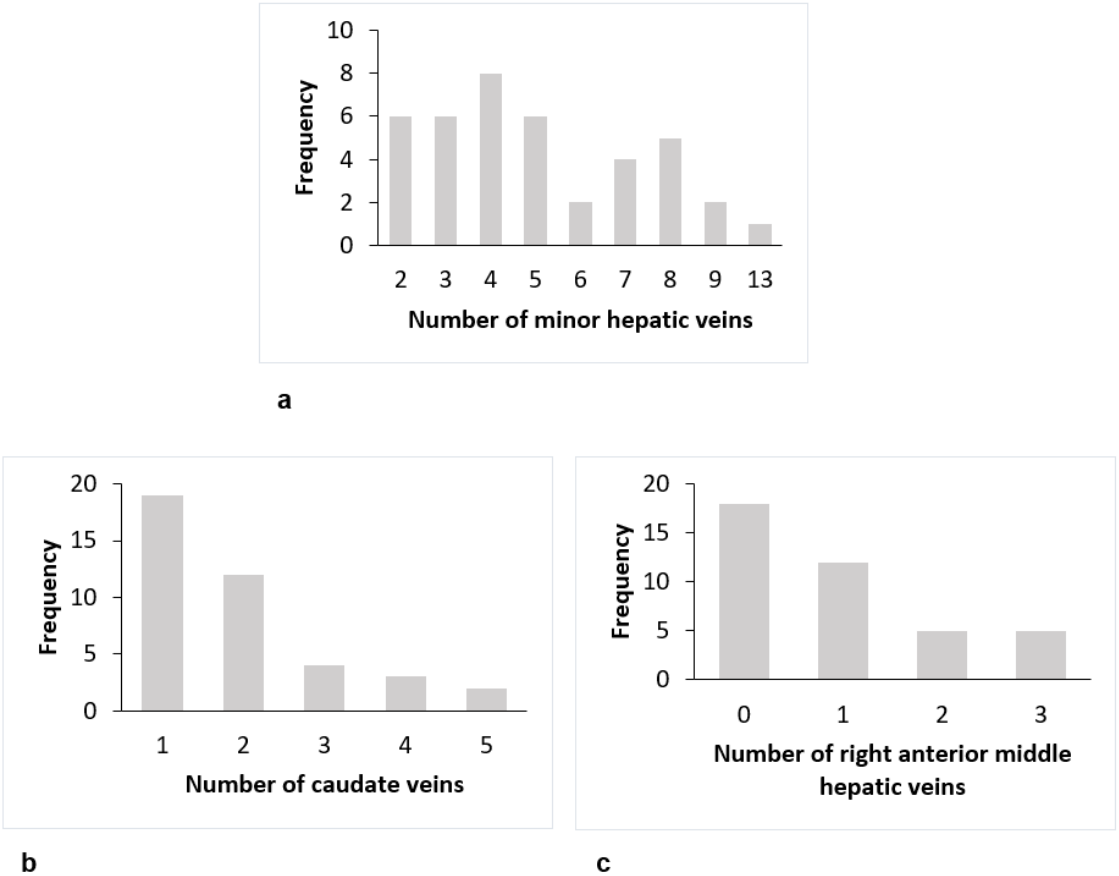

Fig. 5.- The occurrence of the specific hepatic veins under investigation for this research study, recorded as frequencies. (**a**) The frequency for the number of minor hepatic veins present in the livers investigated for this study. Figures 5b and 5c, illustrate the subdivision of the minor hepatic veins of figure 5a. (**b**) The frequency for the number of caudate veins present in the livers investigated for this study. (**c**) The frequency for the number of right anterior middle hepatic veins present in the livers investigated for this study.

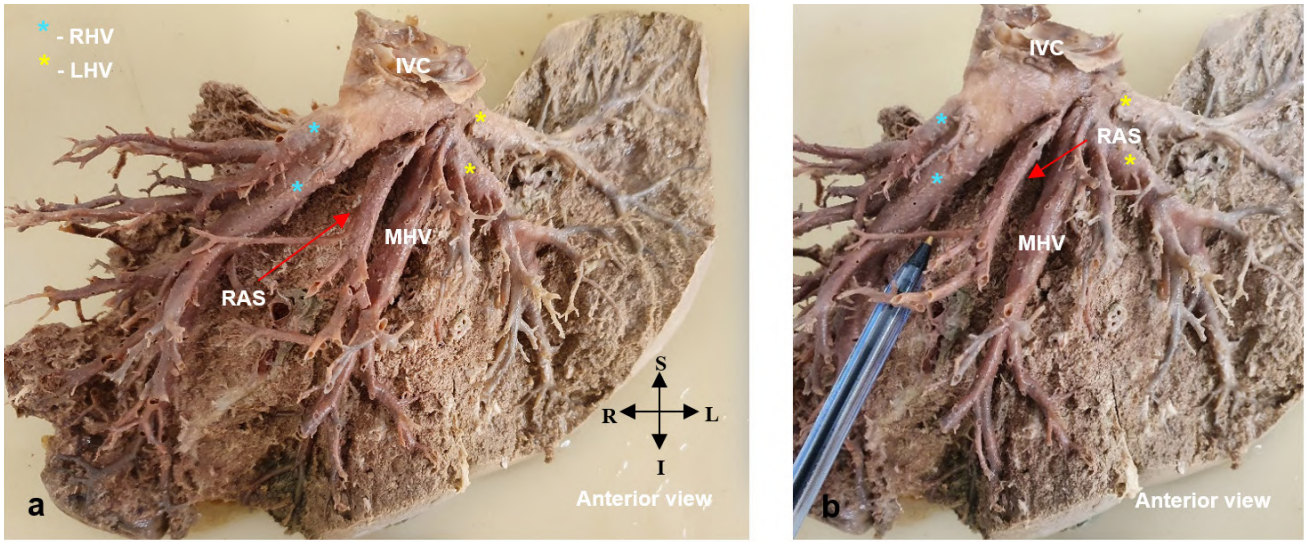

Fig. 6.- The incidence of the right anterior superior (RAS) hepatic veins observed in this study. (**a**) Presents the RAS hepatic vein indicated by the red arrow for the corresponding liver. It was seen to drain separately into the inferior vena cava (IVC) and course between the right hepatic vein (RHV) and middle hepatic vein (MHV) within the right anterior hepatic segment. (**b**) Shows a closer view of this vessel. Arrow key: S – superior; L – left; I – inferior; R – right.

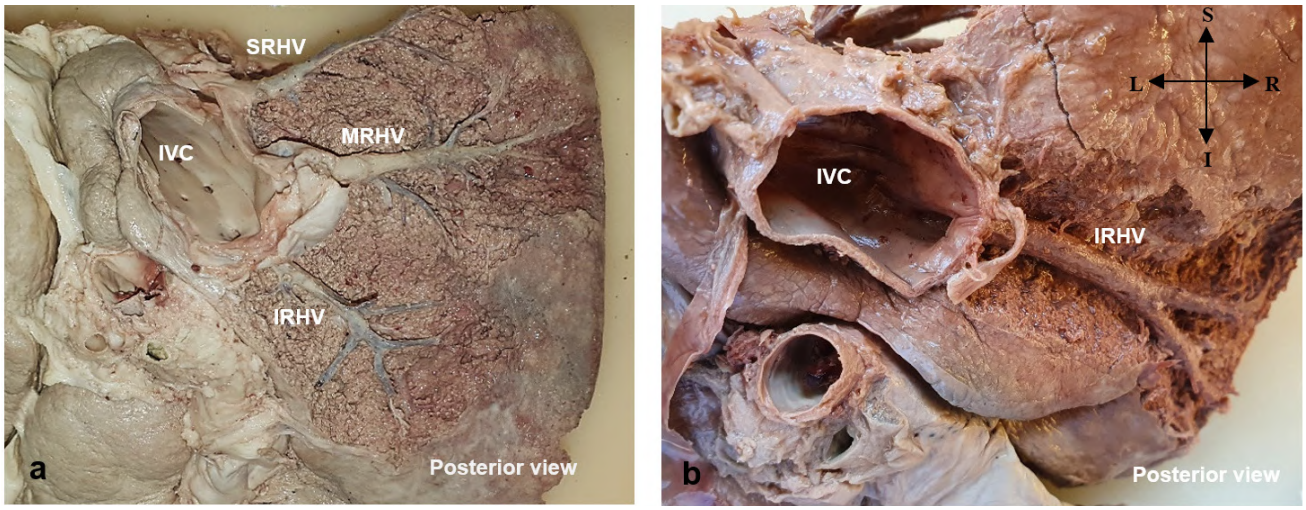

Fig. 7.- Representation of the accessory right hepatic veins observed in this research study. The veins were either all seen to be present as in (**a**), with the superior right hepatic vein (SRHV), middle right hepatic vein (MRHV), and inferior right hepatic vein (IRHV) or only one of these vessels were present as in (**b**) with the inferior right hepatic vein (IRHV). Arrow key: S – superior; R – right; I – inferior; L – left.

Morphological variations

The largest hepatic vein for this study was commonly found to be the RHV which agrees with the literature and general classification of the major hepatic veins (Abdel-Misih and Bloomston, 2010). For the LHV and MHV, contradictory results were found in this study when compared to that of Nand and Rai (2020). This study found the MHV to be the second largest vein to be observed and then the LHV, where Nand and Rai (2020) had opposite results with the LHV being the second largest (n = 10) and no observations for the MHV (n = 0).

Cheng et al. (1996) stated that the formation of a common trunk between the MHV and LHV is of significance during the resection of the left lateral segment of the left lobe together with the general incidence of the formation of a common trunk between the LHV and MHV. This is further supported by the results obtained from this study as well as other studies (Table 3). The major and minor veins accounted for were in line with the description by Standring (2021) and studies such as Nayak et al. (2016). However, Nayak et al. (2016) found six livers (7%) out of the 88 livers investigated that did

Table 3. Literature review results for the formation of a common trunk between the middle hepatic vein and left hepatic vein in cadaveric and clinical studies.

Author/s & Year	Study type	Sample size	Study Setting	Common trunk	
				Yes	No
Soyer et al. (1995)	Imaging (CTAP)	69	France	57 (95%)	3 (5%)
Cheng et al. (1996)	Imaging (ultrasound)	200	Taiwan	140 (70%)	60 (30%)
Wind et al. (1998)	Cadaveric	64	France	54 (84%)	10 (16%)
Singh et al. (2012)	Cadaveric	60	North India	4 (7%)	56 (93%)
Kalaycı et al. (2014)	Imaging (CT)	100	Turkey	70 (70%)	10 (10%)
Ulziisaikhan et al. (2014)	Cadaveric	40	Mongolia	31 (76%)	9 (24%)
Sureka et al. (2019)	Imaging (MDCT)	500	India	405 (81%)	95 (19%)
Nand and Rai, (2020)	Cadaveric	50	India	38 (76%)	9 (18%)
Vinh Tran et al. (2020)	Cadaveric	20	Vietnam	18 (90%)	2 (10%)
Total		**1303 - 32* = 1271**		**939 (74%)**	**332 (26%)**

*Number of livers excluded due to vessels being absent or undetectable.

not have any minor hepatic veins and were solely drained by major hepatic veins, whereas for the current study all the livers were found to be drained by minor and major hepatic veins.

Most minor hepatic veins for this study comprised accessory right hepatic veins where one or more of either one or all the SRHVs, MRHVs, and IRHVs were present. The presence of these veins was supported by previous studies in other populations (Table 4). For this study, the accessory right hepatic veins were mostly equally observed within the liver samples with the SRHV observed to have a slightly higher incidence level (60%), followed by the MRHV (58%) and IRHV (55%) respectively. This observation varies when compared to previous studies where the IRHV is found to greatly contribute to the right accessory hepatic veins (Table 4).

Morphological variation and clinical significance

Ensuring the preservation of the hepatic venous drainage after surgery proves to be of significance as venous obstruction and deferred hemorrhage have been noted (Fang et al., 2012). In the cases where the hepatic veins are partially or fully obstructed; Budd-Chiari syndrome, congestive hepatomegaly, and veno-occlusive diseases can develop (Fang et al., 2012). Thus, any variations encountered within the hepatic veins that could alter the hepatic venous outflow and drainage volume are of importance, especially in cases where the RHV is used as a graft and the presence of accessory veins and tributaries exist (Uchida et al., 2010).

The presence of accessory veins or tributaries from the RHV or MHV is of significance during resections of the right anterior or posterior segments of the right lobe (Sharma et al., 2019; Watanabe et al., 2020). This occurrence of accessory hepatic veins or tributaries is of importance as they could traverse the hepatectomy field and create a source of bleeding and graft ischemia when these vessels are damaged during surgery, leading to cardiac arrest or the origin of an air embolism (Shilal and Tuli, 2015; Paspulati, 2017). Furthermore, during the resection of the left lateral segment of the left lobe, the formation of a common trunk between the MHV and LHV is of significance as resection of the LHV should either be performed above or at the level of formation of the common trunk (Cheng et al., 1996).

The incidence of accessory right hepatic veins can be attributed to the embryological development where the ductus venosus and hepatic sinusoids are in direct contact with one another (Shilal and Tuli, 2015). As the gestation period comes to an end, this point of contact between the vessels generally atrophies, but it is believed that some regions maintain their connection and thus lead to the formation of accessory right hepatic veins such as the MRHV, IRHV, and SRHV (Shilal and Tuli, 2015).

Table 4. Literature review results for the incidence of accessory right hepatic veins in cadaveric and clinical studies.

Author/s & Year	Study type	Sample size	Setting	Accessory vein		
				MRHV	IRHV	SRHV
Cheng et al. (1997)	Imaging (ultrasound)	400	Taiwan	22 (6%)	72 (18%)	-
De Cecchis et al. (2000)	Cadaveric	110	Slovenia	-	23 (21%)	-
Akgul et al. (2004)	Imaging (CEHCT)	308	Turkey	-	65 (21%)	-
Orguc et al. (2004)	Imaging (CT)	100	Turkey	-	60 (60%)	-
Koc et al. (2007)	Imaging (MDCT)	1120	Turkey	-	356 (32%)	-
Uchida et al. (2010)	Imaging (CT)	223	Japan	-	90 (40%)	-
Fang et al. (2012)	Imaging (CT)	200	China	-	42 (21%)	-
Kalaycı et al. (2014)	Imaging (CT)	100	Turkey	36 (36%)	58 (58%)	44 (44%)
Shilal and Tuli (2015)	Cadaveric	60	India	-	46 (76%)	-
Sharma et al. (2019)	Imaging (CECT)	224	North India	-	126 (56%)	-
Sureka et al. (2019)	Imaging (MDCT)	500	India	-	185 (37%)	-
Nand and Rai (2020)	Cadaveric	50	India	-	27 (54%)	11 (22%)
Watanabe et al. (2020)	Imaging (CT)	307	Japan	-	197 (64%)	25 (8%)
Yang et al. (2020)	Imaging (CT)	299	China	-	103 (34%)	-
Cawich et al. (2021)	Imaging (CECT)	118	Trinidad and Tobago	5 (4%)	53 (45%)	-
Total		**4119 – 2473* = 1646**		**63 (4%)**	**1503 (91%)**	**80 (5%)**

*Number of livers excluded due to vessels being absent or undetectable.

When all these points are not taken into consideration, obstruction or ineffective hepatic resections or transplantations can occur and complications such as liver atrophy, infarction, septic shock, and diminished or no hepatic restoration have been seen to occur (Uchida et al., 2010).

CONCLUSION

The findings from the current research study revealed various morphological variations with a high prevalence of accessory right hepatic veins within a South African population. These morphological variations prove to be of clinical significance and contribute to the preoperative understanding of these vessels. Sex and age were not found to be contributing factors to the variations observed and future studies are recommended to further investigate specific aspects of these variations. Future studies could include a biometric study with different scraping techniques and casting or corrosion methods to better represent and measure these veins or an investigation into the relationship of the diameter of the RHV in comparison to that of the IRHV.

ACKNOWLEDGEMENTS

The authors sincerely thank those who donated their bodies to science so that anatomical research and teaching could be performed. Results from such research can potentially increase scientific knowledge and can improve patient care. Therefore, these donors and their families deserve our highest respect.

I would also like to express my gratitude to Mr. Steven Ronald Randall for assisting with the interpretation of the statistical aspect of this project and Ms. Marischka Lee Ford for assisting as my interobserver. I appreciate the support received from the Anatomy Technical staff in the Department of Human Biology for providing the necessary materials to conduct this project and the National Research Foundation (NRF) for their financial assistance.

REFERENCES

ABDEL-MISH SRZ, BLOOMSTON M (2010) Liver Anatomy. *Surg Clin North Am*, 90: 643-653.

AKGUL E, INAL M, BINOKAY F, CELIKTAS M, AIKIMBAEV K, SOYUPAK S (2004) The prevalence and variations of inferior right hepatic veins on contrast-enhanced helical CT scanning. *Eur J Radiol,* 52: 73-77.

ASHWORTH M (2020) Development of the heart and cardiovascular system in relation to cardiac abnormalities. In: Pandya PP, Oepkes D, Sebire NJ, Wapner RJ (eds.). *Fetal Medicine: Basic Science and Clinical Practice, Third Edition.* Elsevier Limited, China, pp 88-102.

BODZIN AS, BAKER TB (2019) Anatomy and Physiology of the Liver. In: Yeo CJ (ed.). *Shackelford's Surgery of the Alimentary Tract, Eighth Edition.* Elsevier Inc., China, pp 1386-1397.

BRENTJIES T, WEYKER PD, WEBB CAJ (2018) Diseases of the Liver and Biliary Tract. In: Hines RL, Marschall KE (eds.). *Stoelting's Anesthesia and Co-Existing Disease, Seventh Edition*. Elsevier Inc., China, pp 345-358.

BRITANNICA DICTIONARY - https://www.britannica.com/dictionary/fabric-softener.

CAWICH SO, NARAYNSINGH V, PEARCE NW, DESHPANDE RR, RAMPERSAD R, GARDNER MT, MOHAMMED F, DINDIAL R, BARROW TA (2021) Surgical relevance of anatomic variations of the right hepatic vein. *World J Transplant*, 11(6): 231-243.

CHENG Y, HUANG T, CHEN C, CHEN T, HUANG C, KO S, LEE T (1996) Variations of the left and middle hepatic veins: application in living related hepatic transplantation. *J Clin Ultrasound*, 24*:* 11-16.

CHENG Y, HUANG T, CHEN C, CHEN T, HUANG C, KO S, YANG B, LEE T (1997) Variations of the middle and inferior right hepatic vein: application in hepatectomy. *J Clin Ultrasound*, 25(4): 175-182.

DE CECCHIS L, HRIBERNIK M, RAVNIK D, GADZIJEY EM (2000) Anatomical variations in the pattern of the right hepatic veins: possibilities for type classification. *J Anat,* 197: 487-493.

FANG C, YOU J, LAU WY, LAI ECH, FAN Y, ZHONG S, LI K, CHEN Z, SU Z, BAO S (2012) Anatomical variations of hepatic veins: Three-dimensional computed tomography scans of 200 subjects. *World J Surg,* 36: 120-124.

KALAYCI TÖ, KUTLU R, KARASU Ş, YILMAZ S (2014) Investigation of right lobe hepatic vein variations of donor using 64-detector computed tomography before living donor liver transplantation. *Turk J Gastroenterol,* 25: 9-14.

KOC Z, ULUSAN S, OGUZKURT L, TOKMAK N (2007) Venous variants and anomalies on routine abdominal multi-detector row CT. *Eur J Radiol,* 61: 267-278.

MCPHERSON AM, ANTHONY EY (2019) Embryology, Anatomy, and Normal Findings. In: Coley BD (ed.). *Caffey's Pediatric Diagnostic Imaging, Thirteenth Edition.* Elsevier Inc., China, pp 393-396.

NAND B, RAI A (2020) Cadaveric study of portal and hepatic venous anatomy with special reference to territory of middle hepatic vein. *Int Surg J,* 7(9): 2980-2984.

NAYAK S, DEEPTHINATH R, KUMAR N, SHETTY P, KUMAR V, AITHAL A, SHETTY S (2016) Evaluation of numerical and positional variations of the hepatic veins: A cadaveric study. *J Cardiovasc Echogr,* 26: 5-10.

ORGUC S, TERCAN M, BOZOKLAR A, AKYILDIZ M, GURGAN U, CELEBI A, NART D, KARASU Z, ICOZ G, ZEYTUNLU M, YUZER Y, TOKAT Y, KILIC M (2004) Variations of hepatic veins: helical computerized tomography experience in 100 consecutive living liver donors with emphasis on right lobe. *Transplant Proc,* 36: 2727-2732.

PASPULATI RM (2017) Liver Transplantation. In: Haaga JR, Boll DT (eds.). *CT and MRI of the Whole Body, Sixth Edition*. Elsevier Inc., China, pp 1375-1405.

SHARMA M, SOOD D, SINGH CHAUHAN N, VERMA N, KAPILA P (2019) Inferior right hepatic vein on routine contrast-enhanced CT of the abdomen: prevalence and correlation with right hepatic vein size. *Clin Radiol,* 74: 735.e9-735.e14.

SHILAL P, TULI A (2015) Anatomical variations in the pattern of the right hepatic veins draining the posterior segment of the right lobe of the liver. *J Clin Diagnostic Res,* 9(3): AC08-AC12.

SINGH D, AGNIHOTRI G, SINGH S, SINGH R (2012) Patterns of tributaries of major hepatic veins by dissection and radiology. *Anat J Afr,* 1(1): 17-19.

SOYER P, BLUEMKE DA, CHOTI MA, FISHMAN EK (1995) Variations in the intrahepatic portions of the hepatic and portal veins: findings on helical ct scans during arterial portography. *Am J Roentgenol,* 164: 103-108.

STANDRING S (2021) The anatomy of the vascular and lymphatic systems. In: *Gray's Anatomy, Forty Second Edition*. Elsevier Ltd., China, pp 1464.e56-1464.e129.

SUREKA B, SHARMA N, KHERA PS, GARG PK, YADAV T (2019) Hepatic vein variations in 500 patients: surgical and radiological significance. *Br J Radiol*, 92: 1-5.

UCHIDA K, TANIGUCHI M, SHIMAMURA T, SUZUKI T, YAMASHITA K, OTA M, KAMIYAMA T, MATSUSHITA M, FURUKAWA H, TODO S (2010) Three-dimensional computed tomography scan analysis of hepatic vasculatures in the donor liver for living donor liver transplantation. *Liver Transplant,* 16: 1062-1068.

ULZIISAIKHAN T, AVIRMED A, ENEBISH S, AMGALANBAATAR D (2014) Variations of hepatic veins: study on cadavers. *Int Asian Res J,* 02(02): 41-45.

VINH TRAN H, THANH VO N, VAN DUONG H, TALARICO EF (2020) Anatomical variations of hepatic veins in Vietnamese adults. *Eur J Anat,* 24(2): 111-120.

WATANABE A, YOSHIZUMI T, HARIMOTO N, KOGURE K, IKEGAMI T, HARADA N, ITOH S, TAKEISHI K, MANO Y, YOSHIYA S, MORINAGA A, ARAKI K, KUBO N, MORI M, SHIRABE K (2020) Right hepatic venous system variation in living donors: a three-dimensional CT analysis. *Br J Surg,* 107(9): 1192-1198.

WIND P, DOUARD R, CUGNENC PH, CHEVALLIER JM (1999) Anatomy of the common trunk of the middle and left hepatic veins: application to liver transplantation. *Surg Radiol Anat,* 21: 17-21.

YANG Y, GUAN T, SI Y, XING X (2020) Correlation of clinical features with inferior right hepatic vein incidence: a three-dimensional reconstruction-based study. *Surg Radiol Anat,* 42: 1459-1465.

YIP VS, FENWICK SW (2013) Hepatic, Biliary, and Pancreatic Anatomy. In: Parks RW (ed.). *Hepatobiliary and Pancreatic Surgery: A Companion to Specialist Surgical Practice, Sixth Edition.* Elsevier Ltd., China, pp 17-40.

Insight into Vietnamese women's internal iliac artery anatomy

Bac Nguyen[1], Tuan Vo[2], Tham Nguyen[2], Hoang Pham[2], Bao Vo[3]

[1] *National Hospital of Obstetrics and Gynecology, Hanoi, Vietnam*

[2] *University of Medicine and Pharmacy at Ho Chi Minh City, Vietnam*

[3] *University of Missouri at Kansas City, USA*

SUMMARY

This study aims to assess the characteristics of the internal iliac artery and to examine correlations between the internal iliac artery and other anatomic structures in the pelvis. A cross-sectional study was conducted in the period between October 2019 and May 2020. Eighteen samples of the left and right internal iliac arteries were taken from formaldehyde-embalmed female cadavers at the Ho Chi Minh City University of Medicine and Pharmacy Department of Anatomy. The study showed that the origins of most internal iliac arteries were located by the lumbar vertebrae 4-5. The mean distance from the origin of the internal iliac artery origin to the sacral promontory was 33.95 ± 3.35 mm (on the left), and 31.70 ± 4.64 mm (on the right). The internal iliac artery always had two big branches – anterior and posterior. A third branch was an ilio-lumbar artery, often seen by 43.33%. The diameters of those internal iliac artery branches were comparable on both sides, and the branches of similar name had a little larger diameter on the left than on the right.

The internal iliac artery always has two large anterior and posterior branches; in some cases, it has a third branch called ilio-lumbar artery. The internal iliac artery's length from its origin to the initial branch division is comparable for both right and left sides. The distance from the internal iliac artery's origin to the sacral promontory is suggestive for surgeons to find the internal iliac artery after determining the sacral promontory.

Key words: Post-partum haemorrhage – Internal iliac artery – Anatomy

ABBREVIATIONS:

Postpartum hemorrhage (PPH)

World Health Organization (WHO)

The American College of Obstetricians and Gynecologists (ACOG)

Obstetrics and Gynecology (OB/GYN)

Digital Subtraction Angiography (DSA)

INTRODUCTION

Obstetrics and Gynecology is a medical domain that raises a considerable interest from experts over the world. Post-partum hemorrhage (PPH) currently remains one of the leading obstetric complications that cause maternal deaths in the world and in Vietnam (Say et al., 2014). There are about 14 million women over the world annually

Corresponding author:
Tuan Vo. 217 Hong Bang, District 5, HCMC, Vietnam. Phone: (+84) 909 727 199, Facsimile: (+84-28) 3855 2304. E-mail: vominhtuan@ump.edu.vn

Submitted: December 19, 2021. **Accepted:** September 7, 2022

https://doi.org/10.52083/FLOT6898

incurring PPH (Miller et al., 2004). The risk of maternal mortality due to hemorrhage is one per thousand live births in developing countries (100 over 100,000 live births). Almost all maternal deaths (about 99%) are due to PPH occur in low- and middle-income countries as compared to 1% in industrialized countries (Knight et al., 2009). As per ACOG statistics, it is estimated that there are about 140,000 maternal deaths due to PPH every year (Casanova, 2018). Currently, the leading cause of maternal mortality is still PPH (Lalonde et al., 2006). As per the World Health Organization (WHO) statistics of 2012, maternal mortality rate due to PPH accounted for 25% in Africa, 43% in Indonesia, and 53% in the Philippines (WHO, 2012). On average, there is a PPH maternal death every four minutes in the world. As per statistics in the United States, PPH rate increased by 26% during the period between 1994 and 2006.

In Vietnam, at TuDu hospital alone, there are 60,000 – 68,000 births per annum, and PPH rate was reported 5.18% (TuDu Hospital, 2018) in 2018. Medical and surgical treatment have been applied for PPH. Surgical intervention such as pressing balloon, hypogastric artery ligation, B-Lynch suture stitch, and uterine artery embolism are contributing to maternal mortality rate reduction (Dilly, 2006).

The internal iliac artery provides blood to nearly all internal and external female genitals. Therefore, the emergency management of bleeding complications such as PPH, placenta accrete, or uterine rupture has a close relation to the internal iliac artery and its branching. Internal iliac artery blockage is one of various treatment approaches to this obstetric accident. There is a considerable amount of literature describing the anatomy of the internal in general and the uterine artery in particular over the world, but there are many inconsistent points overall, and domestic documents are very limited. Clinical practitioners often refer to international documents. The issue is "What characteristics do the internal iliac artery and relevant anatomic changes have in Vietnamese females?"

To answer that question, a study on the anatomy of the internal iliac artery in Vietnamese women was conducted to have a panorama of the characteristics of the Vietnamese women's internal iliac artery for clinical reference. The study also wishes to visibilize references to the internal iliac artery, preluding many other studies on anatomy in the future. The main objective of this study is to define the internal iliac artery in relation to other anatomic structures in formaldehyde-embalmed female cadavers at Ho Chi Minh City University of Medicine and Pharmacy, Department of Anatomy.

MATERIALS AND METHODS

A cross-sectional study was conducted from October 2019 to May 2020. The target population was Vietnamese females aged over 18 years. Study subjects were formaldehyde-embalmed female cadavers who met inclusion criteria such as bilateral internal iliac arteries in dissected bodies to conveniently serve academic training at the University of Medicine and Pharmacy of Ho Chi Minh City.

All cases showing evidence of anatomical damages in the pelvic artery system during dissection process, or signs of pelvic distortions, or evidence of pelvic surgery, or tumor presence might cause changes in pelvic artery network structure. Those were exclusion criteria, as they could change the original vascular structure of interest.

Sample size

Estimated sample size for a mean

$$n = \frac{C}{(\Delta/\sigma)^2}$$

with 95% confidence interval, power 0.8, then C = 7.85

Estimated error in the study was selected 7 mm. Sample size for left internal iliac artery was 15 cadavers. The sample size for right the internal iliac artery was of 18 cadavers.

Sampling method

Random selection of cadavers was conducted at convenience over 23 cadavers dissected for research and training. All selected cadavers met

inclusion criteria.; Once the sample size was completed, the recruitment was stopped. The number of female cadavers available at dissection time was 23 of which 18 were selected (78%).

Data collection

Examination was conducted with dissecting instruments, and measuring was conducted with an electronic ruler of Mitutoyo, model 500-776. The ruler audit on its accuracy was certified and stamped by an independent auditor. The ruler accuracy unit was 0.01 mm. Abdominal viscera were displayed via lower laparotomy.

Fig. 1 describes how to explore the pelvis and the iliac artery system by dissecting and moving internal organs aside. Fig. 2 shows how to measure the artery diameter at its origin. Fig. 3 shows how to measure the distance between the internal iliac artery's origin and the sacral promontory. Fig. 4 shows how to measure the internal iliac artery's length. A thread was placed along and adjusted in form of the artery pathway from the origin to its end, and then two markers were defined on the thread; the distance between two markers was measured, in accordance with Le's method (Le et al., 2020). Fig. 5 shows how to dissect to find the anterior and posterior trunks of the internal iliac artery, and then to separate the branches of the anterior and posterior trunks. it also shows how to dissect external female genitals to the transverse perineal layer; and then determinesthe branches of uterine artery for external genitals. Dissections around to explore uterine artery features was made following Le's method (Le et al., 2020).

Data entry were conducted with Excel program, and coded and processed with IBM SPSS Statistics 20.

Ethics License

The study was approved by the Ethics Council for Bioresearch of the HoChiMinh City University of Medicine and Pharmacy, approval no. 562/ĐHYD-HĐĐĐ, dated 28/10/2019.

Fig. 1.- Dissecting and moving internal organs aside to explore internal iliac artery.

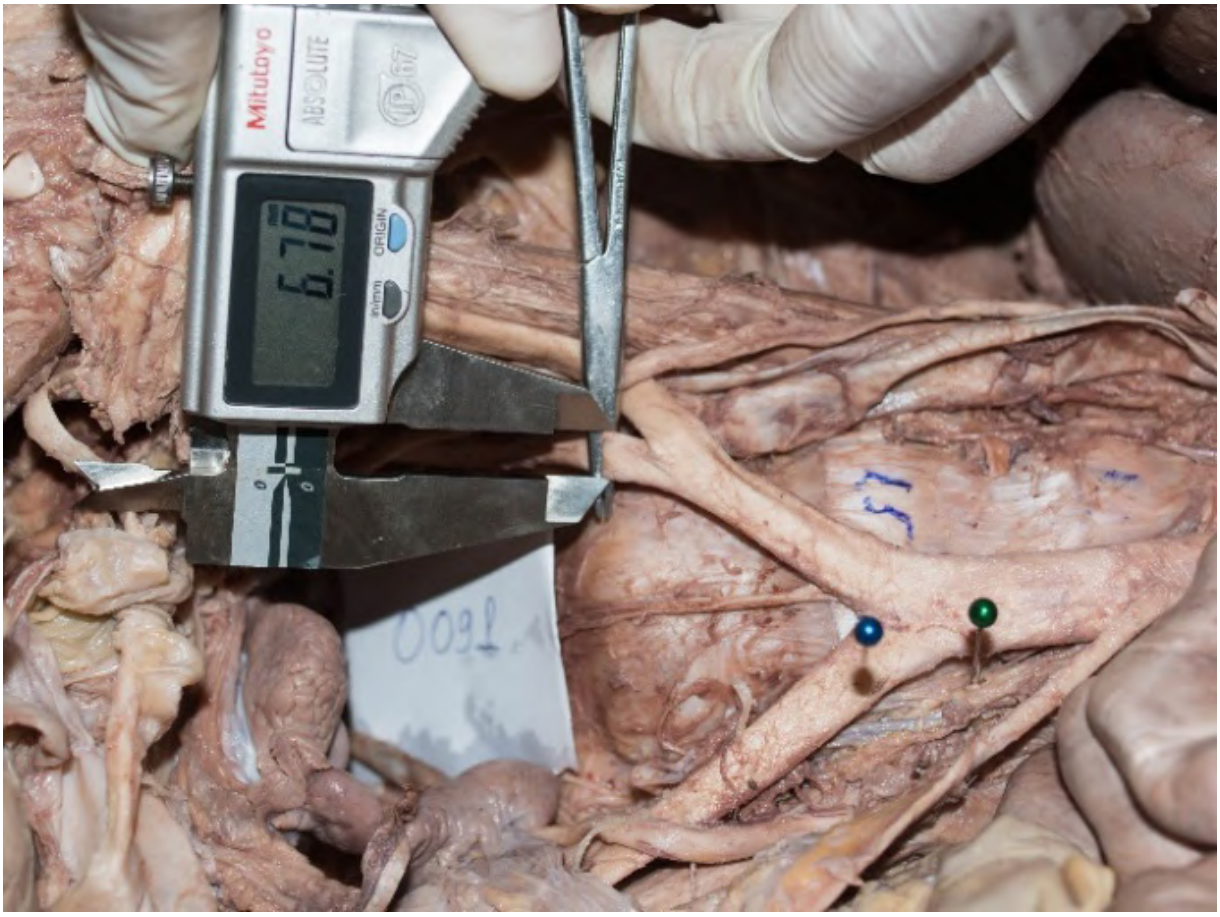

Fig. 2.- Measuring the internal iliac artery diameter at its origin.

Fig. 3.- Measuring the distance between Internal iliac artery origin and sacral promontory.

Fig. 4.- Measuring the Internal iliac artery length.

Fig. 5.- Dissecting to find the anterior and posterior trunks of internal iliac artery.

RESULTS

The mean age of cadavers was relatively high 70.50 ± 17.86 years. The youngest age was 33 years and the oldest 99 years. Cadaver preservation period ranged between 1 and 7 years. Causes of death and maternal parity were not available.

The origin of the internal iliac artery was mostly found at lumbar vertebral levels 4-5. The mean distance from the internal iliac artery origin to sacral promontory was 33.95 ± 3.35 mm (on the left) and 31.70 ± 4.64 mm (on the right) (Table 1).

Table 1. Origins of internal iliac artery.

Internal iliac artery origin by vertebral level	N of cases	
	Left	Right
L3	1 (5.56%)	0 (0%)
Inter-vertebral disc L3 – L4	2 (11.11%)	1 (5.56%)
L4	5 (27.78%)	3 (16.67%)
Inter-vertebral disc L4 – L5	2 (11.11%)	1 (5.56%)
L5	8 (44.44%)	13 (72.22%)

The internal iliac artery always had two large branches – anterior and posterior. A third branch was an ilio-lumbar artery, also frequently found by 43.33% (Table2).

Table 2. Number of Internal iliac artery branches.

N of branches	N of cases	Percent
2	17	56.67%
3	13	43.33%

The diameter of the anterior internal iliac artery branch ranged within 4.74-11.85 mm on the left, and 4.08-11.08 mm on the right. The diameter of the posterior branch ranged within 3.6-10.16 mm on the left, and 2.3-12.16 mm on the right. Ilio-lumbar branch had the diameter range of 1-2 mm (Table 3).

Table 3. Mean diameter of Internal iliac artery branches.

	Mean diameter (mm)		Largest diameter (mm)		Smallest diameter (mm)	
	Left	Right	Left	Right	Left	Right
Anterior branch	7.29 + 1.91	7.03 + 1.78	11.85	11.08	4.74	4.08
Posterior branch	6.03 + 1.86	5.93 + 2.21	10.16	12.16	3.60	2.30
Ilio-lumbar branch	1.49 + 0.29	1.31 + 0.23	2.08	1.68	1.08	1.02

The internal iliac artery's length ranged 30-50 mm (Table 4).

Table 4. Mean length of internal iliac arteries.

	Mean length (mm)		Largest length		Smallest length	
Artery	Left	Right	Left	Right	Left	Right
Internal iliac	42.62 + 2.98	42.28 + 4.31	47.85	50.10	38.06	31.52

Most of uterine arteries had an origin compatible with vertebral levels S2 to S3. The mean diameter of the uterine artery was measured at its origin 3.03 ± 0.85 mm (on the left), and 2.95 ± 0.79 mm (on the right) (Table 5).

Table 5. Origin of uterine artery.

Uterine artery origin by vertebral level	N of samples	Percent
S1	1	3.33%
S2	16	53.33%
Intervertebral S2 – S3	2	6.67%
S3	8	26.67%
S4	3	10%

The largest distance to the sacral promontory was measured 68 mm, and the smallest 33 mm. The largest distance to the vaginal artery was 115 mm, and the smallest 31 mm.

Table 6. Correlation of uterine artery origin.

	Mean distance (mm)		Largest distance		Smallest distance	
	Left	Right	Left	Right	Left	Right
Distance from uterine artery origin to sacral promontory	51.86 + 9.74	45.67 + 9.99	68.54	68.02	35.40	32.76
Distance from uterine artery origin to vaginal artery origin	60.63 + 1.71	64.28 + 25.16	96.32	115.60	32.43	31.30

The distance between the uterine artery and the ureter by the cervical edge was within 3.5-18 mm. The distance of the uterine-artery-ureter crossing point to cervical edge was 11-33 mm (Table 7).

Table 7. Correlation between uterine artery and ureter.

	Mean distance (mm)		Largest distance		Smallest distance	
	Left	**Right**	**Left**	**Right**	**Left**	**Right**
Distance from uterine artery to ureter by cervical edge	7.71 + 3.51	9.38 + 4.16	18.12	16.90	3.56	4.40
Distance from crossing point of uterine artery and ureter to cervical edge	19.28 + 4.01	19.87 + 5.12	26.10	33.16	11.12	13.70

The other branches (i.e., iliolumbar artery, lateral sacral artery, superior gluteal artery, inferior gluteal artery, middle rectal artery, obturator artery, inferior vesical artery, superior vesical artery, obliterated umbilical artery, internal pudendal artery) were also examined. However, those branches' characteristics will be assessed in another article with further study objectives.

DISCUSSION

The origin of the internal iliac artery in this study is comparable with those from the study ny Mamatha et al. (2015), in which 72% of internal iliac artery's origins came by vertebral level S1, 24% by L5-S1, and 4% by L5. The rates by Naveen et al. (2011) were 58.3% (S1), 40% (L5-S1), and 1.7% (L5), respectively.

As per Jean-Pierre Pelage et al., the internal iliac artery ended in two large trunks – anterior and posterior – in 77% of cases, 14% had three trunks, 3% had more than 3 trunks, and 4% had a unique trunk. In this study, all internal iliac arteries had two large branches, anterior and posterior. In some instances, an ilio-lumbar branch deviated ahead of the origins of the other two branches and became the third branch. The cases with a unique branch or more than 3 branches are rare in literature, and in our study, such rare cases were not detected (Pelage et al., 1999).

The internal iliac artery's diameter in this study was measured at 5 mm away from the artery's origin to obtain the most real size and to avoid false increase. The value was 9.69 ± 1.4 mm. According to Fatu et al. (2006), the internal iliac artery's mean diameter in females was 9.83 ± 1.57 mm, within the range of 4-11 mm. That study's results look quite comparable with theirs.

The uterine artery originates from the anterior branch of the internal iliac artery. Some authors considered the uterine artery an anatomic detail to identify the anterior branch of the internal iliac artery (Lipschitz, 2018). The uterine artery had its origin by sacral vertebral levels S2-S3 in about 87% of cases in the study.

At its origin, the uterine artery often sprang ahead of the sacral promontory with a mean distance of 48.77 ± 10.22 mm on both sides, in which the left distance was 51.86 ± 9.74, and the right 45.67 ± 9.99 mm. Almost all previous studies compared the uterine artery's location with the mid-sagittal plane. The selection of the sacral promontory as an anatomical correlation landmark of artery location is the new point of this study.

The ureter is the important mark in Ob/Gyn operations in the pelvis. The mean distance between the uterine artery's origin and the ureter was 8.34 ± 2.90 mm, in which the distances were 8.62 ± 3.33 mm (on the left), and 8.07 ± 2.47 mm (on the right). The ureter often crosses in front of or behind the uterine artery by the upper endocervical level. Eighty percent of cases had a uterine artery crossing the ureter by the upper edge of the cervix. The crossing point was 19.28 ± 4.01 mm away from cervix. This result is quite comparable with the value of 2 cm by other authors (Le et al., 2020).

The quick identification of artery origins has a great meaning in emergency management for PPH (Greenwood, 1987) and other uterine surgeries. The anatomical positions and correlations with surrounding structures provide surgeons with further information for quick and precise manipulation.

Limitations of the study: the anatomical assessment of embalmed cadavers is not as precise as those on fresh ones or by real clinical practice. The study should be conducted on fresh cadavers with better quality. It will be better to assess and measure the internal iliac artery conducted on DSA film, and then to compare results obtained

between formaldehyde-embalmed and fresh cadavers.

CONCLUSION

The internal iliac artery is an important artery providing blood to the pelvis and female genitals. The internal iliac artery always has two large branches, anterior and posterior, and in some cases, it has a third branch – an iliolumbar artery.

The length of the internal iliac artery from its origin to the first division site is equivalent for both sides. The distance from the internal iliac artery's origin to the sacral promontory suggests how to find the internal iliac artery after identifying sacral promontory.

The branches of the internal iliac artery are comparable between the left and right ones, in which uterine artery is an important one. The anatomical correlation of the ureter crossing the unternal iliac artery and the uterine artery, as well as the distance and crossing position are essential to locate the ureter in Ob/Gyn operations.

ACKNOWLEDGEMENTS

The authors wish to express their sincere gratitude to the anatomical donors of Vietnam, who bequeathed their bodies for medical education and basic science research. We also wish to thank each of the patients who agreed to participate in the present work, thus adding new knowledge that might help future patients.

Support: University of Medicine and Pharmacy at Ho Chi Minh City (Vietnam) - Internal Funding.

NOTES ON CONTIBUTORS

Prof. Tuan Vo M.D., Ph.D. Current position: Head of Science-Technology Office and Deputy Chair of Obstetrics & Gynecology Department of University of Medicine and Pharmacy at Ho Chi Minh City (UMP). Academic profiles: Completed an OB/GYN residency at UMP (1995). Earned Ph.D. in University of Texas, then post-doctoral fellowship in OB/GYN at University of Michigan (2006). Research interest: Clinical interests include all aspects of general OB-GYN with interests in Cancer prevention. He published 130 research articles and 9 books. Member of: Vietnam's Obstetrics and Gynecology and Family Planning Association (VINAGOFPA); Ho Chi Minh City Reproductive Endocrinology and Infertility Association (HOSREM).

Tham Nguyen, M.D. was Junior Lecturer in the Department of Anatomy at the University of Medicine and Pharmacy at Ho Chi Minh City, Vietnam. She did a fellowship in OB/GYN with Prof. Tuan Vo at University of Medicine and Pharmacy at HCMC, Vietnam (2020). "Insight into Vietnamese women's internal iliac artery anatomy" was her thesis in the OB/GYN fellowship program.

Bac Nguyen, M.D. was senior physician in the Department of Gynecology at the National Hospital of Obstetrics and Gynecology, Hanoi, Vietnam. Research interest: Clinical interests include all aspects of general OB-GYN.

Hoang Pham, M.D. is Junior Lecturer in the Department of OB-GYN at the University of Medicine and Pharmacy at Ho Chi Minh City, Vietnam. He was Ph.D. student of Prof. Tuan Vo at University of Medicine and Pharmacy at HCMC, Vietnam (2022-2025).

Bao Vo is a third-year student of Biomedical Sciences Department of University of Missouri – Kansas City, USA. Bao Vo did his shadowing with The Ho Chi Minh City University of Medicine and Pharmacy (HCM-UMP) for the period of September 2020 – April 2021. He has been assigned to work with Prof. Tuan Vo during his internship in Vietnam.

REFERENCES

CASANOVA R (2018) Beckmann and Ling's Obstetrics and Gynecology. Lippincott Williams & Wilkins, pp 317-334.

DILDY III G (2006) The pelvic pressure pack. In: A textbook of postpartum hemorrhage. Sapiens Publishing, Dumfriesshire, UK, pp 308-311.

FĂTU C, PUIŞORU M, FĂTU I (2006) Morphometry of the internal iliac artery in different ethnic groups. *Ann Anat,* 188(6): 541-546.

GREENWOOD L, GLICKMAN M, SCHWARTZ P (1987) Obstetric and nonmalignant gynecologic bleeding: treatment with angiographic embolization. *Radiology,* 164(1): 155-159.

KNIGHT M, CALLAGHAN WM, BERG C (2009) Trends in postpartum hemorrhage in high resource countries: a review and recommendations from the International Postpartum Hemorrhage Collaborative Group. *BMC Pregnancy Childbirth,* 9(1): 1-10.

LALONDE A, DAVISS B, ACOSTA A (2006) Postpartum hemorrhage today: living in the shadow of the Taj Mahal. *Sapiens Publishing*, pp 2-10.

LE CV, TALARICO JR, NGUYEN KT (2020) The size of intestines in Vietnamese adults. *Eur J Anat,* 24(3): 169-178.

LIPSHUTZ B (1918) A composite study of the hypogastric artery and its branches. *Ann Surg,* 67(5): 584-608.

MAMATHA H, HEMALATHA B, VINODINI P (2015) Anatomical study on the variations in the branching pattern of internal iliac artery. *Indian J Surg,* 77(2): 248-252.

MILLER S, LESTER F, HENSLEIGH P (2004) Prevention and treatment of postpartum hemorrhage: new advances for low-resource settings. *J Midwifery Women's Health,* 49(4): 283-292.

NAVEEN N, MURLIMANJU B, KUMAR V (2011) Morphological analysis of the human internal iliac artery in South Indian population. *Online J Health Allied Sci,* 10(1): 1-4.

PELAGE J, LE DREF O, SOYER P (1999) Arterial anatomy of the female genital tract: variations and relevance to transcatheter embolization of the uterus. *Am J Roentgenol,* 172(4): 989-994.

SAY L, CHOU D, GEMMILL A (2014) Global causes of maternal death: a WHO systematic analysis. *Lancet Global Health,* 2(6): 323-333.

TUDU HOSPITAL (2018) Annual Review Report by Department of Birth Delivery in 2017-2018.

WHO (2012) WHO recommendations for the prevention and treatment of postpartum hemorrhage, *World Health Organization.*

A cross sectional study on the online teaching strategies of gross anatomy and histology during the COVID-19 pandemic periods

Divia Paul. A[1], Manisha R. Gaikwad[2], Ranajit Das[3]

[1] Department of Anatomy, Yenepoya Medical College, Yenepoya (Demed to be University), Deralakatte, Mangalore-575018, India
[2] Department of Anatomy, All India Institute of Medical Sciences Bhubaneswar – 751019 Odisha State, India
[3] Division of Data Analytics, Bioinformatics and Structural Biology (DABS), Yenepoya Research Centre Yenepoya (Deemed to be University) University Road, Deralakatte Mangalore, Karnataka 575018, India

SUMMARY

The subsequent implementation of social distancing during the COVID-19 pandemic has forced universities to keep the students away from the institutions. The aim of the study was to conduct a survey through medical colleges among anatomy teachers along with an exploration of optimization of the transitions which can assist to improve the quality of online teaching. The objectives were to identify the virtual learning interventions implemented by different medical colleges in India during Covid-19 pandemic periods, and to identify suitable technological intervention for teaching anatomy from the educator's point of view. A cross sectional study was conducted by convenience sampling method. A differential rating scale questionnaire study was conducted. A hundred participants from the department of anatomy of 100 medical colleges with a minimum of 3 years of experience in teaching in the field were the samples. Faculty other than anatomy department of medical colleges was excluded. Consents were taken from each participant and participant information was shared by email.

The teachers were from both from Government and from Private Institutions. For most teachers, the biggest difficulty in implementing online teaching during the initial year of online teaching at 2020 was the unstable online teaching environments, platforms and tools (47%), followed by their unfamiliarity with online teaching techniques, platforms and tools (26%). Further, 17% had problems due to insufficient training and management of online teaching from college. This study assists to improve the design and quality of online teaching by suggesting for the change in infrastructure by arranging online portal hands-on coaching for rendering online education.

Key words: COVID-19 pandemic – Online teaching platforms – Optimization of the transitions – Nationwide survey – Technological interventions

Corresponding author:
Dr. Divia Paul. A. Assistant Professor Department of Anatomy, Yenepoya Medical College, Yenepoya (Deemed to be) University, Deralakatte, Mangalore-575018, India. Phone: +91 8075789347. E-mail: drdiviamanoj@gmail.com

Submitted: April 3, 2022. **Accepted:** August 7, 2022

https://doi.org/10.52083/YRTB9630

INTRODUCTION

Anatomy is the subject that describes the identification as well as the concepts of the body structures of living things. Gross anatomy includes the study of major body structures by dissection and close observation of its narrowest sense, especially when concerned with the human body. Medical students do the dissection of human bodies themselves in anatomy laboratories. This is considered as the most effective method to deliver anatomical knowledge to medical students (Snelling et al., 2003). Web-based anatomy education has used various technologies, such as three-dimensional (3D) computer models (Fellner et al., 2017) but the educational worth and efficacy of these technologies remains controversial (Ghebreyesus, 2020). The subsequent implementation of social distancing during the COVID-19 pandemic has forced colleges and universities to empty their classrooms and keep the students away from the institutions (Kamenetz, 2020). Consequently, there has been a general shift from traditional face-to-face instruction to online teaching. Most institutions have switched to distance learning in the simplest and most convenient ways possible, including conferencing platforms, email, and phone (Lederman, 2020).

As we know, the achievement of online teaching depends on various technologies, including the appreciation of broadband and teaching platforms (Krenacs et al., 2010). Commonly used appreciative techniques includes synchronous live broadcasting teaching platforms, simultaneous live broadcasting software, teaching management platforms, virtual labs projects, screen capture and postproduction units and social media apps. These appreciative techniques were insufficient to meet the basic needs of online education caused medical college closures, as there were few other choices during the pandemic outbreak.

In India, as of 21 May 2020, there are 542 medical colleges recognized by the National Medical Commission (NMC). A nationwide survey among Indian professional anatomy teachers is required to assess the general situation of medical education online during the pandemic periods in India. This can provide teachers with some facts regarding effective online teaching. The aim of the study was to conduct a survey through medical colleges among anatomy teachers along with the optimization of the transitions which can assist the improvement of the quality of online teaching. The objectives were to identify the virtual learning interventions implemented by different medical colleges in India during Covid-19 pandemic periods, and to identify suitable technological intervention for teaching anatomy from the educator's point of view.

METHODOLOGY

A cross-sectional study was conducted from October 2021 to March 2022 and convenience sampling method was adopted. A differential rating scale questionnaire study was conducted. In order to get the correct representation, a multi-center study was conducted for data collection in which centers were selected by randomization from the different states of India. Based on information and queries with faculties working at different medical colleges, the researcher developed the tool for the study. Approval of the Institutional Ethics Committee of parent University, as well as prior permission from the authorized college in-charges of the concerned medical college were obtained. Informed consent was taken from each participant and participant information was shared to the concerned participants via email.

The confidentiality of the participants was maintained and they were assured that their participation and nonparticipation in the study would have no benefits. Faculties from the departments of anatomy from the medical colleges across India with teaching experience of more than 3 years were included in the study. Faculty of anatomy from different colleges other than medical colleges and faculty other than anatomy department of medical colleges were excluded. A hundred participants from 100 medical colleges with a minimum of 3 years of experience in teaching the field were the samples.

The tool consisted of 29 items on multiple choice questions type scale with open-ended answers. Questions were descriptive in nature. There were no negative statements. The items

in the questionnaires were focused on clinical medicine programs. The participants from each college were contacted previously to acquaint them with the study and to check their willingness to participate in it by personal contacting measures. Sample collection is by questionnaire method provided via Google forms and sent to the participant by link to personal email. The researcher developed demographic proforma and online teaching strategies scale based on key variables. The demographic proforma had three items including name of the medical College and university of current employment, current designation at present place of work and years of experience in teaching the field. The online teaching strategies scale based on key variables included 6 major orientations: namely principle implementation tools, mode of delivery, student-teacher interaction methods, perceptions and effectiveness, active learning, problems encountered and success rates. There were questions separately for theoretical and practical sections, which included gross anatomy and histology sections of anatomy based on key variable section.

The questionnaire adopted commonly used synchronous live broadcasting teaching platforms for the development of the tool more effectively. This includes simultaneous live broadcasting software, such as SWAYAM PRABHA (launched by MHRD under NMEICT INFLIBNET centre, Gandhinagar, Gujarat), CLOUDATOMY (Gurugram, haryana, Google suite (Google LLC, Mountain View, California, U.S.), Youtube live stream etc (Google LLC, Mountain View, California, U.S.), along with Zoom (Zoom Video Communications Inc., San Jose, CA), which is also popular in other parts of the world.

Based on various teaching management platforms, there were sections in the tool, such as Microsoft teams, (Microsoft Corporation, Redmond, Washington, U.S.), Google classroom (Google LLC, Mountain View, California, U.S.), Google Hangouts (Google LLC, Mountain View, California, U.S.), Google meet (Google LLC, Mountain View, California, U.S.),, Facetime (Apple Inc. , Cupertino, California, U.S.), etc., which are the most popular choices for anatomy teachers working in India to upload and issue their teaching materials, which includes videos, presentations, exercises, etc. A few teaching management platforms, for example, Google Classroom and Microsoft teams, have upgraded their functions to support live broadcasting teaching.

The open free online courses and details were also used for formulating the questionnaire such as the virtual labs project (SWAYAM PRABHA) launched by MHRD under NMEICT INFLIBNET centre, Gandhinagar, Gujarat), the virtual simulation experiment teaching center: for example, 3D ORGANON VR ANATOMY(Medis Media Pty Ltd, Australia), VR Anatomy- Digital Solutions-Manipal Digital (India Partner & Distributor for 3D Organon to help you to transform Medical Education), ACTS-YEN (Yenepoya university, Mangalore) are also well- recognized on different course platforms as content providers for medical courses in India.

Screen capture and postproduction software, including Adobe premier - Adobe Inc. , San Jose, California, U.S, Adobe after effects - Adobe Inc. San Jose, California, U.S, final cut -Apple Inc., Cupertino, California, U.S. are extensively used worldwide. In addition, some social media apps, for example, WhatsApp (WhatsApp LLC (Facebook Inc.), Mountain view, California, U.S) and Telegram (Telegram FZ LLC, London, United Kingdom), also provided important knowledge about live broadcasting tools in India and helped to finalize the assessment section.

Data were collected by attached excel sheet along with the Google forms. All the 100 participants returned the answered Google questionnaire forms. The tools were pretested among 10 participants of a selected institution. The reliability of the tool was measured by using Crohnbach alpha formula. The calculated 'r' value is $0.8 > \alpha \geq 0.7$ and tool was found reliable and acceptable for assessment. Analysis of the data was done using the Statistical Package for the Social Sciences (SPSS) software package for Windows version 22.0 (SPSS Inc., Chicago, IL). This is to assess the feasibility and predictability of the tool by interpretation of data.

RESULTS

The given questionnaire was completed by faculties of various designations, ranging from lecturers, early-career Assistant Professors with three years of teaching experience to senior Professors with 25-27 years of teaching experience. The teachers were from both Government and Private Institutions. Overall, >90% teachers were used to face-to-face lectures from lecture halls before the COVID-19 pandemic set in and only ~8% teachers had experience in some sort of online teaching (Fig. 1). The scenario changed drastically during the pandemic with ~65% teachers moved to simultaneous live broadcasting where the teacher delivered the sessions live and another 24% opted for a mixed method of simultaneous broadcasting with some recorded broadcasting (Fig. 2).

For teacher and student interactions during simultaneous live broadcasting of online theoretical sessions, the majority (69%) opted for real-time voice communication on platforms such as Google Classroom and Microsoft Teams. Interestingly, only 9% teachers incorporated online assignment questions in PowerPoint presentations based on teaching management platforms. During the simultaneous live broadcasting of online theoretical sessions, 58% teachers talked most of the scheduled time and kept the last 10 minutes for clearing any doubts. However, ~34% teachers stressed more on teacher-student interactions than on pure didactic lectures. While 16% of them kept more than half of the scheduled time for the teacher-student interaction, another 18% kept little less than half of the scheduled time for the same. Unfortunately, 8% teachers did not schedule any interaction time during the simultaneous live broadcasting of online theoretical sessions.

For separate recorded broadcasting of online theoretical sessions, 25% teachers said that they opted for screen capture software to record only the slides and sound of the PowerPoint presentation, and he/she did not appear in the

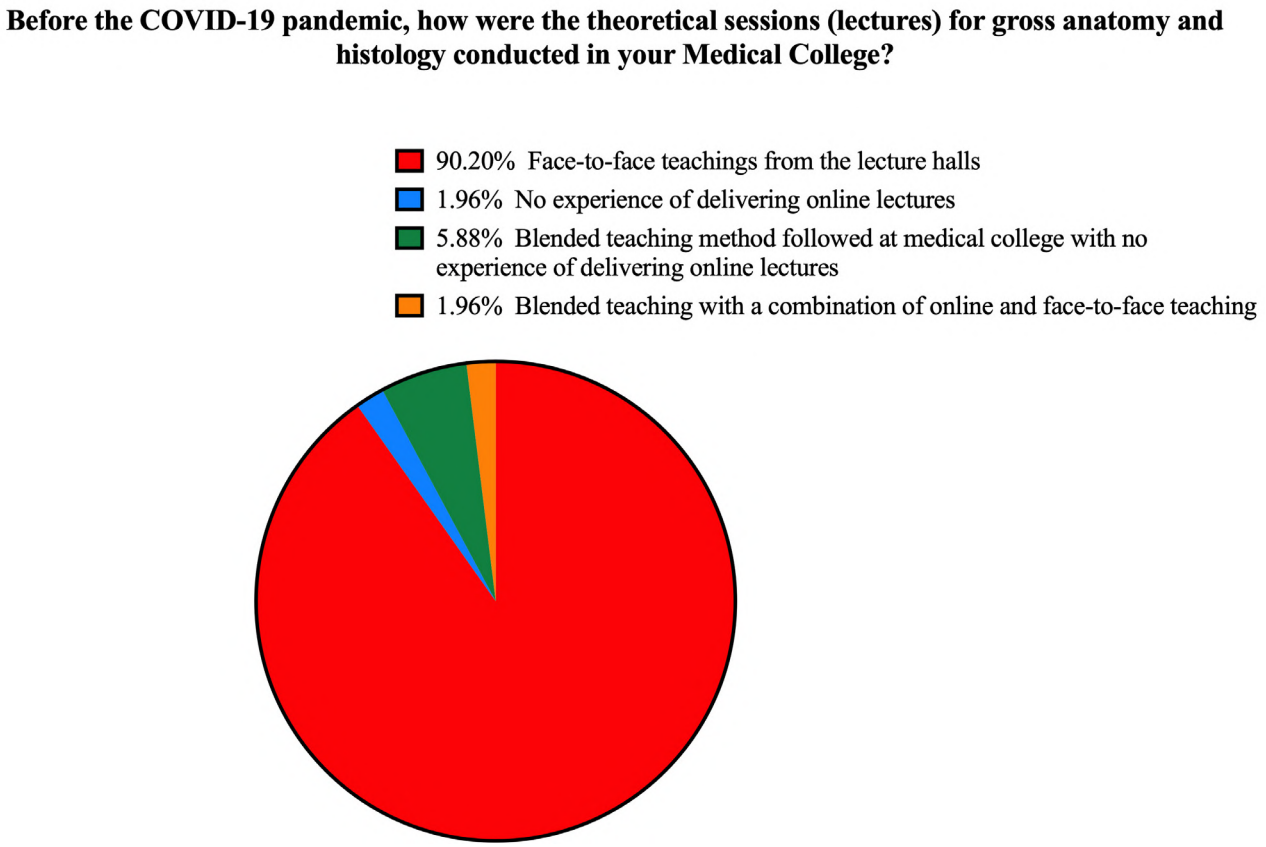

Fig. 1.- Before the Covid-19 pandemic, how were the theoretical sessions(lectures) for gross anatomy and histology conducted in your medical college. The Pie chart was plotted in GraphPad Prism v9. The plot shows that before the pandemic almost all theoretical sessions (>90%) used to be conducted on face-to-face basis.

recorded session. ~29% teachers had access to video cameras to record the session with 13% or without 16% post-production facilities.

However, 33% faculties had no experience of delivering recorded lectures. In terms of the content of the teaching materials, most of the teachers 29% kept the content the same as those for face-to-face teaching and did not change anything to suit online teaching. However, 50% o f teachers did reworking for improving the course content. While 25% of them made slight changes in the content, others completely redesigned the teaching materials to suit online teaching. Intuitively, before the COVID-19 pandemic, >90% of the practical sessions for gross anatomy and histology were conducted via face-to-face teachings from the dissection halls and histology labs.

During the COVID-19 pandemic, the format of the online practical sessions on gross anatomy and histology changed. Expectedly, ~94% medical colleges increased the use of visual media in the practical sessions. Thirty-four percent of teachers opted for simultaneous live broadcasting, where teacher delivers the sessions live for gross anatomy and histology and another 34% explored the mixed methods with some sessions by simultaneous live broadcasting and some by separate recorded broadcasting for gross anatomy and histology practical. During the COVID-19 pandemic, only 17% medical colleges employed some sort of virtual lab or virtual simulation experiments such as Swayam Prabha, 3D Organon virtual anatomy etc. for gross anatomy and histology practical sessions. Unfortunately, 83% medical colleges had no experience of delivering online practical sessions.

Similar to theoretical sessions, during the simultaneous live broadcasting of online practical sessions of gross anatomy and histology, most (44%) teachers talked most of the scheduled time and kept only the last 10 minutes for clearing any doubts. However, 43% teachers focused more on teacher-student interactions during

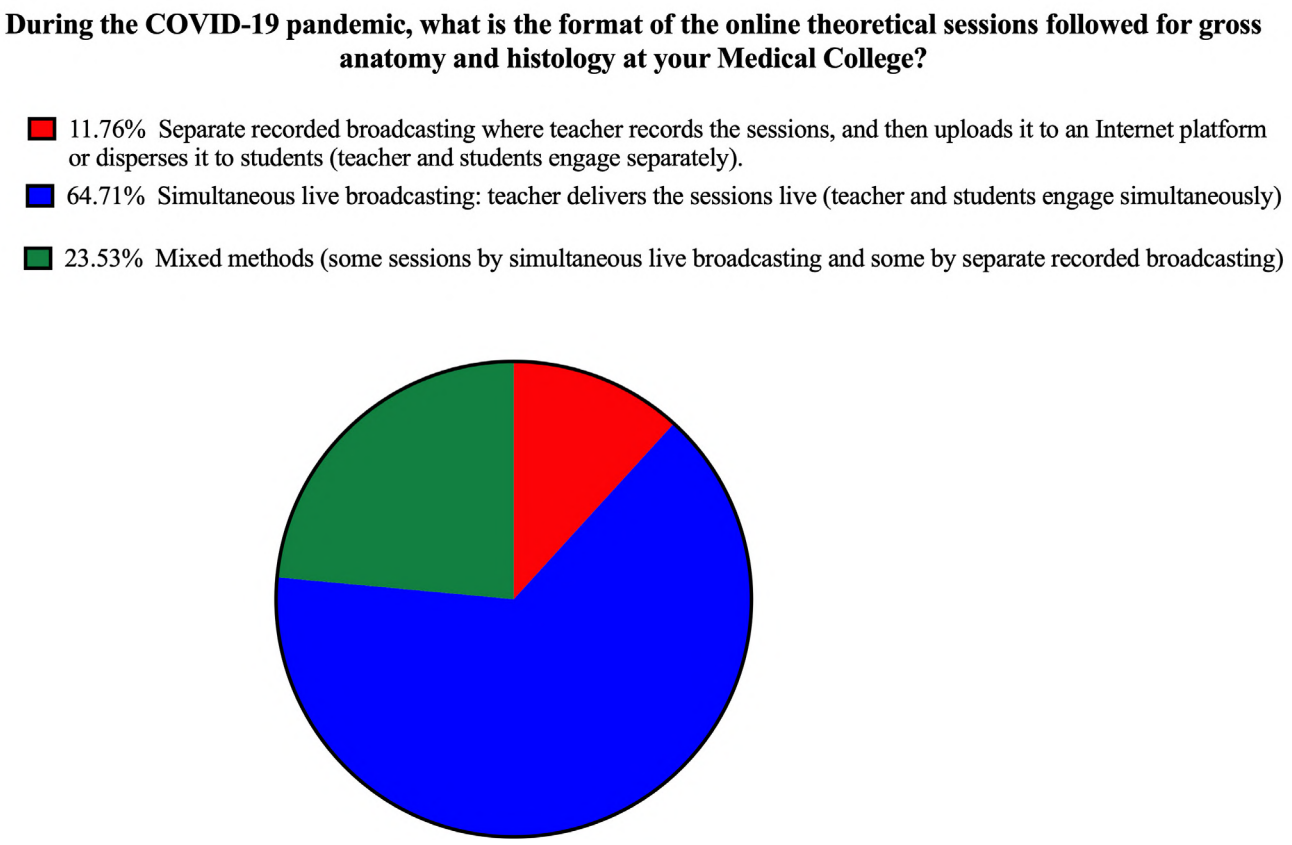

Fig. 2.- During the Covid-19 pandemic, what is the format of the online theoretical sessions followed for gross anatomy and histology at your medical college. The Pie chart was plotted in GraphPad Prism v9. The plot shows that during the pandemic almost all theoretical sessions (>88%) moved to some sort of online mode of teaching.

practical. While 20% of them kept more than half of the scheduled time for the teacher-student interaction, another 23% kept little less than half of the scheduled time for the same. Unfortunately, 12% of teachers did not schedule any interaction time during the simultaneous live broadcasting of online practical sessions, which might have impacted the holistic learning of these students.

During the COVID-19 pandemic, 26% of medical colleges implemented problem-based learning, 45% initiated an online small group discussion, 13% initiated microteaching and individualized tutoring, and 6% introduced term-based learning as means of active online learning for gross anatomy and histology. For the majority of the medical colleges (36%), the active learning program was implemented before the pandemic and has continued to be used during the pandemic. For another 16% medical colleges, some sort of active learning measure was implemented before the pandemic but was used only at selected time intervals and slots.

However, for 32% colleges it was not implemented before the pandemic and only implemented during the same. Further, during the COVID-19 pandemic, most medical colleges (42%) employed platforms for online courses to implement active learning of gross anatomy and histology. Well-known online platforms such as WhatsApp and YouTube were close second (41%) in terms of being implemented as the means of active learning.

The main pattern of online assessment at most medical colleges (73%) during the pandemic was online theory and practical tests, distantly followed by individual online assignments and seminars (12%). Interestingly, 5% of medical colleges did not have any online assessments of students while 6% of colleges employed assessment only by recording the attendance for online sessions. While for 63% of medical colleges, this online assessment was not implemented before the pandemic, 17% of colleges already implemented this, and it continued to be used during the pandemic.

Interestingly, while most teachers (55%) believe that 30-60% of learning outcomes are achieved through online teaching, 23% believe that less than 30% of learning outcomes are achieved and 17% think that 60-80% of learning outcomes are achieved. Only 5% teachers think that 80-100% of learning outcomes are achieved. Overall, 50% of teachers are dissatisfied with the effectiveness of online learning during the COVID-19 pandemic and 38% are neutral about it. Only 13% of them are satisfied about it. According to most teachers (45%), the biggest gain from the online teaching during the COVID-19 pandemic in 2020 was the diversity of teaching methods, followed by the opportunity for developing novel teaching methods (37%) and novel contents (13%). However, in 2021, the biggest gain from the online teaching during the COVID-19 pandemic was the enhancement of interaction between teachers and students (30%) and the development of more individualized instruction (30%), closely followed by expediting the feedback process for students (27%).

For most teachers, the biggest difficulty in implementing online teaching during the initial year of online teaching at 2020 was the unstable online teaching environments, platforms and tools (47%), followed by their unfamiliarity with online teaching techniques, platforms and tools (26%). Further, 17% believe that the main problem was insufficient training and management for online teaching from college. However, for 2021 the biggest difficulty in implementing online teaching was the difficulty in grasping student progress and results of learning (46%), followed by difficulty in efficient interaction with students (36%). Further, 13% of teachers thought that it takes much longer time for preparing online teaching than traditional teaching. Given the current insufficient and inadequate infrastructure for online teaching, unsurprisingly most teachers (68%) prefer returning to traditional face-to-face classes as soon as the pandemic is over. However, 33% teachers are willing to continue some form of online teaching especially, or some theoretical classes even after the pandemic is over. Only 2% teachers want to continue to conduct both theoretical and practical classes online after COVID-19 pandemic.

DISCUSSION

The world has responded to a pandemic of contagious respiratory disease caused by a novel coronavirus, named COVID-19 by different approaches (Jernigan et al., 2020). On March 11, 2020, the World Health Organization declared the coronavirus outbreak a pandemic – i.e., the worldwide spread of a new disease (Ghebreyesus, 2020). The subsequent implementation of social distancing during the COVID-19 pandemic has forced colleges and universities to empty their classrooms and keep the students away from the institutions (Kamenetz, 2020). Consequently, there has been a general shift from traditional face-to-face instruction to online teaching (Lederman, 2020). In the present study, conducted among faculties of anatomy departments of various medical colleges in India, it was noted that though >90% teachers were used to face-to-face lectures from lecture halls before the COVID-19 pandemic set in and only ~8% teachers had experience in some sort of online teaching. The scenario changed drastically during the pandemic, with ~65% teachers moved to simultaneous live broadcasting where teachers delivered the sessions live and another 24% opted for a mixed method of simultaneous broadcasting with some recorded broadcasting. During the simultaneous live broadcasting of online theoretical sessions, 58% of teachers talked most of the scheduled time and kept the last 10 minutes for clearing any doubts. However, ~34% of teachers focused more on teacher-student interactions than on pure didactic lectures. Therefore, interspersing interactive sessions during didactic sessions may help to break the monotony if any. Most institutions, have switched to distance learning in the simplest and most convenient ways possible, including conferencing platforms, email, and phone (Lederman, 2020). As we know, the achievement of online teaching is heavily reliant on various technologies, including the appreciation of broadband and teaching platforms (Krenacs et al., 2010).

In recent years, techniques based on the internet have progressed greatly in India, producing a profound effect on education. Online teaching and learning activities are becoming popular among teaching academics and learners. India could manage to develop live broadcasting platforms and teaching management platforms, although initially there was a dependency from Chinese apps. In the present study, for teacher and student interactions during simultaneous live broadcasting of online theoretical sessions, the majority (69%) opted for real-time voice communication on platforms such as Google Classroom and Microsoft Teams. Interestingly, only 9% teachers incorporated online assignment questions in power point presentations based on teaching management platforms. Currently, technology helps for the transformation of the teaching from a "teacher-centered" approach to the "student-centered" process. Information technology used by teachers can help students improve their academic output. This is achieved by giving students more autonomy in learning (Yao et al., 2020). So, can technology further play an independent role, or even replace teachers to achieve students' completely autonomous learning? A growing number of colleges and universities have been implementing a transition from traditional face-to-face teaching methods to online teaching or a combination of online and traditional teaching (blending) (Orleans, 2014). Unfortunately, it was found in the present study that during the COVID-19 pandemic only 17% of medical colleges employed some sort of virtual lab or virtual simulation experiments such as Swayam Prabha, 3D Organon virtual anatomy, etc. for gross anatomy and histology practical sessions and 83% of medical colleges had no experience of delivering online practical sessions.

In the present study, for the majority of the medical colleges (36%), the active learning program was implemented before the pandemic and has continued to be used during the pandemic. The blended method of teaching involves replacing part of the face-to-face interaction with online instruction (Edginton and Holbrook, 2010). This means that technology is playing an increasing role, but the effective communication between teachers and students face-to-face is still indispensable and is a critical link for students' learning process. In India, well-known online platforms such as WhatsApp and

YouTube were close second (41%) in terms of being implemented as the means of active learning. Although familiarity in the software applications used by the faculties assisted them to blend with the online teaching scenarios in the present study, challenges to online education reported in the medical literature so far include issues relating to time management, use of technology tools, students' assessment, communication, and the lack of in-person interaction (Esani, 2010; Krenacs et al., 2010).

A study from United States indicated that that many teachers are attempting to transform their face-to-face teaching to an online environment of education (Hixon et al., 2012). With the advent of online teaching formats such as MOOC, and some more radical views with the help of artificial intelligence, virtual teachers can replace most of the roles of offline teachers. (Yao et al., 2020; Yu (2018) used large-scale academic monitoring data and found that the teacher-student relationship is the most essential factor that affects student performance. The results of the present study indicate that the main pattern of online assessment at most medical colleges (73%) during the pandemic was online theory and practical tests, distantly followed by individual online assignments and seminars (12%). Besides, online education may not be equitable in terms of access and the quality of teaching (Modna, 2020). Challenges to the online environment during an emergency may delay the adoption of technology-enabled education (Rajab et al., 2020). In contrast, other commentators have predicted that the COVID-19 pandemic would have a positive impact that will lead to wider acceptance of online and technology-enabled education (Krenacs et al., 2010).

Moreover, switching over to online instruction during an emergency acts as a reset button to the ailing traditional educational system (Chiasson et al., 2015). The transition to online education requires mutual support from the faculty as well as from the universities, planning such a transition. The survey indicated 80% of institutions confirmed that faculty members are being offered some support for their online courses (Lion and Stark, 2010). But the present study's scenario shows that, because of the current insufficient and inadequate infrastructure for online teaching, unsurprisingly most teachers (68%) prefer returning to traditional face-to-face classes as soon as the pandemic is over. However, 33% of teachers are willing to continue some form of online teaching especially or some theoretical classes even after the pandemic is over. Only 2% of teachers want to continue to conduct both theoretical and practical classes online after COVID-19 pandemic.

CONCLUSION

The results provided us a summary of current efforts in organizing online teaching of gross anatomy and histology teaching. This study helps to identify the problems faced by the faculty for online medical education during the pandemic periods in India. This study assists to improve the design and quality of online teaching by suggesting for the change in infrastructure by arranging online portal hands-on coa ching for rendering online education.

ACKNOWLEDGEMENTS

We appreciate the great effort of Dr. Ranajith Das,Yenepoya Research Centre, Mangalore, Karnataka, India for analyzing and verifying the data of this study.

AUTHOR CONTRIBUTIONS

All authors hereby declare that their contribution was equal towards the formation of the manuscript.

REFERENCES

CHIASSON K, TERRAS K, SMART K (2015) Faculty perceptions of moving a face-to-face course to online instruction. *J College Teaching Learning (TLC)*, 12(3): 221-240.

EDGINTON A, HOLBROOK J (2010) A blended learning approach to teaching basic pharmacokinetics and the significance of face-to-face interaction. *Am J Pharmaceut Educ*, 74(5).

ESANI M (2010) Moving from face-to-face to online teaching. *Am Soc Clin Lab Sci*, 23(3): 187-190.

FELLNER FA, ENGEL K, KREMER C (2017) Virtual anatomy: the dissecting theatre of the future – implementation of cinematic rendering in a large 8K high-resolution projection environment. *J Biomed Sci Engineer*, 10(8): 367-375.

GHEBREYESUS TA (2020) World Health Organization. WHO Director-General's opening remarks at the media briefing on COVID-19. 25 May 2020.

HIXON E, BUCKENMEYER J, BARCZYK C, FELDMAN L, ZAMOJSKI H (2012) Beyond the early adopters of online instruction: motivating the reluctant majority. *Internet Higher Educ*, 15(2): 102-107.

JERNIGAN DB, COVID C, TEAM R (2020) Update: public health response to the coronavirus disease 2019 outbreak – United States, February 24, 2020. *Morbidity and mortality weekly report*, 69(8): 216.

KAMENETZ A (2020) Panic-gogy': teaching online classes during the coronavirus pandemic. *NPR Special Series: The coronavirus crisis*.

KRENACS T, ZSAKOVICS I, MICSIK T, FONYAD L, VARGA SV, FICSOR L, MOLNAR B (2010) Digital microscopy: the upcoming revolution in histopathology teaching, diagnostics, research and quality assurance. *Microscopy: Science, Technology, Applications and Education*, 2: 965-977.

LEDERMAN D (2020) Will shift to remote teaching be boon or bane for online learning. *Inside Higher Educ*, 18.

LION RW, STARK G (2010) A glance at institutional support for faculty teaching in an online learning environment. *Educause Quarterly*, 33(3): 23-39.

MODNA Y (2020) The importance of online academic counseling meetings during the global Covid-19 pandemic to improve student confidence and academic performance: a review of outcomes.

ORLEANS M (Ed.) (2014) Cases on critical and qualitative perspectives in online higher education. IGI Global.

RAJAB MH, GAZAL AM, ALKAWI M, KUHAIL K, JABRI F, ALSHEHRI FA (2020) Eligibility of medical students to serve as principal investigator: an evidence-based approach. *Cureus*, 12(2): e7025.

SNELLING J, SAHAI A, ELLIS H (2003) Attitudes of medical and dental students to dissection. *Clin Anat*, 16(2): 165-172.

YAO J, RAO J, JIANG T, XIONG C (2020) What role should teachers play in online teaching during the Covid-19 pandemic? Evidence from China. *Sci Insight Educ Front*, 5(2): 517-524.

YU S (2018) The future role of AI teachers. *Open Educ Res*, 24(1): 16-28.

Brief outline of the methodology to be adopted

Development and description of the data collection tool
Data collection tools were the instruments used by the researcher to observe or measure the key variable in the research problem. The data collection tool used for the present study is demographic and key variable proforma which is developed to consolidate our experience in order to identify problems and further improvement the online teaching. The questions are aiming at teaching for the students of clinical medicine program.

Development of tool
The tool was developed by the researcher after reviewing the related literatures and guidance from experts and based on the research personnel experience; initially a first draft of the tool was developed. After validation, the necessary modifications will be made as per the suggestions of the experts. Thus a final draft of the tool was developed with twenty nine key variable related questionnaires which will be shared in Google forms via link.

The following consents were undertaken to prepare the tool
- Review of literature
- Consultation and discussion with experts
- Content validity of the tool
- Preparation of the final draft

The tool consists of two parts
Part l: **Section A: Baseline proforma** (3 questions coupled along with key variable questionnaire)
This section seeks the informations related to socio-demographic data of professionals.
Part ll: **Section B**: **Key Variables**
The key variables are categorised into six major orientations.
A) Principle implementation tools
B) Mode of delivery
C) Student-teacher interaction methods
D) Perceptions and effectiveness
E) Active learning
F) Problems encountered and success rates

TOOL

Title of the topic: A cross sectional study on the online teaching strategies of gross anatomy and histology during the COVID-19 pandemic periods
Instruction to the participants:
You are cordially invited to take part in the research study titled above having participation duration of 20- 25 minutes. The questionnaire contains 29 questions developed in Google forms, shared via link. The questions are aiming at teaching for the students of clinical medicine program.
Description of tools: The questionnaire schedule consists of two parts

PART I: SECTION A: **Baseline proforma** (3 questions coupled along with key variable questionnaire)
This section seeks the informations related to socio-demographic data of professionals.

PART II: SECTION B: **Key Variables**
The ethical responsibilities are categorised into six major orientations. Namely,
A) Principle implementation tools
B) Mode of delivery
C) Student-teacher interaction methods
D) Perceptions and effectiveness
E) Active learning
F) Problems encountered and success rates
This section consists of twenty (26) multiple choice questions.

ART I: SECTION A: BASELINE PROFORMA (First 3 questions coupled along with key variable questionnaire)
Instruction to the participants:
Dear participants,
Kindly read the questions carefully, please provide your frank response, attempt all the items and place the tick **(√)** mark against the appropriate option whichever you feel suitable in the box [ ] provided against each question.
This section seeks the information's related to socio-demographic data of professionals.
CODE NO: _____

STRUCTURED QUESTIONNAIRE (Google form shared via link)
1. **Name of the Medical College and University of your current employment (The answer to this question is for correlation analyses only, and no personal information will be disclosed) [Please fill in the space below]**.....
2. **Your Current Designation at present place of work**.....
3. **Years of experience in teaching field** .....

PART II: SECTION B: KEY VARIABLES

MULTIPLE CHOICE QUESTIONS- 26 Questions (Google form shared via link)
4. **Before the COVID-19 pandemic, how were the theoretical sessions (lectures) for gross anatomy and histology conducted in your Medical College?**
   a) Face-to-face teachings from the lecture halls
   b) Blended teaching with a combination of online and face-to-face teaching
   c) No experience of delivering online lectures
   d) Blended teaching method followed at medical college with no experience of delivering online lectures

5. **During the COVID-19 pandemic, what is the format of the online theoretical sessions followed for gross anatomy and histology at your Medical College?**
   a) Simultaneous live broadcasting: teacher delivers the sessions live (teacher and students engage simultaneously)
   b) Separate recorded broadcasting where teacher records the sessions, and then uploads it to an Internet platform or disperses it to students (teacher and students engage separately).
   c) Mixed methods (some sessions by simultaneous live broadcasting and some by separate recorded broadcasting)
   d) Any Others (please elaborate).....

6. **For simultaneous live broadcasting of online theoretical sessions, which platforms/tools does your Medical College employ?**
   a) Simultaneous live broadcasting software – If Yes, tick the appropriate
   Swayam Prabha ( ), Cloudatomy ( ), Google suite ( ), Youtube live stream ( ).
   b) Teaching management platform with Simultaneous live broadcasting capability –

If Yes, tick the appropriate
Microsoft teams ( ), Google classroom ( ), Google meet ( ), Google Hangouts ( ), Facetime ( ).
c) Social media If Yes, Tick the appropriate WhatsApp ( ), Telegram ( )
d) Any Other (please elaborate) .....

7. For simultaneous live broadcasting of online theoretical sessions at your Medical College, how do the teacher and students interact?
a) Real-time voice communication (on platforms like Google Classroom ( ), Microsoft Teams ( ) or .....
b) Real-time text communication (on platforms like Whatsapp ( ), Telegram ( ) or.....
c) Real-time on-screen doubts via chat box, online voting or.....
d) Incorporating online assignment questions in power point presentations based on teaching management platform
e) Organizing students into teams for online discussions (Small group discussion (SGD), Self Directed Learning (SDL)
f) Almost no interaction between teacher and students
g) Any Other (please elaborate).....

8. For simultaneous live broadcasting of online theoretical sessions at your College, how much time is used for student-teacher interaction?
a) More than half of the scheduled time of the classes are taken with teacher-student interaction
b) Less than half of the scheduled time of the classes are taken with teacher-student interaction
c) Almost no interaction between teacher and students
d) The teacher talks most of the scheduled time and last 10 minutes is scheduled for clearing doubts

9. For separate recorded broadcasting of online theoretical sessions, how does your College record the sessions for delivering it ?
a) Use a video camera to record the teacher delivering the session, without post-production
b) Use a video camera to record the teacher delivering the session, with post-production
c) Use a screen capture software to record only the slides and sound of the PowerPoint presentation, and the teacher does not appear in the recorded session
d) We do not have any such experience of delivering recorded lectures
e) Blended method of certain videos with postproduction and certain without postproduction
f) Any Other (please elaborate) .....

10. For separate recorded broadcasting of online theoretical sessions, what platforms/tools does your school employ for delivering the recorded session?
a) Simultaneous live broadcasting software – If Yes, tick the appropriate,
Swayam Prabha ( ), Cloudatomy ( ), Google suite ( ), Youtube live stream ( ).
b) Teaching management platform with Simultaneous live broadcasting capability –
If Yes, tick the appropriate, Microsoft teams ( ), Google classroom ( ), Google meet ( ), Google Hangouts ( ), Facetime ( ).
c) Social media If Yes, Tick the appropriate WhatsApp ( ), Telegram ( )
d) Any Other (please elaborate) .....

11. For either simultaneous live or separate recorded broadcasting of online theoretical sessions, what changes were made to the content materials? [Single choice] *
a) The content materials have been completely redesigned
b) The content materials have been broken down into smaller parts
c) The content materials have been adjusted slightly
d) The content materials are the same as those for face-to-face teaching, and have not been changed
e) Blended method of adjusting content materials and certain times without adjusting content materials

12. Before the COVID-19 pandemic, how were the practical sessions for gross anatomy and histology conducted in your Medical College? [Single choice]*
a) Face-to-face teachings from the dissection halls and histology labs
b) Blended teaching with a combination of online and face-to-face teaching
c) No experience of delivering online practical sessions
d) Blended teaching method followed at medical college with no experience of delivering online practical sessions

13. During the COVID-19 pandemic, has there been an increase in the use of visual media in the practical sessions at your Medical College? [Single choice] *
a) No change
b) Yes, Increased by less than 50%
c) Yes, Increased by more than 50%
d) Any other .....

14. During the COVID-19 pandemic, what is the format of the online practical sessions on gross anatomy and histology at your medical college? [Single choice] *
a) Simultaneous live broadcasting: teacher delivers the sessions live (teacher and students engage simultaneously) for gross anatomy and histology
b) Separate recorded broadcasting where teacher records the sessions, and then uploads it to an Internet platform or disperses it to students for gross anatomy and histology (teacher and students engage separately).
c) Mixed methods (some sessions by simultaneous live broadcasting and some by separate recorded broadcasting) for gross anatomy and histology
d) Histology practical sessions were temporarily suspended and planned for the make-up sessions will be implemented when face-to-face classes resume while gross anatomy practical classes were continued by online platforms
e) Any Other (please elaborate).....

15. During the COVID-19 pandemic, what platforms/tools does your Medical College employ for gross anatomy and histology practical sessions? [Single choice] *
a) Virtual Labs Project Launched by MHRD under NMEICT (SWAYAM PRABHA)
b) The Virtual Simulation Experiment Teaching Center (e.g 3D ORGANON VR ANATOMY)
c) The virtual simulation experiment platform built by your Medical College (e.g ACTS-YEN)
d) No such experience of delivering online practical sessions

16. How much time is used for teacher-student interaction during the online gross anatomy and histology practical sessions at your medical college? [Single choice]*
a) More than half of the scheduled time of the classes are taken with teacher-student interaction
b) Less than half of the scheduled time of the classes are taken with teacher-student interaction
c) Almost no interaction between teacher and students
d) The teacher talks most of the scheduled time and last 10 minutes is scheduled for clearing doubts

17. During the COVID-19 pandemic, what types of active online learning have been implemented for gross anatomy and histology at your Medical College? [Single choice]*
a) Online small group discussion
b) PBL (Problem-based learning)
c) TBL (Team-based learning)
d) Microteaching and Individualized tutoring
e) Any Other (please elaborate) .....

18. Before and during the COVID-19 pandemic, has active learning (please refer question [17] above for types of active learning) been implemented for gross anatomy and histology at your Medical College?? [Single choice]*
a) It was implemented before and has continued to be used during the pandemic
b) It was implemented before but were used only at selected time intervals and slots
c) It was not implemented before but has been implemented during the pandemic
d) It was not implemented before or during the pandemic
e) It was implemented before but has been temporarily suspended during the pandemic

19. During the COVID-19 pandemic, which tool was employed to implement active learning of gross anatomy and histology at your Medical College?
a) WhatsApp Web and YouTube
b) Email
c) Telephone
d) Platforms for online courses
e) Any Other (please elaborate) .....

20. What is the main pattern of online assessment at your Medical College during the pandemic?
a) Online theory and practical tests
b) Individual online assignments and seminars
c) Subjective assessment by teachers after the sessions
d) Only recording the attendance for online sessions
e) No online assessments of students
f) Any Other (please elaborate).....

21. Before and during the COVID-19 pandemic, has online assessment been implemented for gross anatomy and histology at your Medical College? [Single choice]*
a) It was implemented before and has continued to be used during the pandemic
b) It was implemented before but were used only at selected time intervals and slots
c) It was not implemented before but has been implemented during the pandemic
d) It was not implemented before or during the pandemic
e) It was implemented before but has been temporarily suspended during the pandemic

22. How do you evaluate the extent of effectiveness of online learning performed during the pandemic? [Single choice]*
a) Less than 30% of learning outcomes are achieved
b) 30-60% of learning outcomes are achieved
c) 60-80% of learning outcomes are achieved
d) 80-100% of learning outcomes are achieved
e) More than 100% of learning outcomes are achieved

23. Are you satisfied with the effectiveness of online learning during the COVID-19 pandemic?
a) Very satisfied
b) Satisfied
c) Neutral
d) Dissatisfied
e) Very dissatisfied

24. What is the biggest gain of your Medical College from the online teaching during the COVID-19 pandemic during initial year of online teaching at 2020?
a) Good opportunity for developing novel teaching methods
b) Diversity of teaching methods
c) Development of content materials for teaching
d) Any Other (please elaborate)

25. What is the biggest gain of your Medical College from the online teaching during the COVID-19 pandemic during the current year of online teaching at 2021?
a) Enhancement of interaction between teachers and students
b) Expediting the feedback process for students
c) Development of more individualized instruction
d) Any Other (please elaborate) .....

26. What are the biggest difficulties you have encountered in implementing online teaching during initial year of online teaching at 2020?
a) Insufficient training and management for online teaching from college
b) Unstable online teaching environments, platforms and tools
c) Unfamiliarity with online teaching technique, platforms and tools
d) Not adapting to novel teaching concepts and methods
e) Insufficient online teaching resources

27. What are the biggest difficulties you have encountered in implementing online teaching during this year of online teaching at 2021?
a) Content materials that are not easily amenable to online teaching
b) Difficulty in grasping student progress and results of learning
c) Difficulty in interacting effectively with students
d) The much longer time needed for preparing online teaching than for traditional teaching
e) Any Other (please elaborate) .....

28. Would you like to continue online teaching after the COVID-19 pandemic? [Single choice]*
a) Willing to continue to conduct the theoretical sessions online
b) Willing to continue to conduct practical sessions online
c) Willing to continue to conduct both theoretical and practical sessions online
d) Willing to continue to conduct some theoretical and practical sessions online
e) Prefer returning to traditional face-to-face classes

29. What suggestions do you have for the further development of effective online teaching of gross anatomy and histology [Please fill in the space below]
.....

Author Index to Volume 26, 2022

F

G

H

I

J

K

L

M

N

O

P

Q

R

S

T

U

V

W

Y

Z

European Journal of Anatomy